DIGITAL IMAGE PROCESSING OF LANDSAT DATA FOR MAPPING HYDROTHERMALLY ALTERED ROCKS IN NEW MEXICO

Robert William Magee, BSc.

A thesis submitted for the degree of Doctor of Philosophy of the University of London.

Imperial College of Science, Technology and Medicine
London, England

October 1989

ACKNOWLEDGEMENTS

Throughout my research and during the writing of this thesis many individuals and institutions have given me invaluable support and advice. The following merit particular mention.

John McMahon Moore, Senior Lecturer in geology and remote sensing at Imperial College, for supervising the project and for his advice and criticism of the text.

The Geology Department, and The Remote Sensing Sections at Imperial College and the Geography Department at University College, all of the University of London, for allowing me to carry out my research and for the use of their facilities.

David Norman, Associate Professor, of the New Mexico Institute of Mining and Technology, Socorro, who was instrumental in setting up this project and provided me with logistical support and advice during my field work in New Mexico.

Dr. Stephen Zara of the Applied Botany Department of Imperial College for assisting me with my laboratory reflectance measurements.

To my former fellow students and research colleagues, for their advice and stimulating discussion, particularly Jeremy James, Khatab el Hinai, Jake Brunner, and Graham Oakes.

In New Mexico, Ted Talmon and the staff of the Technology Application Centre, Albuquerque, University of New Mexico, provided me with useful image processing facilities; Richard Robinson and Pioneer Nuclear Inc. (now Mesa Petroleum) provided useful field support in the Summit Mountains, and Professor Anthony Barringer of Barringer Resources, Golden, Colorado, loaned me a field radiometer.

I was supported throughout my research by a postgraduate award from the N.Ireland Education Authority.

My thanks to Culham Laboratory for the use of reprographic facilities, in particular to Stuart Morris for help and advice on graphics.

On a more personal note I thank all the friendly people I met in New Mexico who made my time in the "land of enchantment" a very enjoyable one, particularly Mary Norman, Cheryl Fahringer and Mike and Barbara Phillips.

Finally a thank you to my family and friends who have supported me throughout with patience and good humour.

ABSTRACT

Landsat Thematic Mapper data covering southwest New Mexico is evaluated for mapping hydrothermal alteration in the volcanic terrain of the Datil - Mogollon region of southwest New Mexico.

The epithermal mineral deposit in the Summit Mountains is used as a test area to evaluate the relationship between the imagery and the terrain features. Information was provided by field and laboratory studies, including geological and vegetation mapping, spectral reflectance measurements, geochemical and petrological analyses.

Characteristics of the Summit Mountain epithermal system are described and are used to produce a conceptual remote sensing model, which is used to identify potential epithermal deposits in New Mexico using TM imagery.

All known hydrothermally altered rocks and several previously unknown areas of alteration, greater than 0.1 km^2, were identified, except in mountainous and forested terrain. The main constraints are the vegetation density and distribution and the low sun angle of the imagery. Spectral masking from weathering, surface stains and lichens, although significant on the microscale do not affect results.

Where vegetation cover is less than approximately 70 percent of a pixel, single band TM ratio images are

successful. With increasing vegetation cover, colour ratio composites are superior. Combination 5/7 3/2 4/3 worked well over a wide range of conditions up to about 40 percent total scene vegetation cover.

Alteration could not be mapped satisfactorily in areas of mixed pixels consisting of more than 70 % vegetation and alteration, using either CRCs, Principal Components Analysis, Directed Principal Components Analysis or Mineral Indices.

This study is the first to use Landsat Thematic Mapper data for mapping hydrothermal alteration in southwestern New Mexico. The limitations of TM are documented and the geological knowledge of alteration in New Mexico is improved.

Guidelines are presented for mapping hydrothermally altered rocks using TM imagery in semi-vegetated terrain.

TABLE OF CONTENTS

LIST OF FIGURES

LIST OF TABLES

CHAPTER 1.

AIMS, OBJECTIVES, METHOD AND SCOPE OF THE RESEARCH

1.1 Introduction

Hydrothermally altered rocks are commonly associated with epigenetic mineral deposits, forming alteration zones much larger than the orebodies of these deposits. The study of these alteration zones plays an important part in the detection of many epigenetic mineral deposits. The constituent minerals of hydrothermally altered rocks are often difficult to distinguish in the field, and commonly require geochemical and petrological analyses for detailed and accurate study. The geologist rarely has immediate access to such facilities in the field.

Rocks and minerals can be identified from the measurement and analysis of electromagnetic energy reflected or emitted from the terrain surface. Such measurements made from sensors mounted on aircraft or satellite platforms allow alteration zones to be mapped over large areas. This information can be recorded and analysed by computers and image processors to reveal subtle or apparently hidden spectral information, usually in the form of images. The study of these images to extract useful information is part of the science of remote sensing.

Landsat Thematic Mapper (TM) imagery is important because it gives geologists access to high resolution

imagery over most of the world, capable of detecting the surface presence of common alteration minerals, such as clays, micas, alunite and iron oxides, hence allowing the potential to identify small epigenetic mineral deposits.

This thesis assesses digital image processed Landsat Thematic Mapper imagery for mapping hydrothermally altered rocks. The research was done in the Mogollon - Datil volcanic field of southwest New Mexico where there are numerous areas of hydrothermally altered rocks associated with epigenetic mineral deposits.

1.2 Review of remote sensing of hydrothermally altered rocks.

Remote Sensing is a multi-disciplinary science, whose definition varies with the discipline. It is the observation and measurement of an object without touching it (Fischer 1975). From a geological viewpoint remote sensing may be defined as the use of electromagnetic radiation sensors to record images of the environment which can be interpreted to give useful geological information. Electromagnetic sensors measuring from the ultraviolet to radio waves are used for geological remote sensing, but for remote sensing of hydrothermal alteration the emphasis has been on the visible to the short wave infrared (SWIR) parts of the electromagnetic spectrum. This review and thesis is restricted to sensing in this part of the spectrum.

The difficulty of recognising hydrothermally altered rocks on black and white photographs, delayed the application of aerial photography to alteration mapping until the 1950s when colour photographs became available. Some of the first applications of colour aerial photographs to alteration mapping include mapping supergene enrichment (Lake 1950), and porphyry copper alteration (Kent 1957). Numerous other examples are listed by Norman (1969). Later attempts were made to map alteration from space with colour photography. These were largely unsuccessful because high altitude photography is affected by atmospheric scattering , e.g. Skylab (Rowan and Lathram 1980).

Modern multispectral remote sensing has its origins in the US space missions of the 1960s. Planetary exploration required research on rock and mineral spectroscopy which led to developments in remote sensing of the earth. In the 1970s Hunt and co - workers (e.g. 1970a, 1970b, 1971a. 1971b, 1973b, 1973c, 1974, 1979) produced a series of spectral analyses of many rocks and minerals which showed that many minerals common in altered rocks have diagnostic spectral features, particularly in the short wave-length between 1 and 2.4 μm, which could be utilized for mapping hydrothermal alteration (Appendix 1). However the ability to use the reflectance of altered rocks for alteration mapping on a world wide scale did not occur until the Landsat programme had begun.

The first widely available satellite data was from the Landsat Multispectral scanner (MSS). Initiated

by NASA in 1967 and launched in 1972, Landsat was an experimental system designed to test the feasibility of collecting earth resource information from an unmanned satellite. From its inception Landsat was not designed for geological applications and the data is far from ideal for alteration mapping. The spectral range allows the identification of iron oxide bearing rocks but the resolution is insufficient to discriminate between various iron oxides. More detrimental is the absence of spectral information from the short wave infrared part of the electromagnetic spectrum where many hydrothermal alteration minerals have diagnostic spectral signatures. The 80 metre spatial resolution limits MSS to detecting alteration zones of the order of 2 hectares in area e.g. Baker and Baldwin (1981)[1].

Nevertheless MSS data was widely used with some success for regional alteration mapping in arid and semi-arid areas, e.g. Rowan et al. (1976) (Appendix II). Perhaps of greater importance in the development of geological remote sensing was the exposure of many geologists to the concept of using remotely sensed data for geological applications.

The Thematic Mapper, launched on the Landsat 4 platform on July 1982 was the second generation Landsat sensor designed for multispectral survey. The spectral range and resolution, spatial resolution and radiometric sensitivity are superior to the first generation Landsat MSS (Table 1.1). The TM records

1 *This reported performance is the limit of MSS capability. For mapping in territories where good ground information is absent a figure around 25 hectares would be expected.* *See page 207.*

Table 1.1 Comparison between the Landsat MSS and TM sensors (adapted from Smith, 1985)

	Multispectral Scanning System (MSS)			Thematic Mapper (TM)	
1. Wavebands					
	MSS Bands		Band Width (um)	TM Bands	Band Widths (um)
	Landsat 1 - 3	Landsat 4 on			
	4	1	0.5 - 0.6	1	0.45 - 0.52
	5	2	0.6 - 0.7	2	0.52 - 0.6
	6	3	0.7 - 0.8	3	0.63 - 0.69
	7	4	0.8 - 1.1	4	0.76 - 0.9
				5	1.55 - 1.75
				6	10.4 - 12.5
				7	2.08 - 2.35
2. Nominal Ground Resolution (metres)	79 x 79			30 X 30 in bands 1 - 5 and 7 120 in band 6, resampled to 30 X 30	
3. Grey Levels	64			256	
4. Number of Detectors	6			16	
5. Data Rate	15 Mbps			85 Mbps	

reflected electromagnetic energy in seven discrete bands, 3 visible, 1 near infrared, two mid-infrared and 1 thermal infrared. The nominal 30 metre spatial resolution was chosen principally to allow monitoring of crops in small fields and the spectral bands were chosen primarily for vegetation monitoring with the exception of band 7 (2.08 - 2.35 μm) which was chosen for geological applications (Salomonson et al. 1980).

The main importance of band 7 for geological mapping is that hydroxyl bearing minerals show strong and unique absorptions in this part of the electromagnetic spectrum, which can be used to identify particular minerals, such as clays (Appendix 1). The feasibility of mapping clay minerals using this was known for many years from laboratory and field research e.g. Hunt et al. (1979), but the band was included on the TM after successful lobbying from the geological community and from a successful demonstration of alunite and clay mineral mapping at Cuprite Nevada (Abrams et al. 1977).

Unfortunately the Landsat 4 satellite failed in early 1983, soon after launch. As a result the availability of TM data was severely restricted and many researchers were unable to evaluate the new data. Consequently a research programme using airborne TM data began in the U.S.A.. Hydrothermal alteration was successfully mapped using this Airborne Thematic Mapper data (ATM) at several localities in the western USA, e.g. Abrams et al. (1983), Rickman and Sadowski (1982) and Kruse (1984a). However ATM was collected with superior

resolution and greater spectral range than TM and the results are not representative of TM satellite data.

The first results from Landsat TM satellite data applied to mapping hydrothermal alteration were from the Landsat 4 satellite from imagery covering the southwest USA, e.g. Podwysocki et al. (1984), Magee et al. (1986). This restricted imagery was collected in the winter of 1982/3 and suffers from low sun illumination, snow cover and high vegetation cover. With the availability of Landsat 5 data, TM imagery was used for alteration mapping in regions outside North America for the first time e.g. Rodalquilar, Spain (Huckerby et al. 1986).

The main attention of the research community for alteration mapping in the mid and late 1980s has been on high spectral and spatial resolution data from aircraft sensors measuring infrared and thermal infrared reflectance. Although Landsat TM has inferior performance relative to modern aircraft based sensors, in terms of spatial and spectral resolution, it does have certain important advantages for remote sensing of alteration. These include global availability, the relatively low cost of data acquisition and the easy availability of hardware, software and human expertise to process and interpret the data.

This brief review has not covered the image processing techniques used for alteration mapping, which are described in Chapter 2.

1.3 Objectives and Methodology

This research project began in the autumn of 1983 when TM data in digital form were available only for restricted areas of the continental United States, at which time the capabilities of Landsat TM for alteration mapping had not been assessed. The objectives were to assess TM for mapping hydrothermally altered rocks, using digital image processing techniques, with particular emphasis on mapping alteration associated with epigenetic mineral deposits.

The selection of a suitable study area was limited by the restricted availability of TM data, but the following criteria were of fundamental importance to the project:

1. Hydrothermal alteration developed on the surface related to epigenetic mineral mineralisation
2. Low vegetation cover[1]
3. Ease of access and availability of geological information and logistical support.

With the co-operation of Professor Norman of the New Mexico Institute of Mining and Technology a number of potential sites in New Mexico were investigated, with the Steeple Rock mining district in the Summit Mountains of Grant County, New Mexico being finally

---

1 *Surficial alteration and a lack of vegetation are required because visible and near infrared (VNIR) energy is reflected from the rock surface.*

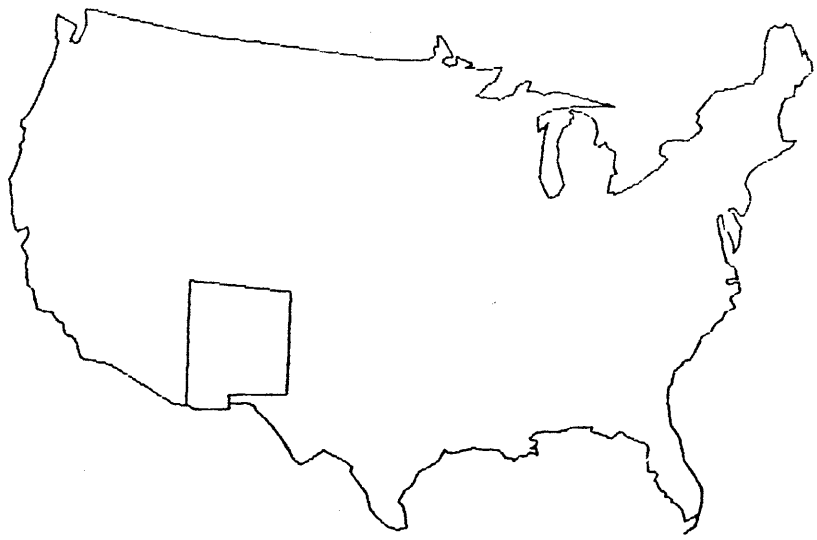

(a) New Mexico, USA

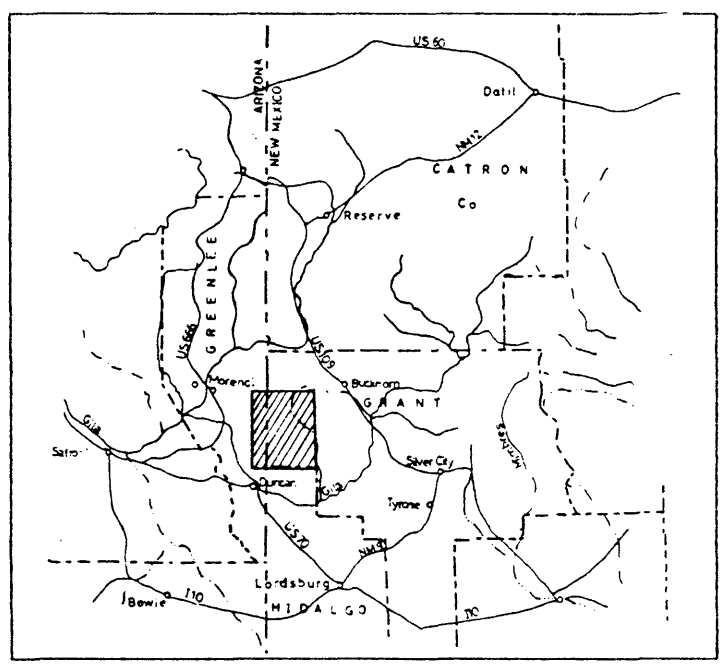

(b) Southwest New Mexico and Arizona

Figure 1.1 Location of the Summit Mountains, New Mexico USA (shaded)

chosen (Fig. 1). The district contains epithermal precious and base metal ores, associated with extensive hydrothermal alteration, in a semi-arid region were vegetation cover is relatively low. Full details are given in Chapter 4.

The research method was to assess the TM data and applied image processing techniques in the Summit Mountain test area, where the complex relationships between the TM data and the ground could be analysed and better understood. From there the techniques would be extrapolated and altered as required for application to regional hydrothermal alteration mapping in southwest New Mexico.

A regional map showing the distribution of alteration zones of southwest New Mexico is one parameter among many geological factors indicative of the presence of epithermal deposits. It was hoped that TM image information, supplemented where necessary with existing geological information would allow the identification of epithermal types in southwest New Mexico. It was not an intention of this study to perform a comprehensive geological exploration programme over the region. This would involve the integration of the remotely sensed data with geological, geophysical and geochemical information with appropriate weighting and interpretation given to each.

1.4 Thesis Structure.

Chapter 1 describes the objectives, methodology and structure of the thesis. Chapter 2 describes the image processing techniques and equipment used in the research and Chapter 3 describes the regional geography and geology of southwest New Mexico and discusses how they affected the research objectives.

Chapters 4, 5 and 6 cover the test area studies in the Summit Mountains. Chapter 4 describes the geography and geology with particular emphasis on the alteration - mineralisation relationships and presents a model describing the epithermal system. Much of the geological data presented is based on new material from my fieldwork in the Summit Mountains and subsequent geochemical and petrological analyses.

Chapter 5 assesses the capabilities of TM imagery for alteration mapping by comparing various processed image types to ground information. Processing techniques to extract this information are presented.

Chapter 6 collates the image processing results with the laboratory and field studies and discusses the main factors which were determined to affect the results from the test area.

Chapter 7 describes the extrapolation of the techniques to southwest New Mexico. A number of areas of hydrothermally altered rocks are identified and evaluated as epithermal deposits. The relative use of band ratios, Principal Components Analysis

(PCA), and other image processing techniques for alteration mapping in terrain with varying vegetation cover are evaluated.

Chapter 8 summarizes the research findings relating to the geological use of the TM data for mapping alteration in southwest New Mexico. From the test area and regional studies the relative importance of those factors which affect alteration mapping using TM data and the optimum processing techniques to use under these conditions are listed. Recommendations are made for the application of remote sensing for mineral exploration and for further research in southwest New Mexico.

[Throughout this chapter and in the rest of the thesis image processing commands of the IIS image processor (Model 70F/4) are referred to by name in block capitals.]

CHAPTER 2

DATA, EQUIPMENT AND IMAGE PROCESSING PROCEDURE

2.1 Data and Equipment

Both Landsat Thematic Mapper and Landsat MSS data were used in this research. The areal coverage of this imagery is shown in figure 2.1 Two Landsat MSS scenes were used, from Landsat 3 and 4 respectively. The Landsat 4 scene (Path 34, Row 37) was acquired in photographic negative form and was used for preliminary geological studies. The Landsat 3 scene (Path 34, Row 34) was acquired in digital format. Processing of this scene was carried out to compare and compliment the TM imagery (Appendix II). The TM data is the third quadrant of a Landsat 4 scene (Path 34, Row 37), (the stippled area on Figure 2.1).

The TM was imaged on 10 January 1983 at 17.14.22 hrs. (GMT). The most important feature of this image is the low sun illumination angle of 27 degrees. Lambertian reflectance of many ground materials may not occur at this low angle (Appendix III).

Most of the digital image processing was done using the facilities of the Centre for Remote Sensing at Imperial College. Basic processing was on the IIS System 500 model 70 F/4 processor, hosted by a PDP-11/24 computer. Details of operation can be found in the operation manual and in Driscoll and Walker (1981).

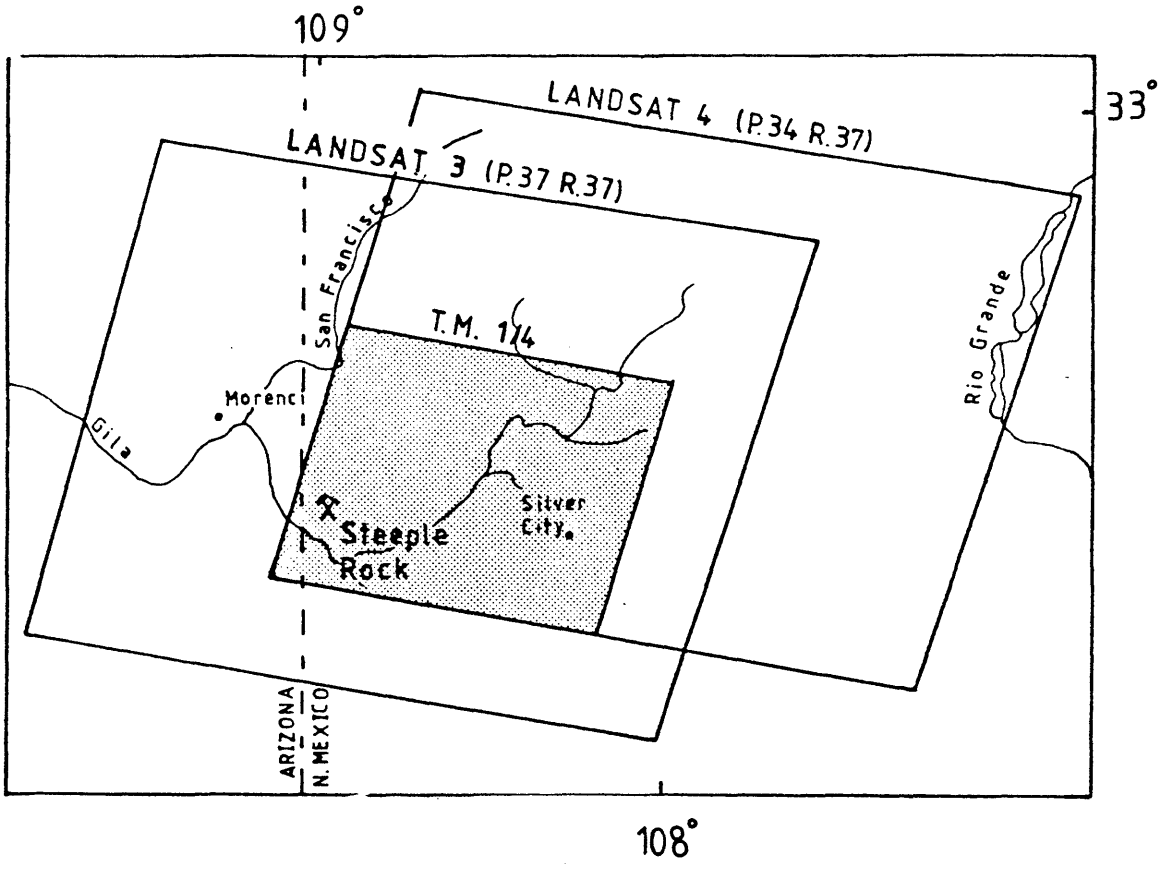

Figure 2.1 Location and area covered by the Landsat Scenes used in this research.

There are many hardware and software limitations on this equipment due to the small memory capacity of the host computer and the age of the software (c. 1979). One of the main limitations was that many of the processes may be applied only on images 512 lines by 512 samples in size. A second was the limited number of refresh channels (4). Processing on larger images and nonstandard processing was done on the more powerful and flexible IIS models 70E and 75 Vax 11-70 hosted system.

Prior to and during field work in New Mexico, use was made of the RIPS image processing system at the Technology Application Centre at the University of Albuquerque, New Mexico. The combination of periods of field work interspersed with periods of processing helped image interpretation and allowed ground checking of areas of alteration identified on the imagery.

The IIS System and the associated ISIS digitising package in the Geography Department of University College London were used to digitise geology and drainage maps for geometric correction of the TM data.

2.2 Digital Image Processing

Digital image processing is a branch of computer graphics concerned with the manipulation of digital images to display an image for interpretation or information extraction. An excellent introductory text to digital image processing is given by Schowengerdt (1982). The operations within digital image processing can be divided

Figure 2.2 The steps of digital image processing

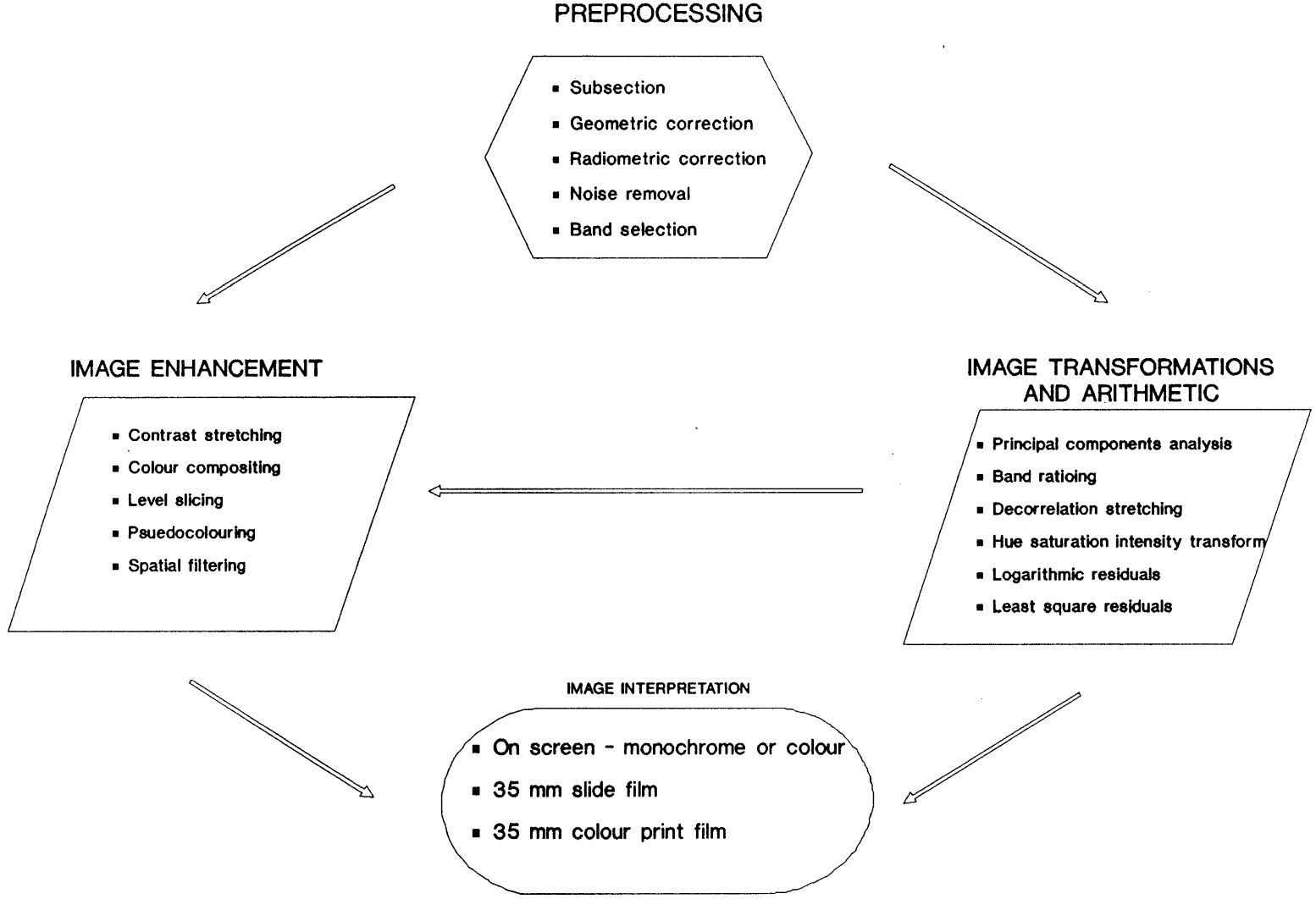

into three main processes shown in figure 2.2, restoration, enhancement and interpretation (Estes et al. 1983).

Restoration refers to those processes which are necessarily applied to the image data prior to image enhancement and includes radiometric calibration, noise removal and correction of geometric distortions. Image enhancement may involve contrast enhancement, colour enhancement, edge enhancement or any process which improves the image visually. Interpretation may involve further processing by the computer and human interpretation skills.

In geological remote sensing image processing has historically been used mainly as a restoration and enhancement tool. Interpretation has been largely left to traditional photo-geological techniques although computers have an increasingly important role to play, because of the growing uses of multispectral data and other remote sensing data gathered outside human sensory experience.

Image transformations such as band ratios, and principal components analysis, are in part computer interpretative. The image products may be interpreted visually or used as input for computer classification. These techniques are both a classification and an enhancement process and have been termed enhancement classification (Schowengerdt 1983).

Image processing was first applied to geological studies in the 1970s, primarily with Landsat MSS data, although

earlier Skylab data was also digitally processed. Many of the standard techniques were first described in the classic paper of Rowan et al. (1976). Comprehensive coverage of both optical and digital image processing techniques applied to geological studies can be found in Skaley (1983) and Gillespie (1983). More recent texts with useful information include Drury (1987) and Sabins (1986).

For alteration mapping using VNIR and SWIR data image processing techniques have all attempted to recognise and exaggerate the unique spectral characteristics of altered rocks and to separate rock spectra from vegetation. Simple band ratios have been very effective (Chap. 2.6a, and 5) but more recent techniques include Directed Principal Components (DPCA) (Chap. 7.3), Logarithmic Residuals (Chap. 2.6), Least-square Residuals (Fraser et al. 1986), Decorrelation Stretching (Chap. 2.5c), and Directed band ratios (Crippen 1988b)[1]. Least-square Residuals was unavailable when my research was undertaken, but is discussed in Chapter 8.

---

1 *Crippen describes a technique for introducing topographic information into ratio images. Band subtraction would be a better technique because they retain topographic information and are computationaly simple to produce and interpret. The principle advantage of the ratio is the supression of topographic information.*

2.3 Data Handling and Image Management

The first step in the processing procedure is to enter the digital data from the computer tape into the computer. For MSS imagery whole bands have to be entered in one stage because they normally require whole scene preprocessing operations to be applied, e.g. geometric corrections (Chap. 2.4a). The imagery is then divided into manageable blocks for rapid handling and screening. On the IIS 500 system these blocks are band multiples of three or four, measuring 512 lines by 512 samples in dimension.

The divisions of the TM imagery are shown on figure 2.3. These image blocks are referred to by name throughout the thesis. The image block names and the regional geographical names are often used synonymously. For example the test area in the Summit Mountains is equivalent to the Summit Mountain image. It is also important to note here that the Summit Mountain area is sometimes called the Steeple Rock district, the main mining area within the area.

To display images larger than the 512 lines by 512 pixels subsampling is necessary. For example, the Blue Creek image was displayed by sampling every third line and pixel. This subsampling and loss of resolution may cause image blockiness whereupon smoothing may be applied, at the expense of loss of information (Chap. 2.4).

Handling of the TM data relative to the MSS presented data handling problems. The scale of the problem can be

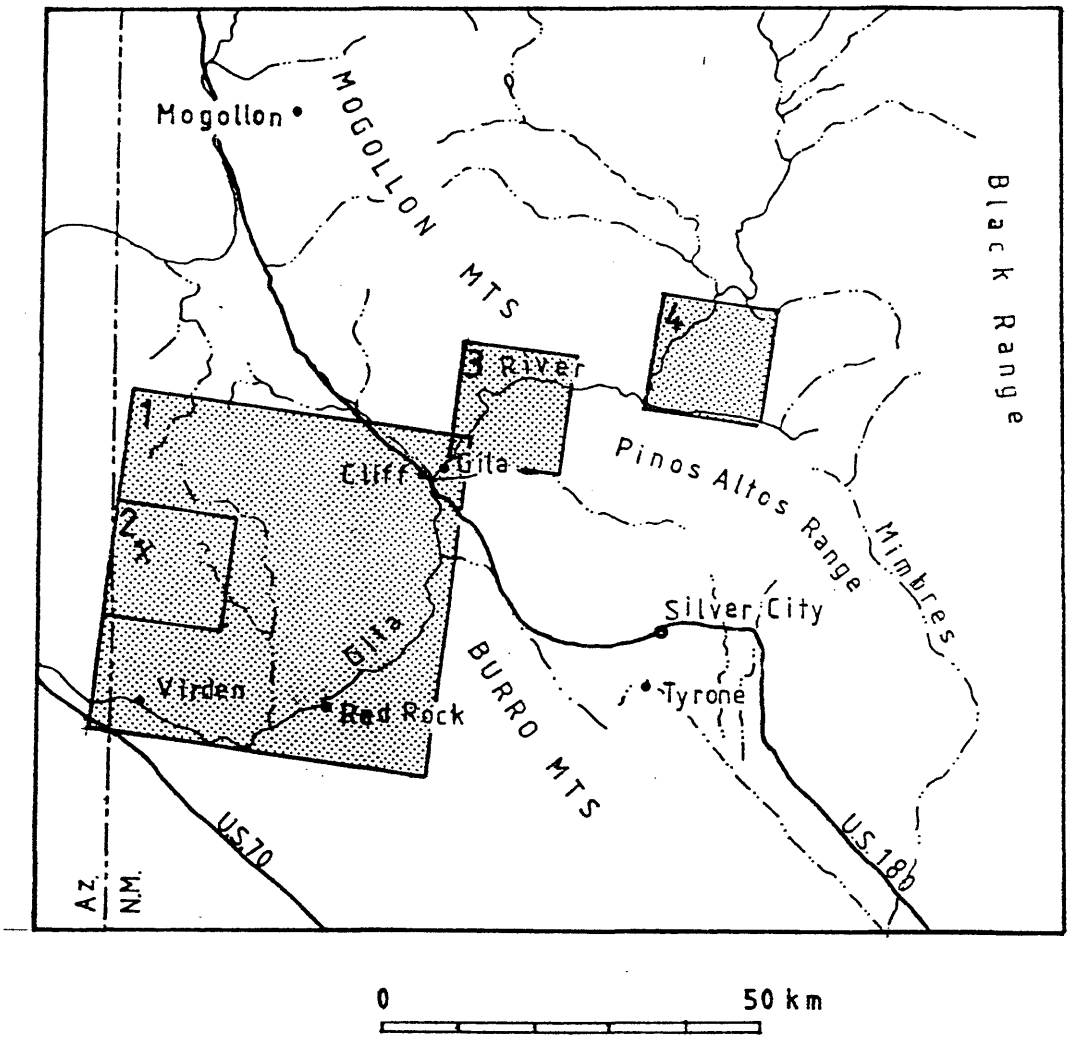

Figure 2.3 Names and location of the TM imagery subscenes.

1 Blue Creek
2 Summit Mountains
3. Brock Canyon
4. Alum Mountain (including Copperas Creek)

Table 2.1 Data Storage and Handling Details

Equipment

Image Processor:	IIS Model 70F/4
Host Computer:	PDP - 11/24
Display:	4 Channels, 512 x 512 pixels
Hard Disc Capacity:	132 Mb

Data

Landsat MSS (full scene - 4 band)	32 Mb
Landsat TM (full scene - 7 bands)	300 Mb
Landsat TM (1/4 scene - 7 bands)	100 Mb
Blue Creek TM scene	14 Mb
Summit Mountain TM scene	1.6 Mb

Management

	MSS	TM
No. of full resolution subscenes per band	100	1008
No. of 3 band combinations	4	20
No. of 3 band ratio combinations	20	455

appreciated by reference to table 2.1, which lists some typical storage and data handling details. Data reduction is an important part of image processing. Reduction may be achieved by compression of the information into fewer images, or by selecting bands according to their information content. The Principal Component Transform (PCT) is a statistically optimum means of data compression, but the resultant images are scene dependent and pose unique interpretation problems to the geologist (Chapts. 2.6b, 5.7 and 7.3). In geological remote sensing band selection is often the preferred option.

To produce colour composite images, three bands are selected and one each is allocated to one of the primary colours, red, green and blue. When colour composites are referred to the band numbers are listed in order of RGB, e.g. the image 352 is the colour composite with band 3 shown in the red, 5 in green and 2 in blue.

The number of unique band combinations, C, of extracting r bands from a total number of N bands is given by:

$$C = N!/(N - r)!\ r!$$

The number of band combinations for typical Landsat MSS and TM colour composite images are shown in table 2.1. The improved spatial resolution of TM over MSS compounds the data handling problem. For example, a 512 x 512 pixel MSS scene covers 1636 square kilometres. The same size of TM imagery covers 236 square kilometres, a reduction in area of a factor of 7.

These figures emphasise the importance of band selection. Selection may be based on numerical measurements of band information content, or on empirical grounds, based on known expected or predicted physical characteristics of the features of interest. Both techniques are described in Chapter 5.1. Extensive spectral data bases exist for remote sensing of alteration.

2.4 Image Restoration

Remotely sensed imagery acquired from satellite or aircraft suffers from electronic, geometric, mechanical and radiometric distortions which can seriously affect the use of the data. Most of the corrections required are made to the data at the ground processing station (ground segment) before distribution to the user.

(a) Geometric Correction

The Landsat TM data used here was fully geometrically and radiometrically processed at the Goddard Space Flight Centre, Maryland, USA. All TM are transformed to a Space Oblique Mercator projection (SOM) a projection especially designed to permit low distortion mapping of the earth from satellite imagery. This is a complex projection in which the groundtrack for the satellite is held to scale and mapping is conformal. Conformal projections are correct in shape for each infinitesimal element of the

map, thus distance and direction between near points is accurate. However when the image consists of more than a small number of elements, distortion in shape and area is appreciable (Berstein, 1983). The distortion across a full resolution TM scene as displayed on the IIS monitor (512 by 512 pixels, representing 14.6 km on the ground) was negligible. However for smaller scale mapping distortion was appreciable and a geometric correction was necessary.

The IIS system has several geometric algorithms (DESKEW, LATLONG, UTM) all of which were designed for Landsat MSS data. None accurately corrected the TM data. Therefore a geometric correction had to be done by other means.

The distortion on the Blue Creek image, which measured 1536 by 1536 pixels was significant, so this image was geometrically corrected to a UTM projection to allow accurate comparisons of the imagery with geological maps and to allow the accurate placement of hydrothermally altered rocks on the topographic base maps. The procedure took the following steps:

(1) Drainage, roads, topographic features and mine positions were traced onto acetate from the Silver City 1:250,000 base map.
(2) The data was digitised using the ISIS digitising package of University College London.
(3) The digitised data was converted to a one band 512 by 512 image compatible with the IIS system also using UCL software.
(4) Ground control points (GCPs) were identified and plotted on the image and on the base map.

(5) The TM imagery was warped to fit the base map using proprietary IIS software (CPU'WARP).

The use of a large number of GCPs reduced the accuracy and increased the processing time. The best fit warp used 16 GCPs and gave an estimated error of 1.2%. A nearest neighbour resampling algorithm was used to avoid changes of the pixel intensities and to maintain radiometric fidelity. The pixel intensities of the warped image and the original image were unchanged by the resampling process. All the Blue Creek imagery described in the regional processing (Chapter 7) were geometrically corrected.

(b) Radiometric Corrections

The second process done on the imagery was radiometric correction. Although radiometric corrections are applied to the data during ground processing, imagery often contains residual bad pixels or striping in the sample direction. Radiometric striping was a common problem with Landsat MSS data, but not with TM. However if the TM data was not "destriped" strong residual striping appeared in ratio images, because ratio images enhance noise.

Striping on Landsat imagery is simple periodic noise, which can easily be removed by convolution, a spatial filtering technique (Chap. 2.5d). Striping was particularly apparent on the TM 5/7 ratio (Fig. 2.4).

Striping was removed by spatial filtering techniques operated by the CONVOLVE command. On the IIS an

[Filtering is performed on the input bands to the ratio and not on the ratio image. The periodic noise shown on figure 2.4c is that removed from bands 5 and 7 before ratioing.]

(a) Original TM 5/7 ratio. Note the periodic and isolated noise

(b) Destriped TM 5/7 ratio

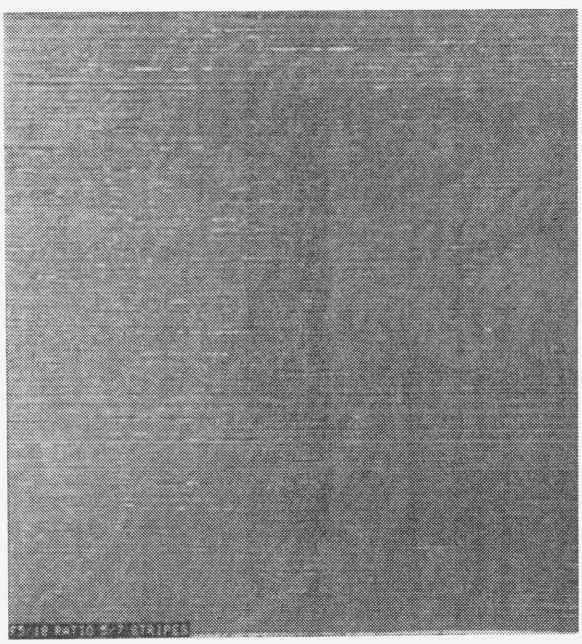

(c) The Periodic noise removed

(d) TM ratio 5/7 after low pass filtering

Figure 2.4 Radiometric processing of the TM 5/7 ratio image of the Summit Mountains. All images are linearly contrast stretched.

especially designed spatial filter called DESTRIPE was available. This filter suppressed sudden changes in mean and variance between adjacent scan lines by means of a box car filter. The weighting of the filter can be changed to lower the noise threshold at the expense of causing blurring on the image.

Random noise can be removed by low pass filtering, which causes image smoothing, or alternatively, if the noise is high frequency by the use of a despiking filter. A despiking filter replaces any pixel above a defined threshold by the average value of the pixels in the filter box. The despike filter used was not a standard IIS software programme, but was developed at Imperial College by Graham Oakes (Oakes 1988).

Isolated noise, such as bad pixels and lines can be removed on the IIS by an editing function called EDIT. This filters noise on a line, line segment or on a pixel in the horizontal or vertical directions by a median filter, similar to a low pass filter but which replaces each pixel by the median neighbourhood value rather than the mean.

The low pass spatial filters available on the IIS were assessed together with the despike filter. The despike filter was very flexible and superior to the median and low pass filters for noise removal while retaining image information, but it took up to 30 minutes for each 512 by 512 size band. Low pass 3 x 3 filters were flexible and rapid, typically taking a few seconds processing time. However they caused distinct image blurring. The median filter was very rapid and caused less blurring than the

low pass filters, however it caused an unpleasant blocky image texture. The square and cross filters were harsher than the x filter which removed less noise.

2.5 Image Enhancement and Display

a) Contrast Enhancement

To aid the human analyst in the extraction and interpretation of image data images are displayed and manipulated to give the optimum display for interpretation by the eye.

Contrast enhancement is a pixel by pixel radiometric transform where each pixel is changed by a specified transform independent of neighbouring pixels to make optimum use of the dynamic range of the display device, which is usually 255 levels (2^8). The IIS system has several contrast enhancement functions which are virtually instantaneous in operation, for both automatic and interactive processing of display resident images. These are:

1. Linear stretches

a) Linear - rapid and simple but cause some data saturation, implemented by SCALE.
b) Piecewise linear - allows more control over image contrast and is useful for asymmetric histogram,

implemented by PIE.[1] A very powerful tool when used with the 'Breakpoints'option together with the analysis of the image histogram.

c) Interactive - very flexible, implemented by TLM.[2]

2. Automatic non-linear stretches

a) Gaussian - implemented by HISTOGRAM'N or ADJUST

b) Cumulative density function - implemented by HISTOGRAM EQUALISATION

c) Logarithmic - implemented by LOG

d) Exponential - implemented by EXP

e) Negative - implemented by NEGATE

Contrast within a image can vary locally and an optimal enhancement may be achieved by using an adaptive algorithm whose parameters are determined by local image contrast, e.g. Fahnestock and Schowengerdt (1983). On the IIS this is done by the LOCAL ENHANCE space variant contrast stretch. This gave a pleasing contrast to most images, but it alters the radiometric values of the image irreversibly and took considerable computation time (20 minutes for a one band 512 by 512 scene).

Density slicing, implemented by LEVEL SLICE is a contrast stretch useful for visual analysis. All grey levels falling within a specified range are mapped to a single DN level output value which can be coloured. This is a special enhancement which actually decreases the image data range, and is a very useful analytical tool for single band ratio images (Chap. 5.3).

---

1 *PIE - Piecewise Linear Enhancement.*

2 *TLM - Trackball Linear Mode, the IIS command for an interactive linear contrast stretch via a mouse.*

(b) Colour Display

Although the human eye can adapt to an enormous number of brightness levels of the order of 10^{10}, this impressive performance cannot be achieved simultaneously, and for a complex image only approximately 12 to 24 grey levels can be discriminated at any one point (Gonzalez and Wintz 1977). By contrast the average human eye can discriminate approximately 200 different hues (Coren et al. 1978). Colour display dramatically improves image interpretability.

In digital image processing colour display is achieved by simultaneously displaying each of the three spatially registered images individually through red, green and blue filters. This process is known as colour compositing and the resultant image a colour composite. Figure 5.3 is a colour composite of the Summit Mountain test area, of bands 4, 3 and 2 through red, green and blue filters. All the colour composites described in this thesis are in the filter assignment order of red, green and blue.

Colour compositing is a powerful interpretation tool because reflectance information in three separate images can be represented on one image and if the spectral signatures of the features in the scene are known, the hue and the resultant cover type on an image can be controlled or predicted.

Contrast stretching is an important step in colour composite production. The aim is to have all colours

equally represented, i.e. colour balance. Which is achieved by placing the data cluster centrally over the achromatic or grey point. If this is not done the image may appear monochromatic. The invariant contrast stretch described earlier (LOCAL ENHANCE) produces monochromatic images when applied to individual bands prior to compositing.

The examination of the individual image histograms to find out the mean, maximum and minimum grey levels followed by a piecewise linear stretch using the breakpoints 0 128 and 255 gave the best colour composite images.

(c) Colour Transforms

In common with many Landsat multispectral images of arid and semi-arid terrain, those of New Mexico are highly correlated and contain very little spectral information (Chap. 5.2). The composites remain essentially monochromatic because stretching of the three highly correlated bands expands the intensity range but does little to expand the range of colours (Gillespie et al. 1986). Colour transforms are processing techniques used to expand the range of colours of composite imagery. There are two common types, hue saturation intensity, known as HSI and decorrelation stretching.

Intensity hue and saturation are terms used to describe the subjective sensations of brightness, colour and colour purity. The process involves transformation of a colour composite from red, green and blue components to HSI components. Effective enhancement is done by stretching

[The main advantage of the HSI technique over decorrelation stretching for my work is that HSI is scene independent whereas decorrelation stretching (and principal components analysis) are scene dependent. Thus the HSI techniques successful in the test area can be extrapolated with confidence to the region where ground information is lacking. Decorrelation stretching processes are difficult to extrapolate from image to image.]

the S component prior to transformation back to the original RGB component for display. Retransformation is important because the colour composite image is interpretable in terms of the original colour composite. However, if the H component is stretched the resultant colours of the retransformed RGB image may not resemble those of the original, but it may be necessary to slightly stretch H to improve image colour.

A second method which has been favoured recently is the decorrelation stretch. Decorrelation stretching was not used in my research because while the technique certainly produces colour enhanced imagery, the technique is scene dependent. Decorrelation stretching involves transformation of the data to PCA (Chap. 2.6b) followed by a transformation into RGB. The resultant colours on the enhanced image are not necessarily interpretable in terms of the original colour composite image because the new bands contain admixtures of all the bands both positive and negative. This means that a low DN value in a particular band does not necessarily mean there is low reflectance in that band.

Gillespie et al. (1986) discuss both the HSI and decorrelation stretches in detail and give the mathematics of the transforms. The uses of the HSI transform in my research are described in Chapters 5.2 and 7.4.

(d) Spatial filtering

Geologists have always used geomorphological information to relate surface topography and drainage to underlying

geology. Air photographs have been used extensively for structural mapping and analysis (Blanchet 1957, Lattman 1958). However the use of satellite imagery for structural studies is controversial, because of the unclear relationship between structures identified on the ground and lineaments observed on the imagery (Wise 1982). Satellite imagery can only observe the broad relationships between the terrain and geological structure because the practical limit of resolution from digital imagery is 3 times the pixel size (Drury 1986), giving a minimum ground feature size of 240 and 90 metres resolution for Landsat MSS and TM imagery respectively.

Some lineaments are clearly identifiable as faults, but most appear to be zones of more intense joint development and fracturing, thought to originate from erosion and weathering of more subtle underlying structural features (Wise et al. 1985).

In geological remote sensing spatial filtering is an enhancement technique applied to imagery to enhance geological structure by sharpening edges of images or by producing edge maps, often for regional structural studies. A regional structural study was not an objective of this research, except in so far as it relates to the identification of epithermal deposit types. Simple edge enhancement techniques were used to improve imagery for visual interpretation. No attempt was made to analyse, classify or otherwise map lineaments.

Spatial filtering like contrast enhancement is a pixel by pixel transformation, but unlike contrast enhancement the DN of a pixel is altered according to the DN of the pixels

in the immediate vicinity. Filtering can be achieved in the frequency or spatial domain. On the IIS it was done in the spatial domain using the CONVOLVE command using 3 x 3 pixel size convolution filters.

The two commonly used filter types are high pass and low pass filters. The use of low pass filters for noise removal was described in Chapter 2.4b. High pass filters are used to filter out low and medium frequency information, to leave those image feature with high spatial frequencies, such as topographic features related to geological structure. These features are observed better on monochrome images. Colour images emphasise gross variations in surface cover which may relate to rock type (Drury 1986).

In southwest New Mexico there is a good relationship between topography and geological structure, because the region is geologically young. Where there is little superficial cover, bedrock structures exert a strong influence over the topography and drainage. In the basins where thick conglomerates and other unconsolidated superficial deposits occur, tectonic trends are often visible, probably from joint and fault propagation upward to the surface. These areas are often noisy with high frequency drainage features (highest frequency information can be removed by a despiking filter).

There is a strong bias toward the detection of structural features lying orthogonal to the direction of illumination of the imagery. To overcome this, directional high pass filters can be used. These filters must be used with care as spurious linear features can be introduced on the

imagery.

On the New Mexico imagery, Laplacian (simple multi-directional) filters added back to the original imagery produced good quality sharpened imagery suitable for structural interpretation. Convolution reduced image contrast and consequently gave dull colour images. An HSI colour transform counteracted this effect.

It is beyond the scope of this thesis to fully describe spatial filtering techniques. Comprehensive details can be found in Schowengerdt (1983, section 2.3) and Oakes (1988).

2.6 Image Arithmetic and Transforms

Image transforms are mathematical processes performed on the image data and include simple arithmetic operations such as addition, subtraction, multiplication and division, and more complex operations such as the Principal Components transform, Log. Residuals and Least-square Residuals. All the processes may be considered as enhancement operations if the output is the final image product for interpretation, or as a preclassification technique if the processed images are input features for computer classification. In my work the processes were used exclusively as an enhancement operation.

Addition and multiplication of bands are non-linear

operations[1] which tend to enhance common information, which is mainly topographic. Multiplication is rarely used as it produces very harsh images due to the severe image compression which occurs during scaling of the output image for the image to be displayed on the VDU. Addition is a useful display operation; addition of a broad band TM and MSS data approximates to a panchromatic band and information from more bands than there are display channels available can be done.

Both band subtraction and division enhance spectral features and are used to extract spectral information. Band subtraction is an attractive proposition as the technique is simple and interpretation of the resultant image is easy. However simple band differences do not suppress band independent radiance variations from topographic slope and aspect and other temporally or spatially varying gain and bias factors, which are removed by band division, the effect of which is the introduction of topography into difference images. The low sun angle of the TM imagery used in this study (27 degrees) caused strong topography and shadow which does not favour the use of band differences.[2]

---

1 *Non linear on the image processor due to rescaling of real numbers to fit the image display range.*

2 *Canas (pers. comm., 1989) has developed a differencing technique which overcomes the problems of topography on difference images. The technique applies a contrast stretch to both images before subtraction which ensures each band has the same histogram width and mean value. On subtraction information common to both images is cancelled leaving spectral differences which can subsequently be enhanced by contrast stretching. (Canas, A.D., Applied Optics Group, Blackett Laboratory, Imperial College, University of London).*

Log. Residuals were developed to remove varying albedo and illumination effects on imagery on a per-pixel basis to leave residual values approximating to surface reflectance (Green and Craig, 1985). The technique was not used in my work because of the unavailability of the software. However, Hook and Munday (1988) report that Log. Residuals produce numerous false anomalies when used for mapping advanced argillic alteration in vegetated terrain of Queensland, Australia.

Band division, commonly referred to as band ratioing, was the main technique used to extract spectral information.

(a) Ratios

Band ratioing techniques have been widely used for spectral remote sensing of multispectral imagery for many applications in geological, landuse and vegetation studies, because they have the ability to suppress common information and simultaneously enhance spectral differences.

In its simplest form, band ratioing involves the division of two spatially registered bands on a pixel by pixel basis. The utility of the ratio image lies in its simplicity, ease of implementation and in the properties of the product image. Spectral information in two images are presented in one image which is interpretable in terms of the spectral signatures of the ground features. For example a feature with low reflectance in band 1 and high reflectance in band 2 will have a low 1/2 ratio and appear dark on the 1/2 ratio image.

Slater (1980) lists many of the radiometric problems which are overcome by using spectral band ratios. The most important of which is the removal of variations in reflectance due to topography. However the suppression of brightness information may cause spectrally dissimilar materials to appear similar (Sabins 1978, p.262).

A major disadvantage is caused by the non-linear way in which ratios treat input data, so an appreciation of the properties of ratios is important to ensure that the best image processing techniques are used. Ratio intensities are represented on the feature space by lines radiating from the origin, the slopes of which represent constant grey levels (Fig. 2.5). Clusters of classes which occur on the same slope will have the same ratio value or range of values. Thus the data range occupied by a cluster depends upon its position relative to the origin and on the range of angles it subtends.

Because TM data is highly correlated from band to band and class to class, the range of ratio values is small. No amount of contrast stretching can rectify this problem. The angles that a class or classes subtend and hence the ratio value range of the class(es) can be increased by negating one of the input bands to improve discrimination, but this re-introduces topographic information (Fig. 2.6), (Chap. 5.5).

The output values on a ratio image are scaled for display on the VDU from 16 bit word information to bytes. This compression is unequal across the image intensity range, the net result of which is that ratio x/y may not be the

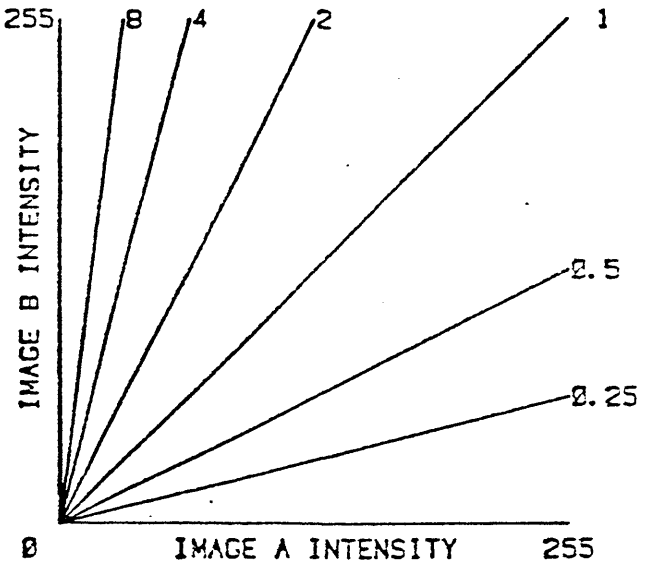

Figure 2.5 Division of feature space on simple ratios.

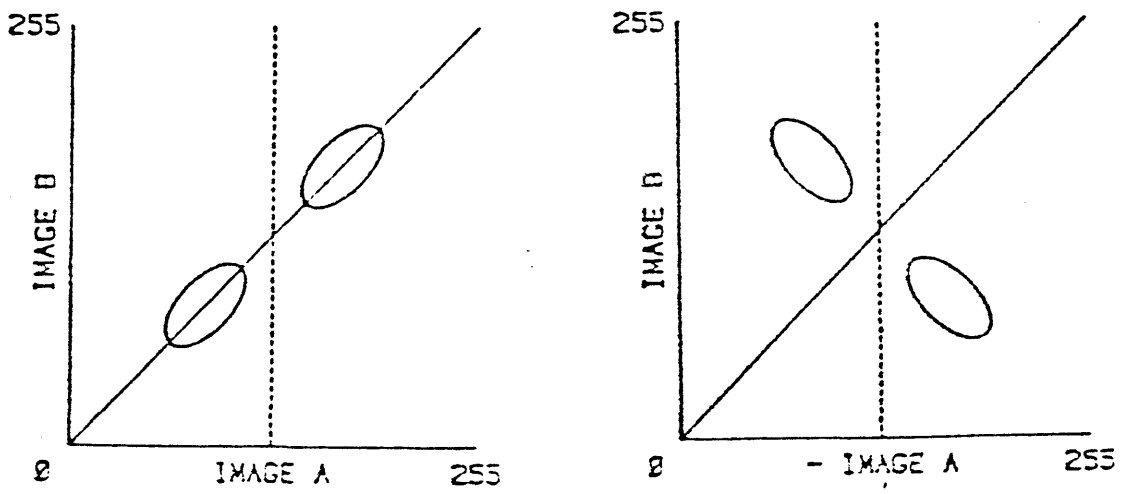

Figure 2.6 Improved cluster discrimination with simple ratios by image negation.

direct negative of ratio image y/x. Thus where classes have high or low ratios values intra and inter class separability may be improved.

Full details of the ratioing procedures are described in Chapter 5.3.

b) The Principal Component Transform

Principal Components Analysis (PCA) has been widely applied to multispectral data as an image enhancement technique, a preclassification process and as a means of reducing image dimensionality i.e. data compression (Jenson and Watts, 1979). For geological usage image enhancement has been the main use, although data compression is becoming increasingly important, particularly as multispectral channels increase in number.

The original N features of a data set are transformed by means of a linear transformation to a new N dimensional set, of which the features are uncorrelated and are ordered by decreasing variance. The net result is to produce new uncorrelated images equal in number to the original bands, which retain all the original variance, but now separated into levels of decreasing image variance. The first PC has the greatest variance, commonly greater than 50%. This is usually information common to all the bands, such as topography.

Mathematically the transform is implemented in three stages (Canas and Barnett 1985);

1. Calculation of the variance - covariance matrix for the image data.
2. Computation of eigen-values and eigen-vectors of the variance - covariance matrix.
3. Implementation of the PCT by forming a weighted sum of the original images using the eigen vector components as the weighting factors.

Like band ratios the PCT eliminates topographic - illumination brightness differences and enhances spectral information. The PCT has several advantages over the ratio, including greater spectral detail, and the separation of noise from signal. The main disadvantage is the images are uniquely scene dependent. The results of the PCA are given in Chapter 5 and a related technique called Directed Principal Components Analysis (DPCA), developed for separating alteration from vegetation features, is described in Chapter 7.

2.7 Interpretation Methods

The objectives were to accurately transfer the image features to the base maps, so that the image features could ultimately be identified on the ground. The procedure followed can be divided into four steps:

(i) Visual image assessment - compare the image to other data sources (field data, maps, photos etc.). Use IIS facilities such as TLM or an automatic contrast enhancement and ZOOM.

(ii) Class Assessment - analyse cover class spectral features using statistical output, histograms and feature space scattergrams.
(iii) Improved image enhancement (Chap. 2.2)
(iv) Data output - compile, compare and interpret the image data with other information sources.

The main problem is to transform the high quality image information on the screen into a form which can be easily compiled, compared and interpreted with other data. This can be done either by putting all the relevant information onto the computer and displaying it on the screen, or by taking the imagery information off the screen.

Putting all the information into the image processor and displaying it on the screen is an attractive proposition. The powerful image processing facilities can then be used to merge, process and display many different types of spatial information, such as geology, topography, and vegetation. However the information has to be taken off the screen for presentation purposes. A 1:250,000 scale geologic map was digitised using the ISIS system, and put into the IIS system using a procedure identical to that described for the geometric correction. This geologic map was useful for interpretation of the regional imagery.

However, this option was not pursued for two reasons; the map data for southwest New Mexico are of different scales and coverage, and it would have taken a great deal of time to digitise and input the information into the computer. Secondly, the IIS system had only four display channels, which effectively limited the display to either one colour TM image and a map or one monochrome TM image and three

maps.

Hardcopy output is best for interpretation but is prohibitively expensive when large amounts of imagery are required, so 35 mm colour film was used. The main technique used in my research was to photograph the VDU screen using colour slide film with a 35 mm camera resting on a tripod. A zoom lens was used to minimise distortion around the screen edges. The colour slides were then projected using a standard slide projector onto a specially designed light box with a 45 degree angled mirror and reflected onto a glass plate. The image was clearly visible on the plate through acetate or tracing film placed on the surface. This system although crude gave considerable flexibility as the image could be interpreted at various scales simply by moving the projector backward or forward.

For the test area studies all the imagery, maps, and aerial photographs were interpreted and or compiled at 1:50,000 scale. For the regional work 1:250,000 was the working scale.

CHAPTER 3

GEOLOGY AND GEOGRAPHY OF SOUTHWEST NEW MEXICO

3.1 Geography

Southwestern New Mexico extends westwards from the Rio-Grande to the Arizona stateline and southwards from Socorro New Mexico to the Mexican border, a huge area of some 50,000 square kilometres (Fig 3.1). This vast region is one of the most isolated areas in the USA and much is designated as National Forest.

The region contains two distinct physiographic provinces. The southern and western parts belong to the Mexican Highland section of the Basin and Range Province, characterised by scattered fault block ranges and broad intermontane basins. The central and western parts represent a transition zone between the Basin and range Province and the Colorado Plateau to the north, called the Datil-Mogollon section. This consists of rugged volcanic terrain dominated by high table lands, broad structural basins and scattered fault block ranges.

The Datil-Mogollon section is comprised mainly of highlands known as the Mogollon Plateau. The eastern margin is marked by the forested Black Range which rises to over 2438 metres (8000'). The dissected interior rises in elevation from 2286 m in the east to 2591 metres in the west and on the western rim the rugged Mogollon Mountains rise to above 3048 metres (10000'). Southwest of the Mogollon Mountains lies the relatively subdued volcanic

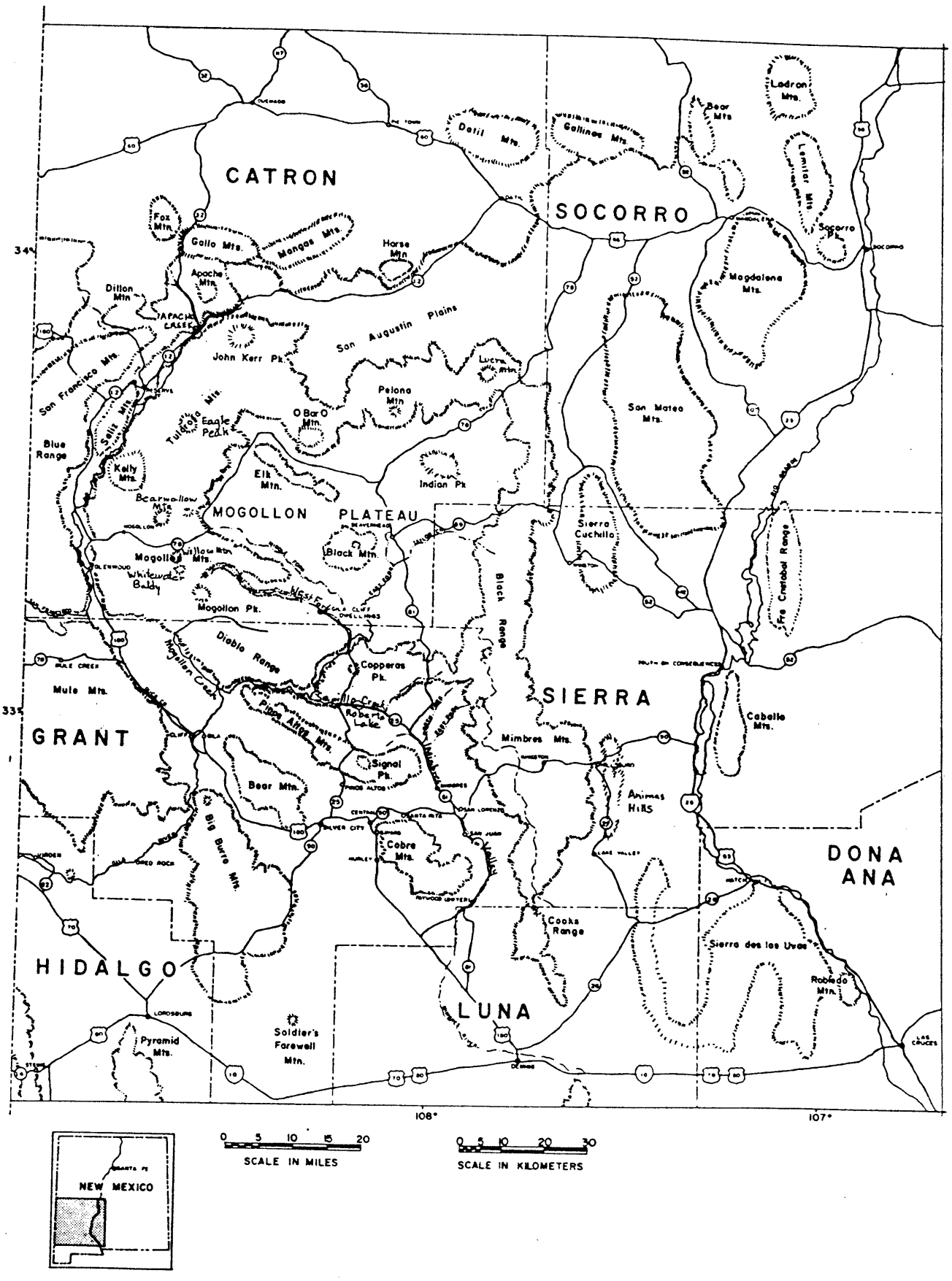

Figure 3.1 Geography of southwest New Mexico (from Elston et al. 1976)

terrain of the Summit and Mule Mountains, separated from the Mogollon Plateau by a prominent structural feature, the Mangas trench. The lowland areas surrounding the plateau; the Mangas Trench, the Mimbres and Sapillo Creek valleys and the San Vicente Basin, are composed of Quaternary age alluvium, colluvium, river terraces and pediment gravels.

The west of the region is drained by the Gila river, whose headwaters drain the interior plateau and high mountains, flowing south and then westwards to Arizona. The Gila occasionally runs dry in summer and most of the larger tributaries are perennial in their upper parts. The western slopes of the Black Range, the Pinos Altos mountains and the lowlands southeast of the Burro mountains are drained by the Mimbres, San Vicente Arroyo and Whitewater Creek systems southward into the desert. To the northwest, Mule Creek and Little Dry creek drain westward to the San Francisco river and west of the Black Range drainage is eastward to the Rio Grande.

The climate is continental semi-arid to semi-desert and varies considerably according to altitude, season and to a lesser extent aspect. Average annual temperature ranges from 21 degrees centigrade in summer to 2 degrees centigrade in winter with a maximum diurnal variation of 30 degrees. Table 3.1 shows the average temperatures for the lowland deserts and high mountain regions.

Average precipitation is around 300 mm, ranging from less than 250 mm in the desert plains to over 460 mm in the Mogollon and Black Range mountains. Most precipitation falls as rain between July and September, carried by the

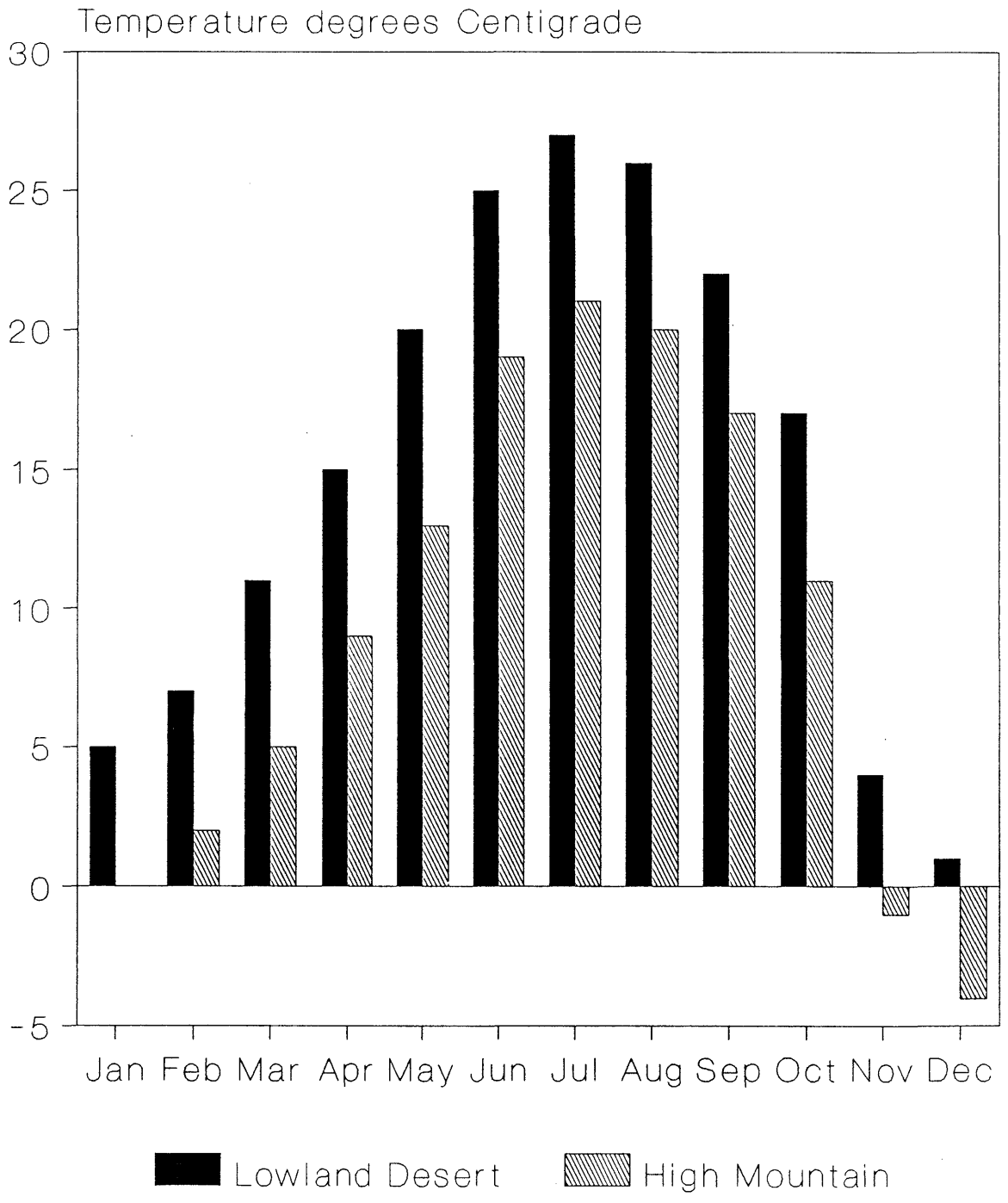

Table 3.1 **Average temperatures in the lowland desert and high mountain regions of southwest New Mexico.**

southwestern winds from Baja California. Snow occasionally falls in winter on the higher mountains. Vegetation type, distribution and density are controlled by topography in so far as it controls precipitation and temperature. There are five types of natural vegetation (Fig 3.2). In Grant County three types are dominant; Grasslands and shrub steppe occur below 1370 m, Woodlands between 1370 m and 2286 m and Coniferous forests above 2134 m.

The basinal areas and lower hills are mainly covered in desert shrubs and grasses with aspens (called Cottonwoods in the USA) and Walnut in the dry washes. Grasses include Gramma grass (*Bouteloua eriopoda*), tobosa grass (*Hilaria*) and beargrass (*Nolina*). Shrub steppe includes species of Creosote bush (*Larrea*), mesquite (*Prosopis*) and various species of cacti, including Cholla (*Opunta bigelovii*) and Prickly pear (*Opunta phaeacontha*).

The woodland association is dominant west of the Mogollon mountains covering most of the mountain slopes and low hills. It favours elevations above 1717 m and on north and east facing slopes. The woodland consists of Juniper (*Juniperus*), Pinyon (*Pinus*) and scrub Oak (*Quercus*), with an understudy of shrub steppe or grasses. The trees are small, usually less than 12 m, and well spaced, although areas of continuous canopy cover occur locally in watered areas.

The Coniferous forests consist of Ponderosa pine (*Pinus Ponderosa*) and Douglas Fir (*Psuedo Tsuga*), with Aspen (*Populus angustifolia*) and Oak. Engleman Spruce (*Picea englemannii*) occurs on the higher and wetter areas. The Coniferous Forest association is found above 2134 m where

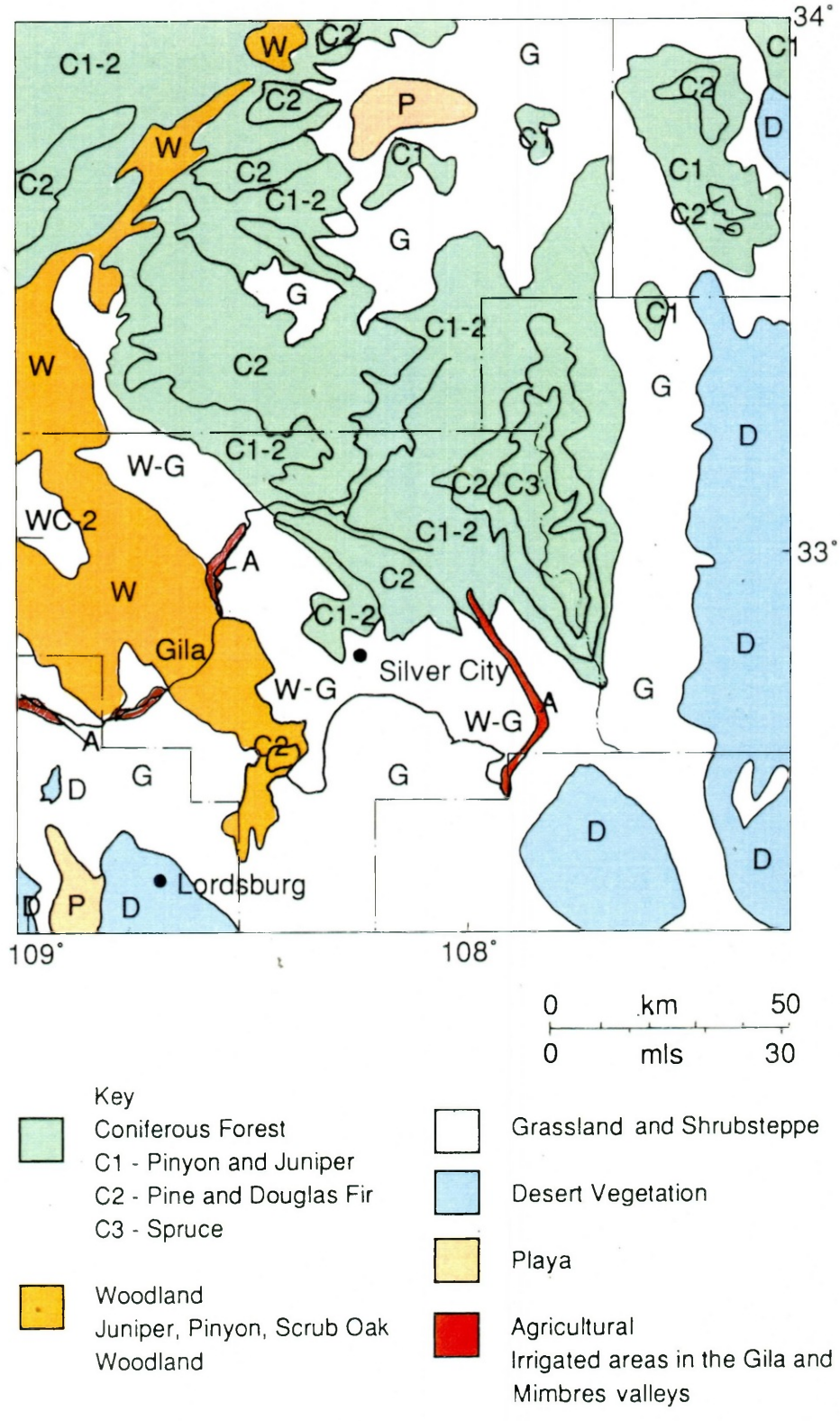

Figure 3.2 Vegetation type and distribution of southwest New Mexico (adapted from Morain et al. 1977).

precipitation exceeds 400 mm per year and is best developed on the western and southern parts of the Mogollon mountains. Smaller stands occur to the north west of the Summit Mountains and in the Burro mountains.

Agricultural land is restricted to irrigated parts of the Gila river valley south of Cliff and to the Mimbres valley.

The region is thinly populated. Communities are restricted to the desert basins of the south where the largest towns are Lordsburg and Demming and to the fertile Rio Grande basin where Las Cruces is the main city. The settlements of the interior owe their existence to mining, lumbering and ranching. Mining is the most important economic activity and supports Silver City, the largest interior settlement. Details of the mining are given in Chapter 3.6.

3.2 Regional Geology

The geology of the region is poorly documented due to three main factors; the large size and rugged nature of the terrain, the relatively small number of geologists working in the area, and the complexity of the geology.

Prior to 1960 very little was known about the geology of the region. Early studies, such as those of Gillerman (1964) and Lindgren (1905), understandably concentrated on descriptions of the numerous mining districts. They referred to the regional geology in a general way.

During the last three decades the works of Elston, Seagor, Clemons, Coney, Smith and Rhodes have contributed significantly to the understanding of the regional geology. United States Geological Survey (USGS) studies looked at the regional geology and mineralised areas in the western Mogollon-Datil volcanic field and in the Silver City Quadrangle.

South west New Mexico forms part of the North American Cordillera and its geology is typical of that found in the southwestern United States. Three main events characterize the region; the late Cretaceous early Tertiary age Laramide orogeny, the Mid-tertiary period of volcanism and tectonism and the Basin and Range tectonism of late Tertiary and Quaternary age. Coney (1972) and Elston (1976a) have described and interpreted these events in terms of plate interactions between the Farallon plate and the North American plate.

In the American Southwest the Laramide orogeny was characterized by northeast directional compression, uplift, intrusion, calc-alkaline volcanism and the emplacement of the porphyry copper plutons (Titley and Hicks 1966). In New Mexico traces of the Laramide orogeny are slight; the present geology and topography are inherited from Tertiary age events.

The Mogollon-Datil volcanic field forms one of several major Tertiary-Quaternary age volcanic fields that lie at the edge of the Colorado Plateau Province (Fig. 3.3). The central part of the field is interpreted as a cauldron complex which has been described as the surface expression

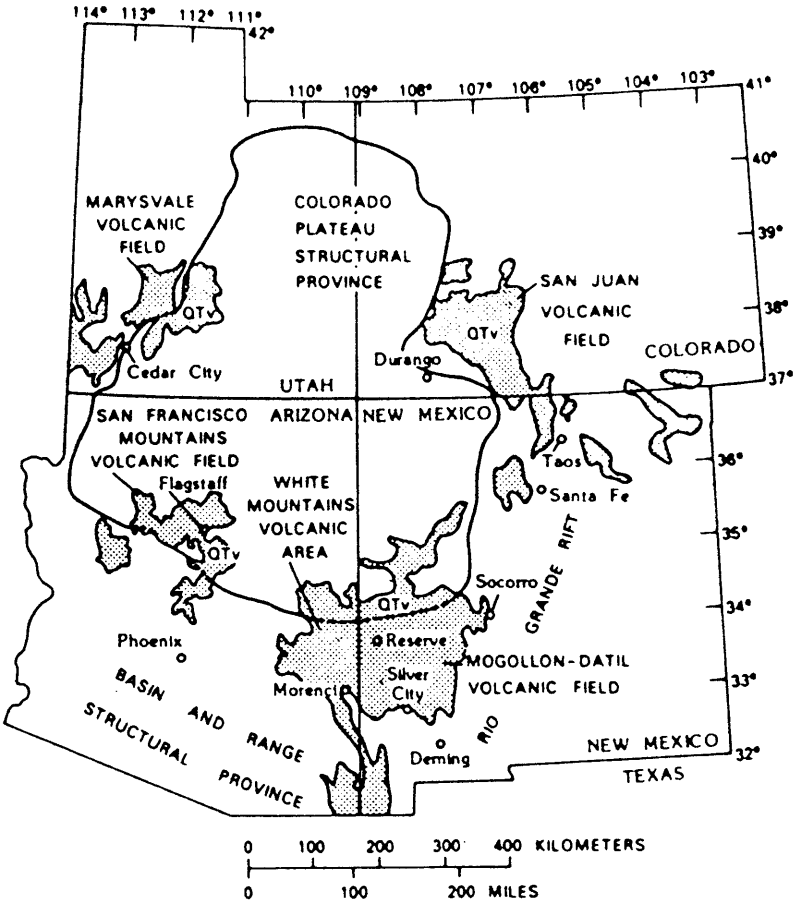

Figure 3.3 Location of the Mogollon-Datil volcanic field in relation to other major Cenozoic volcanic fields near the margins of the Colorado Plateau province (from Ratte et al. 1979).

of a major batholith (Rhodes 1976b)[1]. A further 28 cauldrons are known or suspected to exist in the region (Elston 1984b). The nature of these cauldrons and the related volcanism are discussed in Chapter 3.4.

3.3 Pre Tertiary Geologic History

Precambrain, Palaeozoic and Mesozoic age rocks form the basement on which the Laramide and Tertiary age volcanics lie (Table 3.2). The basement rocks lie on the margins of the volcanic province and reach a thickness of several hundred metres in the Silver City area.

Precambrian rocks are restricted mainly to the Burro Mountains and smaller outliers at Silver City, and south of the Summit Mountains in western Grant County (near the test area). They include an early granodiorite to granitic group forming large plutons and dykes and later gneisses of sedimentary and volcanic origin. The Burro Mountain granites are intruded by later Laramide age quartz monzonite masses.

A maximum thickness of 900 metres of Palaeozoic rocks, consisting of fossiliferous carbonates and clastics, have been recorded at Silver City. They thin westward to 300 metres at Morenci, Arizona (Lindgren 1905) and northwards. Mesozoic strata are thin in the region. Triassic and Jurassic and lower Cretaceous formations are absent.

---

1 *Cauldron is a structural term used here to include all volcanic subsidence structures, regardless of shape, size, depth of erosion or connection with surface volcanism.*

Table 3.2 Palaeozoic and Mesozoic rocks at Silver City New Mexico (after table 1, Hernon et al, 1967)

AGE	FORMATION	LITHOLOGY	MAXIMUM EXPOSED THICKNESS REPORTED (METRES)
Late Cretaceous	Colorado Fm.	Interbedded sandstone and shale	550
	Beartooth Quartzite	Massive orthoquartzite, minor shale	47
		unconformity	
Early Permian	Abo Fm.	Calcereous sandstone and shale	88
Pennsylvanian	Syrena Fm.	Grey limestone	117
Pennsylvanian	Oswaldo Fm.	Massive limestone, shale at base	140
		unconformity	
Mississippian	Lake Valley Limestone	Blocky massive limestone	160
Late Devonian	Percha Shale	Upper: Shale with limestone nodules Lower: Black fissile shale	137
		unconformity	
Silurian	Fusselman Dolomite	Massive dolomite	100
Late Ordovician	Montoya Dolomite	Dolomite; interbedded chert in middle; sandstone at base	117
		unconformity	
Early Ordivician	El Paso Limestone	Blocky dolomite and limestone	173
Early Ordivician to Late Cambrian	Bliss Fm.	Dark massive orthoquartzite, locally hematitic or glauconitic, minor dolomite	63
		unconformity	
Precambrian		Granite, quartzite	

Upper Cretaceous rocks are widespread at Silver City where they reach a maximum thickness of 600 metres. Like the Palaeozoic they are believed to thin northward.

Rocks of Laramide age include the porphyry copper stocks and numerous small unmineralised intrusions and the remnants of probably extensive volcanics. Outcrops are scattered and small as much of the record has been obliterated by Tertiary erosion, volcanism and tectonism (Titley 1983).

3.4 Tertiary Volcanism

The vast 65,000 square kilometre Mogollon-Datil volcanic province dominates southwest New Mexico. The rocks are classified as cauldron related, mainly rhyolite from ash flow tuff cauldrons and non cauldron related, mainly andesites from stratovolcanoes. Taken as a whole the rocks are mildly bimodal calk-alkaline volcanics emplaced in a back-arc tectonic setting (Elston and Bornhorst 1979, Elston 1984a).

The volcanics have been arranged in three main groups which have been related to the plate interactions and associated volcanic and tectonic evolution of the southwest USA (Elston 1984a, 1984b).

1. Calc-alkaline volcanism (40 - 30 m.y.)
   Andesitic becoming rhyolitic with local basaltic volcanism

2. High silica rhyolite (30 -20 m.y.)
Rhyolite and quartz latite ash flow tuffs eruptions from cauldrons with voluminous basalt eruptions peripheral to the cauldron centres.

3. Bimodal basaltic-rhyolite volcanism related to basin and range volcanism.

Middle Tertiary age calk-alkaline volcanism began at the end of the Laramide orogeny. Early eruptions began from andesitic stratovolcanoes which continued to erupt for most of the Tertiary, but with the composition becoming more rhyolitic. Many of the early centres are dominated by andesite and rhyolite vent complexes, commonly with extensive hydrothermal alteration. Known examples in southwest New Mexico are Alum Mountain, Copperas Creek, and Brock Canyon and possibly the Steeple Rock area in the Summit Mountains.

High silica rhyolite volcanism began about 30 m.y.. They are interpreted as partial melts of lower crustal granulite and gneiss with heat provided by ponded mafic magmas. Quartz latite ashflow tuffs erupted from numerous volcanoes in sufficient volumes to cause cauldron subsidence. Twenty-eight of these rhyolite ash flow tuff cauldrons are known or suspected to exist in southwest New Mexico (Elston 1984b), (Fig. 3.4).

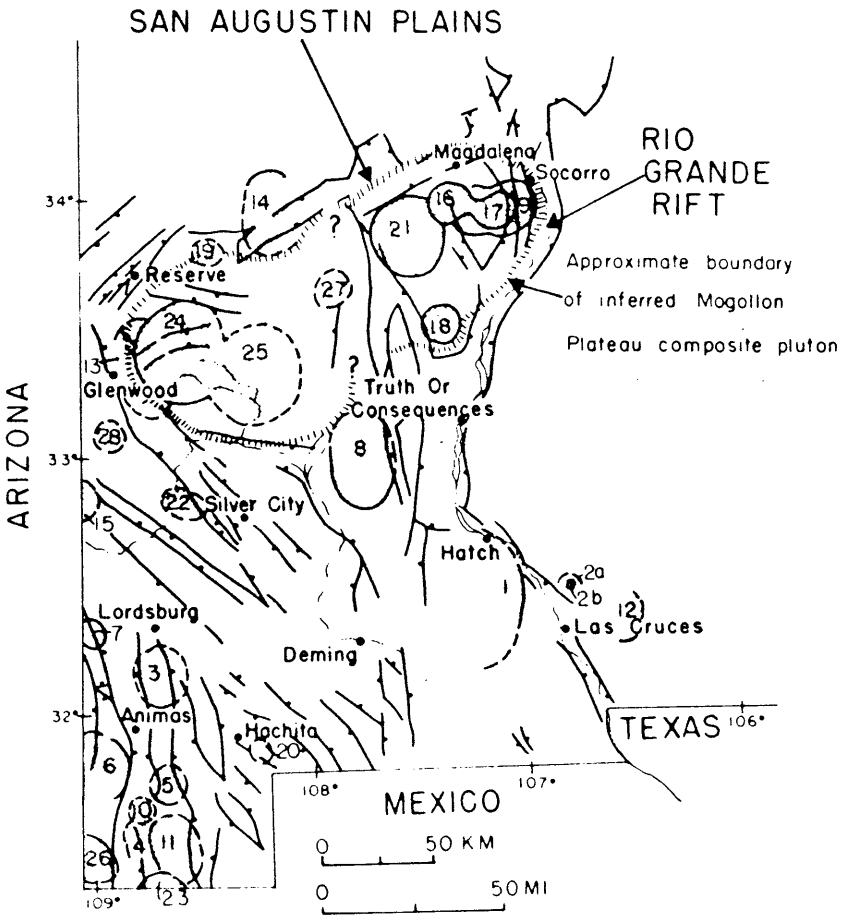

Figure 3.4 Proposed mid-Tertiary age ash flow tuff (ignimbrite) cauldrons of southwest New Mexico (from Elston, 1984b).

Elston (1984a) proposed five principal stages for cauldron development of resurgent cauldrons in southwest New Mexico (Fig. 3.5). The stages are;

(1) Precursor (ring fracture)
(2) Caldera collapse
(3) Post collapse volcanism
(4) Major ring fracture volcanism
(5) Hydrothermal alteration

The best documented cauldron complex is the Mogollon Mountains and consists of four known cauldrons and eight major ash flow units, each greater than 100 km^2. The complex is believed to be the surface expression of a composite batholith, analogous to and contemporaneous with the San Juan volcanic field of Colorado (Ratte et al. 1984a).

The southwestern part of the Mogollon-Datil volcanic field is less well known. Wahl (1980) described it as a volcano-tectonic depression filled with 4 kilometres of volcanics of middle Tertiary age, and named it the Blue Creek basin. This basin is believed to be underlain by an apophysis of the inferred Mogollon batholith. It has been postulated that three cauldrons exist in the area; the Schoolhouse Mountain Cauldron (Wahl 1980), the Mule Creek Cauldron (Rhodes and Smith 1972a) and an unnamed cauldron in the Summit Mountains (Powers 1976). Evidence for the existence of the latter is poor (Chap.4) and later work in the Mule Mountains failed to corroborate the existence of the Mule Creek Cauldron (Ratte et al. 1984b).

Basaltic volcanism began locally around 30 m.y. and between 30 and 20 m.y. huge volumes were erupted

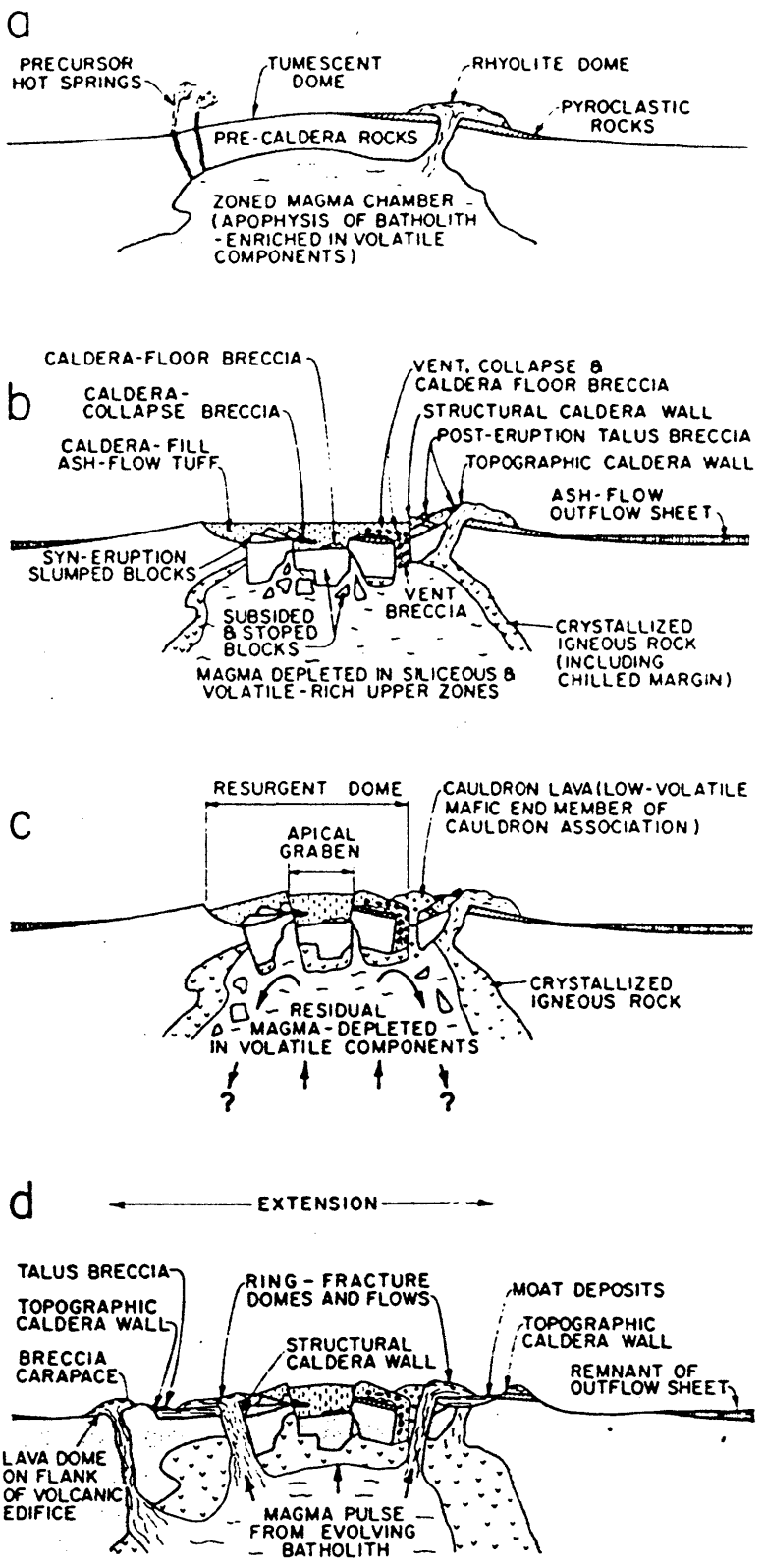

Figure 3.5 Evolution of a typical main stage resurgent cauldron, southwest New Mexico (from Elston, 1984a).

peripheral to the Mogollon plateau. Volcanism was basaltic andesite from stratovolcanoes e.g. the Bearwallow Mountain formation and the Amygdaloidal Andesite unit in the Blue Creek basin. Activity declined after 21 m.y with the onset of basin and range tectonism.

The third phase of bimodal basalt and rhyolite phase appeared in areas peripheral to the Mogollon Mountains between 21-18 m.y and continues to the present. This appeared with the inception of basin and range extension and appears to be controlled by basin and range faults (Ratte 1984a). Tholeiitic and alkali basalt have predominated since 15 m.y .

3.5 Structure

Three main stages of deformation are recognisable in southwest New Mexico (Fig. 3.6); a Laramide event (Late Cretaceous to early Tertiary), a Middle Tertiary event and Basin and Range tectonism. The Laramide and earlier periods of deformation are largely masked or over printed by the middle and late Tertiary events; however rejuvenation causes difficulty in distinguishing the phases.

Pre Laramide structures appear to have involved epirogenic movements consisting of broad uplifts and depressions (Ratte et al. 1979). Two blocks which occur in the region are the Burro Uplift, a core of Precambrian rocks overlain by Cretaceous sediments (Elston 1958) and the Florida Uplift , of Palaeozoic origin (Kottlowski 1965). The

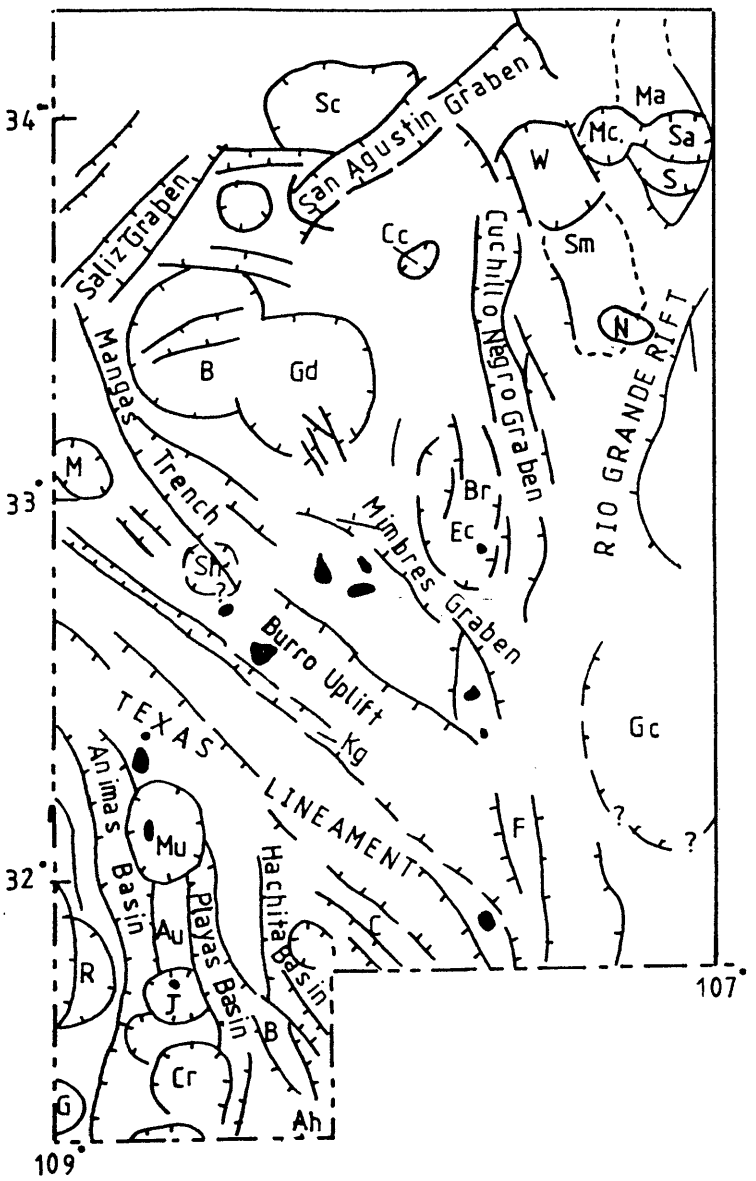

Index to structures

Ah	Alamo-Hueco uplift	Gd	Gila Cliff Dwellings caldera
Au	Animas uplift	Kg	Knight Peak graben
B	Bursum caldera	M	Mule Creek caldera
Bh	Big Hatchet uplift	Ma	Magdelena uplift
Br	Black Range uplift	Mc	Magdelena caldera
C	Cedar uplift	N	Nogal Canyon caldera
Cc	Corduroy Canyon uplift	S	Socorro caldera
Cr	Cowboy Rim caldera	Sa	Sawmill canyon caldera
Ec	Emory caldera	Sc	San Agusta caldera
F	Florida uplift	Sh	Schoolhouse Mountain caldera (?)
Gc	Goodsight Cedar Hills volcano-tectonic depression	Sm	San Mateo uplift
		W	Mt. Withington caldera

Figure 3.6 Tectonic map of southwest New Mexico (adapted from Kelly 1982).

uplifts form a part of the controversial "Texas lineament", a west northwest trending zone of faults and geologic and topographic discontinuities. The nature of the zone is disputed, but there is an apparant deflection of Basin and Range structures (Turner 1962) and the zone forms a barrier between Palaeozoic and Mesozoic platform sediments in the north from geosynclinal sediments of the Sonoran and Mexican troughs to the south (Elston 1958). Wertz (1970) discussed the tectonic control of the lineament on the localisation of the porphyry copper deposits.

In the American Southwest Laramide deformation is characterized by wide belts of interspersed centres of intra-arc volcanic and plutonic activity, north to northwest striking elongate basement cored uplifts flanking intermontane basins and marginal upthrusts along ranges (Titley 1986). In southwest New Mexico rocks of this age are the Palaeozoic and Mesozoic sediments of Silver City and the PreCambrian Burro Mountains, (Chap. 3.3) intruded by numerous stocks, sills, plugs and dykes. These include the porphyry copper stocks (Chap. 2.6b). In the Silver City area Laramide movement on northwest and northeast faults are documented (Jones, Hernon and Moore, 1967, p12).

Middle Tertiary age constructional volcanism and volcano-tectonic processes involved pluton emplacement and cauldron subsidence (Chap. 3.4). The Bursum caldera first formed a subsidence feature 40 km in diameter and remains the dominant structural and topographic feature of the region. The less well defined Gila Cliff dwellings caldera is expressed mainly by thick sections of Bloodgood

canyon tuff exposed in the middle and west forks of the Gila river (Ratte et al. 1979).

Basin and range tectonism is characterised by a large number of horsts and grabens and north and northwest trends. Prominent horst and grabens occur along the Mogollon front and extend into the Mimbres fault zone. Other graben include the Mangas trench, Mimbres graben and the Cuchillo-Negro graben.

The Mogollon pluton appears to have acted as a relatively rigid block around which Basin and range structures have been wrapped. The San Agustin Plains, Reserve graben and Saliz mountains, Mangas trench, Mimbres graben and the Gila - Sapillo - Mimbres valleys border the north, northwest, west and south sides. The eastern flank is complicated by the Rio Grande rift.

Basin and range extension reactivated and enhanced both Laramide and Tertiary structures.

3.6 Mineral Resources

Southwest New Mexico is a region of considerable mineral wealth and mining has been central to the regions physical and cultural development. Before 1800 Indians mined turquoise near Tyrone in the Big Burro Mountains and in 1801 the Spanish mined and shipped copper from Chihuahua and Mexico City from the Santa Rita mine (Gillerman 1964). Large scale development did not begin until the gold rushes of the 19th Century. Many of the eastern mining

towns, including Georgetown, Chloride Flat, Hillsboro and Chloride appeared in the 1830s and in the 1880s exploration moved westward to develop Mogollon, Winston and Steeple Rock. The fortunes of these towns were inextricably tied up with metal prices, particularly gold, and many have been ghost towns throughout much of the 20th century and remain so to this day. The current high precious metal prices of the 1980s have led to speculation about their revival.

Two main mineralising periods are recognized; one of Laramide age and the other of Oligocene - Miocene age, of which the former is vastly more important in terms of production and economic value.

b) Laramide mineralisation

Laramide mineralisation is centred on two main areas; the Central Mining area around Silver City and the Burro Mountains area to the south and west (Fig. 3.8). The porphyry copper mines at Santa Rita have produced an estimated $630 million worth of copper between 1930 and 1977 and the Tyrone open pit copper mine produced 855,137 tons of copper between 1967 and 1979 (Kolessar 1986), worth over one billion dollars at 1989 prices.

The Burro mountains area includes the Blackhawk, Round Ranch, Gold Hill, Malone, Telegraph, Tyrone and White Signal mining districts. Most of these districts were discovered in the 1880s and abandoned by the early 1900s. The White Signal district experienced a uranium boom in the 1920s and drilling in the late 1970s discovered a sulphide porphry copper system at depth. The Tyrone

porphyry copper deposit is the main producing mine of the district and is one of the largest copper producers in the USA. The deposit was discovered in 1879 where high grade oxidised ore occurred in a northeast trending fracture zone in the Tyrone quartz-monzonite stock. No mining occurred between 1920 and 1950 and in 1969 open pit mining began.

Other deposits in the region include numerous hydrothermal veins of copper, Ag-Pb,(Cu-Bi-U), gold base metal, Ni-Co-Ag(U) and manganese. Most are related to the Laramide age intrusions and are found in the intrusions and the Precambrian granitic country rock. The deposits are small in size, worked out in many cases and as a consequence are of little economic value.

The Central mining area includes many mining districts occurring on the southern margins of the Tertiary volcanic field, including the Central, Chloride Flat, Fierro-Hanover, Fierro-Manganese, Fleming, Georgetown, Lone Mountain, Pinos Altos, Santa Rita and Silver City districts. The two major porphyry copper deposits at Santa Rita and Hanover Mountain are related to the Santa Rita quartz-monzonite porphyry stock and the Fierro-Hanover granodiorite stock. Massive sulphide and oxide replacement deposits of Fe, Zn, Cu-Fe, and Zn-Pb occur in Palaeozoic carbonate rocks, crudely zoned around the Laramide stocks to which they are spatially and genetically related.

Other deposits include Ag(Pb-Mn) vein and replacement deposits (Georgetown, Lone Mountain and Chloride Flat), Zn-Pb(Cu-Ag-Au) vein and replacement deposits (Bayard Zone) and post porphyry Au-Ag base metal vein deposits at

Pinos Altos, most of which were exhausted by the beginning of the 20th century.

Detailed references to all these mining areas can be found in Richter and Lawerence (1983).

c) Tertiary Mineralisation

The main mining districts range in age from Oligocene to Quaternary and are scattered throughout the region (Fig. 3.7). Mineralisation is dominantly epithermal precious and or base metal vein deposits, although tin occurs at Mount Taylor and there are base metal replacement deposits in the Black Range near Silver City.

There were at least two periods of mineralisation. Oligocene mineralisation is associated with calk-alkaline stratovolcanoes, e.g. Alum Mountain, Copperas Creek and Brock Canyon; and post Miocene mineralisation e.g. Mogollon. Mineralisation at Mogollon is dated at 18 m.y. and is possibly related to the post caldera bimodal rhyolite volcanism (Ratte et al. 1984a).

The value of production while small relative to the Laramide porphyry copper deposits, is significant. The Mogollon district, one of the richest deposits, produced over 362,000 ounces of gold and 17 million oz. of silver between 1879 and 1959 (North and M^{c}Lemore 1986), worth greater than $130 million and $86 million respectively (September 1989 prices).

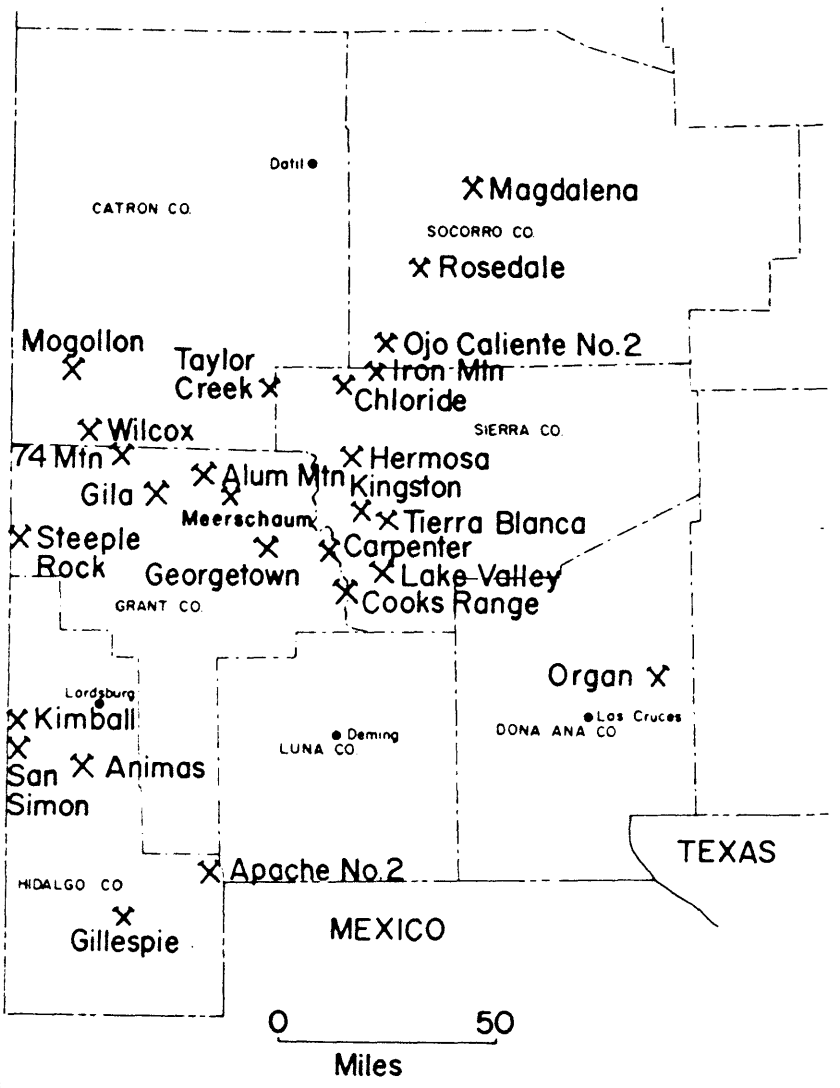

Figure 3.7 Tertiary age mining districts of southwest New Mexico (from Elston, 1976b.)

Host rocks are mainly andesites and flow tuffs, commonly occurring in the vicinity of, or associated with cauldrons (Elston et al. 1976b). Similar associations between cauldrons and mineralisation have been noted throughout the American Southwest, e.g. in Nevada (Albers and Kleinhampl 1970), Arizona (Lipman and Sawyer 1985) and Colorado (Steven 1984). McKee (1979) has shown that in Nevada there is no genetic relationship between cauldron formation and mineralisation and in New Mexico most of the deposits where dated, are 10 to 20 million years younger than the host cauldron formations (Moore and McLemore 1986). The close spatial arrangement between the caldrons and the mineral deposits is probably due to the favourable structural zones provided by the cauldrons, which tapped later hydrothermal fluids.

Modern studies (Heald et al. 1987, Hayba et al. 1986) classify volcanic hosted epithermal deposits into two types, adularia sericite and acid sulphate (Chap. 4.7a). The deposits in New Mexico are difficult to classify because of a lack of up to date geological information. However generally the post Miocene age deposits are mostly adularia sericite type and the older deposits are acid-sulphate.

d) Mineral Potential

The mineral resource potential of the region is considerable. The potential for porphyry copper or molybdenum mineralisation is high in the Tyrone and Burro Peak areas, and around the Pinos Altos Stock in the Central Mining district, and to the west of the area in the Safford area of Arizona. Other deposits with good

potential include, stockwork molybdenum, rhyolite hosted tin, uranium and the widespread deposits of manganese and fluorite.

The relatively high precious metal prices of the 1980s have made epithermal precious metal deposits a focus of exploration. There have been several studies on the mineral potential of the region, including studies in the Gila Wilderness (Ratte et al. 1979), Hells Hole (Ratte and Hedlund 1981, Ratte et al. 1982) and in the Silver City quadrangle (Drewes et al. 1985). From these studies several areas with high epithermal deposit mineral potential can be identified (Fig. 3.8):

i) The Mogollon front range; a northwest trending zone of faulting and intrusions, and particularly the intersection of this zone with the Bursum caldera.

ii) The older (Miocene) calk-alkaline stratovolcanoes, e.g, Alum Mountain, Copperas Creek, Brock Canyon and perhaps Steeple Rock in the Summit Mountains.

iii) Mineralisation related to intrusive centres of middle to late Tertiary age, e.g. Hells Hole.

On figure 3.8 there is a large area in which the mineral potential is largely unknown because of a lack of geologic information. This area covers much of the central and western part of the Blue Creek basin, stretching from Cliff in the east to the Summit Mountains in the west.

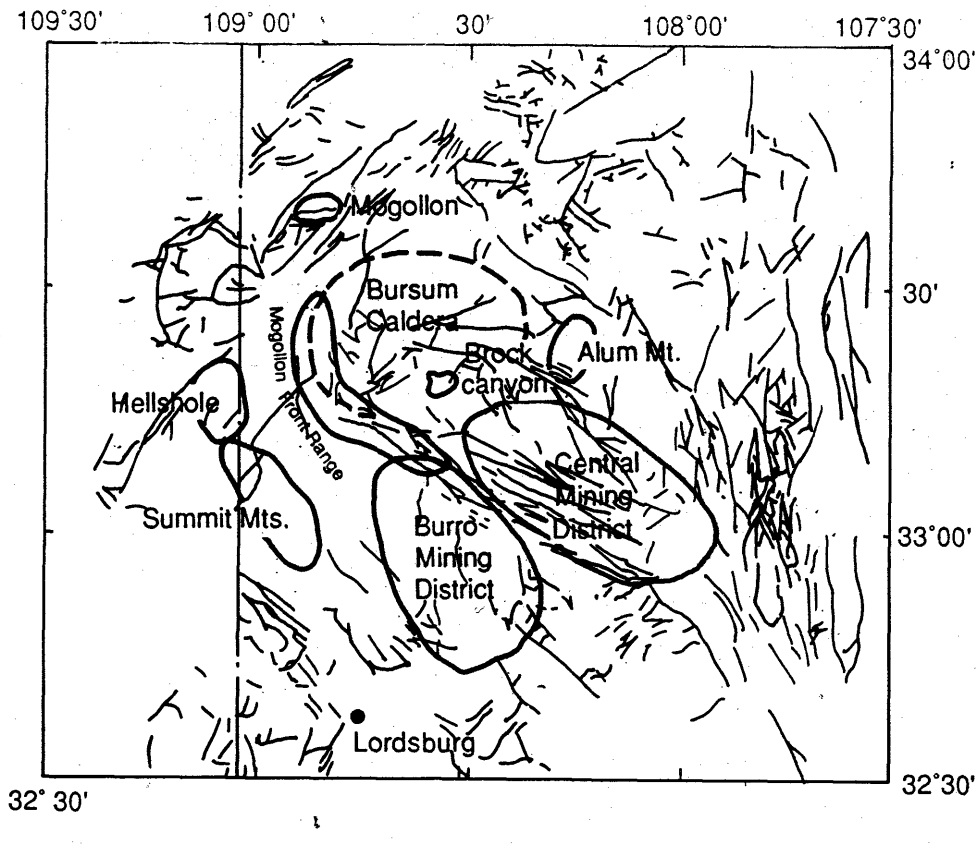

Figure 3.8 Areas of high mineral potential in southwest New Mexico. The areas are superimposed upon a regional structural map from Ratte et al. (1979)

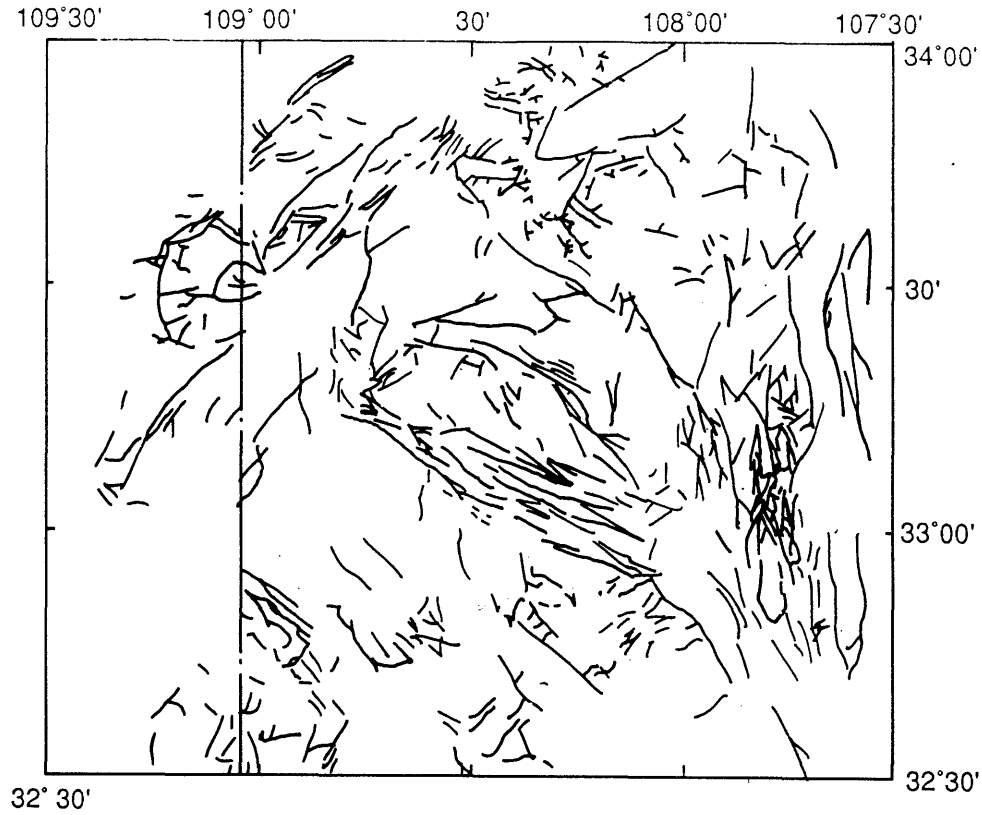

Figure 3.8 Areas of high mineral potential in southwest New Mexico. The areas are superimposed upon a regional structural map from Ratte et al. (1979)

3.7 Discussion

An assessment of alteration mapping with Landsat data in southwest New Mexico could use as a subject any one of or all of the alteration types present. But given the time limit of the research, it is both necessary and desirable to define closely the objectives and restrict the study to specific areas. This section sets out the possible alternatives and discusses the selection of the objectives chosen.

The Laramide porphyry copper deposits of southwest New Mexico (and elsewhere), generally have large and well developed alteration haloes of a size and type well suited to study by Landsat satellite data. While the New Mexican deposits themselves have not been studied using such techniques, others occurring in broadly equivalent semi-arid terrain have been the subject of several remote sensing studies, e.g. Schmidt and Bernstein (1977), Abrams et al. (1983) and Kepley et al. (1982). The terrain around the New Mexico deposits is largely affected by mining activities and is easily visible on Landsat MSS data and on aerial photographs.

The numerous vein and replacement deposits in the Central and Burro mountains have alteration zones which are limited in type and too small for identification by Landsat satellite data. Further they are of marginal economic value as their distribution is geographically limited and most are either well developed or exhausted.

I decided not to include the porphyry copper deposits or the vein and replacement deposits in this research. The Tertiary age epithermal deposits, by contrast, have the

following characteristics which make them a suitable target and topic for the regional research study.

1. Widespread occurrence in southwest New Mexico

2. High economic value

3. Genetically associated with hydrothermally altered rocks in well defined zones of a size potentially detectable by Landsat TM, a capability which was generally not possible with Landsat MSS data.

4. The regional geological environment is suitable for the existence of further deposits (Chap. 3.6d), and the current state of geological knowledge is such, that information from TM can make a significant contribution to known geology.

5. Because the Summit Mountain study area is a Tertiary age epithermal deposit its characteristics may not be similar to epithermal deposits of Laramide age.

6. There have been no previous remote sensing studies using TM data in southwest New Mexico, except for the application of ATM data (Kruse 1984a) and MSS data (Kruse 1984b) in the Lordsburg mining district, some 40 kilometres to the south.

The geology was not the only determining factor in the selection of the regional study objectives. The physical nature of the terrain affects remote sensing studies, particularly the type and distribution of vegetation (Chap. 6.4). The thick and extensive coniferous forests

which cover much of the Mogollon-Datil volcanic field (Fig. 3.2) are likely to affect direct spectral remote sensing of hydrothermally altered rocks. Spectral remote sensing is likely to be restricted to areas peripheral to the plateau where vegetation types are Woodland, Grassland and desert.

The largest non-coniferous forested area occurs in western Grant County, the geological sub-region known as the Blue Creek Basin, approximately coincident with the area were the geological data is lacking.

CHAPTER 4.

THE SUMMIT MOUNTAINS TEST AREA

4.1 Introduction to the test area studies

This chapter describes the geography, geology, hydrothermal alteration and mineralisation in the Summit Mountains. Those aspects of the geology and geography which characterise the terrain surface were studied for evaluation of the processed TM imagery (Chapter 5). For the first time the hydrothermal alteration in the Summit Mountains is described in detail and is compared with current epithermal deposit types.

4.2 Geography

The Summit Mountains test area is situated on the Arizona-New Mexico state line, some 60 kilometres west of Silver City. It occupies western Grant County, New Mexico, and a small part of Greenlee County, Arizona (Fig. 4.1). Access to the area is by dirt road from Duncan, Arizona, 25 kilometres distance to the southwest.

Figure 4.1 shows the main geographical features and the location index. Topography varies from the moderately rugged volcanic mountains in the north and west to the low alluvium filled valleys and hills to the south. Altitude ranges from 1500 metres to 2160 metres above sea

The grid on figure 4.1 is the standard map reference system used in the USA. Each state is divided into 36 square mile divisions each identified by a Township (T) and Region (R) prefix. Each square mile (section) in the division is numbered consecutively from 1 to 36 from top to bottom and side to side following on from the previously numbered square. For example Kemp Peak is positioned in the south west corner of section 35, Township 16 South, Region 20 West, New Mexico, written as SW Sec. 35, T.16S R20.W NM.

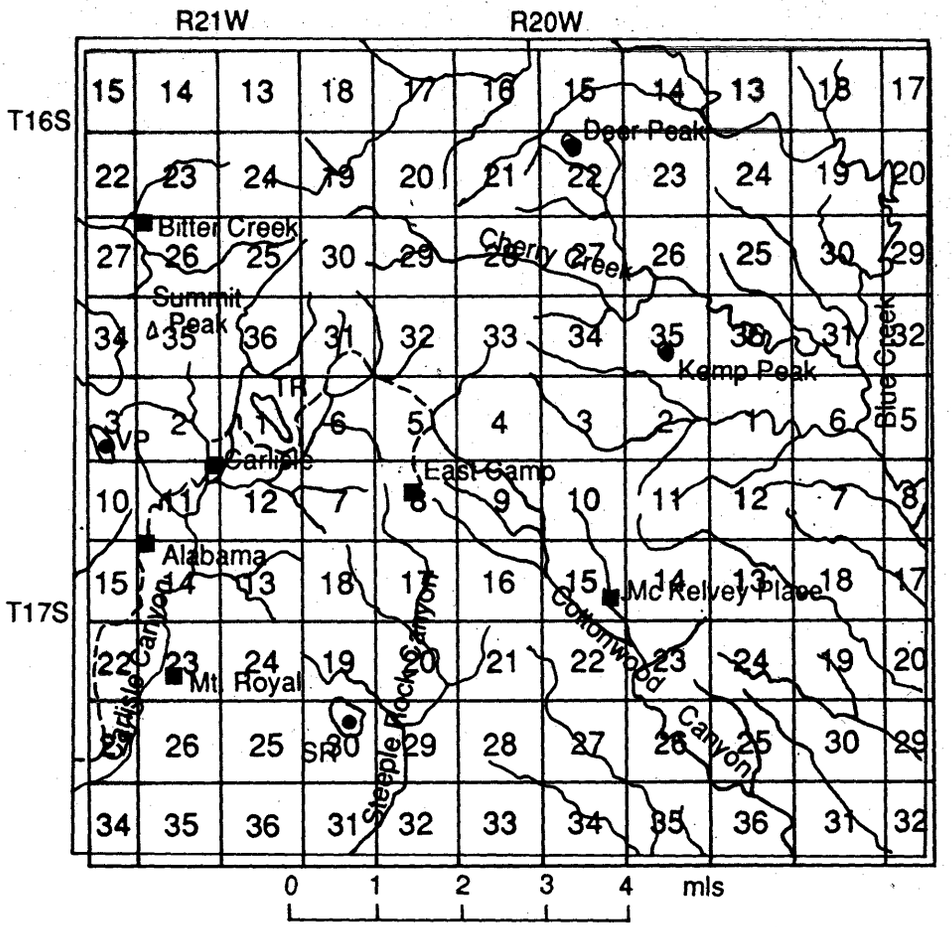

Figure 4.1 Main geographical features and location index of Summit Mountains test area.

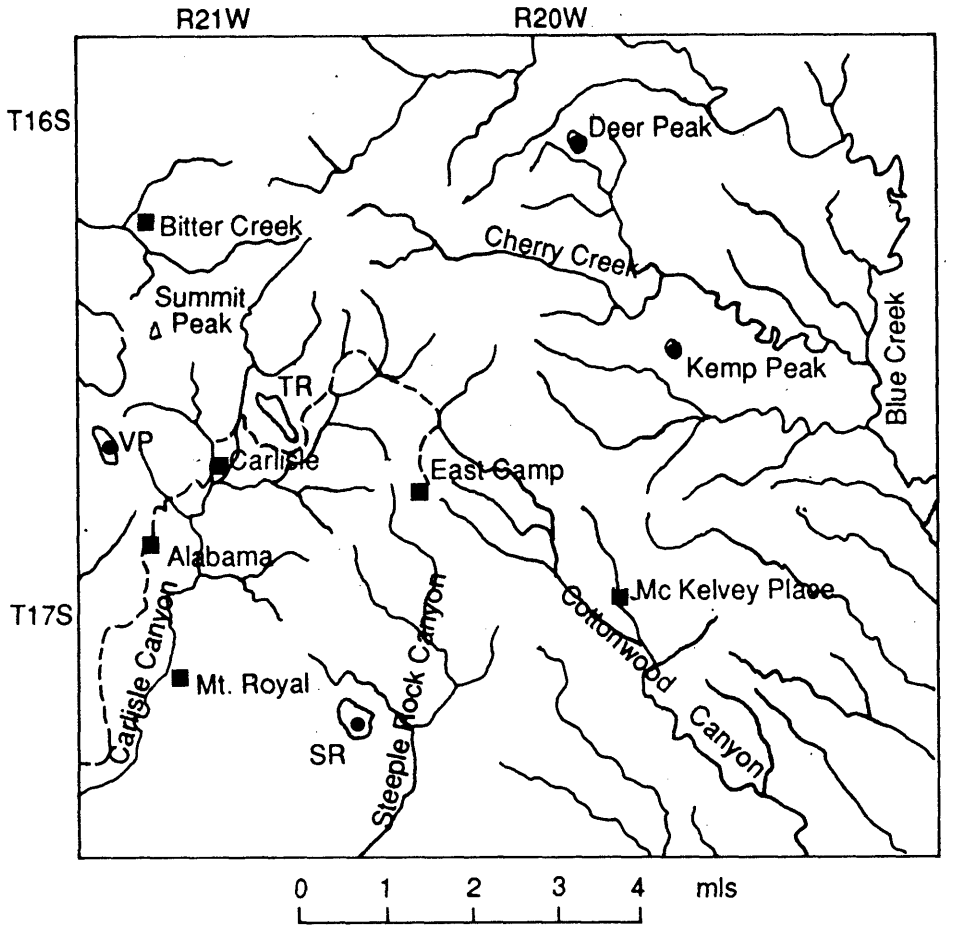

Figure 4.1 Main geographical features and location index of Summit Mountains test area.

level. The numerous perennial streams are steep and rocky in their upper parts with wide meandering sandy or rocky lower channels. During the rainy season flash floods are common. The main southward flowing channels are Carlisle Canyon and Steeple Rock Canyon. Bitter Creek drains eastward into Arizona. The north eastern and eastern areas drain into Blue Creek. All drainage is to the Gila River.

The climate is semi-arid; annual precipitation averages 325 mm, most of which falls as summer thunderstorms. Vegetation is the Woodland Association (Fig. 2.1) and canopy cover ranges from zero to 100 % (Fig. 6.11). Approximately 70 % of the area has less than 10 % vegetation cover. Vegetation cover is dependent on aspect, altitude and rock type. It is greater on north and east facing slopes because it is sheltered from the hot afternoon sun, and on ground above 1700 metres because of greater rainfall and lower temperatures. On acid and hydrothermally altered substrates vegetation is absent or reduced, except on north or east facing slopes where vegetation canopy cover can be up to 90 %. The surface is covered by thin rocky soils, with talus and landslide debris on steeper mountain slopes. Less than 5 % of the area is estimated to be exposed bedrock.

An early pioneer's comment on the flora and fauna of the region is particularly apt " If you touch it, it stings you,if you pet it, it bites you, and if you eat it, it kills you" (Corle 1951). The fauna includes rattlesnakes, scorpions and coyotes and Dee et al. (1970) report that infection from bubonic plague remains a hazard.

4.3 Geology

a) Introduction

The Summit Mountain rocks are almost all Tertiary age volcanics forming part of the Blue Creek Basin which in turn is a part of the Mogollon-Datil volcanic field.

The first documented geological reports concerned individual mine and mineral descriptions, e.g. Graton (1910), Johnson (1943), Russel (1943), Trace (1947) and Wilson (1950). The first published geological map appeared in 1960 (Elston 1960) as part of the reconnaissance map of the Virden quadrangle. Gillerman (1964) briefly described the geology and gave a thorough account of the areas mineral deposits.

Griggs and Wagner (1966) produced the first detailed geological description, based on field investigations done in 1942 and 1943. Biggerstaff (1974) and Powers (1976) produced the first modern works on the geology and mineral deposits in their Masters theses. Biggerstaff's work was based largely on that of Griggs and Wagners, while Powers described several new units and attempted to explain the origin of the hydrothermal alteration (Chap. 4.5). Wahl (1980) described the area in the regional context of the Blue Creek Basin and produced a detailed reconnaissance map.

The most recent geologic work by Hedlund (1979-80) of the USGS is unavailable, but is accessible in a less detailed form as it is incorporated in a regional 1:250,00 scale map of the Silver City quadrangle (Drewes et al, 1985).

This latest map only became available at the end of my research period.

The compilation of the geological data from these diverse sources was a considerable task. The maps and reports covered different areas, using different scales and nomenclature. Table 4.1 compares the volcanic stratigraphy used in this thesis to that of previous workers.

It was never intended to produce a geological map of the Summit Mountains. However because of the uncertainty and inconsistencies of the available information and because of the need for a reliable geologic database a composite map was produced (back folder). This map combined my own field observations, and air photo interpretations made from 1:30,000 scale photographs, with the sources found to be most reliable, mainly from Wahl (1980) and Griggs and Wagner (1966).

A simplified geological map is shown on figure 4.2, and the simplified geological stratigraphy is shown on table 4.2.

b) The Older Volcanic Series

The oldest rocks outcrop south and east of Steeple Rock Peak. The flows thicken and outcrop more extensively to the east. Drewes et al (1985) named the unit rocks of the "Cliff Eruptive Centre", reflecting his opinion that the rocks are from an (as yet) unidentified cauldron source in the Cliff area (Chapter 3.4). Wahl (1980) speculated on a source in the Schoolhouse Canyon area and termed the unit

TABLE 4.1 CORRELATION OF STRATIGRAPHY USED IN THIS THESIS TO PREVIOUS WORK

STRATIGRAPHY USED IN THIS THESIS	WAHL (1980)	POWERS (1976)	BIGGERSTAFF (1964)	ELSTON (1960)	GRIGGS & WAGNER (1943)
Gila Conglomerate	Gila Conglomerate				
Sycamore Camp Eruptives	Upper Rhyolite			Upper Rhyolite	
Bearwallow Mountain Fm.	Bearwallow Mountain Fm.			Bearwallow Mountain Fm.	
Hells Hole Group	Twin Peaks Rhyolite		Upper Rhyolite	Intrusive Rhyolite	
Cherry Creek Rhyolite (Dacites and Rhyolites)	Black Jack Canyon Rhyolite	Flow banded Rhyolite Complexes			
Amygdaloidal Andesite	Amygdaloidal Andesite	Amygdaloidal Andesite	Brown Andesite Porphry Andesite - Basalt unit	Andesite	Brown Andesite Porphry Amygdaloidal Andesite - Basalt
Bloodgood Canyon Tuff	Noeh Mesa Tuff	Rhyolite Ashflow Tuff	Rhyolite Welded Tuff	Rhyolite	
Virden Dacite	Virden Dacite	Purple Ashflow Tuff Andesite Porphry Unit	Purple Andesite Porphry	Dacite	Purple Andesite Porphry
Steeple Rock Rhyolite	Steeple Rock Rhyolite				
Older Volcanic Series	Upper Andesites Mud Springs Tuff Lower Andesites				

The Older Volcanic Series is known as the Schoolhouse Mountain Formation (Wahl, 1980) and the Cliff Eruptive Centre (Drewes, 1985)

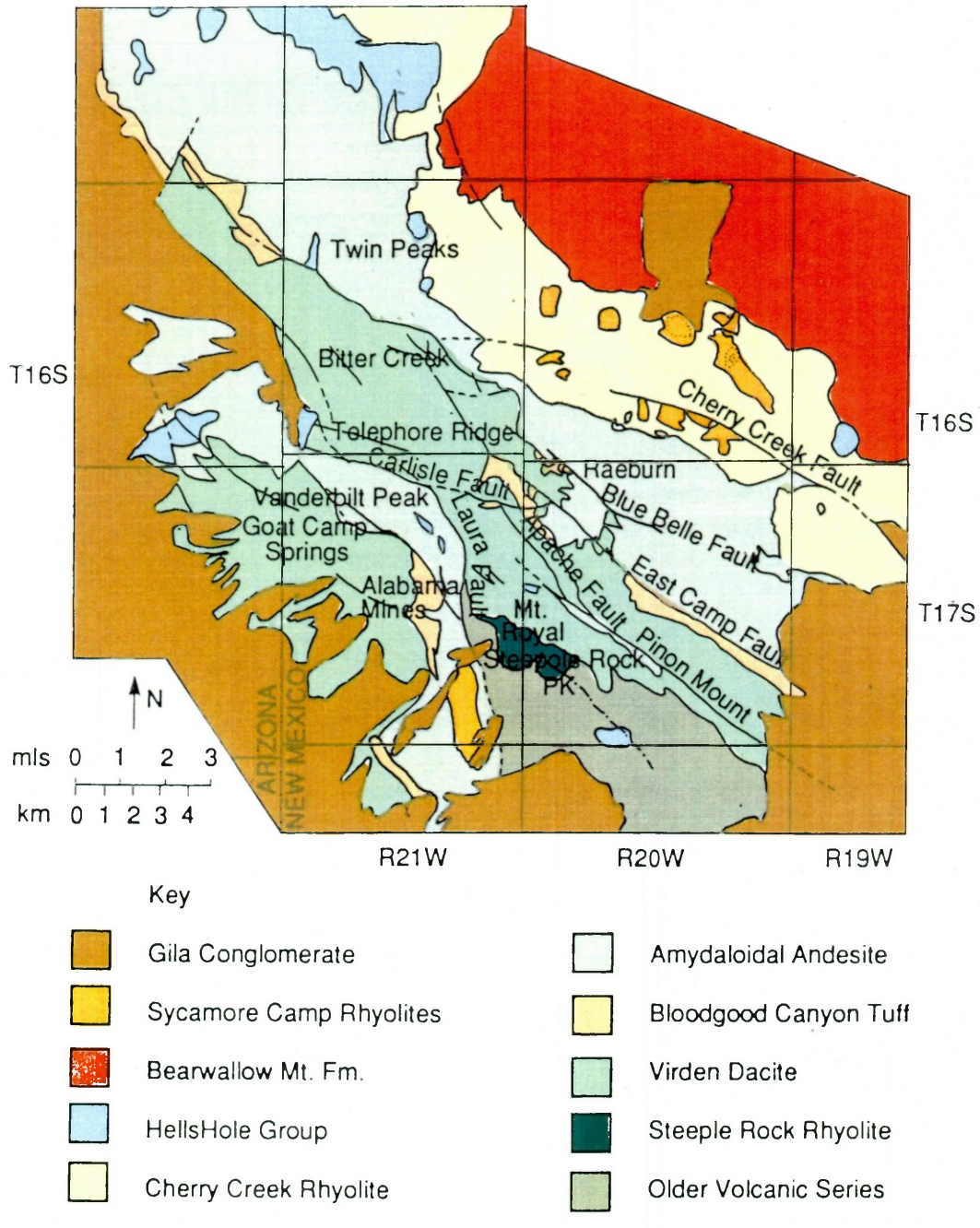

Figure 4.2 Simplified geological map of the Summit Mountains (a detailed map can be found in the back pocket).

TABLE 4.2 SIMPLIFIED DESCRIPTION OF THE STRATIGRAPHY

GILA CONGLOMERATE	Alluvial & lacustrine deposits (Coarse grained alluvium and fanglomerate)	Pliestocene to Upper Miocene
SYCAMORE CAMP ERUPTIVE CENTRE	Rhyolite flows, domes and pyroclastic deposits with intercalated tuffaceous sandstone beds	Miocene 20 - 18 m.y.
BEARWALLOW MOUNTAIN FORMATION	Andesite and basaltic andesite flows	Miocene
HELLS HOLE CENTRE	Rhyolite intrusive - extrusive flow complex consisting of large dome flow complexes, dikes, plugs and diatremes of fresh fine grained equi-granular to porphritic rhyolite and rhyodacite	Upper Oligocene
CHERRY CREEK RHYOLITE	Thick silicic flows of dacite and rhyolite possibly related to the Hells Hole Centre	Upper Oligocene - Miocene 27 m.y. ?
AMYGDALOIDAL ANDESITE	Rhyodacite to basaltic andesite lava flows and flow breccias with discontinous felsic tuff and volcanoclastic lenses	Upper Oligocene
BLOODGOOD CANYON TUFF	Poorly to densely welded rhyolite ashflow tuff derived from the Bursum Caldera	29 - 28 m.y.
VIRDEN DACITE	Porphritic flows of dacite and latite with intercalated lenses of felsic tuffs and tuffaceous sandstone	Middle Oligocene
STEEPLE ROCK RHYOLITE	Massive flow banded rhyolite	
OLDER VOLCANIC SERIES	Moderately welded rhyolite to latite ash flow tuffs interbedded with porphritic andesite flows	Late Eocene - Oligocene

the Schoolhouse Mountain Formation.

The unit is reported to be at least 860 m thick in Carlisle Canyon (Wahl 1980), consisting of a well bedded ash flow tuff, air fall deposits and volcanoclastics of rhyolite to quartz in composition, sandwiched between porphritic andesite flows. They form low lying terrain cut by numerous dry washes. There is a thin sandy to rocky soil, supporting shrub steppe. The larger silicic tuff members form bulbous upstanding features devoid of vegetation.

c) The Steeple Rock Rhyolite

The Steeple Rock Rhyolite is a massive flow banded rhyolite which outcrops on Steeple Rock Peak and Mount Royal, directly overlying the Older Volcanic Series. All workers prior to Wahl placed the rhyolite into the Older Volcanic Series. The bulbous nature of the flow and localised extent suggest that it erupted from a single vent as a highly viscous flow. The district takes its name from the prominent Peak. (Fig. 4.3).

d) The Virden Dacite

First termed a dacite by Elston (1960) and has since been called the purple andesite porphry (Griggs and Wagner 1966, Biggerstaff 1974), the andesite porphry (Powers 1976) and the Virden Dacite (Wahl 1980). In broad composition the unit is a trachyandesite (latite in US terminology), however in this thesis I have adopted Wahl's terminology of Virden Dacite.

Figure 4.3 Looking north to the peaks of the Steeple Rock rhyolite with the Older Volcanic Series in the foreground.

Figure 4.4 Middle (foreground) and Upper (Juniper Peak) flows of the Amygdaloidal Andesite unit with characteristic rocky soils and scrub vegetation.

It is made up of a series of andesite to trachyandesite flows, tuffs and volcanoclastics, interbedded with felsic tuff horizons and has a thickness of over 1300 metres. The rocks originate from local stratovolcanoes of which several have been recognized in the district (Wahl). In places there is considerable alteration to a propylitic facies, some of which is related to hydrothermal activity around local vents. The uppermost rocks are highly tuffaceous and silicic. Lenses of volcanoclastics including mudstones and bedded sandstones at the top of the unit are evidence of a period of quiescence before the deposition of the Bloodgood Canyon tuff.

Rocks of this unit are the main host to the mineralisation and alteration; over wide areas the rocks are stained by iron oxides, bleached and coloured (Chap. 4.6). Vegetation is often sparse on these altered substrates.

e) The Bloodgood Canyon Tuff

This is believed to be a regional outflow tuff sheet from the Bursum Caldera (Ratte et al, 1984) and represents the first influx of high silica rhyolite into the Summit Mountains. It is a 30 to 50 metres thick welded rhyolite tuff which lies with a prominent unconformity on the upper felsic and volcanoclastic rocks of the Virden Dacite. It is a useful lithostratigraphic and time stratigraphic unit, dated at 26.5 m.y (Drewes et al, 1985).

It is hydrothermally altered near the main mineralised areas to silicic and advanced argillic assemblages. Where silicification is intense it is difficult to separate it from the underlying Virden Dacite tuffs. It forms flat,

well bedded resistant outcrops low in vegetation cover, and is clearly visible on aerial photographs (Figs. 4.9 and 4.10).

f) The Amygdaloidal Andesite

The thick flows of basaltic andesite and thin tuff beds of this unit lie slightly unconformably on the Bloodgood Canyon tuff, and where the tuff is absent, with a prominent unconformity on the Virden Dacite.

The unit is at least 1300 metres thick and can be divided into four major sub-units. The lower rocks are amygdaloidal to aphanitic flows and flow breccias between 1 and 10 metres thick, much altered to a propylitic assemblage, particularly at Goat Camp Springs, north of the Blue Bell fault and between the Steeple Rock and Alabama faults. Where alteration is severe the rock appears as a greenish brown coloured poorly consolidated mass with distinctive pea like inclusions.

The middle flows are 800 metres thick and are unaltered and have been mapped as separate unit called the Dark Thunder Andesites (Ratte and Hedlund 1981). They are vesicular to massive, aphanitic to porphritic andesites with a few volcanoclastic lenses. In Apache Creek, to the northwest of the area is a more felsic phase of trachyandesite flows 200 metres thick. The uppermost flows occur on Vanderbilt Peak, Juniper Peak (Fig. 4.4) and on the hills around Little Sycamore Creek south of Cherry Creek.

The unit forms low step like hills, with a brown to red

thin rocky soil. In some areas the staining is very strong and is visible on aerial photographs e.g. east of East Camp. Vegetation is widely scattered scrub with scattered trees, with denser tree cover on northern and eastern slopes.

g) The Cherry Creek Rhyolite

A thick sequence of flow banded rhyolites intrude and unconformable overlie the Amygdaloidal Andesite flows in the north of the area. This unit is equivalent to the Blackjack Canyon Rhyolite (Wahl 1980) and Flow Banded Rhyolite (Powers 1976) of earlier workers. The rocks may be related to the Hells Hole volcanics.

A sub-unit, called here the Anderson Ranch unit, occurs on the north eastern boundary of the Summit Mountains area. It consists of felsic flows and tuffs which appear to have erupted contemporaneously with the middle flows of the Amygdaloidal Andesite unit. On aerial photographs the Anderson Ranch unit appears reddened and is intruded by a small rhyolitic body and a major dyke, probably related to the Hells Hole phase (See Map in back pocket).

h) The Hells Hole group

The flows of the Amygdaloidal Andesite unit were followed by a 10 m.y. period of acidic intrusive and extrusive volcanism centred to the north of the Summit Mountains at Hells Hole. The Hells Hole volcanic complex consists of andesite to high silica rhyolite flows, and subvolcanic intrusives which overlie or intrude the older calcalkaline

rocks of the Summit Mountains. The presence of a rhyolitic stock or small batholith at depth is suggested from the arcuate outcrop pattern of the rhyolite and a coincident aeromagnetic low (Ratte and Hedlund 1981).

The numerous rhyolite dykes, and intrusives which intrude the Summit Mountain rocks in a northwest belt extending from Pinion Mountain (north of Steeple Rock Peak) to Twin Peaks (Bitter Creek) and beyond, probably belong to this group.

The rocks of this group are easily identified on the ground and on air photographs. They form positive, intrusive features circular or linear in plan. They have high albedo, are often spatially associated with hydrothermal alteration and have sparse vegetation.

i) Bearwallow Mountain Formation

This unit is composed of dark vesicular, locally porphritic flows which are indistinguishable from the Amygdaloidal Andesites where the two units are not separated by the felsic Cherry Creek or Hells Hole units. It is likely the Bearwallow Mountain formation and the Amygdaloidal Andesite units are one phase of continuous basaltic andesite volcanism (Chap. 3.4).

The flows are about 400 metres thick and are exposed in the north of the Summit Mountains area, forming a relatively low plateau from which shield volcanoes such as Bear, Applegate and Brushy Mountain arise. The formation has surface features similar to those of Amygdaloidal Andesite except for the presence of scattered pine trees.

j) Sycamore Camp Eruptives

Rhyolite flows, domes and pyroclastics with interbedded tuffaceous sandstones ranging in age from 21.3 to 17. 2 m.y (Drewes et al, 1985) represent the final volcanic activity in the area. The eruptions took place from tuff rings and vents such as Deer Peak, aligned north westerly, possible reflecting early Basin and Range control. Material from these vents forms the Mule Mountains (north of the Summit Mountains) and infill Sycamore Creek. The Upper rhyolite of Wahl (1980) and Elston ((1960) and other rhyolitic rocks of the Blackjack Canyon Rhyolite belong to this unit. Surface features are similar to those of the of the Hells Hole Rhyolites.

k) Gila Conglomerate

Lying above and in some places interbedded with the Bearwallow Mountain formation and the Sycamore Camp Eruptives is the Gila Conglomerate, a massive to poorly bedded, poorly sorted, coarse grained alluvium and fanglomerate which reaches a thickness of 1000 metres.

4.4 Structure

A dominant northwest structural trend is present throughout the area (Fig. 4.5). Major normal faults divide the areas into horst and graben blocks tilted at an

angle of 25 to 30 degrees to the north east.

At the eastern end of the area faults of the Eastcamp system downthrow to the northeast, while in the central and western parts of the area faults of the Laura, Carlisle, and Mayflower systems are downthrow to the southwest, producing a northwest trending horst block across the district. The higher horst areas are Summit Peak and Telephone Ridge.

Where silicified, faults often have prominent ridges. The East Camp fault, divides into a 150 metre wide zone of anastomising quartz veins at Bitter Creek. The Carlisle fault is silicified from the Ontario mine to the head of Whiskey creek. A tensional origin of the faulting is indicated by normal fault movement and by the growth of vein quartz in open spaces (Griggs and Wagner 1966). Recurrent movement occurred throughout the Tertiary period.

Several workers have suggested a cauldron origin for the Summit Mountain area, probably because of the large number of cauldrons proven or thought to exist in the volcanic fields of southwest New Mexico and generally in the American Southwest (Chap. 3.4). Powers (1976) proposed a possible cauldron centred on Goat Camp Springs and Wahl (1980) noted that an eroded cauldron may be the source of the altered tuffs at Bitter Creek. However evidence for the existence of a cauldron in the area is weak. If one existed it is deeply eroded or buried, or both. The ashfalls and tuffs can be satisfactorily sourced outside the Summit Mountains, i.e. the Cliff eruptive Centre and the Bloodgood Canyon Caldera.

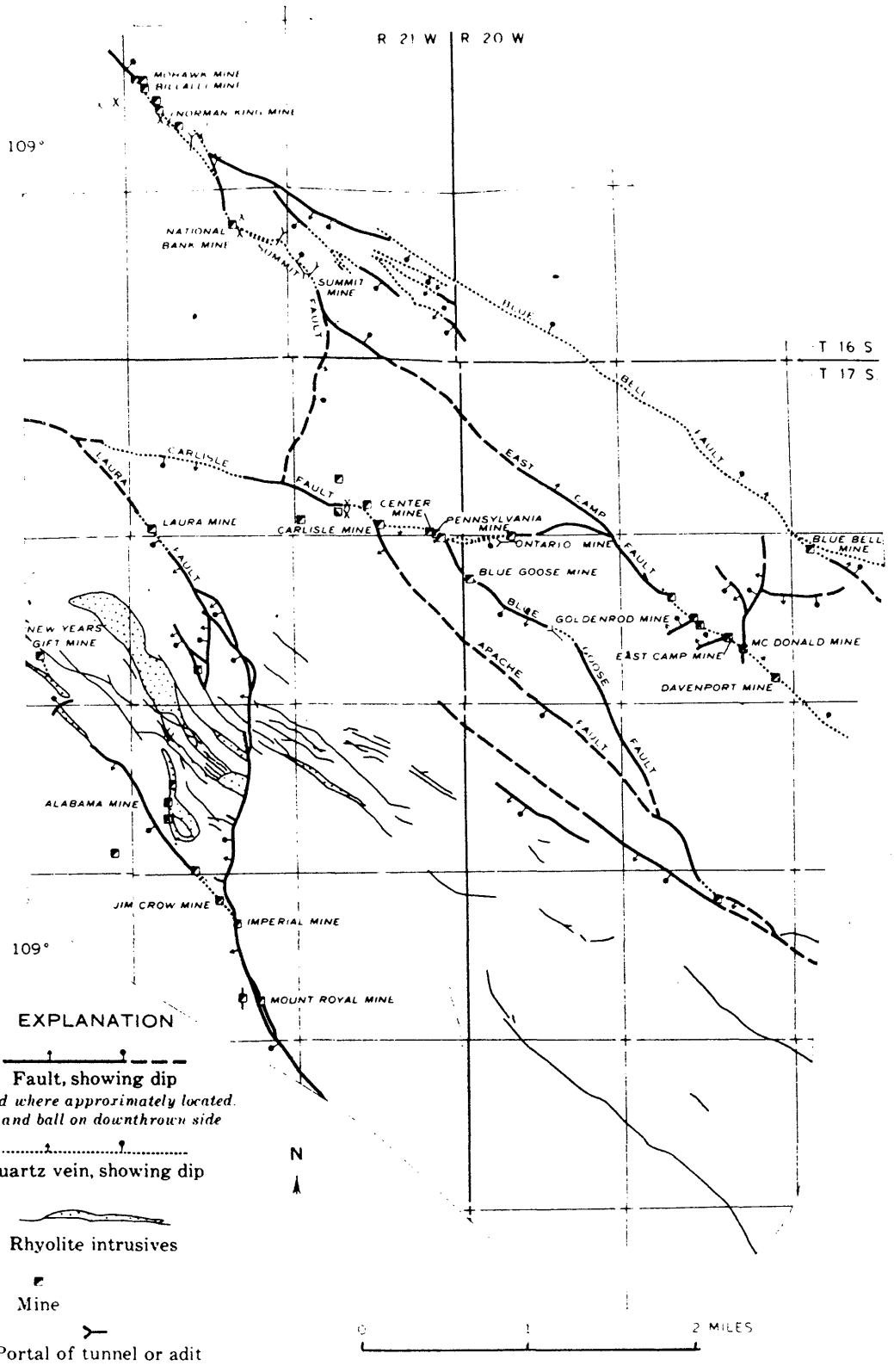

Figure 4.5 Faults, quartz veins and rhyolite dykes in the Steeple Rock Mining district of the Summit Mountains test area (from Griggs and Wagner, 1966).

Basement structures trending west north west and north east have been identified from geophysical data (Fraser Martin Mines in Wahl 1980). Wahl (1980) suggested these are due to plutonic control of Basin and Range structure, similar to that described by Elston and others (1976a) for the Mogollon pluton. The Mogollon pluton is believed to have acted as a relatively rigid block around which Basin and Range structure is wrapped. Many similarities between the Mogollon plateau and the Blue Creek Basin were listed by Wahl and he postulated that the Blue Creek basin is underlain by an apophysis of the Mogollon pluton.

A middle Tertiary age volcanic centre with an underlying subjacent shallow stock or small batholith of acid to intermediate composition has been identified from geological (Ratte and Hedlund 1982) and geophysical (Martin 1981) evidence in the Hells Hole area. The intrusive rhyolite dykes and plugs related to the Hells Hole complex postdate Basin and Range extension.

4.5 Economic Geology

a) Introduction

The Summit Mountains area contains the Steeple Rock mining district and the Duncan fluorspar district. There are also a number of smaller mines to the northwest of the area, around Hells Hole.

Mining records begin around 1880 for the Steeple Rock

district, although there is a military record noting the despatch of troops from Fort Thomas (on the approximate site of Duncan, Arizona) to protect the miners from Apache Indians in 1860 (Russel 1947). Since records began 36,675 ounces of gold and 1,533,041 ounces of silver have been mined in addition to copper lead and zinc. Actual production has been estimated to be 135,000 troy ounces of gold and 4.5 million ounces of silver (North and McLemore 1986), worth an estimated $70 million (September 1989).

Most production occurred between 1882 and 1946, and up to 1897 nearly all came from the Carlisle mine. Between 1897 and 1933 no production was recorded. Details of the early mining history can be found in Gillerman (1964, pages 180 - 184) and Griggs and Wagner (1966).

The rise in precious metal prices in the 1980s led to a resurgence of mining activity in the area. Several mines including the Summit, Eastcamp, Center and Laura have been refurbished and operated. In 1984, during my field visit there was no active mining. The Center and Mount Royal mines were operating on a care and maintenance basis and ore from recent production was being transported to the smelter at the nearby Santa Rita copper porphyry mine. Exploration for precious metals continues in the area. Telephone Ridge was drilled in the winter of 1984-85 by Pioneer Nuclear but work ceased soon after when the Company was taken over by Mesa Petroleum.

The Duncan fluorite district was mined between 1937 and 1945 and is now inactive (Powers 1976). What little is known about the district is summarised in Richter and Lawerence (1983).

b) Mineralisation

The fluorite veins of the Duncan district occur mainly as fracture fillings and small stockworks along northwest trending faults. Vein minerals are chiefly quartz mixed with fluorite, calcite coated with manganese oxides and locally pyrite (Richter and Lawerence 1983). No precious metal mineralisation is known.

At Steeple Rock ore minerals include native gold, galena, sphalerite, chalcopyrite, argentite and tetrahedrite in a gangue of quartz (locally amethystine), pyrite and calcite with minor barite and fluorite (Powers 1976). They occur mainly as epithermal fissure fillings along brecciated northwest and west northwest trending faults. Ore shoots are localised at fault intersections or at abrupt changes in fault strike or dip (Griggs and Wagner 1966) and many are marked on the surface by prominent silicified breccia zones known locally as "blow outs". (Fig. 4.7).

Mineralisation textures are open space fillings and replacements. Several mineralising periods accompanied by recurrent fault movement are known. The first was barren, followed by a base metal and then a precious metal phase. The mineralisation is in pre-mineral faults. Base metal mineralisation occurs along the Carlisle fault where it intersects the Apache fault. At the Carlisle, East Camp, Center, Pennsylvania and Ontario mines (Fig. 4.5) gold and silver occur in the upper parts of the ore shoots, grading with depth into base metals. Traces of base metals sulphides have been found in dumps of the Vanderbilt and Mount Royal mines (Powers 1976).

The East Camp group of mines in the eastern part of the Summit Mountains account for the greatest aggregate gold production in the district. Ores are native gold, argentite, native silver, ceragyrite and secondary coppers with chalcopyrite, galena and sphalerite at depth, in a gangue of quartz, calcite, limonite and minor fluorite (Gillerman 1964).

4.6 Hydrothermally Altered Rocks

a) Introduction

Early workers described the strong silicification, brecciation and alteration associated with the mineralisation (Graton 1910, Griggs and Wagner 1966). Elston (1960) was the first to map and describe the alteration which he described as "characterized by silicification and brecciation near veins, and widespread sericitisation, associated with small plugs and dykes of banded intrusives rhyolite believed to be of late Cretaceous age". Today the mineralisation is known to be middle Tertiary in age. The incorrect Laramide age led to several efforts to find porphyry copper deposits in the 1950s and 1960s.

Powers (1976) recognised an argillic assemblage characterised by alunite, diaspore and kaolinite; a propylitic assemblage characterised by montmorillonite, epidote, chlorite and calcite; and alteration restricted to within 10 metres of the veins consisting of quartz, sericite, adularia, chlorite, calcite and kaolinite. He

noted the alteration was not locally associated with the silicic intrusives and proposed the alteration and mineralisation to be "hot spring and epithermal type, originating from deuteric alteration processes from within the volcanic pile".

Wahl (1980) noted at least three phases of hypogene alteration with superimposed supergene processes. He considered the extensive argillic and propylitic alteration to have occurred before the mineralisation. Hall (1978) described the alteration at Bitter Creek as "metasomatic replacement alunite deposits", similar to those at Alum Mountain (Chap. 7) and Goldfield Nevada.

Previous work did not provide information of sufficient detail or reliability to provide the basis for the development of a conceptual alteration model to describe the Summit Mountain epithermal system. My studies included detailed field mapping, air photo interpretation, and petrological and geochemical analyses to determine the types of alteration and to better understand the relationship with the mineralisation.

The alteration was studied in five main localities; Bitter Creek, Telephone Ridge, Raeburn, Laura-Alabama and East Camp. The mineralised and altered areas at the western end of Bitter Creek and at Goat Camp Springs (Duncan Mining District) were not studied in detail as they lay outside the coverage of the TM imagery used in this research.

Figure 4.6 shows an alteration map produced from my field and laboratory studies.

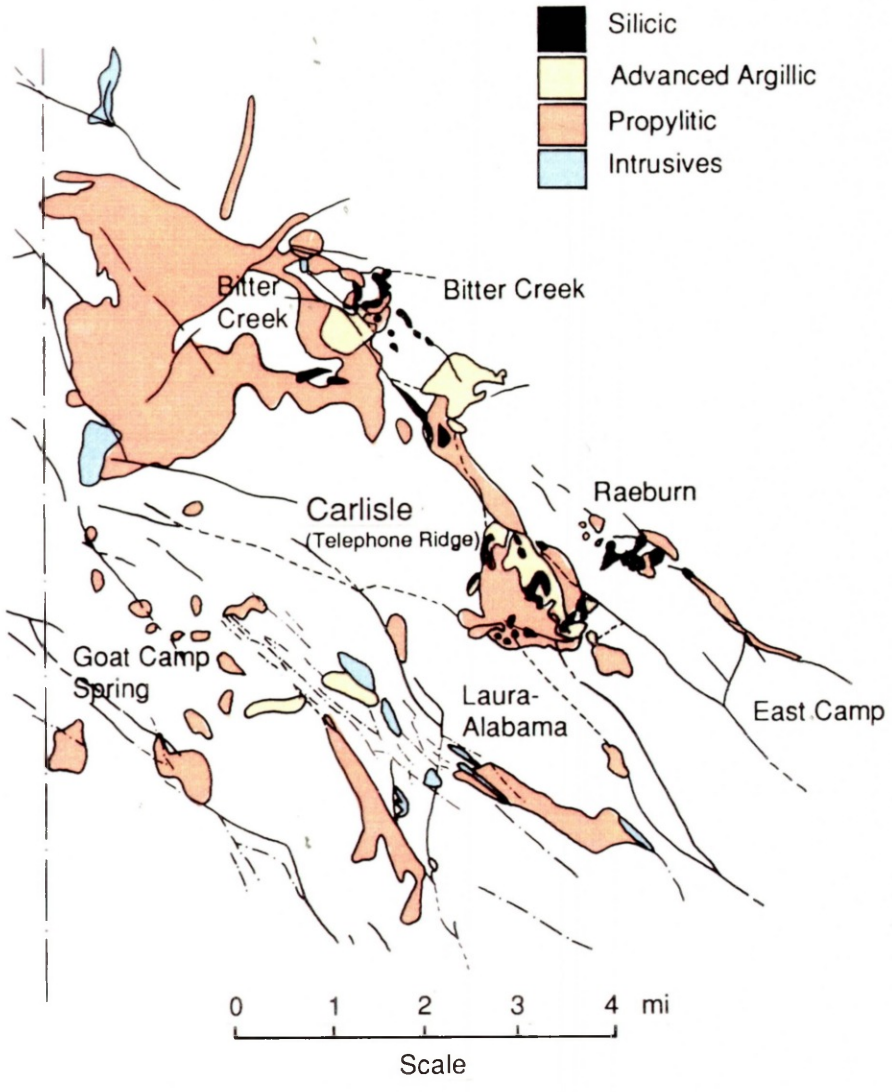

Silicic	includes sericitic and argillic around mineralised veins and faults
Advanced Argillic	includes argillic
Propylitic	In Bitter Creek includes smaller areas of argillic-sericitic assemblages and extensive supergene alteration

Figure 4.6 Distribution of hydrothermally altered rocks and intrusives of the Hells Hole unit of the Summit Mountains.

b) Alteration Assemblages

Forty samples of altered rocks and representative unaltered rock were thin sectioned for petrographic study under the microscope and 25 of these were crushed in preparation for X-ray diffraction analysis (Table 4.3)

From the laboratory analyses and field studies five alteration types were recognised.

(i) Silicic alteration
Occurring as resistant craggy, commonly brecciated and resilicified outcrops with iron oxides stains, or less commonly as pervasive alteration. In places flooded silica cappings occur. The silicic alteration forms ridges, low hills and "blow outs" commonly aligned along major faults (Fig. 4.7). The mineralogy is predominantly quartz with or without minor natro-alunite, pyrophyllite, kaolinite and diaspore.

(ii) Advanced argillic alteration
The altered rocks are pink to buff in colour and form well bedded and jointed outcrops which are composed mainly of interlocking grains of quartz and alunite or natro-alunite, pyrophyllite and kaolinite (Fig. 4.10). The original volcanic depositional features are recognisable - its survival indicates a metasomatic replacement process. This assemblage is restricted exclusively to silicic rocks, mainly the Bloodgood Canyon tuff and the upper tuffs of the Virden Dacite unit.

(iii) Argillic
Is spatially restricted to narrow zones around mineralised fracture zones and faults. It consists mainly of

Table 4.3 Mineralogy of various rock samples as determined from XRD from selected localities of the Summit Mountains test area

Sample	Alteration Type	Rock Type	Location	Mineralogy
M24A	Advanced Argillic	Silicified tuff	East Summit Ridge	Q Nal;Dl Hm Ml (Mu Verm)
M4	Advanced Argillic	Bloodgood Canyon tuff	Estes Ranch	Q;K Py;Dia An Hm
M24B	Advanced Argillic	Bloodgood Canyon tuff	East Summit Ridge	Q Py K;Sm Le Fe
14B	Advanced Argillic	Bloodgood Canyon tuff	Pennsylvania Canyon	Q Nal Py;Dia K Le
420	Advanced Argillic	Silicic Capping	Telephone Ridge	Q Nal;Le;Mn
M26C	Advanced Argillic	Bloodgood Canyon tuff	Whiskey Creek	Q D K;Py;Fe
430C	Advanced Argillic	Silicified tuff	Telephone Ridge	Q Nal;An Fe
M26A	Advanced Argillic	Bloodgood Canyon tuff	Whiskey Creek	Q Nal:K Sm;Hm An
16R	Argillic	Virden Dacite	Carlisle Fault	Q Py K G Ja Hm
M20A	Propylitic	Virden Dacite	Blue Goose Fault	Q Na-Ca Feld Ml (Chl Ser Vm);Hm Mag An
B1	Propylitic	Virden Dacite	Telephone Ridge	Q;Na-Ca Feld Px? Ml(Chl Mu) Clay (Sm Verm K)
M20B	Propylitic	Virden Dacite	Blue Goose Fault	Q Na-Ca Feld; Ca Feld; Px; Ser;Mu Hm; Bro
M21	Propylitic	Amygdaloidal Andesite	Blue Bell Fault (north of)	Kspar Ca-Na Feld Px? Bro Q;Chl-Liz Serp Hm
M132	Sericitic-Argillic	Clay vein	Telephone Ridge	Mu-Q;K-Al
41E	Sericitic-Argillic	Virden Dacite	Angelo Windmill, Carlisle Canyon	Q;Fe K;Ml (Mu);Mn Py?
M22B	Silicic	Amygdaloidal Andesite	Blue Bell Fault	Q;Ja;Mu Feld? Px?
M22A	Silicic	Quartz vein	Blue Bell Fault	Q(90%);K(Dl) Verm;Go Hm
17B	Silicic	Rhyolitic tuff	Raeburn Peak North Slope	Q;K(Dl) Dia Fe
19	Silicic	Rhyolitic tuff	Raeburn Peak NW	Q:K;An Ca
NB	Silicic	Rhyolitic tuff	Raeburn Peak SW	Q;K(Dl) Fe Mn Mu
432A	Silicic	Silicified tuff	Telephone Ridge	Q;N Dia Fe;An st Mn Le
M23	Silicic	Silicified tuff	East Summit Ridge	Q;Nal K;Py Verm
46C	Silicic	Silicic Capping	East Summit Ridge	Q;K;Fe An
414X	Unaltered	Virden Dacite	Charlie Hill	Q-NA-Ca Feld; Ca Feld; Am Ser Hm; Kspar Clays
M25	Unaltered	Virden Dacite	Laura Canyon	Q Na-Ca Feld Px;Ml(Chl Verm Bio);Ca Hm An?
M27X	Unaltered	Amygdaloidal Andesite (tuff horizon)	Mount Royal	Q;Ca-Na Feld Px Hm Ml Ca

Key

Alunite	Al	Dickite	Dl	Magnetite	Mag	Pyroxene	Px
Amphiboles	Am	Ferrihydrite	Fe	Manganese Oxides	Mn	Quartz	Q
Anatase	An	Goethite	Go	Micas	Ml	Sericite	Ser
Biotite	Bio	Hematite	Hm	Muscovite	Mu	Serpentinite	Serp
Brookite	Bro	Jarosite	Ja	Nacrite	N	Smectite	Sm
Calcite	Ca	Kaolinite	K	Natroalunite	Nal	Sodium Feldspar	Na Feld
Calcium Feldspar	Ca Feld	Leucoxene	Lx	Potassium Feldspar	Kspar	Stilpnomelane	St
Chlorite	Chl	Lepidolite	Le	Pyrophyllite	Py	Vermiculite	Verm
Diaspore	Dia	Lizardite	Lz				

Figure 4.7 "Blowouts" of the Carlisle fault near the Center mine. Looking west.

Figure 4.8 A one metre wide vein of the sericitic-argillic assemblage cutting through the bedded tuffs on the southern end of Telephone Ridge.

kaolinite and smectite.

(iv) Sericitic-argillic
Characterised by the occurrence of both white mica and assemblage of quartz, sericite, chlorite, calcite and kaolinite. This assemblage is commonly found around the mineralised veins and faults (Fig. 4.8).

(v) Propylitic
Propylitic alteration is widespread in the whole district and is preore in age. It is particulary common in the trachyandesite flows of the Virden Dacite unit and in basal andesites of the Amygdaloidal Andesite.

Generally the alteration appears to have a crude three dimensional zonation, from an inner silicic and ferric zone outwards through advanced argillic or sericitic-argillic to propylitic. In the field it is difficult to separate the argillic from the sericitic-argillic assemblage. The dimensions of the alteration zones are summarised on table 4.4.

c) Telephone Ridge - Carlisle Area

The Carlisle mining area is dominated by Telephone Ridge rising steeply north of the Carlisle fault to a height of 1830 metres (Fig. 4.9), 370 metres above the mines. The ridge is centred on the largest area of hydrothermal alteration in the Summit Mountains, covering 2.4 square kilometres, and is the only area in the district where significant amounts of precious and base metal ore occur together.

Table 4.4 Approximate dimensions of hydrothermal alteration zones in the Summit Mountains.

Locality	New Mexico Map location	Area (Hectares) Silicic	Advanced Argillic	Argillic Sericitic	Propylitic	Total
Telephone Ridge	Sec.1,T17S,R21W,NM.	9	89	2	200	300
Bitter Creek	Secs.19-22,26-30,T16S,R21W,NM	180	1620	minor	?	1800
Raeburn	NW 1/4 Sec.6,T17S,R20W,NM	9	small	minor	12	22
Laura - Alabama	S 1/2 Sec.3,T17S,R21W,NM	1.5	10	0.5	25	27.5
East Camp	NW 1/4 Sec.8,T17S,R20W	1	0	3	20	24

Structurally the ridge forms a north west trending horst block, bounded on the north by the East Camp fault, and on the south by the Carlisle fault. The western boundary is delineated by East Summit Ridge, a north trending ridge of silicified and argillised rocks running parallel to and above Carlisle canyon. The eastern boundary is marked by the thick unaltered Virden Dacite flows lying above the Ontario mine in Pennslyvania canyon.

Telephone Ridge is made up of trachyandesite flows, volcanoclastics and a purple ash fall tuff forming the upper part of the Virden Dacite unit, overlain by the Bloodgood canyon tuff. These units dip from 10 to 40 degrees to the north east, although in the central saddle of the ridge there is a north trending synclinal structure. Running along the top of the ridge is a prominent resistant, well jointed, welded rhyolite tuff which trends north west, controlling the trend of the whole ridge.

The main host to the alteration is the distinctive Bloodgood Canyon tuff which outcrops extensively on and around Telephone Ridge. It is a pink to buff coloured, and well bedded with circular iron weathering patterns. The tuffs are replaced by a fine grained matrix of quartz and clay minerals. X-ray diffraction (Table 4.3) shows the assemblage to be characterised by quartz, natro-alunite, kaolinite, diaspore, pyrophyllite with accessory ferrihydrite, leucoxene and manganese oxides. A general layering is apparent with an upper silicic capping composed of quartz, with minor kaolinite and diaspore, a lower advanced argillic assemblage of natro-alunite kaolinite and diaspore and a lower zone of kaolin and

Figure 4.9 Bleached and reddened volcanics on the south face of Telephone Ridge, with the Carlisle mine workings on the right.

Figure 4.10 A typical outcrop of altered Bloodgood Canyon tuff, the common host to the advanced argillic assemblage. South face of Telephone Ridge.

pyrophyllite. The trachyandesites flows below are propylitically altered.

Silicified and brecciated tabular pipe structures cut across the general strike of the rocks in a north to north east direction. A one metre thick vein of sericite and kaolinite (Sericitic-argillic alteration, also known as argillic or phyllic) trends north east into the hillside on the east end of the ridge (Fig. 4.8).

The relationship between the silicic, advanced argillic, sericitic-argillic and propylitic alteration and the precious and base metal mineralisation on the Telephone Ridge - Carlisle area is not clear. However around the ore bearing veins there is a separate sericitic-argillic alteration phase noted by Griggs and Wagner (1966) and Powers (1976), consisting of quartz, sericite, adularia, chlorite, calcite and kaolinite.

d) Bitter Creek & Goat Camp Springs Area

The rocks in this area are extensively sheared and fractured by northwest, northeast, east and north trending faults and shear zones which cut across the altered rocks and are well-marked by dykes and veins (Fig. 4.11). The Bitter Creek shear zone is 200 to 1000 metres wide zone of fractured rocks, quartz pyrite veins, discontinuous gouge zones and a recent tufa deposit. The alteration is advanced argillic, sericitic-argillic and propylitic. The silicic and advanced argillic assemblages are restricted to replacements of acid tuff beds, similiar to Telephone Ridge. The sericitic-argillic alteration and propylitisation are more restricted to areas around

faults, intrusions and veins and do not appear to be restricted to any one host. Drilling in Bitter Creek has revealed that supergene alteration is presently active (Wahl 1980).

e) Raeburn Area

Two kilometres north of Telephone Ridge are low hills of trachyandesite flows of the Virden Dacite unit capped by a silicified tuff, tentatively identified as the Bloodgood Canyon Tuff. Amygdaloidal Andesites lie unconformably over the tuffs to the north and north east. Pennyslavania Canyon cuts a steep gorge through the hills.

The tuffs are strongly welded and are capped by a dense flooded quartz capping, and are locally silicified brecciated and stained with iron and manganese oxides. Silicification is concentrated along linear zones in faults, fractures, joints and more permeable beds. The mineralogy is quartz,with minor kaolinite (dickite) and diaspore, with accessory leucoxene, muscovite, calcite and manganese oxides. The trachyandesite flows are altered to a propylitic assemblage. The advanced argillic alteration dominant at Telephone Ridge is absent.

No mineral deposits of any importance are known in the area. An old shaft and several pits occurring on a quartz vein running sub parallel to the East Camp fault, known as the Carnation mine was drilled in 1959/60 (Gillerman 1964). The north eastern boundary of the area is marked by the Blue Bell fault where the Blue Bird mine shaft is sunk into a vein on the north east side of a rhyolite dyke. Here there is mineralogical evidence for a prograde

alteration phase from earlier propylitic to sericitic-argillic alteration.[1]

f) Laura-Alabama Area

In the southwest of the area the north trending Steeple Rock fault and the adjoining north north west trending Laura and Alabama faults have several small mines including the Mount Royal, Jim Crow, Alabama, New Years Gift and Laura (Fig. 4.5). These mines occur in silicified and brecciated zones along the faults or in veins along rhyolite intrusions or fractures parallel to the faults. Unlike Telephone Ridge there is extensive intrusive activity, but the ore phases are post intrusive.

Ores are gold and silver with traces of base metal sulphides. Alteration is silicification and sericitisation with smaller areas of argillisation along and close to the veins. Extensive chloritisation for the Amygdaloidal Andesite unit occurs.

South of the Mount Royal mine on the Steeple Rock fault, there is a 20 mete wide silicified and brecciated zone, surrounded by argillic alteration and pervasive iron staining. Relations at the mine show the ore phase occurred after the rhyolite intrusives (Griggs and Wagner 1966). The Jim Crow and Imperial mines are also on silicified and brecciated zones of the Steeple Rock fault. Between them and the Alabama mine is a wide area of chloritised and reddened Amygdaloidal Andesite, below a white ash flow unit, which is clearly visible on aerial

[1] *Remobilisation and recrystalisation of quartz and epidote replaced by sericite.*

Figure 4.11. "Blowouts" and hydrothermally altered rocks at Bitter Creek, looking south east to Telephone Ridge.

Figure 4.12 Looking north to East Camp Ridge. Note the lack of the advanced argillic alteration assemblage and the increased vegetation cover.

photographs (and Landsat TM).

Between the Jim Crow and Laura mines are numerous rhyolitic intrusives of the Hells Hole series. The Alabama mine is situated on a silicified brecciated zone with surface reddening within a dyke. On the west side of Carlisle Canyon at the confluence with Silver Bar canyon is a large rhyolite stock with brecciated sides and iron stained quartz veins. Extensive argillic alteration occurs on the southwest side of Vanderbilt Peak. At the Laura mine alteration is restricted to within several metres on either side of the Laura fault, the footwall Amygdaloidal Andesites and the trachyandesites of the hanging wall are unaltered.

g) East Camp Area

The mineralisation at East Camp occurs in brecciated wall rock of the northwest trending Eastcamp fault. Details of the mineralisation are in Chapter 4.5. The hanging wall is composed of resistant pervasively iron stained Amygdaloidal Andesite, penetrated by quartz stringers up to several centimetres wide. This forms a prominent ridge some 25 to 30 metres wide running parallel to the vein which outcrops on the southeast side of the ridge (Fig. 4.12). The footwall comprises less resistant Amygdaloidal Andesite on the surface and deeper in the mine tuffs of the Virden Dacite unit. The alteration is restricted to a 30 metre wide zone in the hanging wall. Unaltered Virden dacite flows outcrop 100 metres southeast of the fault. No advanced argillic or argillic alteration occurs at Eastcamp.

4.7 A MODEL FOR THE SUMMIT MOUNTAINS

(a) Epithermal Mineralisation and Alteration Relationships

The development of a model describing the alteration and mineralisation in the Summit Mountains is necessary for two reasons.

(1) Such a model provides a suitable framework to which remote sensing characteristics can be examined and assessed and

(2) Categorisation of the Summit Mountain epithermal system allows comparison of the system with other epithermal deposits and therefore gives some indication of the usefulness of the model and its remote sensing characteristics for identifying other epithermal deposits in New Mexico (and elsewhere).

Since the term epithermal was defined (Lindgren 1922), geologists have attempted to categorise epithermal deposits into descriptive or genetic subsets. Descriptive classifications have been based upon various parameters including gold silver ratios (Ferguson 1929), ore content (Loughlin and Behre 1933) and mineral assemblages (Lindgren 1933).

Genetic classifications have included a depth related continuum (from near surface hot spring deposits to disseminated replacement deposits and deeper bonanza systems), related to convergent plate boundaries (Giles and Nelson, 1982), and relationships with the tops of copper porphyry systems (Sillitoe, 1983). Other

classifications have included those of Berger and Eimon (1983) who defined three end member models; hot spring, stacked cell convection and closed cell convection; Sillitoe and Bonham (1984) based on volcanic landforms and Silberman and Berger (1986) based on high or low sulphur bearing hot spring or bonanza types.

Heald et al (1987) based on a detailed study of 16 well documented epithermal districts, recognised two mutually exclusive end member epithermal types, they termed adularia-sericite and acid-sulphate. The types were distinguished mainly on the basis of alteration and vein mineralogy, although a large number of variables were used (Table 4.5). The type characteristics compiled by Heald, Holey and Hayba are a useful framework to categorise the Summit Mountain epithermal system.

Although both types form under similar pressure and temperature conditions they are believed to represent distinct geothermal environments (Fig. 4.13). Acid-sulphate types are believed to form in the upper core of volcanic domes which are flooded by meteoric waters, and adularia-sericite type deposits form in an extensive meteoric lateral flow system, high above and perhaps offset from a heat source at depth.

(b) Comparison of the Summit Mountain epithermal system to the acid-sulphate and adularia-sericite epithermal types

Three of the 12 characteristics of table 4.5 point to an adularia-sericite type (the size length: width ratio, timing of ore and host, and the vein mineralogy); the remainder are either known in insufficient detail to

Table 4.5 Distinguishing characteristics of the adularia-sericite type and acid-sulphate type deposits of volcanic hosted epithermal systems (adapted from Hayba 1986, Table 7.1)

Characteristic	Acid-Sulphate	Adularia-Sericite
Structural Setting	Intrusive centres, often related to caldera margins	Structurally complex environments, commonly in calderas
Size: length/width ratio	Relatively small; Equidimensional	Variable, some very large; Commonly 3:1
Host Rocks	Rhyodacite	Silicic to intermediate volcanics
Timing of ore and host	Similiar age of ore and host	Distinct age difference, often > 1 m.y.
Mineralogy	enargite, pyrite, native gold, electrum and base metal sulphides, Chlorite rare No selenides, Mn minerals rare, Sometimes bismithinite	argentite, tetrahedrite, tennanite, native silver and gold, and base metal sulphides, Chlorite common Selenides present, Mn gangue No Bismithinite
Production Data	Both gold and silver rich Significant copper	Both gold and silver rich Variable base metal
Alteration	Advanced argillic to argillic (+/- sericitic)	Sericitic to Argillic
	Extensive hypogene alunite Major hypogene kaolinite No adularia	Supergene alunite Occasional kaolinite Abundant adularia
Temperature (degrees C)	200 - 300	200 - 300
Salinity	1 - 24 Wt% NaCl eq.	0 - 13 Wt% NaCl eq.
Source of Fluids	Dominantly meteoric Possible significant magmatic component	Dominantly meteoric
Source of Sulphide Sulphur	Deep-seated, probably magmatic	Deep-seated, probably derived from leaching wallrocks deep in system
Source of Lead	Volcanic rocks or magmatic fluids	Precambrian or Phanerozoic basement rocks

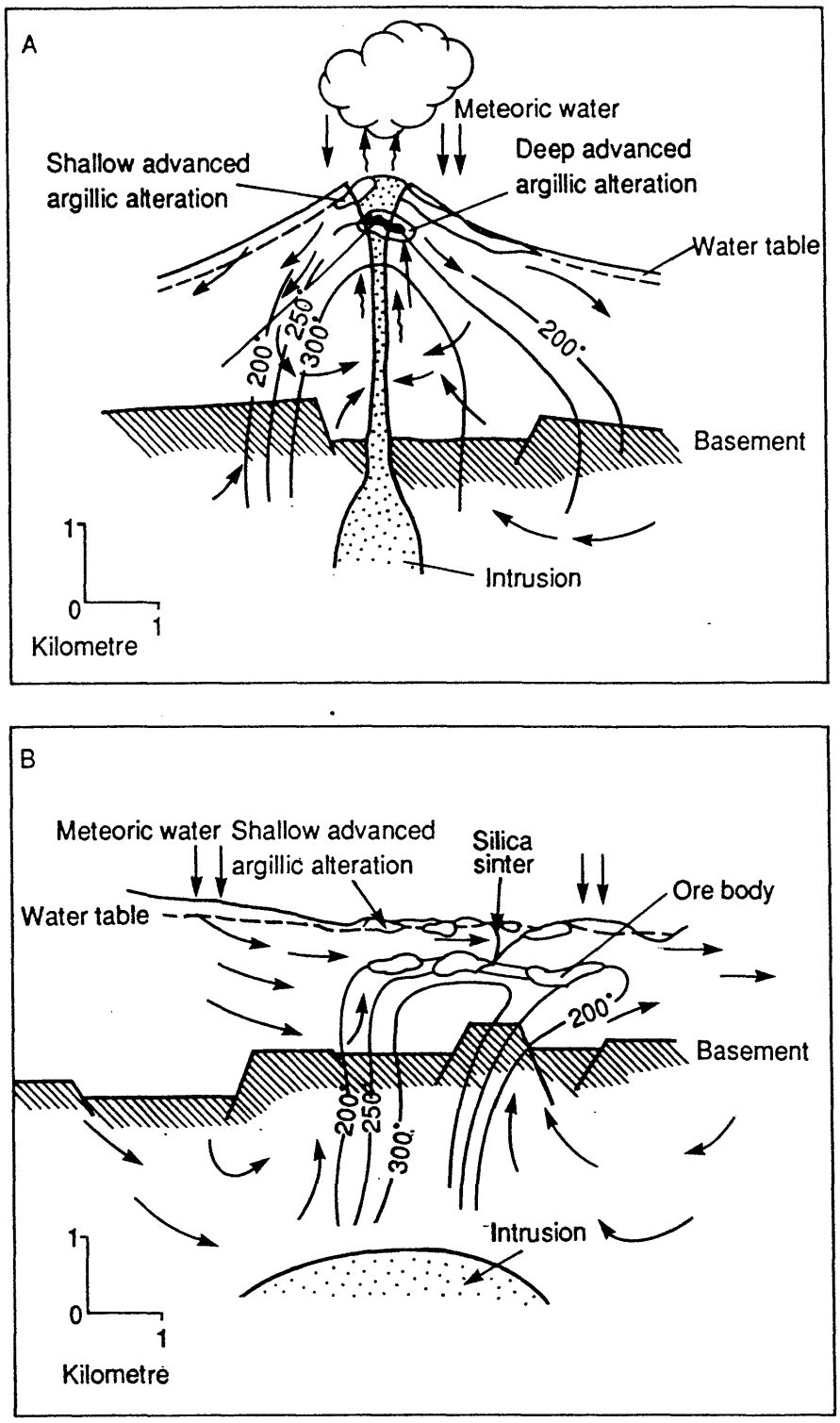

Figure 4.13 Occurrence models of the two types of epithermal ore deposits in a geothermal system.
A. Acid-sulphate type, B. Adularia-sericite type (from Heald et al. 1986).

ascribe to one or another of the types, or are ambiguous.

The temperature of formation, salinity, source of fluids, and the origin of the sulphide and lead of the system are unknown, although none of these characteristics are by themselves definitive. The structural setting and production data are also not exclusive to one type or the other, although intrusive centres are fairly common to acid-sulphate types. The Summit Mountains has a known intrusive centre (Hells Hole) and such centres with acid-sulphate type alteration are known elsewhere in south west New Mexico (Chap. 4.3h).

However the geothermal setting of the adularia - sericite type is on balance more favourable in the Summit Mountains. The Hells Hole volcanic centre to the northwest of the district may have provided a suitable heat source for the hydrothermal system.

The length-width ratio of the ore shoots, the host rocks and the timing of the ore and host are characteristic of an adularia-sericite type. However the key characteristics are (1) the vein and (2) the alteration mineralogy.

Evidence from the alteration mineralogy is ambiguous as there are both advanced argillic and sericitic alteration types present. However there is evidence that the advanced argillic alteration is pre-ore and not related to the ores. This includes:

(i) The centres of strong alteration and mineralisation do not coincide. e.g. at East Camp and Laura Alabama (Chapts. 4.6f and g) metals are rich

and alteration is relatively restricted, the converse is found at Bitter Creek and Goat Camp Springs (Chap. 4.6d).

(ii) The main ore bearing zones cut through the advanced argillic areas of hydrothermal alteration.

(iii) Brecciated pipes and an argillic-sericitic vein cut through the altered tuffs on Telephone Ridge (Chap. 4.6c). Phase equilibrium data suggest the vein formed in a higher temperature less acid regime than the surrounding advanced argillic assemblage.

(iv) Late stage prograde sericitic alteration occurs at the Blue Goose fault (Carlisle area) and the Blue Bell fault (Raeburn area).

There is strong evidence that the ore mineralisation is related to the late stage sericitic-argillic and argillic assemblages because of the close association of these assemblages with the main ore bearing veins on the Carlisle, Blue Bell, Steeple Rock, and Alabama faults.

Vein mineralogy evidence also indicates an adularia-sericite type (Chap. 4.5b). There is no hypogene alunite or enargite associated with the ores. The absence of enargite and the presence of vein adularia and sericite is definitive of the environment of the adularia-sericite type deposit. Chloritisation and manganese oxides found in the Summit Mountains ores are common in the adularia-sericite and rare in acid-sulphate types.

c) Origin of the Advanced Argillic Alteration

If the mineralisation is unrelated to the advanced argillic alteration, as suggested, then the presence of the extensive advanced argillic alteration at Telephone Ridge and Bitter Creek requires explanation. Acid-sulphate alteration forms by three mechanisms, primary hypogene, primary supergene and secondary supergene (Hayba et al, 1986).

Primary hypogene acid-sulphate alteration occurs in the deeper parts of acid sulphate deposits and involves the disproportion of magmatically exsolved sulphur dioxide gas into sulphuric acid and hydrogen sulphide gas.

Primary supergene acid-sulphate alteration involves the simple oxidation of hydrogen sulphide and is the solfataric alteration seen commonly on the surfaces of modern geothermal systems. Oxidation of H_2S occurs when the vapour phase generated by boiling of deep waters contacts the atmosphere above the water table. The sulphuric acid generated percolates downward and acidifies the steam heated groundwaters which overlie the deeper circulating hydrothermal cell. The alteration is intense but is rarely developed more than 50 metres below the paleosurface, and is rarely preserved.

Secondary supergene acid-sulphate alteration results from the production of sulphuric acid during supergene alteration of sulphide ore, postdating the hydrothermal system.

Primary hypogene forms in the deeper parts of acid-sulphate deposits, while primary and secondary

supergene can form in the shallower parts of both epithermal types.

The main area of acid sulphate alteration on Telephone Ridge does not readily fit into any of the three mechanisms. There are characteristics of both primary hypogene and primary supergene alteration. As a secondary supergene origin is very unlikely because of the high temperature mineralogy, the explanation may be that the acid-sulphate alteration resulted from an earlier associated hydrothermal system. This has occurred in the adularia-sericite deposits of Comstock and Rochester Neveda (Heald et al, 1987).

However at Bitter Creek both primary and secondary supergene alteration have operated and secondary supergene alteration is occurring today (Wahl 1980).

The origin of the acid sulphate alteration could be determined by light stable isotope analysis and K-Ar determinations (Hayba et al, 1987, page 12). Sulphur isotopes can be used to distinguish primary hypogene alunite from supergene alunite, but cannot distinguish primary from secondary supergene alunite. These studies were beyond the scope of this research project, but are reccommended for further geological studies on the hydrothermal alteration and mineralisation.

4.8 DISCUSSION

The Summit Mountains area is a volcanic centre of middle Tertiary age consisting of a series of flows, tuffs, intrusives and minor volcanoclastics, ranging in composition from basaltic andesite to rhyolite. Basin and Range tectonism resulted in high angle normal faulting and horst and graben development, which emphasised the earlier volcanic structure and prepared the region for the later hydrothermal flow regimes. The epithermal system(s) may be related to the Hells Hole centre, which may have provided at least the heat source to drive the system.

The epithermal precious and base metal ores occur along brecciated northwest and west-northwest trending faults in silicified and brecciated zones spatially associated with the widespread hydrothermal alteration.

At least five separate periods of hydrothermal alteration are recognisable:

1. Early propylitic with minor primary supergene alteration associated with vents in the Virden Dacite and Amygdaloidal andesite.
2. Primary hypogene alteration centred on Telephone Ridge and Bitter Creek (probably) of acid-sulphate type.
3. Regional adularia-sericite alteration associated with the precious and base metal mineralisation.
4. Deuteric alteration associated with tuff ring vents e.g. Deer Peak.
5. Late stage secondary supergene alteration mainly at Bitter Creek.

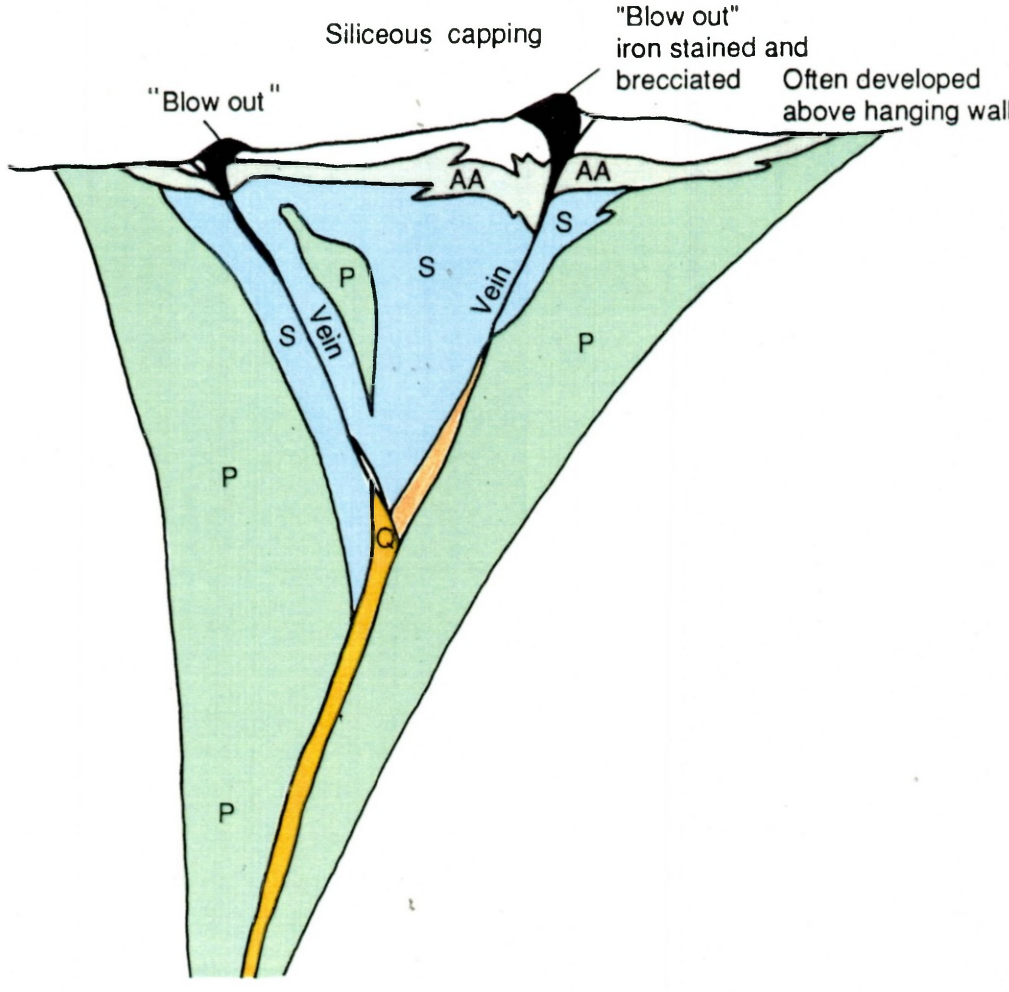

Figure 4.14 Idealised section representation of the alteration - mineralisation relationships in the Summit Mountains.

Thus the epithermal deposit is of the adularia-sericite type with an earlier acid-sulphate phase. The earlier phase may be associated with the adularia-sericite system or be from a separate epithermal system. The superimposition of the two types complicate the development of a simple epithermal model to be used as the basis for a remote sensing study. But based on the relationships found in the area, several common geological factors are recognisable. These are:

(1) Major through-going faults, often kilometres in length and a few metres in width, mostly with a northwest trend but also north - south and east - west.
(2) Silicification of faults and major mineralised areas forming positive iron stained "blow outs"
(3) Narrow zones of sericitic-argillic alteration, often less than 5 metres in width, often iron stained.
(4) Extensive zones of advanced-argillic alteration, many tens of hectares in area, often with smaller silicic iron oxide stained cores.
(5) Widespread propylitic alteration, many tens of hectares in area.

The advanced argillic alteration and iron oxide staining are not always concurrent with mineralised areas. These characteristics are summarised on Figure 4.14.

CHAPTER 5

IMAGE PROCESSING AND IMAGERY ANALYSIS

5.1 Introduction

The objectives of studies reported in this chapter were to assess TM imagery and image processing techniques for mapping the alteration types in the Summit Mountains. More specifically the following questions required answers: Can alteration assemblages be separated from each other ?; can alteration be discriminated from the country rocks ?; and does the imagery show altered areas not known on the ground ? The effective image processing techniques used to extract this information are described.

To achieve these objectives three main image types were quantitatively and qualitatively assessed; TM single bands and colour composites, band ratio images, and principal component images. The quantitative analysis involved statistical separability measurements of cover types selected from training areas from the Summit Mountains. Qualitative analysis was based on comparison of the image products to the geologic maps and information described in Chapter 4.

The selection of training classes required thorough knowledge of the geography and geology of the area and of the spectral signatures of the features being analysed. The former, described in Chapter 4, were provided by geological mapping and field surveys. Spectral information was provided by *in-situ* radiometer

measurements and by high resolution laboratory measurements (Chapter 6). Details of the field spectral studies are given in Chapter 5.3 (Band ratioing) and in Appendix III. The laboratory studies are described in Chapter 5.8 and Appendix V.

(a) Training Classes

Initially I intended to perform the quantitative analysis using the rock types and alteration types mapped in the field, as described in Chapter 4. However preliminary analysis showed that many of the rock types were spectrally inseparable (e.g. Table 5.10), so rocks were categorised into three main rock types based on composition; rhyolites, trachyandesites and andesites (Table 5.1). It proved impracticable to identify and separate individual alteration assemblage on the TM imagery, because of their small size and because of the difficulty of ensuring that "pure" alteration classes were selected. Inadvertent inclusion of mixed pixels for pure pixels would invalidate quantitative analyses and produce misleading results.

The training classes were identified using information collected from the field studies, from colour aerial photographs and from preliminary analysis of TM imagery.

Telephone ridge, Bitter Creek and the southwestern slopes of Vanderbilt Peak were used as training areas for the alteration class. These include mainly silicic and advanced argillic alteration assemblages with lesser propylitic and sericitic-argillic types (Fig. 4.9).

Table 5.1 Geological units and their Training Classes equivalents

Rhyolite	Unaltered Bloodgood canyon tuff Steeple Rock Rhyolite Rhyolites from the Hells Hole Centre Cherry Creek Rhyolites (altered) Sycamore Camp Eruptive Centre
Trachyandesite	Virden Dacite
Andesite	Amygdaloidal Andesite Bearwallow Mountain Formation
Colluvium	Gila Conglomerate
Epithermal Alteration	Telephone Ridge Bitter Creek Vanderbilt Peak

Figure 5.1 Training site for the Trachyandesite class; Looking west to the flows of the Virden Dacite unit at Charlie Hill.

Figure 5.2 Training site for the vegetation class; Woodland vegetation east of the East Camp area on soils of the Amygdaloidal Andesite unit.

Data for the rhyolite class was taken from the unaltered Bloodgood tuff, the rhyolites of Steeple Rock, Hells Hole, Cherry Creek, Sycamore Creek and from sub-units occurring in the Virden Dacite. Trachyandesites were taken from the Virden Dacite unit south of Telephone Ridge and from Charlie Hill (Fig. 5.1). Andesites were from the Older Volcanic Series, the Amygdaloidal Andesite and the Bearwallow Mountain formation.

Larger numbers of pixels were used for the andesite class to take into consideration the greater class variability, caused by variations in scrub vegetation and iron oxide cover (Fig. 4.4). Colluvium and alluvium were taken from the Gila Conglomerate south of Steeple Rock Peak. This class also contains a significant amount of scrub vegetation. Vegetation was chosen from apparent (from the imagery and air photographs) areas of continuous canopy cover from stands of pines occurring on the northern slopes of Steeple Rock Peak, east of East Camp and from grasses along Cottonwood Canyon (Fig. 5.2).

Where possible the training areas were taken on flat or southwest facing slopes toward the sun, to minimise the effects of specular reflectance. Care was taken to ensure that no shadowed pixels were included in the sets.

5.2 Thematic Mapper Bands

(a) Individual bands

Each TM band was contrast stretched and compared with the geology to determine the utility of each for mapping.

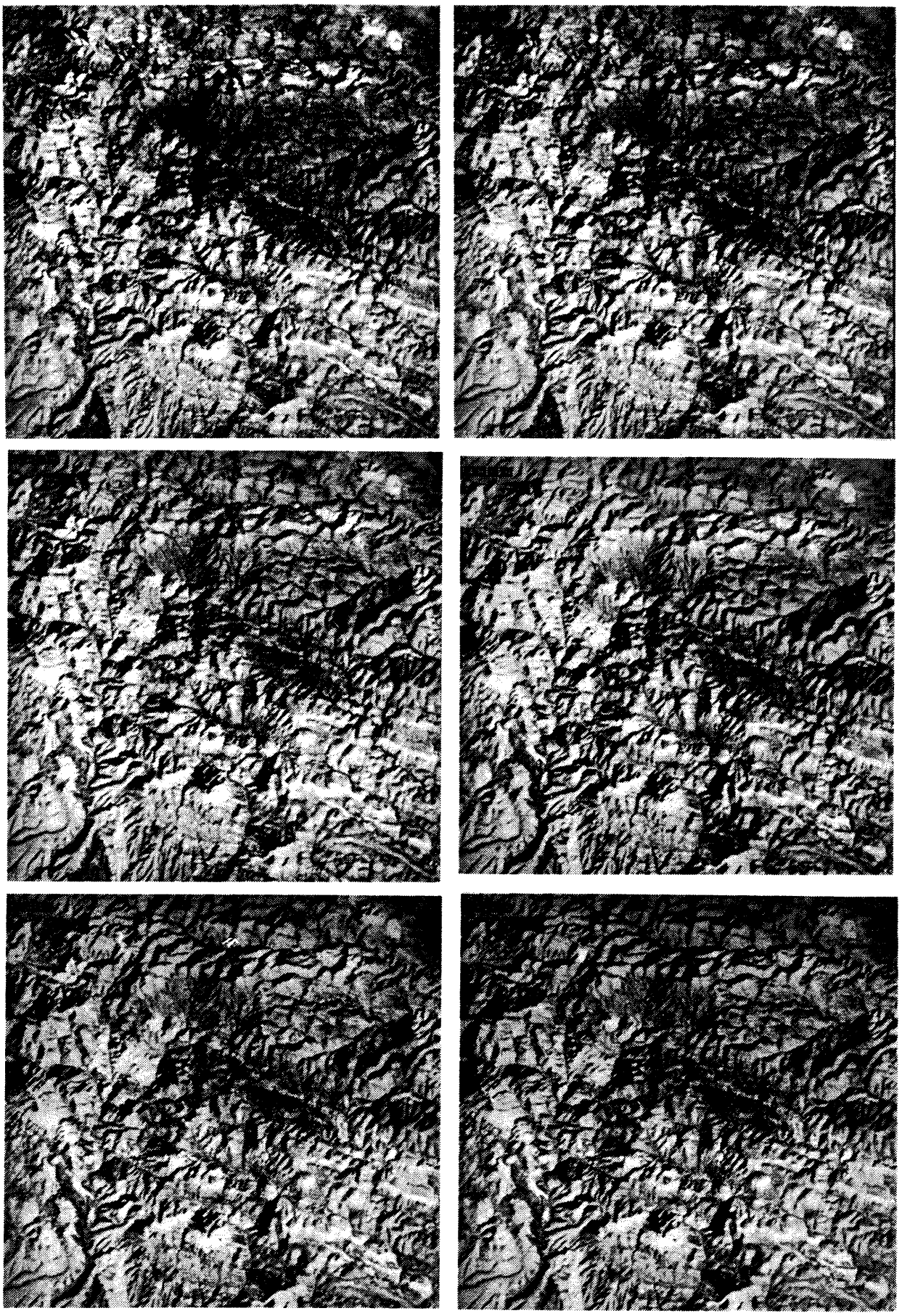

Figure 5.3 Contrast stretched images of TM bands 1 - 5 and 7 of the Summit Mountains.

Figure 5.3 shows the enhanced images. Generally all the bands were poor for lithological and alteration mapping, although they were good for structural interpretations. Statistical analysis of the six classes back up the visual analysis. Table 5.2 shows co-incident spectral plots of the six classes. Band 5 has the greatest scatter of information. There is significant overlap between virtually every class in each band. However alteration is separable from vegetation and andesite in all the bands. The brightest rocks in all the bands are rhyolite followed by alteration, except in band 5 were alteration and rhyolite are indistinguishable.

(b) Colour Composites

The first step in producing colour composite images is the selection of the three bands from the six available (there are actually 7 TM bands, but band six is the thermal band which contains little useful information when imaged during daylight hours, and in addition has 120 m resolution). The objective was to produce the best image for lithological discrimination, in particular the discrimination of the alteration from the other cover types. Initially the standard false colour composite image comprising bands 4 3 and 2, assigned to the colours red, green and blue was produced, giving the familiar red colour to vegetation. This image gave very low contrast images, even after harsh contrast enhancement (Scale or Histogram Equalise), because of the high correlation between the bands.

To help with band selection quantitative analysis of the TM bands was done. Unlike Landsat MSS imagery there is no

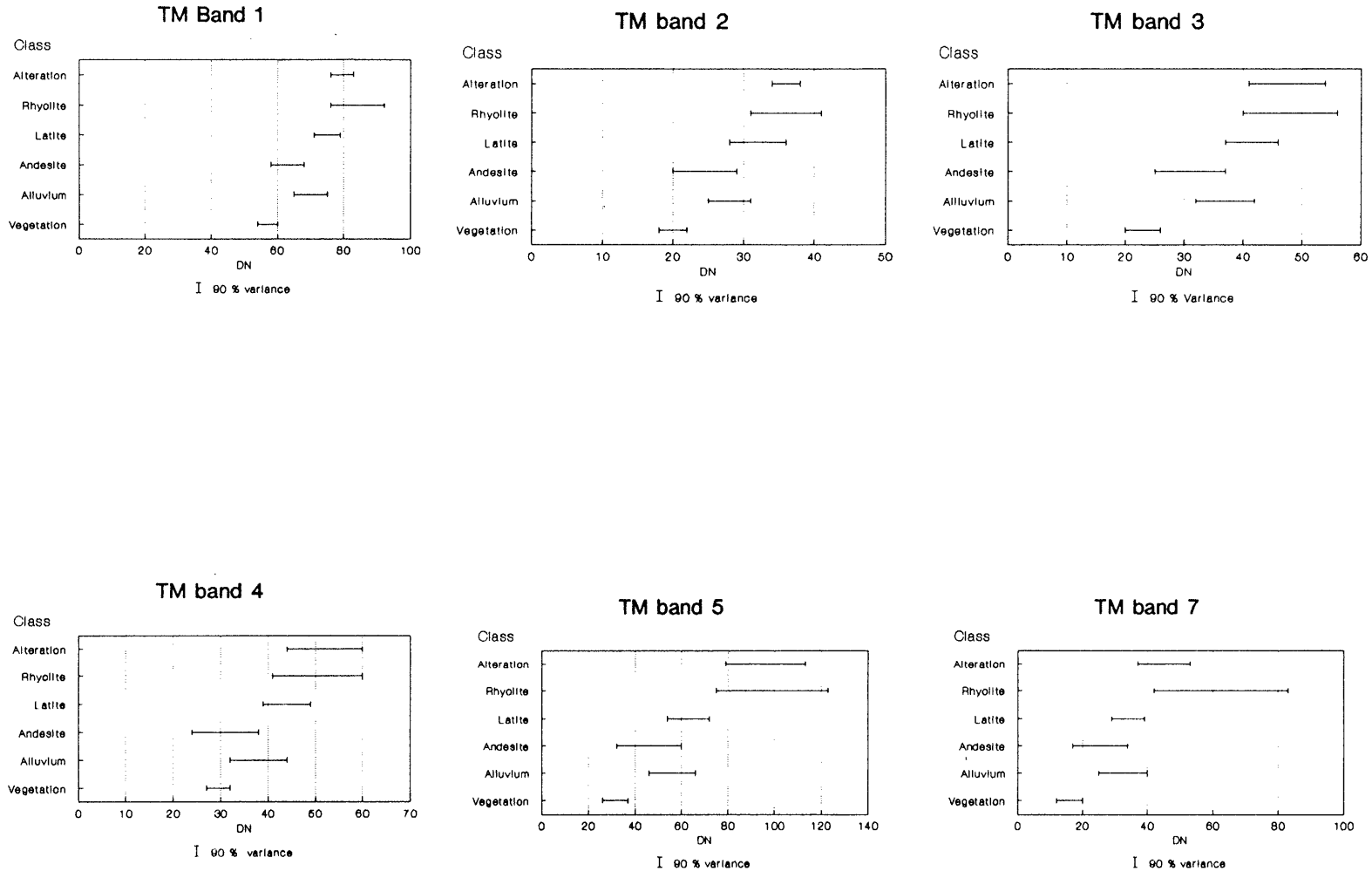

Table 5.2 Co-incident spectral plots for the six cover classes in TM bands 1 - 5 and 7

generally accepted best band combination for TM imagery. Several authors have suggested TM 7 4 2 (RGB) as the best band combination for geological mapping in semi-arid terrain. Loughlin and Tawfiq (1985) suggested 7 5 2 for discriminating argillic and ferruginous alteration.

Rothery (1986) advocated individual visual band assessment and the choice of those bands showing the best diagnostic features, usually containing band 7, the clay band, and band 5, the peak reflectance band. He found combination 7 5 4 to be the best composite. Crippen et al (1987b) recommended combination 1 4 7 as it commonly provides more spectral information than other band triplets.

(c) Automatic band selection

The statistical approach to band selection based on the work of Sheffield (1985) was used on both TM bands and on ratios. The best colour composite may be the one which has the greatest combined image variability. This can be measured by a technique called the Optimum Index Factor (OIF), developed by Chavez et al (1982) for selecting band ratio combinations from Landsat MSS data. The OIF weights the variance of the individual bands by using their standard deviation and correlation between the bands and is defined as:

$$OIF = \sum_{i=1}^{3} SDi \Big/ \sum_{j=1}^{3} |CCj|$$

where
SDi = standard deviation of band i
CCj = absolute value of the correlation coefficient between any 2 of the 3 bands.

The OIF is computed for all possible band combinations by dividing the sum of the standard deviations of each combination by the absolute value of the correlation coefficient computed for the same three ratios taken two at a time. Table 5.3 ranks the TM composites from best to worst from top to bottom.

The OIF is a simple technique prone to errors from duplication. A more complex and statistically thorough technique is that described by Sheffield (1985), called here the Maximum Ellipsoid Volume technique (MEV). This measures the volume of the ellipsoid occupied by the data from the three input bands, rather than the maximum variance as with the OIF. Ranking based on the MEV is shown in table 5.4.

Both the OIF and the MEV produce broadly similar results, both showing that the commonly used false colour composite image (432) followed by the natural colour composite (321) have the lowest scene information content than all the other possible combinations.

However, since not all of the information in the image is important geologically (it is made up of water, soil, vegetation and so on), non-rock information was removed from the imagery in an attempt to isolate geological spectral information. Knepper and Raines (1985) used such a technique to improve contrast stretches of MSS ratio images. It was hoped that a similar process would help produce information for improved contrast enhancements to emphasise lithological discrimination. The masking technique used is described in Chapter 7. The new MEV rankings and the correlation coefficients between the original and masked imagery are shown in tables 5.5 and

Table 5.3 OIF rankings of the TM Colour Composites

Rank	Band Composite	Comment
1	157	
2	145	
3	135	
4	457	Rothery (1986) recommendation
5	345	
6	257	Loughlin (1985) recommendation
7	125	
8	245	
9	235	
10	147	Crippen (1987) recommendation
11	137	
12	357	
13	347	
14	127	
15	247	General recommendation
16	134	
17	237	
18	124	
19	123	Natural colour
20	234	False colour

Table 5.4 MEV rankings of the TM Colour Composites

Rank	Band Composite	Comment
1	145	
2	135	
3	157	
4	147	Crippen (1987) recommendation
5	457	Rothery (1986) recommendation
6	125	
7	357	
8	137	
9	345	
10	245	
11	257	Loughlin (1985) recommendation
12	127	
13	347	
14	235	
15	247	General recommendation
16	134	
17	124	
18	237	
19	123	Natural colour
20	234	False colour

Table 5.5 Comparison of MEV rankings of the TM Colour Composites for original and HSI Vegetation masked imagery

Rank	Original band Imagery	Masked band Imagery	Relative Movement
1	145	145	0
2	135	135	0
3	157	157	0
4	147	147	0
5	457	125	-4
6	125	137	1
7	357	127	-1
8	137	357	3
9	345	457	-4
10	245	245	0
11	257	257	0
12	127	235	5
13	347	345	-6
14	235	247	2
15	247	134	1
16	134	124	-2
17	124	237	1
18	237	123	1
19	123	347	1
20	234	234	0

Table 5.6 Comparison of correlation coefficients between the original amd masked imagery

Original

	1	2	3	4	5
1					
2	0.85				
3	0.83	0.97			
4	0.80	0.93	0.95		
5	0.68	0.77	0.80	0.82	
7	0.69	0.79	0.82	0.85	0.97

Masked

	1	2	3	4	5
1					
2	0.99				
3	0.97	0.99			
4	0.97	0.99	1.00		
5	0.91	0.94	0.95	0.96	
7	0.90	0.93	0.95	0.95	0.99

5.6 respectively.

As can be seen from the tables the MEV rankings from the four best composites are unchanged. Clearly the removal of non geological spectral information has little affect on the imagery. Table 5.6 shows that the removal of the non geological spectral information increases the band correlation, reduces image variance and compounds the poor contrast problems of the TM data. It would seem that much of the image variation is due to the presence of vegetation, particularly because of the large spectral reflectance differences between the visible and NIR for vegetation.

(d) Colour Transforms

Once the best bands were selected they were evaluated visually to determine their geological use. The bands with the greatest variance (MEV and OIF) were the best image products for geological interpretation. However the contrast of the composites wes poor, even after contrast stretching, because the rocks and soils of the test area have very small spectral variation in the TM bands. The high correlation is shown statistically in table 5.6. An HSI colour space transform (Chap. 2) was applied to improve image contrast in an attempt to improve discriminability.

Figure 5.4 shows the best colour composite (145) and figure 5.5 is an HSI transformed 432 composite. Clearly the HSI composite is a much improved image for

Figure 5.4 Colour composite 1 4 5 of the Summit Mountains. PIE stretch with breakpoints. The best image from the MEV and OIF.

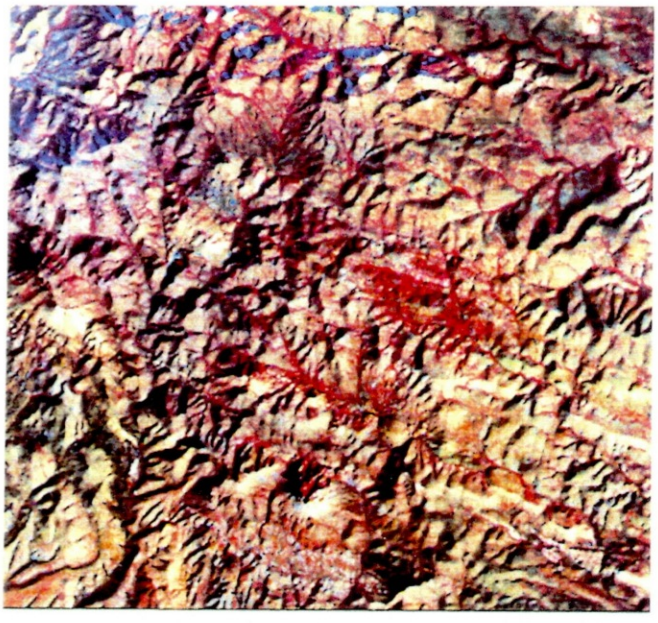

Figure 5.5 False Colour Composite 4 3 2 of the Summit Mountains. HSI transformed with hue and saturation increased and displayed in RGB.

interpretation.[1] The main geologic lithologies can be seen (Compare to Fig. 4.2) and broadly mapped. Based on colour and texture, volcanic rocks are separable from alluvial and colluvial materials. Intrusive volcanics such as dykes and plugs are recognisable and distinct from the host volcanics. It was possible to broadly discriminate the volcanic rock type composition e.g. acid, intermediate and basic and type, tuff, flow, or volcanoclastic, from colour and texture.

However it is not possible to consistently identify altered rocks, which generally appear similar to acid volcanics.

5.3 Band Ratios

a) Introduction

Iron oxides which occur on the terrain surface can be identified with several TM band ratios. The most widely used has been the 1.65/0.48μm (TM 5/1), e.g. Podwysocki et al (1983) at Cuprite, Nevada and Abrams et al (1977) in southern Arizona. Others have used 0.66/0.56 μm (TM 3/2) (Abrams et al 1983, Sadowski and Abrams 1982, Kepley et al 1982), 0.66/0.48 μm (TM 3/1) (Elvidge 1983,) and 1.65/0.8 μm (TM 5/4) (Loughlin and Tawfiq 1985). In contrast, the identification of surface clay bearing minerals is best done with the 1.65/2.22 μm ratio (TM 5/7), which has been shown by experimental work to be

---

1 *The resolution of Fig. 5.5 is superior to Fig. 5.4 because because the former was produced on a high quality colour film writer instead of being photographed from the VDU.*

directly related to the intensity of the 2.2 μm absorption feature (Buckingham and Sommer 1983).

All these ratios were assessed in the test area, using TM imagery and field spectral measurements. This section describes this work. The results are given in the following sections of this Chapter (Chap. 5.4 and 5.5).

b) Field Radiometry

The measurement and analysis of field reflectance data helps understand the relationship between the imagery and the ground features. Band ratio measurements were taken using a Barringer Hand Held Ratioing Radiometer on 33 sites, including a variety of hydrothermally altered rocks, volcanics and vegetation type (Tables 5.7 and 6.2).

The use of a ratioing radiometer simplifies the collection of reliable and usable results, because many of the complex factors which affect field reflectance measurements, such as topography, atmosphere, surface features and instrumentation, are eliminated or greatly reduced (Whitney et al. 1983). Nevertheless there were problems in collecting reliable data (Appendix III).

(c) Class Statistical Analysis

The six cover classes in the test area were examined to determine class separability with band ratios by using scatter plots and co-incident spectral plot (Table 5.9). A special procedure was written on the IIS system to display and merge spectral plots of the classes (Appendix

Table 5.7 Ratioing Radiometer Measurements of rocks in the Summit Mountains

No.	Alteration type	Locality	Iron Minerals	Clay Minerals	Ratio Type						
					Clay	Vegetation	Iron				
					5/7	4/3	5/1	5/4	4/2	3/2	3/1
1	Advanced Argillic	East Summit Ridge	Hematite	Nacrite, Kaolinite	1.80	1.05	1.33	0.99	1.23	1.30	1.64
2	Advanced Argillic	Whiskey Creek	Pervasive hematite, ferrihydrite	Diaspore, Kaolinite	1.50	1.05	2.70	1.60	1.39	1.36	2.12
3	Argillic	Blue Bell fault	Jarosite	Chlorite, Serpentinite	2.20	1.00	2.20	2.20	0.96	1.21	1.09
4	Propylitic	Blue Bell Fault	Hematite	Unknown	1.70	0.94	3.40	2.30	1.64	1.50	1.34
5	Propylitic	Blue Bell Fault	Hematite	Unknown	1.04	0.99	1.80	1.00	1.56	1.17	1.30
6	Propylitic	Laura Canyon	Hematite	Micas	1.17	1.00	1.13	1.04	1.47	1.27	1.40
7	Silicic	Blue Bell fault	Jarosite, Goethite ,Hematite	Dickite	2.56	0.92	3.90	2.62	1.37	1.34	1.05
8	Silicic	East Summit Ridge	Hematite	Nacrite, Diaspore	1.27	1.12	0.90	0.90	0.93	1.11	1.16
9	Silicic	East Summit Ridge	Ferrihydrite	Pyrophyllite, Kaolinite	1.59	1.00	1.22	0.90	1.12	1.10	1.24
10	Silicic	Blue Goose fault	Hematite, Magnetite	Micas	0.99	1.11	1.10	1.03	0.88	0.93	1.00
11	Unaltered	Blue Goose fault	Hematite	Micas	1.05	0.95	0.63	1.04	1.47	1.29	1.59
12	Unaltered	Mount Royal	Hematite	Micas	0.57	1.60	0.59	0.56	0.83	1.45	1.60

IV). Six TM ratios were assessed, 5/7, described in section 5.5, four iron oxide ratios, 5/1, 5/4, 3/1 and 3/2 described in Chapter 5.4 and a vegetation sensitive ratio, 3/4.

(d) Image processing and display

This section describes the ratio processing procedures used in my research and outlines guidelines for ratio processing. Ratio processing was divided into four stages, preprocessing, computation, enhancement and display, and photography, shown on figure 5.6.

FIG 5.6 RATIO PROCESSING STAGES

1. PREPROCESSING
Radiometric Correction
Geometric Correction
Atmospheric Correction
Noise Removal

2. COMPUTATION
Simple Ratio
Complex Ratio

3. ENHANCEMENT AND ANALYSIS
Ratio Selection
Histogram Analysis
Contrast Stretch
Filtering
Density Slice
Pseudo Colour
Filtering-noise removal
Colour Balance Check

4. PHOTOGRAPHY

All the preprocessing steps are required to produce good quality ratio images, although the geometric correction and the final noise removal are not essential. The radiometric correction is applied by using the IIS DESTRIPE function (Chap. 2.4), essential to remove serious image striping illustrated on figure 2.4.

The geometric correction was not necessary for the test area imagery, but was applied to the regional images (Chap. 2 and 7). If it is essential to retain radiometric fidelity, geometric corrections which involve resampling should be avoided, such as bilinear, or cubic convolution interpolation. Nearest neighbour resampling, which maintains the original pixel brightness values but gives inferior accuracy was adequate for my work.

Atmospheric corrections are essential for optimum performance of band ratios (Kowalik et al 1983, Crippen 1988a). Kriegler et al (1969) defined atmospheric effects on imagery as the sum of multiplicative and additive effects to scene radiance. The multiplicative component which includes atmospheric transmission, target reflectance and solar irradiance variables, is reduced by band ratioing. Additive effects, described as the diffuse light scattered into the path between the target and the sensor by the atmosphere and into the sensor from the environment (Vincent 1972) reduce image modulation (contrast) on satellite data and must be corrected before ratioing.

Crippen (1988a) describes several of the methods devised to correct for atmospheric and solar irradiance variations. A simple correction described by Ross (1976) which uses dark ground features to determine atmospheric path radiance, attributing the measured irradiance to atmospheric radiance, was applied to the TM data. This involved measuring the lowest intensity values for each band in an area of shadow or deep water and subtracting this value from all pixels in each respective band. This technique assumes that areas of shadow and deep water will

return zero intensity, any non-zero zero intensity are attributed to atmospheric scattering and sensor offset.

Problems can occur where there are no suitable shadows or deep water bodies, or where scattering is not uniformly distributed across the image. In the test area the offset was determined from a shadowed area of Steeple Rock Peak (Table 5.8). On the regional imagery the offset varied across the scene. The importance of the atmospheric correction is illustrated on Figure 5.7, a 5/1 ratio image of the test area.

Table 5.8 Atmospheric scatter and sensor offset for the Summit Mt. TM imagery

Band	Offset (DN)
1	50
2	16
3	15
4	13
5	6
7	2

Ratio computation involves the choice of the desired ratio type, either simple or complex. Complex ratios are where ratio band sums or differences are ratioed. Several complex ratios were used for vegetation assessment (Chap. 7.4). Image normalisation is a complex band ratio where each band is divided by the sum of all the bands. The effect is similar to a simple band ratio, in that common information is supressed. Rothery (1982) recommended the use of normalised band ratios for lithological discrimination within the Oman ophiolite using Landsat MSS data. Normalised ratios gave poor results for alteration

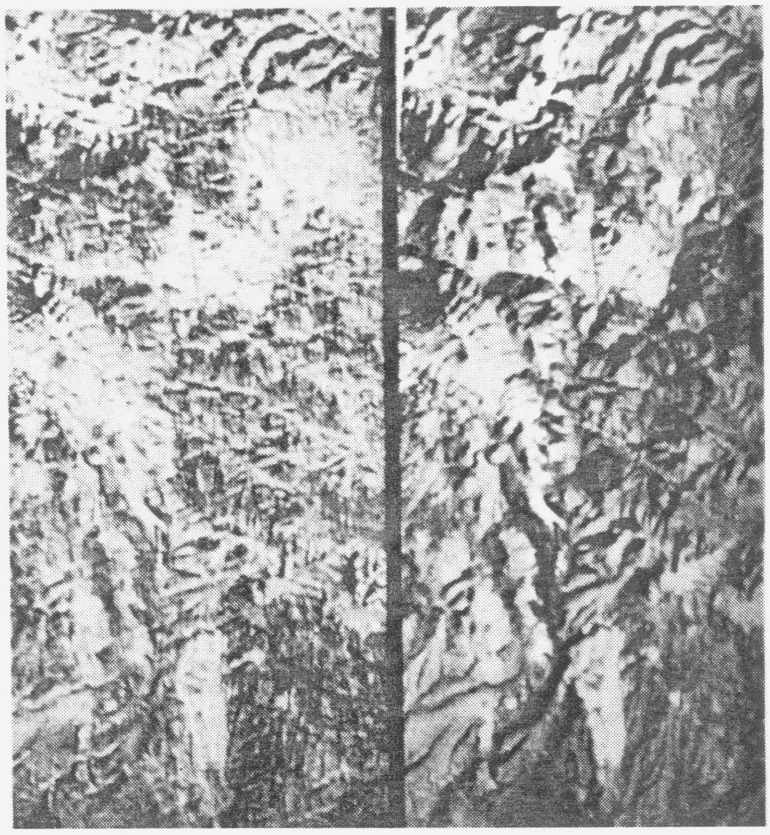

Figure 5.7 The importance of atmospheric corrections for ratio imagery illustrated on the TM 5/1 ratio of the western part of the Summit Moutains. The left side of the split screen is the corrected imagery and the right side is the uncorrected imagery.

mapping in the test area and so simple ratios were used.

The Enhancement and Analysis stage depends on whether the ratio image is to be used as a single band ratio or combined in a colour composite. For either, histogram analysis and contrast stretching are required. Contrast stretching is required because the dynamic range of the ratio is less than that of the original bands because radiance extremes caused by topography are removed (Schowengerdt 1983 page 58). In practice ratios seldom fall outside the range 0.25 to 4 (Drury 1986). Careful analysis of the ratio histogram enables optimum contrast stretches to be applied. Normally a linear stretch is applied to fill the full dynamic range of the display device (Sabins 1978), done on the IIS by SCALE. However this is not the best procedure because important information may be suppressed, e.g. due to compression if information lies on the tails of a histogram.

Initial preliminary assessment of ratios was done using automatic stretches which are quick and easily implemented. The IIS system supported several types (Chap. 2.5). The automatic linear stretch (SCALE) gave harsh images, saturated at the black and white ends. These images are not easy on the eye and there is information compression at the data range edges. Histogram equalisation reduced the contrast in very light or very dark areas and expanded the middle grey regions towards the low and high ends of the radiance scale, and the contrast was often harsh.

The most acceptable automatic stretches were the normalised stretches and adjusted stretches (HIST'N and ADJUST). For both, the mean and standard deviation of the

resultant image could be defined. The manipulation of the standard deviation was a rapid and effective way to display imagery with balanced contrast.

Best results were achieved by defining individual stretches following examination of the scene histogram and the identity of the classes of interest prior to stretching. The automatic functions could be used in this way by defining classes on the screen using a 'blotch' function, but better results were achieved by using a piecewise linear stretch with breakpoints specified from analysis of the histogram.

Filtering involved smoothing and edge enhancement operations (Chap. 2.5d). Smoothing of ratio images was used for simplifying images by removing noise and clutter. Median and low pass filters were used. Smoothing causes unpleasant blurring which was rectified by using the edge enhancement filter shown below, followed by a SCALE or PIE stretch.

A useful lowpass filter was

$$\begin{matrix} 1 & 2 & 1 \\ 2 & 3 & 2 \\ 1 & 2 & 1 \end{matrix}$$

and the edge filter was

$$\begin{matrix} -1 & 0 & -1 \\ -1 & 7 & -1 \\ -1 & 0 & -1 \end{matrix}$$

5.4 MAPPING IRON OXIDES

Iron occurs in hydrothermally altered rocks pervasively and as surface stains in the form of various oxides; hematite, goethite and ferrihydrite and as the sulphate jarosite. In the test area the iron oxides are predominantly surface stains of ferrihydrite - a poorly crystalline hydrated iron oxide. Hematite and goethite and less frequently jarosite occur around the mineralised areas, around and on the veins, on the silicified cappings and blowouts. Staining is also common throughout the propylitically altered volcanics, giving the characteristic reddening and coloration to the district. These iron oxides are readily visible in the field and on colour aerial photographs.

a) Ratio TM 5/1 (1.65/0.48μm)

When iron oxides are present this ratio emphasises the large reflectance difference between band 5, the peak infrared rock reflectance band, to band 1, which has low reflectance chiefly due to the intervalance charge transfer absorption centred in the ultraviolet. Ratio 1.65/0.48μm (TM 5/1) has been widely used for mapping iron oxides (Podwysocki et al 1983; Abrams et al 1977, and Rickman and Sadowski 1982).

The sensitivity of this ratio to iron oxides is illustrated by the field measurements (Table 5.7). The jarositic stained quartz vein (No.7), the pervasively hematised tuff (No.2) and the reddened andesite (No. 4) all have large ratio values. Generally all the altered rocks have ratio values above unity while unaltered rocks

were below unity.

Table 5.9 and Figure 5.8a demonstrates the class separability. The separability of the ratios are briefly discussed facing page 148 (in addendum).

Figure 5.9a is the fully processed ratio image. Optimum contrast was achieved from analysis of the scene histogram followed by a piecewise linear stretch. The atmospheric correction was particularly important for this ratio as image modulation effects are at a maximum between band 1 and band 5. Offsets were 50 and 6 DN for bands 5 and 1 respectively (Table 5.8, Fig. 5.7).

The brightest areas coincide with the most altered areas of Telephone Ridge (T), Bitter Creek (B), Raeburn (R), Vanderbilt Peak (V) and the Laura Alabama (LA) areas. Others include the Sycamore Creek (SC) extrusives and the andesites at McKelvey Place (M).

McKelvey Place was studied in detail because no alteration or mineralisation was known to exist there. Colour aerial photographs and a field visit showed that the high ratio value was caused by extensive surficial ferric oxide staining occurring on the propylitically altered basal unit of the Amygdaloidal Andesite unit. No signs of precious or base metal mineralisation were found, although there are several prospect pits where the micaceous mineral celadonite occurs, a mineral similar in appearance to oxidised copper minerals.

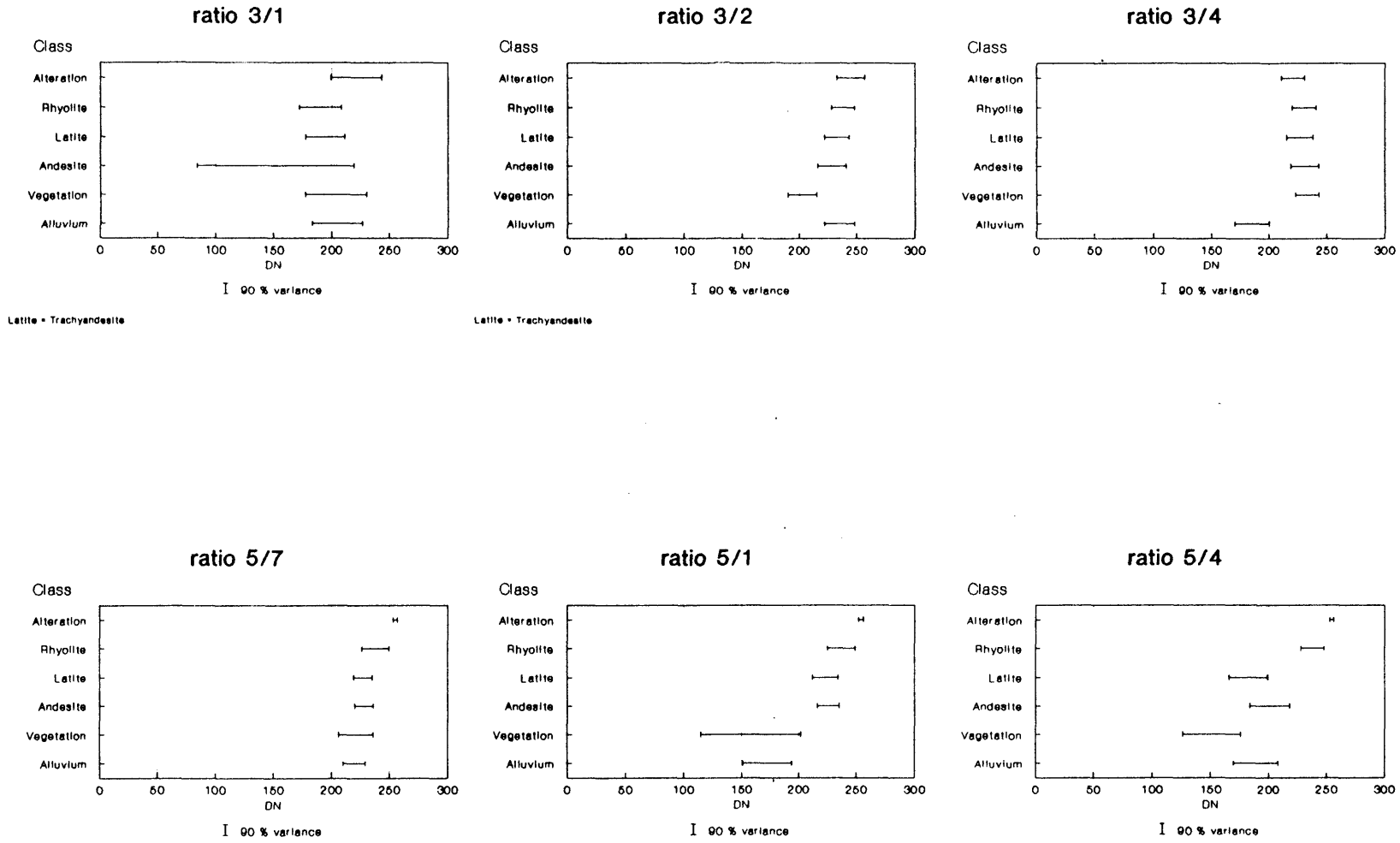

Table 5.9 Coincident spectral plots for the six cover classes in various TM ratios

Note on the scattergrams on Figure 5.8

[Because of the way class clusters are separated in ratio feature space (Fig. 2.5) ratio 5/1 and 3/2 are poor for class separation; on ratio 5/4 vegetation is partially separable from alteration, but there is significant overlap between volcanics, alteration and vegetation; and on Ratio 3/1 volcanics are partially separated from alteration, but vegetation and alteration are similar.]

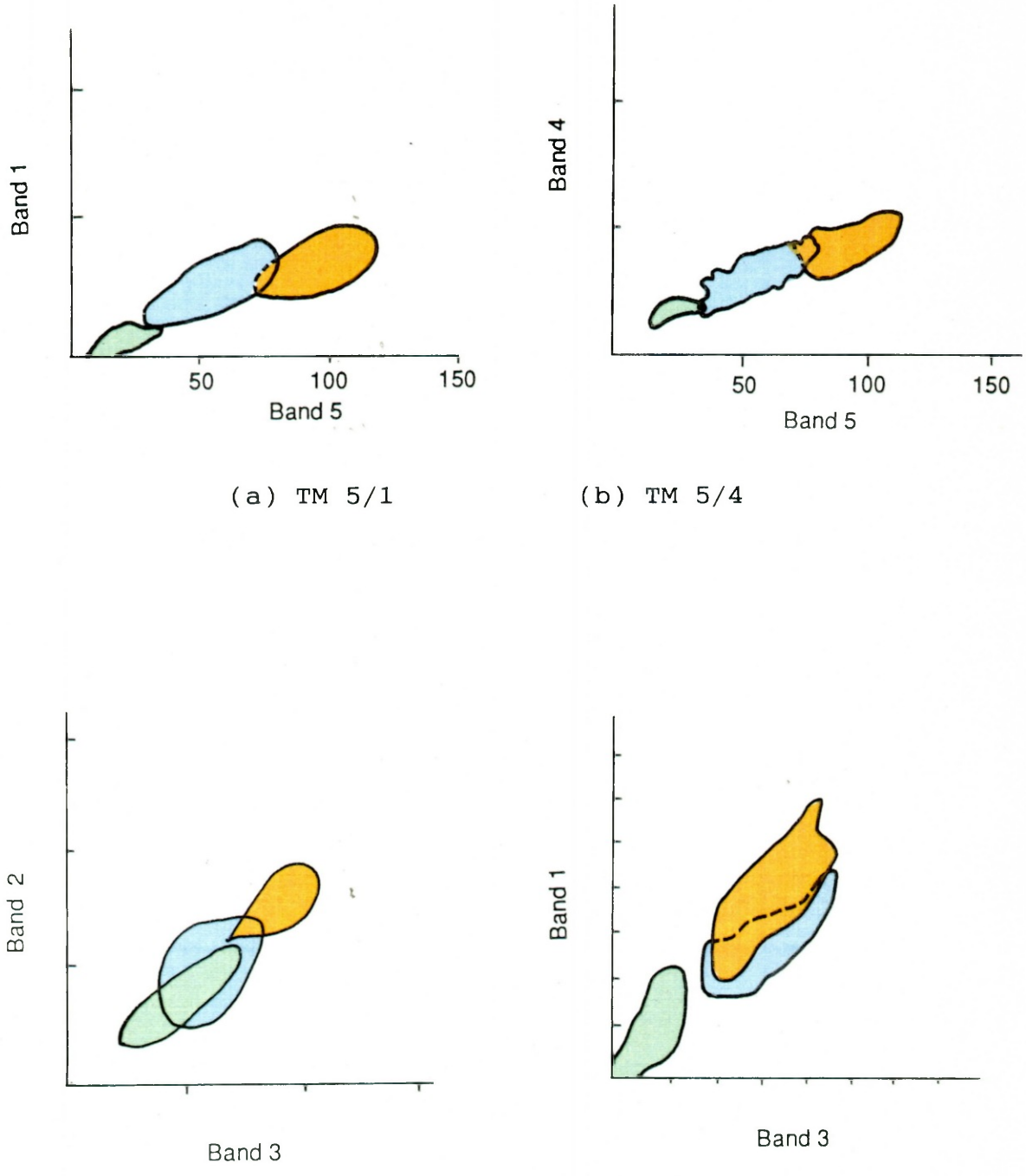

(a) TM 5/1 (b) TM 5/4

(c) TM 3/2 (d) TM 3/1

Figure 5.8 Scattergrams of the cover classes in the Summit Mountains in iron oxide ratio feature space.

Key:

Orange = Altered rocks
Blue = Volcanic rocks
Green = Vegetation

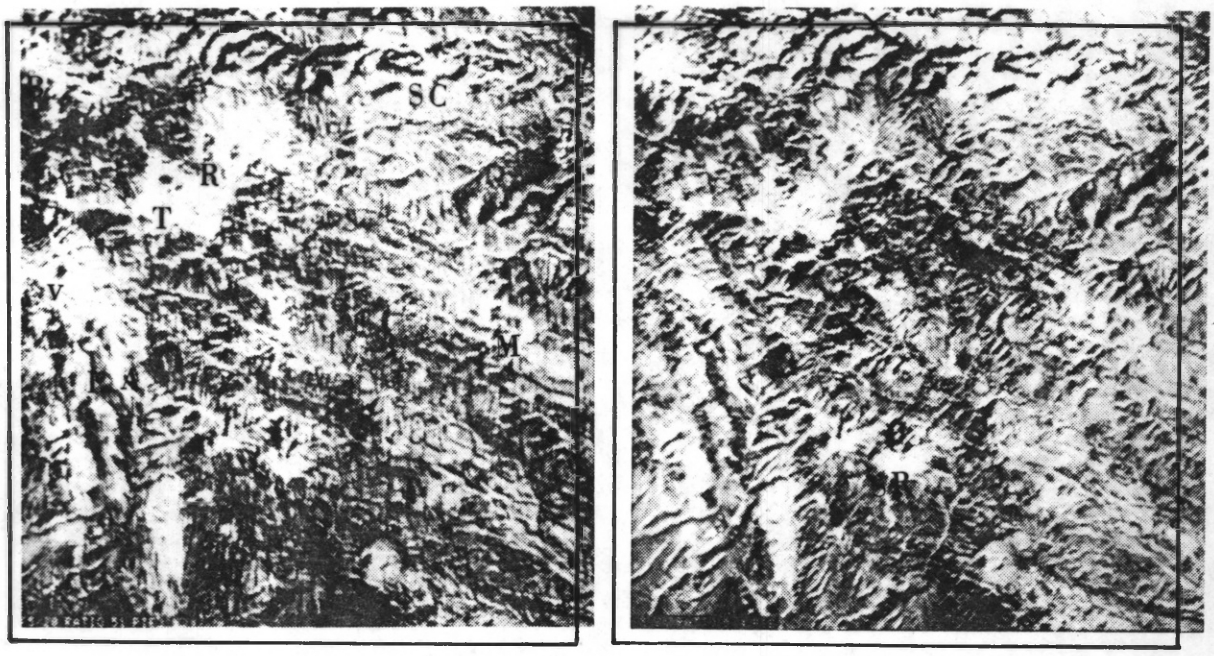

(a) TM ratio 5/1 (b) TM ratio 5/4

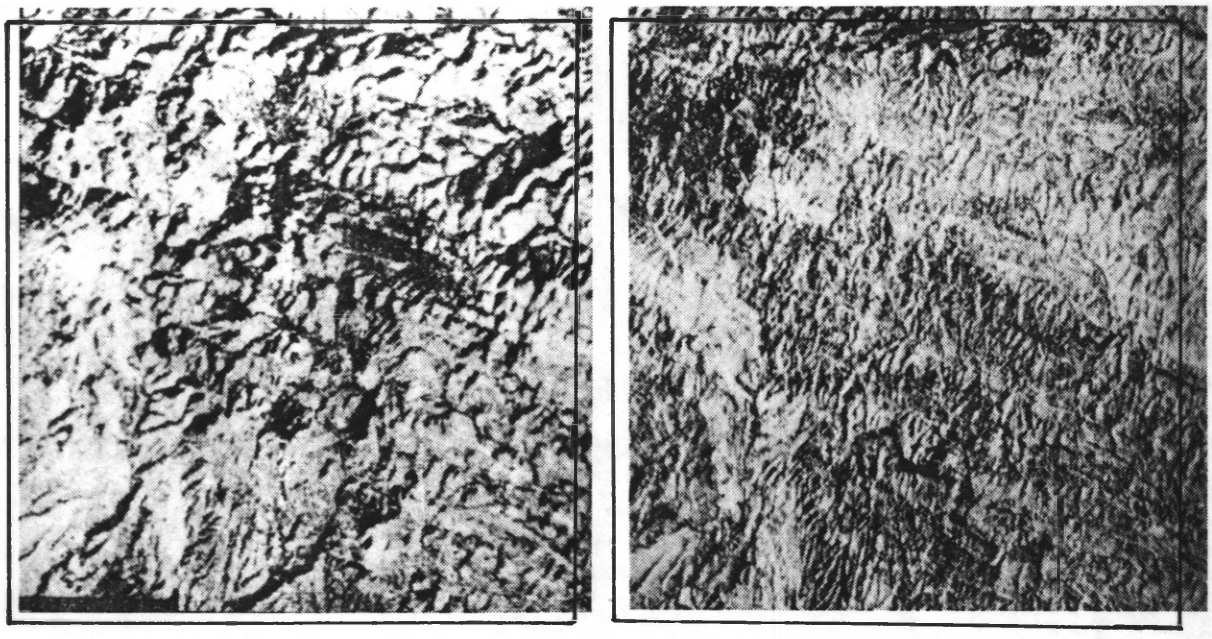

(c) TM ratio 3/2 (d) TM ratio 3/1

Figure 5.9 Iron oxide ratios of the Summit Mountains.

(a) TM ratio 5/1

(b) TM ratio 5/4

(c) TM ratio 3/2

(d) TM ratio 3/1

Figure 5.9 Iron oxide ratios of the Summit Mountains.

b) Ratio TM 5/4 (1.65/0.8 μm)

The hematite 0.85 μm absorption band and the weaker hematite-jarosite 0.9 μm absorption band both occur within TM band 4 (0.69 - 0.97 μm). Spectral reflectance (Appendix I) data show these absorptions may be resolvable yet this ratio has rarely been used.

Field measurements of the ratio (Table 5.7) show similar results to those of ratio 5/1. For altered and rhyolitic rocks there is high correlation (0.8) between the two ratios indicating that they are both good indicators or surface iron oxides.

Generally the 5/4 image is similar in appearance to the 5/1 (Fig. 5.9b) with the important addition of the clear separation between alteration and vegetation on the 5/4. Bright areas correspond to the main altered areas and McKelvey Place. However the rhyolitic rocks at Steeple Rock Peak (SR) are also bright and inseparable from the altered rocks. Table 5.9 and Figure 5.8b illustrate the overlap between the rhyolites and altered rocks, which are separable from the other classes.

c) Ratio TM 3/2 (0.66/0.56 μm)

The Landsat MSS band 5/4 ratio has been widely used with some success for mapping iron oxides (Vincent 1972). The TM equivalent of this ratio, ratio 3/2, has been used by several workers (Sadowski and Abrams, 1982, Kepley et al. 1982 and Abrams et al. 1983).

Field reflectance values (Table 5.7) did not show any

absorptions or correlation between the amount of alteration and the ratio value. Further the scattergram (Fig. 5.8c) and the coincident plot (Table 5.9) shows there is significant overlap between the classes. Nevertheless the ratio image (Fig. 5.9c) shows the altered areas at Telephone Ridge, Bitter Creek, and along the Laura-Alabama fault zone. Only altered areas are bright, vegetation is dark and all the unaltered rocks including the troublesome rhyolites are mid grey in tone.

d) Ratio TM 3/1 (0.66/0.48 μm)

Theoretically this ratio recognizes iron oxides because of the strong absorption of iron oxides in TM band 1 relative to TM band 3.

Field reflectance ratio values are high for all the rock types and like the 3/2 ratio there is no apparant relationship between the ratio value and the alteration. Like the 3/2 ratio the scattergram and coincident plot show considerable class overlap, however there is no separation of alteration from vegetation. On the image (Fig. 5.9ad) bright area include Telephone Ridge, Vanderbilt Peak, McKelvey Place and the Laura-Alabama area. The alteration at Bitter Creek is much less clearly defined. Non altered areas north of the East Camp fault also appear bright causing confusion on the image. Vegetation is mid to light grey in tone.

5.5 THE CLAY MAPPING RATIO

The hydrothermally altered rocks in the Summit Mountains contain several important hydroxyl bearing minerals including alunite kaolinite, pyrophyllite and sericite (Table 4.3). These minerals have absorptions occurring within the range of the TM band 7 (2.0 - 2.5 μm) which may be detected by dividing this band by TM band 5 (1.65 μm), the rock reflectance maximum.

Table 5.7 shows the TM 5/7 ratio (1.65/2.22 μm) field radiometer measurements. The ratio values for silicic and argillic rocks are high, averaging 1.8, while all other rocks, including propylitically altered rocks, have values around one. This shows that the hydroxyl absorptions in the altered rocks (except propylitic) are sufficient to be recognised by the ratio.

Figure 5.10 shows an interpretation of the fully processed 5/7 ratio image of the test area (Fig. 2.4). The brightest areas on Figure 2.4 are the pixels with the highest ratio values, and hence represent the areas with the greatest concentration of hydroxyl bearing minerals. The brightest and largest area occurs at Telephone Ridge, followed by Bitter Creek. These areas coincide with the silicic and advanced argillic alteration mapped on the ground (Fig. 4.6).

Smaller but equally bright areas occur at Raeburn, Vanderbilt Peak, Park Spring and in the volcanics of the Sycamore Group around Cherry Creek. Hydrothermal alteration is known at Raeburn (Chap. 4.6e) and Vanderbilt Peak which is part of the Laura-Alabama area (Chap. 4.6f),

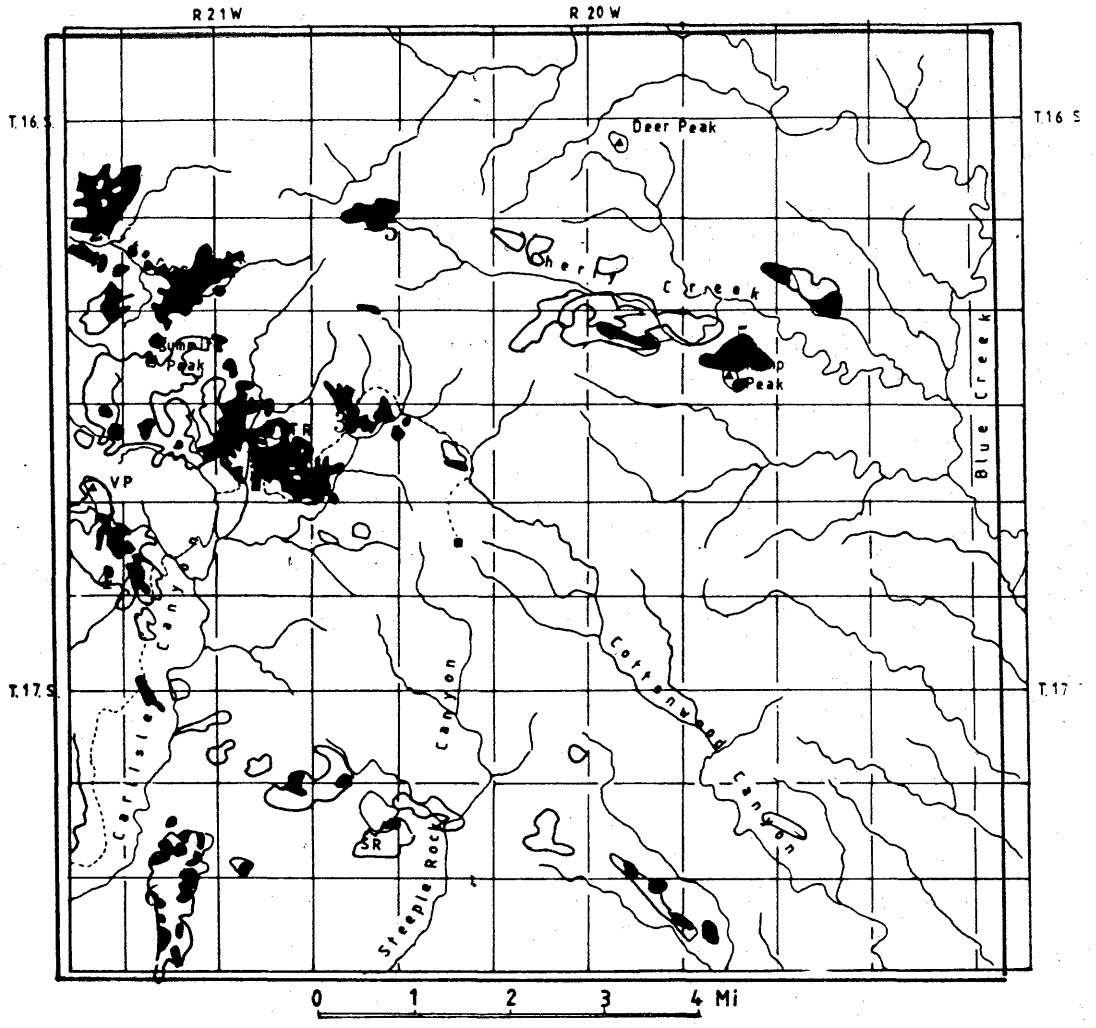

Figure 5.10 Areas with high hydroxyl aborptions as identified on the TM 5/7 ratio image of the Summit Mountains.

Localities:

1. Telephone Ridge
2. Bitter Creek
3. Raeburn
4. Vanderbilt Peak
5. Cherry Creek
6. Park Spring

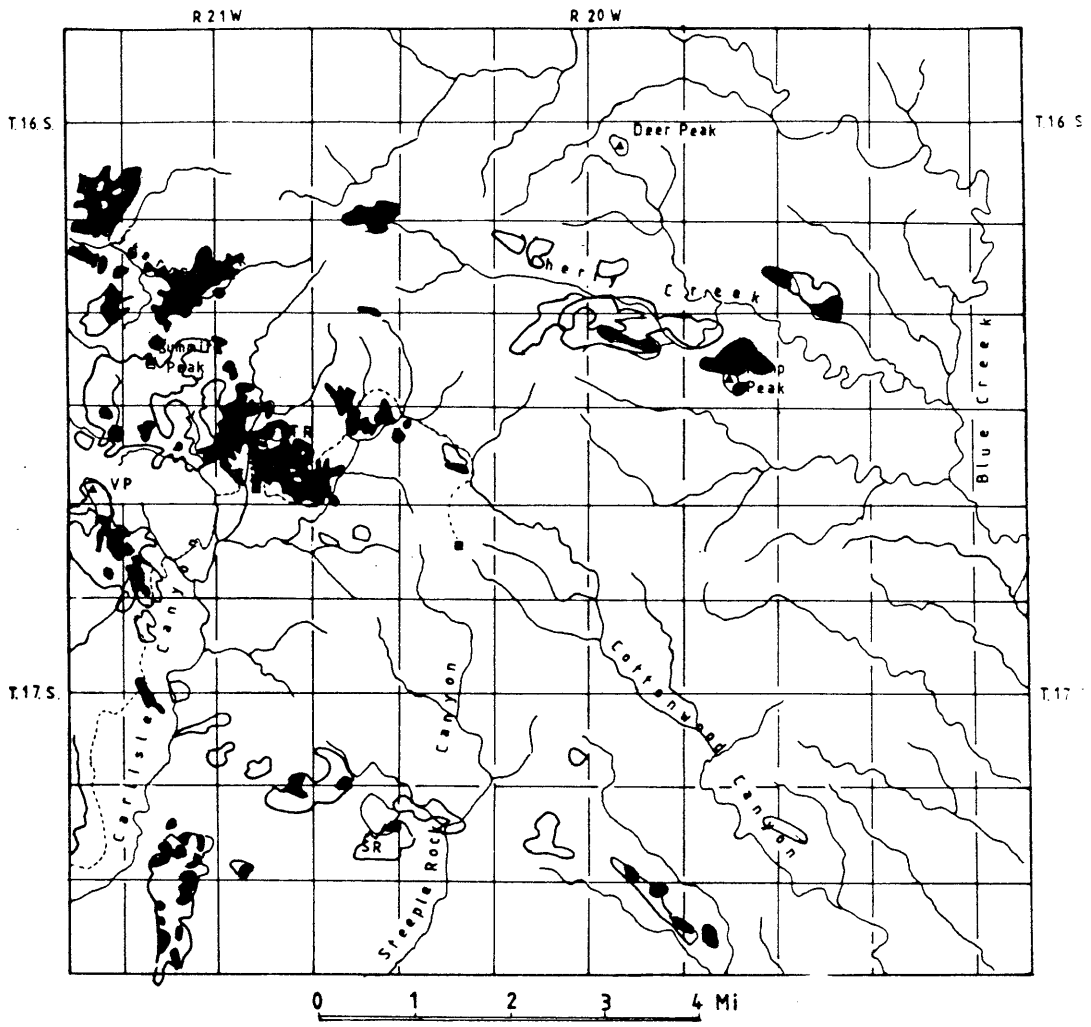

Figure 5.10 Areas with high hydroxyl aborptions as identified on the TM 5/7 ratio image of the Summit Mountains.

Localities:

1. Telephone Ridge
2. Bitter Creek
3. Raeburn
4. Vanderbilt Peak
5. Cherry Creek
6. Park Spring

but no alteration is documented at Park Spring, or around Cherry Creek.

The rocks around Cherry Creek are rhyolite flows, tuffs and pyroclastics of the Sycamore Camp eruptives (See 4.3j). Detailed mapping of the same unit at Deer Peak by Wahl (1980) revealed a tuff ring vent, capped by a rhyolitic plug and surrounded by a brecciated collar. Such tuff ring vents are commonly altered by post eruptive hydrothermal activity, or less commonly by reactions with high temperature water during eruptions or by slow alteration from ground water percolation (Heiken and Wohletz 1985).

The high TM 5/7 ratio absorption at Cherry Creek indicates the presence of alteration similar to that at Deer Peak. A radial intrusive feature visible on the aerial photographs coupled with the absorption evidence is strong evidence for the presence of a tuff ring vent at Cherry Creek.

The Park Spring area, southwest of Mount Royal, has been mapped as a tuff ring vent (Wahl 1980, Powers 1974) and as alluvial fan and pediment material (Elston 1960, Drewes et al, 1985). Wahl has attributed the confusion to a thin veneer of alluvial material covering the tuffs. The strong hydroxyl absorption recorded here indicates the presence of alteration and lends weight to the presence of a tuff ring vent, probably belonging to the Sycamore Camp eruptives.

Other less bright areas on the image are rhyolitic volcanics of the Bloodgood Canyon Tuff, and felsic units in the Virden Dacite.

[The intensity saturation on the TM 5/7 ratio is caused by the position of the alteration cluster in band 5 - 7 feature space (Fig. 5.11), because of the way in which feature space is divided by ratios (Fig. 2.5, page 38).

However, given the discrimination limits imposed by the ratio technique, it is possible to get around the intensity saturation caused by the scaling of the ISS, by comparing real ratio numbers to the distribution of the hydrothermally altered rocks.]

Class statistics from the main altered areas, rock units and terrain types are shown on table 5.10. Quantitative analysis of the 5/7 ratio image is instructive:

(1) All the classes occupy a narrow range and there is significant overlap of both the individual locality sets and the generic classes.
(2) The altered rocks have the highest values which are clustered around 255. Examination of the altered pixels showed the median value to be 255.

The intensity saturation of the altered pixels, means that variations in hydroxyl intensity are not measurable. Contrast enhancement cannot get around this problem as single intensity DN values cannot be divided and stretched.

In Chapter 2.6 two techniques for improving class discrimination were described, inverse ratios, and negative band ratios. These techniques were applied to the intensity saturation problem of the alteration on the 5/7 ratio but made no difference to image discriminability.

The negative band ratio technique was assessed on the six classes using scattergrams on the IIS system. A special display technique was devised to capture and display the clusters from several classes on one scattergram (Appendix III). In TM band 7, band 5 feature space (Fig. 5.11a) alteration is separable from andesites and latites. There is however a small overlap with rhyolites and vegetation. In band 7 negative band 5 feature space alteration and all the other classes have greater ratio intensity values as

Table 5.10 Co-incident spectral plot of various cover types in TM ratio 5/7

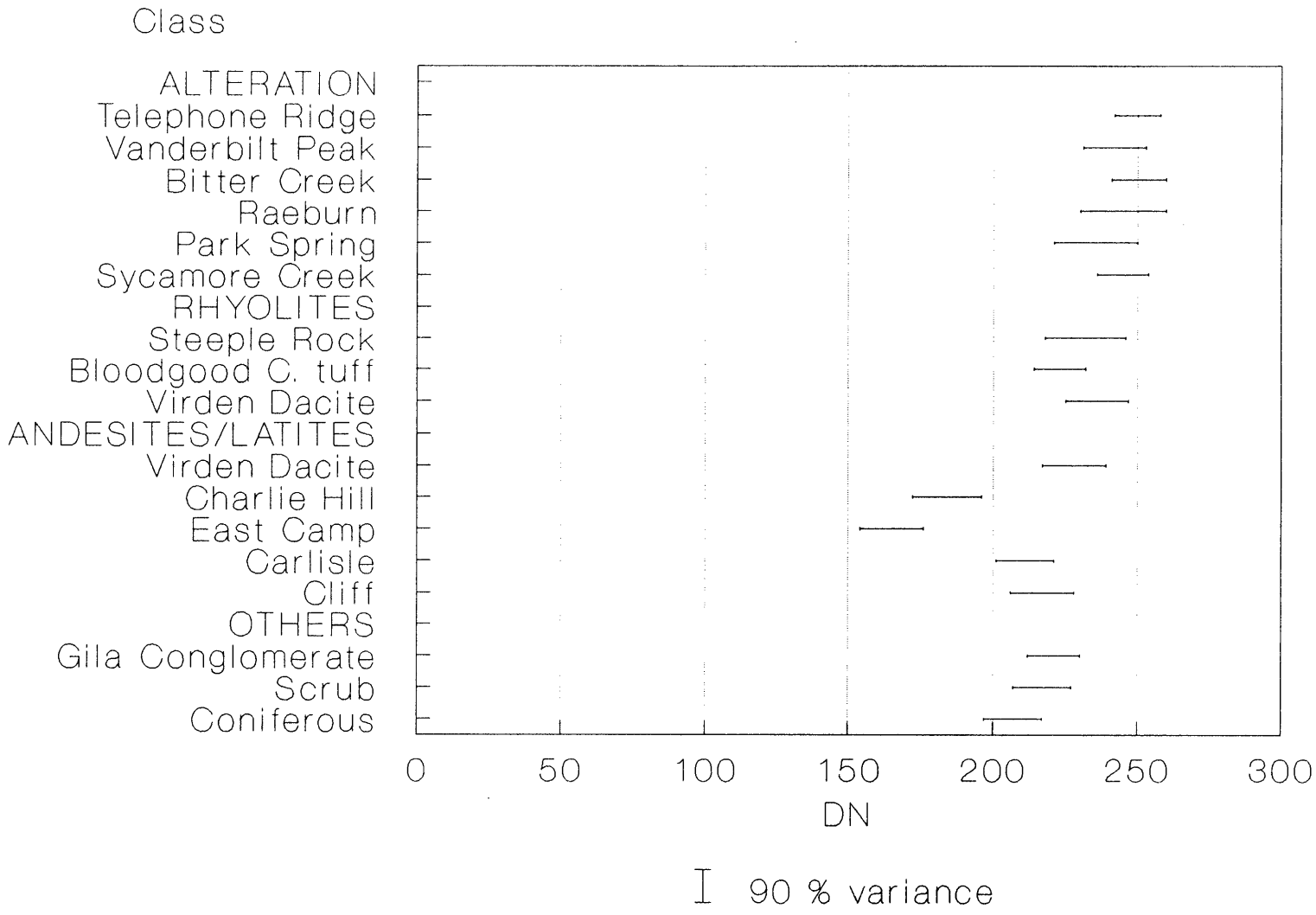

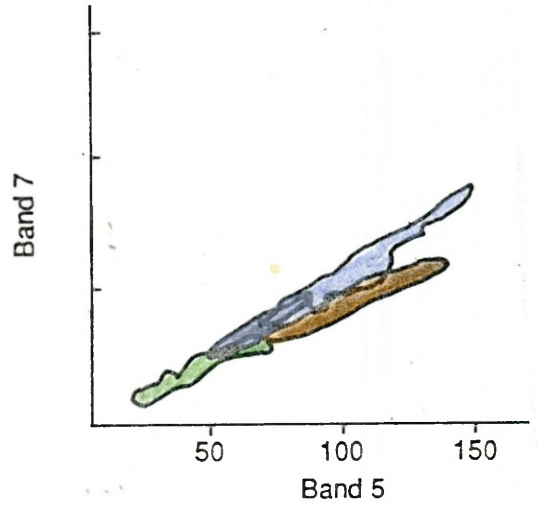

(a) TM band 7 band 5 feature space

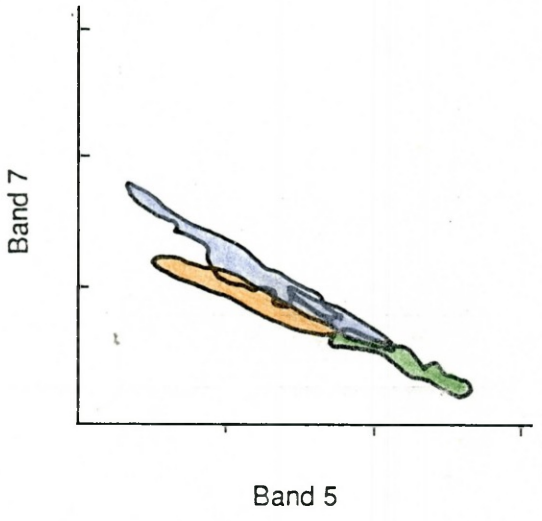

(b) TM band 7 negative band 5 feature space

Figure 5.11 Scattergrams of the Summit Mt. ground classes in TM 7/5 and TM 7/-5 feature space. Key as in figure 5.8.

predicted. However the ability to discriminate alteration from the other classes is lost; alteration, rhyolites, andesites and latites all have similar ratio values (Fig. 5.11b).

If all classes except alteration were masked prior to the ratio computation then variations in the 5/7 intensity and hence hydroxyl intensity could be mapped. This was attempted by level slicing of bands 5 and 7 to isolate altered pixels. Using the IIS Level Slice and Feedback operations all pixels outside a defined area of interest may be given an arbitrary intensity value, in this case zero, while pixels within the area of interest remain unchanged. Alteration could be isolated satisfactorily in band 5 but not in band 7, where there was significant overlap between alteration rhyolites and latites.

Attempts to extract information from the TM data on alteration intensity based on hydroxyl absorptions were unsuccessful.

Although variations in the intensity of alteration within the altered rocks could not be extracted, useful information was provided using standard enhancement techniques, such as contrast stretching, low pass filtering and psuedo-colouring of the 5/7 ratio image (Fig. 5.12).

Filtering removed noise and simplified the image structure. An exponential stretch simultaneously expanded the range of the upper ratio levels (but not those at 255) and decreased the range of the lower levels. While not allowing discrimination between altered rocks, differences between the altered and rhyolitic rocks are enhanced.

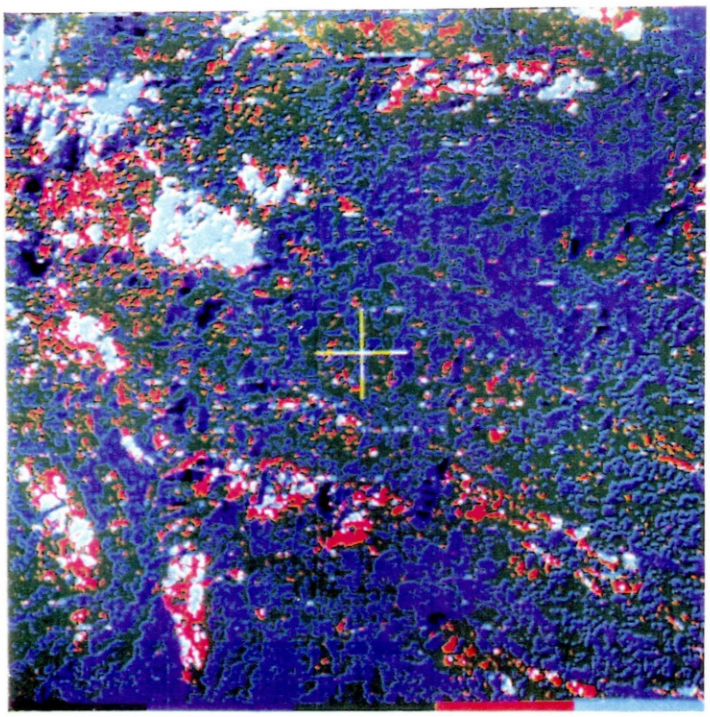

Figure 5.12 Processed TM 5/7 ratio image. Contrast stretched (exponential) low pass filtered, level sliced and psuedo-coloured.

Key:

Cyan	Alteration
Red	Rhyolitic rocks (& minor propylitic)
Green	Trachyandesites
Blue	Andesites basalts and vegetation
Black	Shadow

Light blue colours on the image represent the most altered rocks (and some rhyolites), red is predominantly rhyolitic flows, tuffs and volcanoclastics, green is trachyandesites and blue andesitic to basaltic rocks and vegetated areas.

5.6 RATIO COLOUR COMPOSITES

a) Introduction

The combination of three ratio images in a colour ratio composite (CRC) is an effective way to display and combine spectral information from three ratio bands in one colour image. Image processing steps were as set out in Chapter 5.3d. The most important step is band selection. With TM data there are 455 ratio combinations possible (Chap. 2.3). Selection can be based on statistical measurements of information content (Chap. 5.2) or on empirical based critria, such as the known or predicted spectral signatures of the features of interest.

Ideally, each ratio combination should be photographed, analysed and compared with all other ratios to give a qualitative assessment. However the large number of ratios preclude this systematic approach. The colour ratio composites were produced using rapid automatic contrast stretches and were assessed visually on the VDU. Ratios which appeared promising for alteration or lithological discrimination were retained for further image processing and analysis.

b) Statistical Ratio Selection

The MEV statistical routine described for the TM band analysis (Chap. 5.2) was applied to CRC selection. This was done under the assumption that the three combined ratios images with the largest volume of information, would contain the most spectral information and would hence be a good image for interpretation.

The MEV routine was applied to both the simple ratios and to the simple ratios with vegetation removed (for details of the masking operation see Chap. 7.4). Table 5.11 show the top ten ranked CRCs with and without vegetation.

Visual analysis of these CRCs showed all were high contrast noisy images which were poor for discriminating alteration. Figure 5.13 shows the positions of the useful CRC images for alteration mapping superimposed on the complete MEV curve for all 455 possible CRCs.[1] The highest ranked CRC useful for alteration mapping (5/7 5/1 3/1) was ranked number 43. Other useful CRCs were ranked at 151 (5/7 5/4 5/7), 159 (5/7 5/4 3/1), 205 (5/7 5/1 4/3), 248 (5/7 5/1 3/2), 277 (5/7 3/4 3/1), 350 (5/7 5/4 3/4) and 384 (5.7 5/4 3/2). Clearly CRCs useful for alteration mapping are unrelated to the total volume of image content.

The removal of vegetation from the imagery had little affect on the MEV rankings. However the ranking of CRCs containing the 3/4 ratio are decreased, i.e. the removal of vegetation increases data redundancy.

---

1 *Interestingly Figure 5.13 shows a significant reduction in data volume after rank 400. These tend to be CRCs containing visible bands e.g. TM 1/2 1/3 2/3.*

Table 5.11 Comparison of top ten MEV ranked CRC's for original and HSI vegetation masked imagery in the Summit Mountains

	Original imagery	Vegetation masked imagery	
Rank	Combination	Combination	Change
1	1/4 1/5 1/7	1/4 1/5 1/7	0
2	1/3 1/5 1/7	1/3 1/5 1/7	0
3	1/2 1/5 1/7	1/2 1/5 1/7	0
4	1/5 1/7 4/7	1/5 1/7 4/7	0
5	1/4 1/7 5/7	1/4 1/7 5/7	0
6	1/3 1/7 5/7	1/3 1/7 5/7	0
7	1/3 1/7 4/7	1/5 1/7 3/7	3
8	1/3 1/4 1/7	1/4 1/7 4/7	3
9	1/2 1/4 1/7	1/2 1/4 1/7	0
10	1/5 1/7 3/7	1/5 1/7 5/7	4

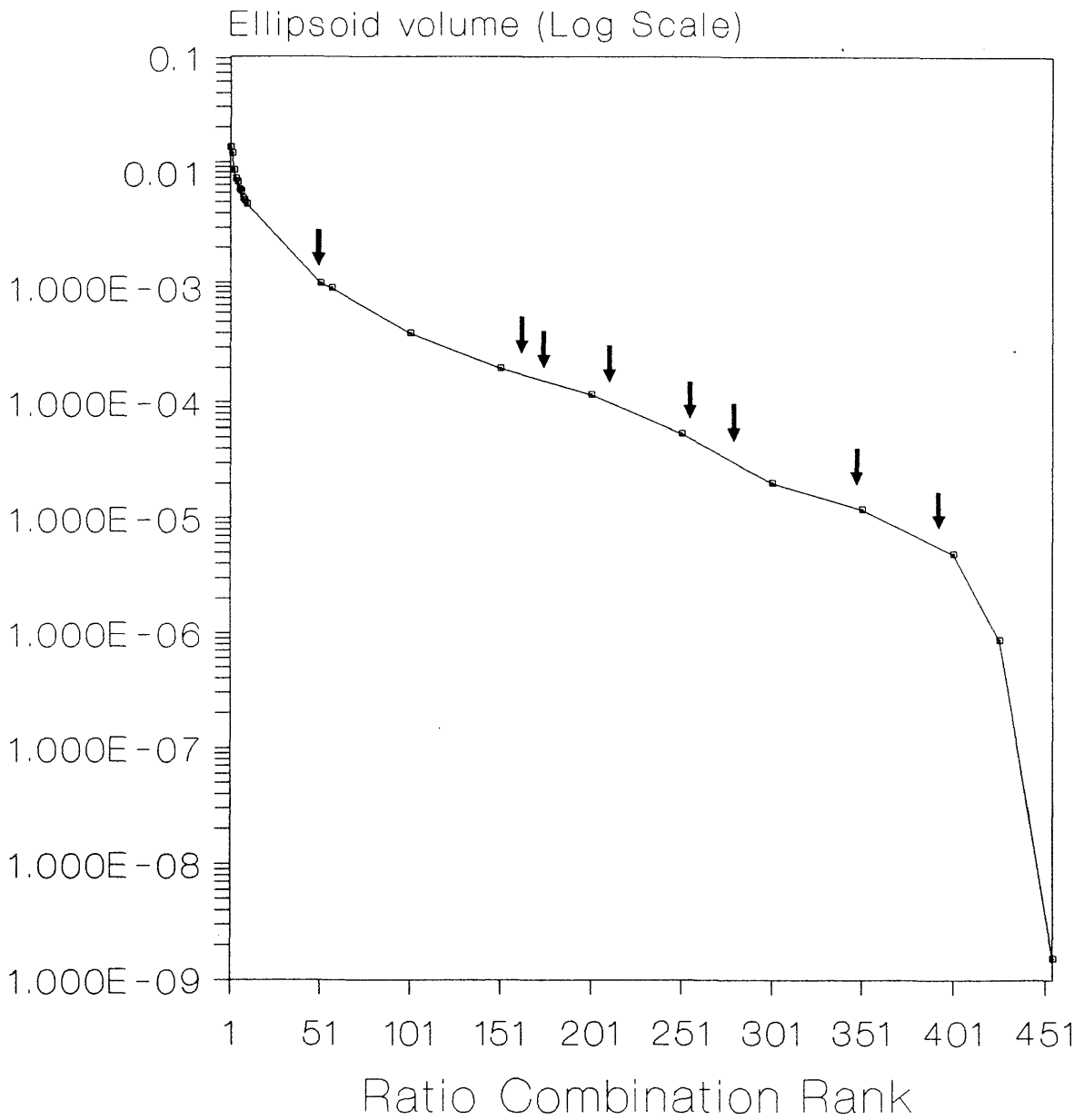

Figure 5.13 Positions of the best CRCs for alteration mapping on the MEV curve for all 455 possible CRC combinations.

c) Empirical CRC Selection

The number of CRC combinations remains large even when the choice of ratios is restricted to those with known or predicted results. The possible CRCs were categorized into three types, depending on the properties of the ratios with respect to clay, iron oxides and vegetation. The types are:

Type 1 CRCs with ratios sensitive to clay, iron oxides and vegetation.

Type 2 CRCs with ratios sensitive to clay and iron oxides only.

Type 3 CRCs without the clay sensitive ratio.

The ratios are listed on table 5.12. For processing details refer to Chapters 2.5a and 5.3.

Type 1 Combinations

CRC with a clay and iron oxide sensitive ratio and a vegetation ratio have been widely used for alteration mapping in arid and semi-arid terrain e.g. Podwysocki et al (1983). If there is a standard colour composite ratio for alteration mapping then a combination within this group is it.

The reasoning behind these CRCs is based on the common observation of the sensitivity of the 5/7 ratio to both hydroxyl bearing minerals and leaf water moisture which potentially renders altered and vegetated areas spectrally similar on the 5/7 ratio image. The combination of a negative vegetation index, usually in the form of the TM 3/4 biomass sensitive ratio, visually untangles the effects of competing 5/7 and 3/4 ratios, hence separating clay alteration from vegetation.

Table 5.12 Colour Ratio Composite Groups

Group 1

5/7	5/1	3/4
5/7	5/4	3/4
5/7	3/2	3/4
5/7	3/1	3/4
5/7	4/2	3/4
5/7	5/1	4/3
5/7	5/4	4/3
5/7	3/2	4/3
5/7	3/1	4/3
5/7	4/2	4/3

Group 2

5/7	5/1	5/4
5/7	5/1	3/2
5/7	5/1	3/1
5/7	5/1	4/2
5/7	5/4	3/2
5/7	5/4	3/1
5/7	5/4	4/2
5/7	3/2	3/1
5/7	3/2	4/2
5/7	3/1	4/2

Group 3

5/1	5/4	3/1 or 4/3 or 3/4
5/1	5/4	3/2 ..
5/1	5/4	4/2 ..
5/1	3/1	3/2 ..
5/1	3/1	4/2 ..
5/1	3/2	4/2 ..
5/4	3/1	3/2 ..
5/4	3/1	4/2 ..
3/1	3/2	4/2 ..

All of the type 1 CRCs were assessed. Examples are shown on figures 5.14 and 5.15. Figure 5.14 is a 5/7 5/1 3/4 CRC with a PIE contrast enhancement (Chap. 5.3d). Notice alteration on Telephone Ridge and Vanderbilt Peak is a bright yellow with minor pink and and red areas. Yellow indicates clay and iron oxides are present, and red indicates clay alone.

Rhyolitic rocks are a dull yellow and are a possible source of spectral ambiguity. Trachyandesites appear purple to reddish purple. The redder hues appear in the areas of propylitic alteration, possibly due to stronger hydroxyl absorptions. Andesites and basaltic rocks are blue except were there are dense areas of vegetation or areas of intense iron surface stains without clay alteration, where they are cyan. Both vegetation and iron oxides appear green due to high 5/1 ratio values (See Table 4.7). Reversal of the vegetation index made little difference to the image.

Figure 5.15 is CRC 5/7 5/4 3/4 with a histogram equalisation contrast stretch. Alteration is yellow on Telephone Ridge, Raeburn, Bitter Creek and Vanderbilt Peak, with smaller areas at Summit Peak and Kemp Peak (part of the Sycamore Camp Eruptives).

Rhyolitic rocks are cyan indicating high 5/4 and high 3/4 ratio values. Andesites and trachyandesites are blue indicating high 3/4 values. The propylitised volcanics on Summit Peak appear yellowish green and red indicating the presence of iron oxides and clays but in amounts less than on Telephone Ridge. Vegetation appears dark reddish

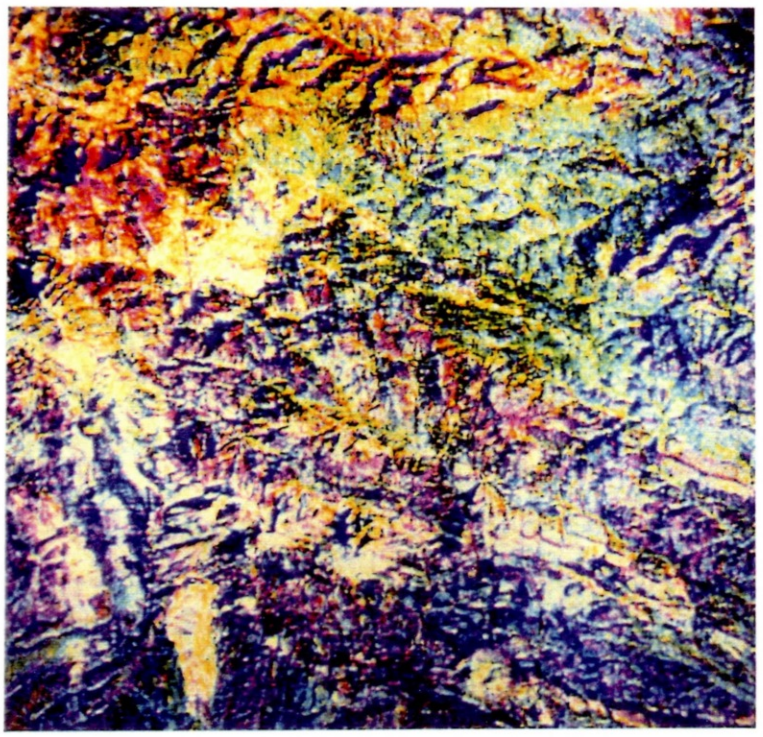

Figure 5.14 Colour Ratio Composite 5/7 5/1 3/4 of the Summit Mountains. Piecewise linear stretch. (See text for description).

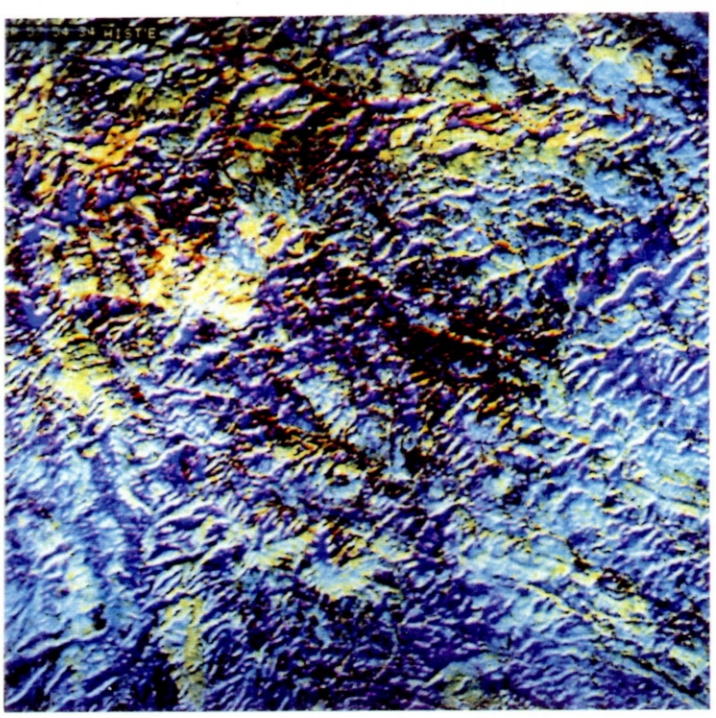

Figure 5.15 Colour Ratio Composite 5/7 5/4 3/4 of the Summit Mountains. Histogram equalisation stretch (See text for description).

brown. The Cherry Creek rhyolites in the north of the image are green because of high iron content.

This CRC is superior to the former because vegetation is separated from iron oxides and rhyolites are separated from altered rocks.

Type 2 Combinations

It may be possible to dispense with a vegetation index because of the the relatively low amounts of vegetation in the test area, allowing the attractive combination of a clay ratio with two iron oxide sensitive ratios.

Ten type 2 CRCs were evaluated and all gave satisfactory results, except for CRC 5/7 5/1 3/1 on which vegetation and iron oxides could not easily be separated because both have high 3/1 and 5/1 ratio values. Figure 5.16 (5/7 5/1 5/4) is an example of one of the better CRC images. The clay and iron oxide rich areas are white because of the strong absorptions occurring in all the ratios. Where clay alteration is dominant red colours occur e.g the top of Telephone Ridge, East Summit Ridge Vanderbilt Peak and Kemp Peak. Other areas of iron oxides without clays occur at Mckelvey Place and north of the Blue Bell fault.

The trachyandesites appear purple and andesites cyan, showing the higher clay content of the former and the greater iron content of the latter. Vegetated areas are blue or cyan the high 5/1 ratio values.

Type 3 Combinations

CRCs without the 5/7 ratio were poor for alteration

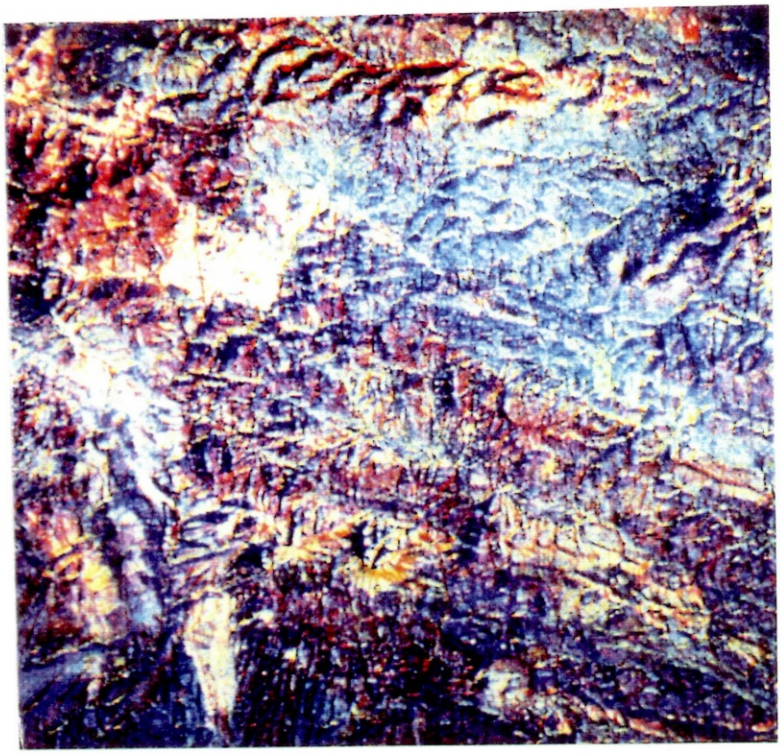

Figure 5.16 Colour Ratio Composite 5/7 5/1 5/4 of the Summit Mountains.

mapping because iron oxide by itself is not diagnostic of hydrothermal alteration.

5.7 PRINCIPAL COMPONENTS ANALYSIS

(a) Single Bands

The six PCT images are illustrated in figure 5.17. Each PC image has been normalised and given a linear contrast stretch.

PC1 shows all the common spectral information of the TM data, showing topography, drainage features and vegetated areas (dark tones). Altered rocks and acid volcanics appear as bright tones. If one monochrome image is to be chosen for geological interpretation the first principal component is the optimum choice. PC2 appears like a negative image of PC1. Little geological information on lithology is shown.

On PC3 altered areas in the Laura Alabama area, Telephone Ridge, Pinon Mountain and Bitter Creek are represented by light tones. Middle grey tones on the centre right of the image correspond to iron rich Amygdaloidal Andesites. PC3 appears to be responsive to the degree of surface iron content (compare with a 5/1 or 5/4 ratio).

On PC4 the darkest areas approximate to the distribution of silicic, advanced argillic, argillic and argillic-sericitic alteration, and also to some acidic

Eigenvectors of the Summit Mountain Image

	TM Bands					
	1	2	3	4	5	7
PC1	0.24	0.17	0.29	0.31	0.73	0.44
PC2	0.54	0.29	0.44	0.41	-0.47	-0.21
PC3	-0.80	0.12	0.33	0.48	-0.10	0.00
PC4	-0.03	0.08	0.20	-0.03	-0.44	0.82
PC5	0.12	-0.38	-0.55	0.64	-0.19	0.31
PC6	-0.06	0.85	-0.52	0.04	-0.02	0.05
% PC Variance						
	89.10	7.44	2.06	0.79	0.46	0.15

The high contribution of band 7 to PC4 clearly shows that PC4 is showing the greater part of the hydroxyl absorptions.

(a) PC 1

(b) PC 2

(c) PC 3

(d) PC 4

(e) PC 5

(f) PC 6

Figure 5.17 Principal Component Images 1 - 6 of the Summit Mountains. Normalised and linear contrast stretched.

rocks. The silicification along the Blue Bell fault, the argillic alteration on Vanderbilt Peak and the altered tuffs of the Cherry Creek rhyolite and Sycamore Camp Eruptives are particularly well shown. However not all dark areas are altered areas related to epithermal mineralisation; note the silicic flows of the Virden Dacite.

PC5 is not affected by striping which is prevalent on PC4, indicating the striping is caused by a systematic sensor error and is not random (Chap. 2.4b). The image shows vegetated areas in bright tones. The silicic and advanced argillic alteration on Telephone Ridge appear black. PC6 shows noise.

PC1 holds nearly 90 % of the image variance, leaving 10 % for the remaining PCs. Alteration contributes mostly to PC4 (mainly clay) with smaller amounts in PC3 (iron) and PC5 (intense hydroxyl).

Further processing on PC4 to enhance the silicic and advanced argillic alteration is shown on figure 5.18. The image is centred on Telephone Ridge. A low pass rectangular filter reduced noise and striping, and a logarithmic stretch brightened up the darker areas to improve discrimination between the altered rocks. Psuedocolouring brings out the intensity of alteration from the greatest (dark blue) to the least (light green). Pink is intermediate and the light blue areas are unaltered.

The alteration on the Telephone Ridge, Bitter Creek, and Raeburn areas is clearly shown. On Telephone Ridge there are three areas of intense alteration; on the southeast

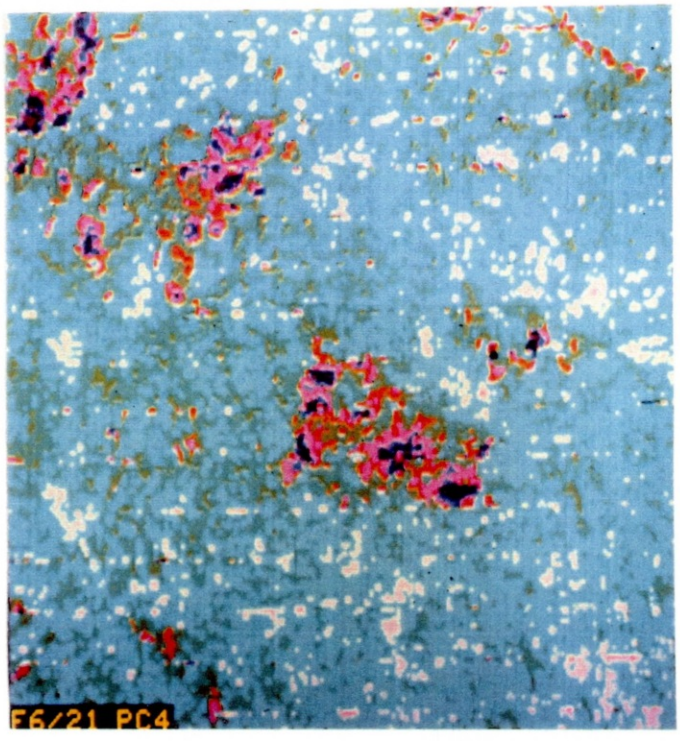

Figure 5.18 Psuedocoloured PC 4 image of Telephone Ridge. Logarithmic contrast stretch. Note the centres of intense alteration (dark blue). See text for full discussion.

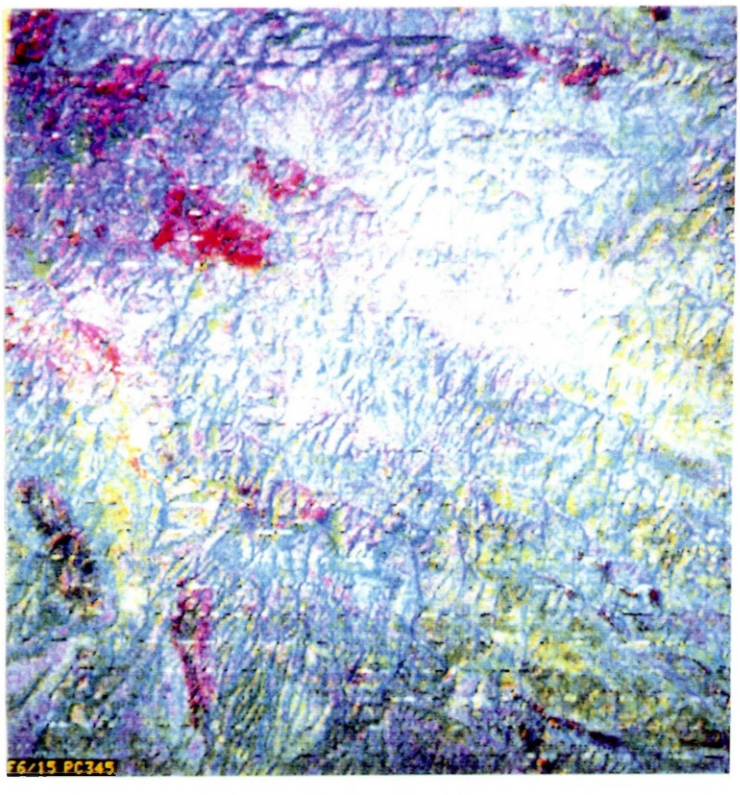

Figure 5.19 Principal Components 3 4 5 of the Summit Mts. displayed as a colour composite. See text for discussion.

end of the ridge, the centre, and across Carlisle Canyon on the west side Of East Summit Ridge. These correspond to the most intense silicic altered areas and the area where there are north trending silicic pipes cutting through the surrounding argillised tuffs (Fig. 4.6). The light green areas broadly represent propylitic alteration on the periphery of the higer grade altered areas.

(b) Colour Composites

Colour composite PC images allow most of the image scene imformation to be displayed in one image. Any of the combinations using PC1 introduce drainage and topography, which may be useful for location purposes. The best composite for alteration mapping was PC345 (Fig. 5.19) Silicified and argillic alteration assemblages appear red, iron oxides green and vegetation magenta. However the image is poor for lithological discrimination - andesites, trachyandesites and rhyolites all appear similar (cyan).

5.8 DISCUSSION

(a) Image Processing techniques

A range of image processing techniques were used to enhance and extract TM imagery to map alteration types and to provide geologic information to help characterise the epithermal system type in the Summit Mountains. Of the three image types used band ratios and PCs were most effective for alteration mapping.

The individual TM bands were poor for lithological and alteration mapping (altered areas could not be discriminated from rhyolites). For lithological discrimination the best colour composites were combinations 135 and 145. There was little difference between the 5 top ranked combinations from the 20 possible. Composites 321 (natural colour), 432 (false colour) and 752, recommended for mapping in mineralised terrain (Loughlin and Tawfiq 1983), were poor for lithological mapping.

Ratio images with the input bands corrected for additive atmospheric radiance, reduce the dominant topographic illumination affects and enhance spectral information of the imagery. Ratio image 5/7 allowed hydroxyl bearing minerals to be mapped. All the iron oxide sensitive ratio images detected the presence of surface iron oxides, although spectral ambiguity occurred with ratio 3/1. Ratio images 5/4 and 3/2 were superior to the more commonly used 5/1 4/2 and 3/1 ratios.

Colour ratio composites (CRCs) not containing the 5/7 ratio were poor for alteration mapping (because iron oxides alone are not sufficiently diagnostic of hydrothermal alteration). The commonly used CRCs e.g. 5/7 5/1 3/4, identified the altered areas. However the best results were achieved using the 5/7 ratio with either the 5/4 or 3/2 iron oxide ratio in combination with the standard vegetation ratio. It made no difference whether the vegetation ratio was positive or negative i.e. 4/3 or 3/4. Information on the relative distribution of clay and iron oxide minerals was possible with CRCs.

The PC4 image clearly delineated the distribution of the epithermal alteration assemblages, but did not discriminate between them. An exponential contrast stretch, low pass filtering, and colour level slicing produced a very good representation of the degree of hydroxyl development in these areas. However unlike the TM 5/7 ratio, without ground control it would not have been possible to identify these areas as altered. Colour composite PC images did not give any information not observed on the ratio or TM band imagery.

Statistical band selection for colour composite generation worked well for TM bands but was poor for CRC selection. Empirical selection of CRCs gave the best results.

The HSI transform applied to TM band colour composites produced excellent images for lithological discrimination. Intrusives were separable form volcanics and sedimentary rocks and acid, intermediate and basic volcanic flows, tuffs and volcanoclastics were discriminated. However hydrothermally altered rocks appeared similar to rhyolites.

Spatial filtering techniques for image enhancement were useful for both simplifying and removing noise on spectral images e.g. ratio and PCs, and for reducing noise and edge enhancement on single band and colour composites. Simple multi-directional 3x3 convolution filters were best for colour images, although they reduce image contrast. Good colour rendition was achieved on such images by use of the HSI transform. Directional filters were not required, because the bedrock geology exerts a strong influence over topography and can be observed directly on the imagery.

(b) Mapping hydrothermal alteration in known areas

Alteration was mapped at all the main localities except East Camp.

At Bitter Creek the known alteration distribution was improved but alteration assemblages or the individual silicified ledges, and veins, could not be mapped. The alteration at Bitter Creek can be divided into two areas - those areas with high hydroxyl and iron oxide absorptions (mainly the silicic and advanced argillic assemblages) and those with high iron oxide absorptions (mainly the propylitically altered rocks of the Virden Dacite unit on Summit Mountain).

At Telephone Ridge there are three areas of intense alteration, on the southeast end of the ridge, the centre, and across Carlisle Canyon on the West side Of East Summit Ridge correspond to the most intense silicic altered areas. On the southeast end of the ridge there are north trending silicic pipes cutting through the surrounding advanced argillic altered tuffs. Propylitically altered areas on the periphery of the higher grade altered areas were mapped.

In the Laura - Alabama area alteration on the SW side of Vanderbilt Peak was easily mapped, and some of the sericitic alteration running aside the rhyolite veins on the west side of the Alabama fault are visible, but the alteration associated with the Laura, Alabama and Steeple

Rock faults is shown only by iron oxide staining - there are no hydroxyl absorptions visible.

In the Raeburn area the boundaries of the silicic tuffs to the northwest and the argillic-sericitic alteration associated with the Blue Bell fault are mapped.

None of the images or image processing techniques indicated the presence of hydrothermal alteration in the East Camp area. There are no absorptions visible on the clay mineral bearing, or iron oxide sensitive ratios, or from the PCA imagery. The main reason for this is the small size of the surface alteration zones which cover an area of less than 4 hectares (Table 4.4).

(c) New altered areas

Previously unknown areas of hydrothermally altered rocks were identified by the processed TM imagery at Park Spring and in the volcanics of the Sycamore Camp Eruptives. Both areas are interpreted as tuff ring vents with deuteric alteration, not related to the epithermal mineralising events. Other areas of deuteric alteration were detected in various felsic tuff horizons of the Amygdaloidal Andesite and unaltered Bloodgood Canyon tuff. Two areas with strong iron oxidised were detected at McKelvey Place and in the Cherry Creek rhyolite.

(d) Remote sensing characteristics of the epithermal model

The epithermal type model characteristics described in Chapter 4.8 can be divided into two types of information:

[PC2 of PCA of bands 5 and 7 would probably allow hydroxyl intensity mapping. See note facing page 158.]

(1) Direct. Specific features of the epithermal system directly observable by remote sensing. (Faults, silicification, advanced argillic alteration, regional and propylitic alteration)

(2) Indirect. Secondary geologic information interpreted from the imagery indicative of an epithermal type. (Regional structure, intrusions, vents, country rocks)

The direct information was obtained from the TM imagery using the various image processing techniques described above. Efforts to find quantitative differences in reflectance between the alteration assemblages were thwarted because of the difficulty of identifying pure altered areas of one type or another on the imagery. Therefore it was difficult to assess whether alteration assemblages are separable using TM data. However qualitative image analysis of ratio and PC images suggests that separation is possible. Although the single band 5/7 ratio suffered from alteration intensity saturation and attempts to solve this problem were limited by the capabilities of the IIS software (Chap. 5.5), it is probable that if these extraction problems could be overcome then hydroxyl intensity mapping should be possible. The DN intensity on the PC4 image appeared to reflect the degree of hydroxyl development and it was possible to broadly match this image to the occurrence of silicic, advanced argillic and propylitic alteration around Telephone Ridge.

TM imagery improved by edge enhancement techniques showed the main through going faults controlling the

mineralisation.

Under terrain and exposure conditions similar to that in the Summit Mountains direct information can easily be extracted. It is posssible to identify all hydrothermal alteration with a high degree of certainty, so long as they cover an area greater than approximately 5 hectares, except for narrow alteration zones of silicification, without accompanied zones of surficial iron oxides, advanced argillic, argillic, or sericitic-argillic assemblages.

Sufficient indirect (geological) information was extractable from edge enhanced HSI processed TM colour composite bands using conventional photogeological interpretation techniques (Chap. 5.2d) to identify the Summit Mountains epithermal deposit. The identification of volcanic vents indicates at least some of the alteration may be acid-sulphate, but most evidence indicates an adularia-sericite type deposit; i.e. abundant linear fault and fractures systems often controlling the alteration, and intrusives indicating the possible existence of a significant intrusion at depth providing a heat source for the epithermal system.

It is not possible to determine the detailed geologic history of the Summit Mountains or to identify the details of the epithermal system (Chapter 4) from TM information alone. Nevertheless a significant amount of geological information is extractable and sufficient improvements were made to the known geology to clearly identify the area has a epithermal system.

CHAPTER 6

FACTORS AFFECTING ALTERATION MINERAL MAPPING IN THE TEST AREA

6.1 Introduction

To determine the applicability of the test area results to other areas in south west New Mexico it is necessary to understand the relative importance of the factors which affected the results.

The ability to map alteration using remote sensing depends on the unique spectral characteristics of the altered rocks and minerals on the ground. It is necessary to know the spectral signatures of the target and surrounding country rock and to understand how these signatures are affected by other physical features in the landscape, including vegetation, soil, lichens and weathered rock surfaces.

6.2 Spectral signatures of the Summit Mountains Rocks

(a) Introduction

Spectral data from the visible and NIR have been collected for numerous rock and mineral types, for example Adams et al. (1967, 1972,), Ross et al. (1969) and Burns (1970). The most comprehensive study was undertaken by Hunt and co-workers published in a series of papers covering all

the main rock and mineral types (Hunt and Salisbury 1970a, 1970b; Hunt, Salisbury and Lenhof 1971a, 1971b, 1973b, and 1974). The usefulness of these extensive records for the interpretation of field data is limited, because the data were collected from powdered and particulate samples measured under laboratory conditions, very different from the complex natural targets and variable measuring conditions found in the field. For this reason spectral studies were done on the rocks from the test area. Laboratory based high resolution spectroradiometry and field based ratio radiometry measurements were done, backed up with petrological and geochemical analyses.

The laboratory spectral measurements were done on approximately 100 samples in the spectral range of the TM, between 0.46 and 2.409 μm but with a resolution of 10 nanometres using the prototype Barringer Refspec spectroradiometer (Appendix V). For the field spectral studies a Barringer hand Held Ratioing Radiometer (HHRR) was used in two modes of operation. Narrow band spectral resolution filters were used to identify the mineralogy of altered rocks at selected sites, and broad band TM equivalent filters were used to assess the performance of TM bands. Only the broad band TM results are discussed here (Table 5.7). The Narrow band results are given in Appendix III.

Petrological analyses involved examination of thin sections to determine petrology and the degree of alteration. Geochemical analyses of the altered rocks to determine the alteration mineralogy was done by X-ray diffraction techniques (Table 4.3).

(b) Spectral Characteristics

(i) Silicic Alteration

The normalised spectral reflectance from a typical silicified tuff from the Telephone Ridge area is shown on Figure 6.1. The mineralogy is predominantly quartz, with minor nacrite, diaspore and ferrihydrite, with accessory anatase and stilpnomelane. The spectrum shows the characteristic 2.16-2.21 µm doublet and sharp 1.4 µm absorptions of kaolinite, the broad flattening centred on 1.8 µm is characteristic of diaspore and the broad absorption between 0.8 and 0.7 µm indicates the presence of iron oxides.

Siliceous rocks composed entirely of quartz (opaline) have no spectral characteristics in the visible and near infrared because silica has no intrinsic spectral characteristics in this area (Hunt and Ashley 1979). Figure 6.2 is the normalised spectral reflectance from a flooded silica capping from Telephone Ridge. The spectrum is flat with minor clay features at 2.21 and 2.3 µm, characteristic of kaolinite. Ferric iron absorption features occur at 0.8 and below 0.6 µm.

Generally siliceous rocks have flat spectra from 1.0 to 2.4 µm. If iron oxides are present a broad absorption centred at 0.85 µm accompanied by a marked fall off in reflectance from 0.7 to 0.4 µm is present. The presence of clay minerals, diaspore or alunite, even in small amounts causes distinct and recognisable absorptions.

The ease by which the TM 1.65/2.2 µm ratio identified silicified areas in the Summit Mountains (Chap. 5.5) indicates that these areas have an hydroxyl content large

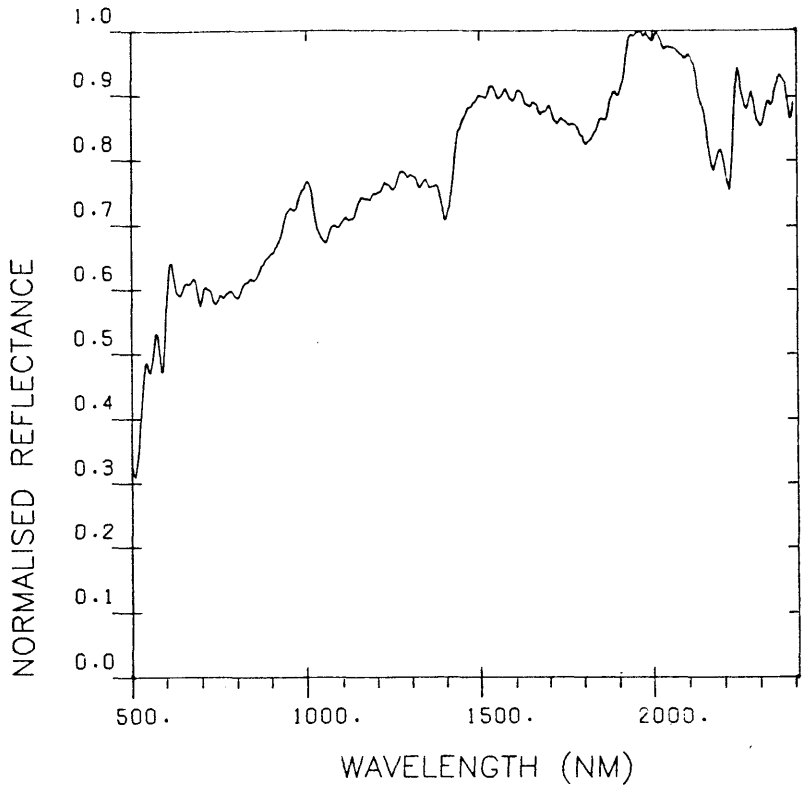

Figure 6.1 Normalised spectral reflectance of a silicified tuff from Telephone Ridge.

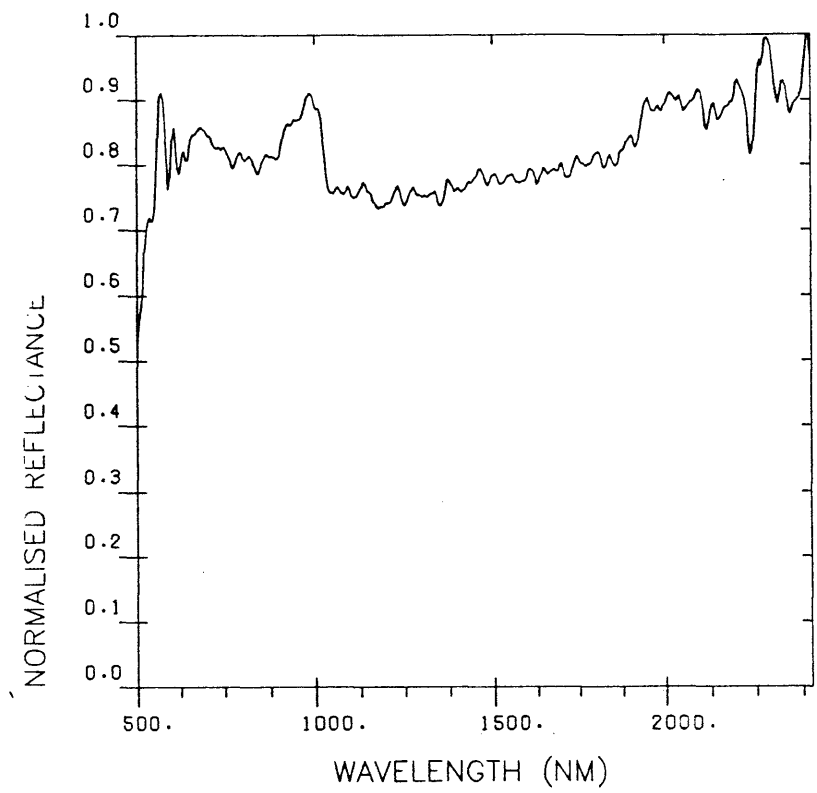

Figure 6.2 Normalised spectral reflectance of a silicified capping from Telephone Ridge.

enough to cause absorptions detectable on TM data. The silicified ledges at the Telephone Ridge, Raeburn and Bitter Creek areas are particularly clear on the imagery. Several of the main ore bearing quartz veins also stand out, probably because they contain hydroxyl bearing minerals both within the vein and in the surrounding sericitic-argillic alteration zone, e.g. the Carlisle vein from Pennsylvania mine west to the junction with the Laura fault, the East Camp fault from Pennsylvania Canyon to Bitter Creek and beyond, and the Bluebell fault from the Bluebell mine to Raeburn Peaks, and finally the Alabama mine area. However where there is not a surrounding hydroxyl bearing alteration zone, the vein was not identified e.g. East Camp.

The HHRR measurement taken from the Blue Bell vein (Sample M22) has a very high 5/7 ratio despite the vein being greater than 90% quartz. Thus clay or phyllosilicate content of less than 10% of the rock is enough to give hydroxyl absorptions sufficiently strong to be detectable by the Landsat TM sensor, although on TM imagery this response would be diluted by other surface features.

ii) Advanced argillic alteration

The dominance of phyllosilicates, mainly kaolinite, dickite and pyrophyllite and the sulphates alunite and natro-alunite, cause distinctive absorptions in this assemblage. In many cases the dominant individual minerals present could be identified from the high resolution laboratory spectra. For example Figure 6.3 illustrates the typical spectrum from an advanced argillic altered tuff from Estes Ranch north of Telephone Ridge. The sharp 1.4 μm feature, the strong sharp 2.17 μm feature

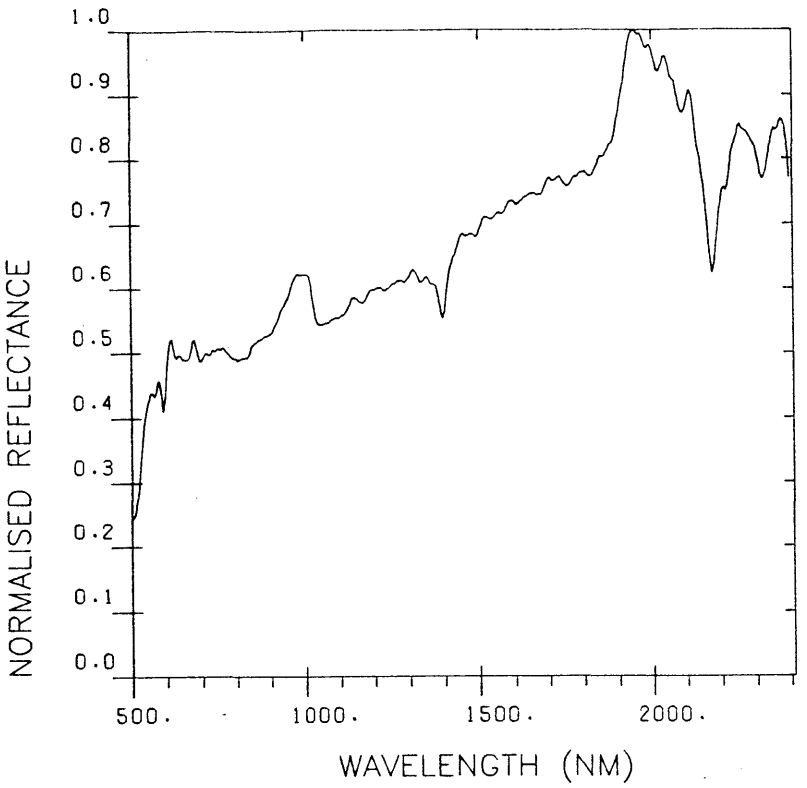

Figure 6.3 Normalised spectral reflectance of a tuff from north of Telephone Ridge altered to the advanced argillic asemmblage.

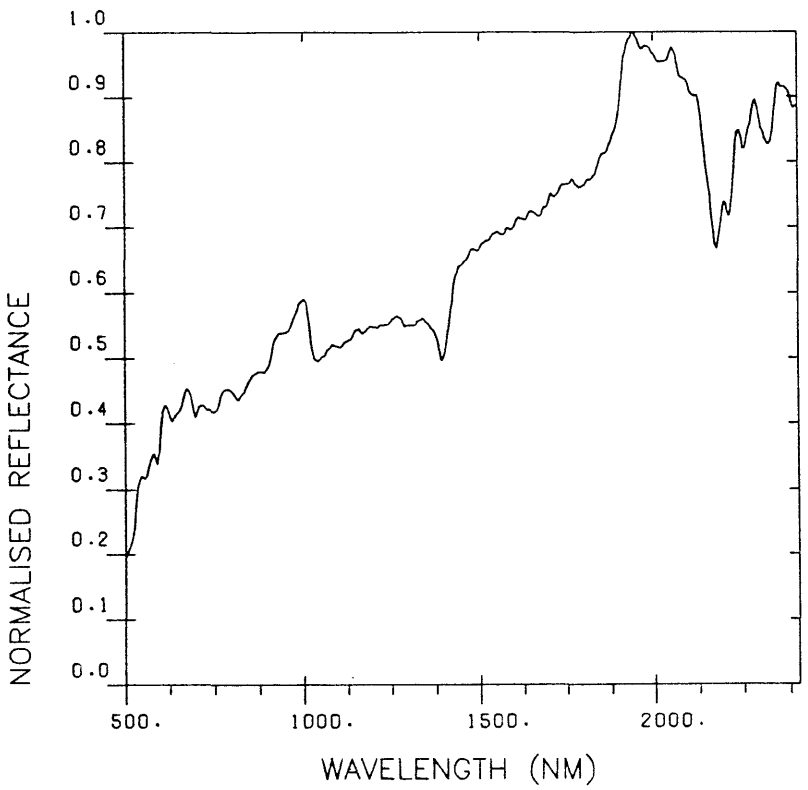

Figure 6.4 Normalised spectral reflectance of a silicified tuff from East Summit Ridge altered to the advanced argillic asemmblage.

and the sharp 2.32 μm feature are diagnostic of pyrophyllite. Geochemical analyses indicated quartz, natro-alunite, pyrophyllite with minor diaspore, kaolin and leucoxene. Surprisingly the spectrum has no features diagnostic of alunite, probably because there is a mineralogic difference between the surface and the powdered sample.

The normalised spectrum from the altered tuff rock from East Summit Ridge shown in figure 6.4 is similar to figure 6.3. The mineralogy is quartz, pyrophyllite and kaolinite, with a quartz content of approximately 50%. The HHRR measurement of this sample gave a high 1.6/2.22 μm ratio value (Table 5.7).

(iii) Sericitic-Argillic

Included with this assemblage is argillic alteration. They show distinctive absorptions on the high resolution laboratory spectra. Figure 6.5 from Telephone Ridge illustrates the normalised spectrum from a sericitic-argillic vein which cuts across the Bloodgood Canyon tuff (Chap. 4.6c). The spectrum has well defined absorptions at 1.4, 1.9 and 2.2 μm diagnostic of sericite. The small 2.3 μm feature indicates kaolinite. Mineralogy is sericite and quartz with minor kaolinite.

(iv) Propylitic alteration

Propylitic altered rocks in the Summit Mountains contain the hydroxyl minerals epidote and chlorite in significant amounts. The small hydroxyl absorptions of propylitic rocks are not visible in the HHRR measurement or on the 5/7 ratio imagery. However propylitic areas were

identified on the TM band ratio colour composites (See figures 5.14 and 5.16). On CRC 5/7 5/1 3/4 and 5/7 5/1 5/4 propylitic areas are a red-purple colour; although it was not identifiable on CRC 5/7 5/4 3/4 (Fig. 5.15). These hues are interpreted as due to surficial iron oxide staining and bleaching of the propylitically altered rocks.

(v) Unaltered volcanic rocks

Unaltered volcanic rocks are abundant in the Summit Mountains even though hydrothermal and deuteric alteration have affected the volcanics. Acidic volcanics commonly have water and clay absorption bands similar to those occurring in hydrothermally altered rocks, often due to microscopic fluid inclusions and deuteric alteration of feldspars to sericite. The water bands at 1.4 and 1.9 μm are visible only in the laboratory as water in the atmosphere absorbs electromagnetic energy at these wavelengths. Thus only the clay bands are troublesome. The difficulty of separating altered rocks from acid volcanics with TM imagery in the Summit Mountains is attributed to these clay bands occurring in the acid volcanics.

In intermediate volcanics only accessory mafic minerals contribute to visible and NIR spectral absorptions, due to ferrous and ferric iron and OH bands. Hornblende has ferric, ferrous and OH bands, biotite has ferric bands at 0.6 -1.5 μm and olivine rich in fayalite may show a ferrous band at 1.0 μm and serpentine hydration at 1.4 and 1.9 μm. Pyroxenes also have iron absorptions. On the laboratory spectra the hydroxyl and water bands were small

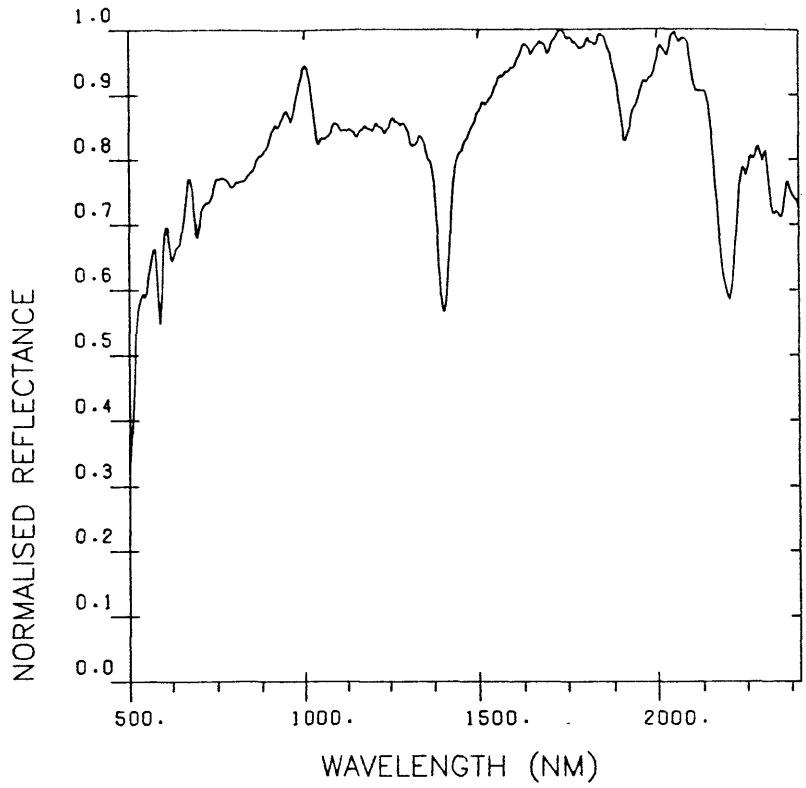

Figure 6.5 Normalised spectral reflectance of altered tuffs of the sericitic-argillic assemblage (From the vein shown on Fig. 4.8).

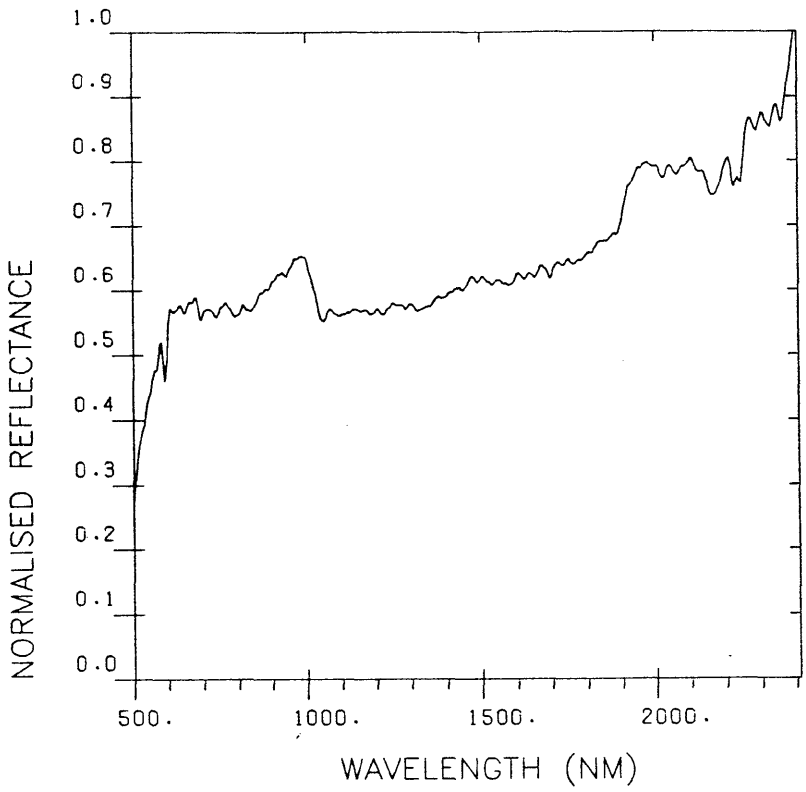

Figure 6.6 Normalised spectral reflectance of an andesite from the Amygdaloidal Andesite unit at Bitter Creek.

and barely visible amongst the sensor noise, and the presence of opaque minerals such as magnetite reduced reflectivity decreasing the absorption contrasts causing what Hunt (1971) termed spectral quenching.

Figure 6.6 illustrates the spectrum from an andesite of the Amygdaloidal Andesite unit from the Bank mine in Bitter Creek. The mineralogy is plagioclase, quartz, amphiboles and serpentinite with minor clays, chlorite and hematite. The spectrum is generally flat with a sharp absorption below 0.6 μm and a weak band at 0.85 μm from ferric iron. It is flat between 1.0 and 1.9 because of spectral quenching from magnetite and ferrous iron. Minor absorptions at 2.15, 2.25 and 2.3 μm are presumably from the amphibole and chlorite. The spectrum of a basaltic rock from the Laura-Alabams area is similiar (Fig. 6.7).

The high resolution laboratory and field ratio radiometry provide a useful insight into the results of the TM imagery. Generally the hydroxyl absorptions in the unaltered rocks were difficult to detect even with the high resolution spectroradiometry done in the laboratory. The difficulty in discriminating altered rocks from acidic volcanic rocks is due to the presence of clays from devitrification, spherulites and fluid inclusions in the acid volcanics giving spectral features similar to but generally slightly weaker than those of hydrothermal alteration assemblages associated with the mineralisation. Deuteric alteration around volcanic vents (Chap. 5.5) also produced hydrothermally altered rocks inseparable from the epithermal assemblages.

Both the high resolution spectroradiometry and the *in-situ*

ratio radiometry showed that absorptions from iron minerals, particularly ferric iron oxides, could be easily detected by remote sensing in TM wavebands (Chap. 5.5). However because iron oxides are widespread in both the altered and unaltered volcanics in the Summit Mountains the visible absorption features are less diagnostic of altered zones than the near infrared absorptions features of hydroxyl minerals.

The diagnostic absorptions of individual alteration minerals found in the silicic, advanced argillic, argillic and sericitic-argillic alteration assemblages are too small to be resolved by the TM sensor and could not be discriminated from each other using the TM imagery.

6.3 THE EFFECTS OF WEATHERING AND LICHENS ON SPECTRAL SIGNATURES

(a) Introduction

Penetration experiments done to determine the depth of rock which contributes to a remotely sensed signal in the visible and near infrared (VNIR) and short wave infrared (SWIR) have shown that the surface mineralogy is of dominant importance. Buckingham and Sommer (1983) have reported varying penetration depths for different materials, ranging from 12 to 28 μm for goethite and 17 to 21 μm for haematite at 0.9 μm wavelength. For clays the upper 50 μm contribute to the signal at 2.2 μm wavelength.

The effects of weathering, lichens, surface stains and

other surface coverings on the spectral signatures of fresh or altered rocks have not been well studied. Pontual (1988) has reported weathering to cause both spectral masking of primary mineralogy and enhancement of mineralogical differences through oxidation of opaque minerals. This laboratory work was done to determine the effect of surface coverings on the spectral signatures of primary mineralogy of hydrothermally altered rocks.

(b) Weathering in semi-arid terrain

In arid and semi-arid terrain , rock surfaces which are mineralogically different from the underlying substratum are formed by *in-situ* weathering reactions or by desert varnish. *In-situ* weathering involves mechanisms of oxidation, hydration and hydrolyses, reactions which are extremely slow and which do not occur at all without the presence of water.

Mafic minerals decay more rapidly than felsic minerals, liberating magnesium,iron and lesser calcium and alkalis. The iron is largely oxidised to form insoluble ferric oxides, mainly the anhydrous oxide, haematite, and the hydrates goethite and lepidocrocite.

From the felsic minerals calcium,sodium and potassium are removed, the remaining Al-SI-O structure may be in part decomposed and partly reconstituted into the framework of clay minerals. The resultant coating of ferric iron oxides, which is mainly fine grained goethite and clays, is commonly termed limonite (Krauskopf 1982).

Manganese oxides also commonly occur on rock surfaces and

cracks in arid and semi-arid areas, forming brown or black stains. The oxidation process is similar to that of iron described above.

Another common weathering process is the oxidation of sulphides occurring in volcanics or around mineral veins. Oxidation of pyrite forms insoluble ferric oxides and hydroxides and high acidity because of hydrolysis of the dissolved metal ion. Various iron oxides and ferrous and ferric sulphates result in yellow, brown and red stains around the veins. Such staining is common in the Summit Mountains.

External processes in arid environments include the build up of coatings on stable substrates, e.g. desert varnish and silica gel varnish. Desert varnish is a surface coating of manganese, ferric oxides and clays which is commonly 100 μm thick. The processes of accumulation are not well understood but are thought to involve chemical and biological processes (Potter and Rossman 1977).

Several workers have studied desert varnish in a remote sensing context. Adams and others (1982) listed the salient points of importance to remote sensing studies as follows:

(1) Composition of clay, iron and manganese oxides
(2) Strong spectral signature
(3) Chemically and mineralogically unrelated to the substratum
(4) Accumulation occurs on substrates stable from between 1000 and 10,000 years
(5) Airborne clay rich source necessary for development

The formation of silica gel coatings is thought to be similar to desert varnish. Farr (1981) reported that gels found in Hawaii and in the western United States are transparent for wavelengths in the visible and NIR. However when contaminated they become translucent below 1.0 μm where they can cause spectral masking.

(c) Spectral masking in the Summit Mountains

To determine the presence and possible spectral effects of surface coatings from weathering surfaces, lichens, or desert varnishes, 23 rock samples were studied using the Refspec (Table A5.1, Appendix V).

The measurement equipment and procedure were as for the spectral signature determinations (Chap. 6.2a), except that the sample was measured on the natural weathered surface and on a fresh surface. In certain cases (noted on Table A5.1) the fresh surface was measured from a flat cut surface which effects scattering and absorption properties (see Salisbury and Hunt 1968) and makes absorption features more pronounced (Hunt 1981).

Little or no difference was found in the spectral signatures between the weathered and fresh surfaces of the unaltered and propylitically altered samples, e.g. Figure 6.7, a basalt from the Amygdaloidal Andesite unit. However, large differences occurred in several of the silicic and advanced argillic altered samples.

Figure 6.8 is a silicified tuff from the Raeburn area. The fresh surface has strong absorptions at 1.75, 2.2 and

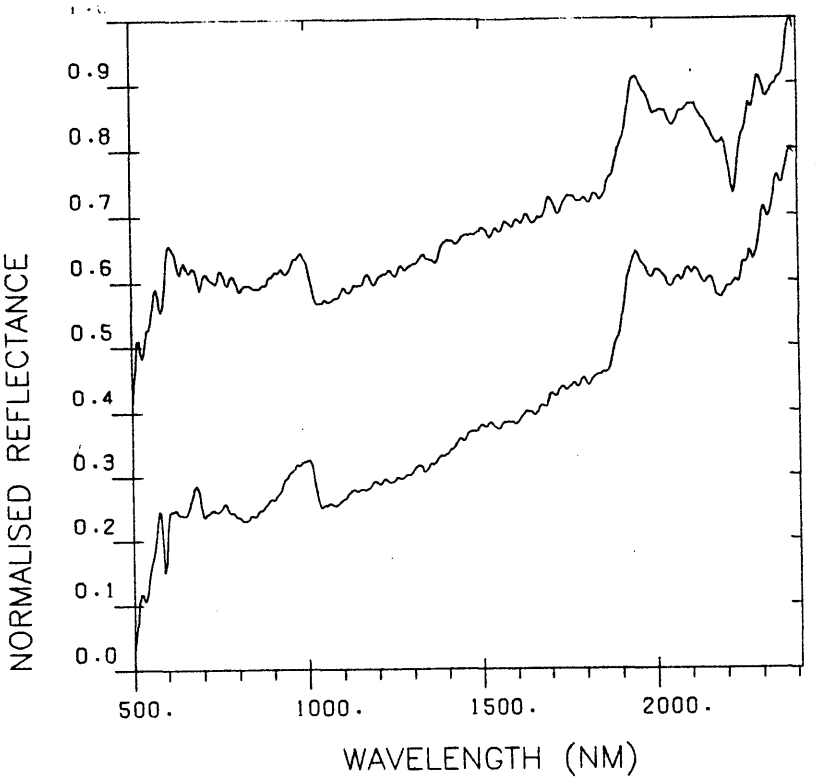

Figure 6.7 Comparative normalised spectral reflectance from the weathered (lower plot) and fresh surfaces (upper plot) of a basalt from the Amygdaloidal Andesite unit.

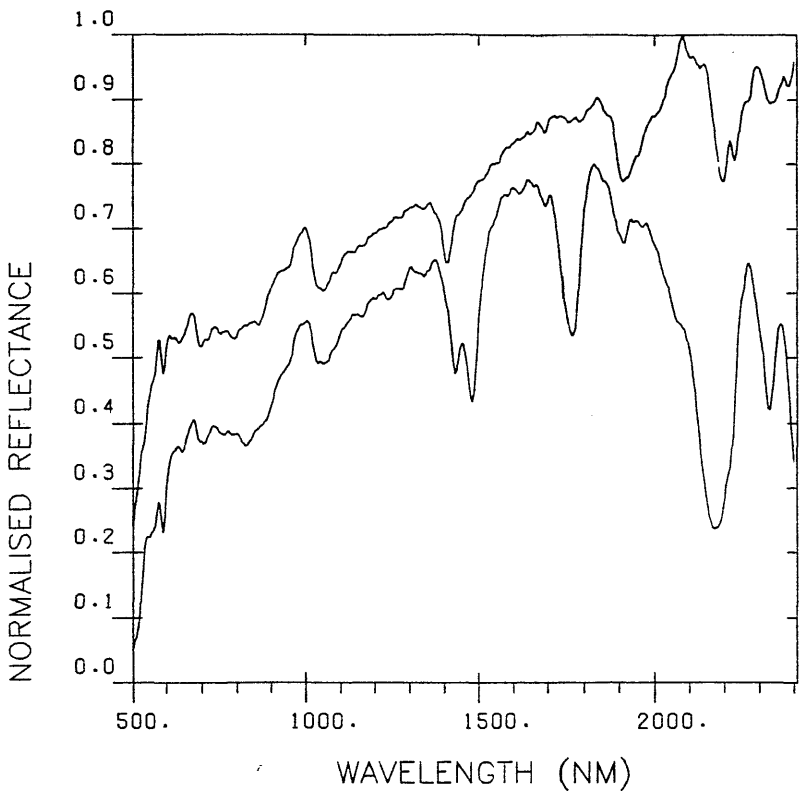

Figure 6.8 Comparative normalised spectral reflectance from the weathered (upper plot) and fresh surfaces (lower plot) of a silicified tuff from the Raeburn area.

2.33 μm and a strong double absorption at 1.4 - 1. 48 μm, diagnostic of alunite (Figure A1.1). The weathered surface spectrum is more subdued, with strong absorptions at 1.4, 1.9 and 2.2 μm. The 1.75 absorption is absent and the 1.9 μm absorption more pronounced. These features are indicative of the presence of kaolinite or diaspore, or molecular water in the lattice.

X-ray analysis of the weathered surface shows kaolinite and diaspore. The mineralogical difference between the weathered and fresh surfaces may be due to a surface coating of kaolinite and diaspore from weathering processes.

Lichens on the surface of three silicified samples caused spectral flattening, e.g. figure 6.9. Here the fresh spectrum, confirmed by XRD analysis, indicates alunite. The lichen covered weathered surface has completely masked the alunite signature, leaving only subdued indications of its presence. Satterwhite (1985) has reported that differences in visible and NIR reflectance (0.4 - 1.1 μm) caused by lichens are mainly due to albedo. My results show that lichens considerably mask and alter rock reflectance in the SWIR out to 2.5 μm.

Manganese and ferric oxide coatings also mask the diagnostic absorptions. Iron oxide absorptions are present on the weathered surfaces of several of the altered and non-altered samples (Table A5.1).

No evidence for the presence of desert varnish or silica gels was found, although it is possible that some of the manganese oxides observed on rock surfaces, cracks and joints could in part be attributed to desert varnish like

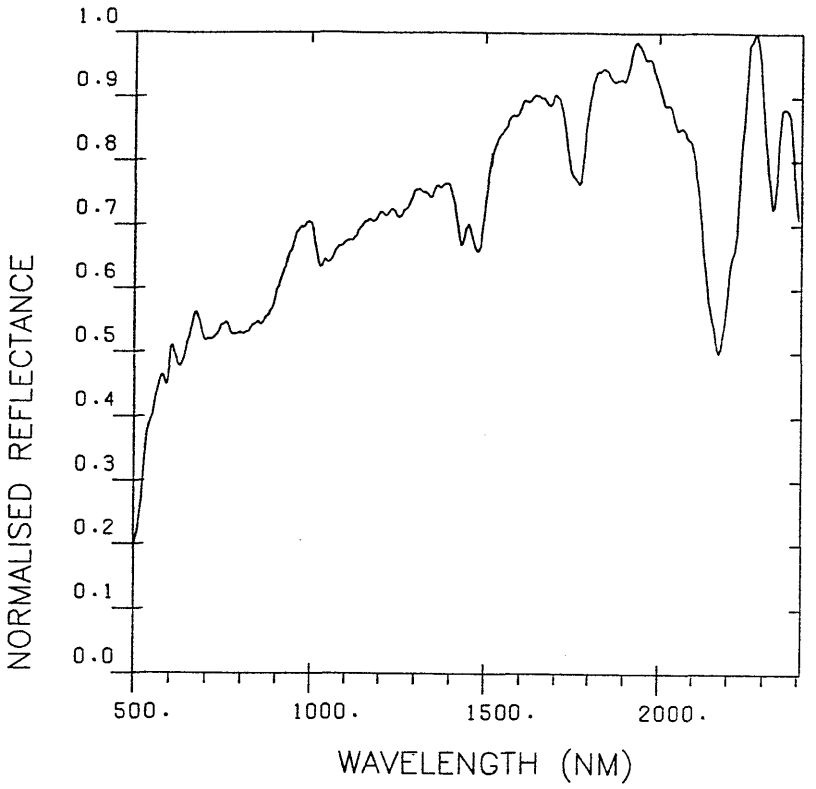

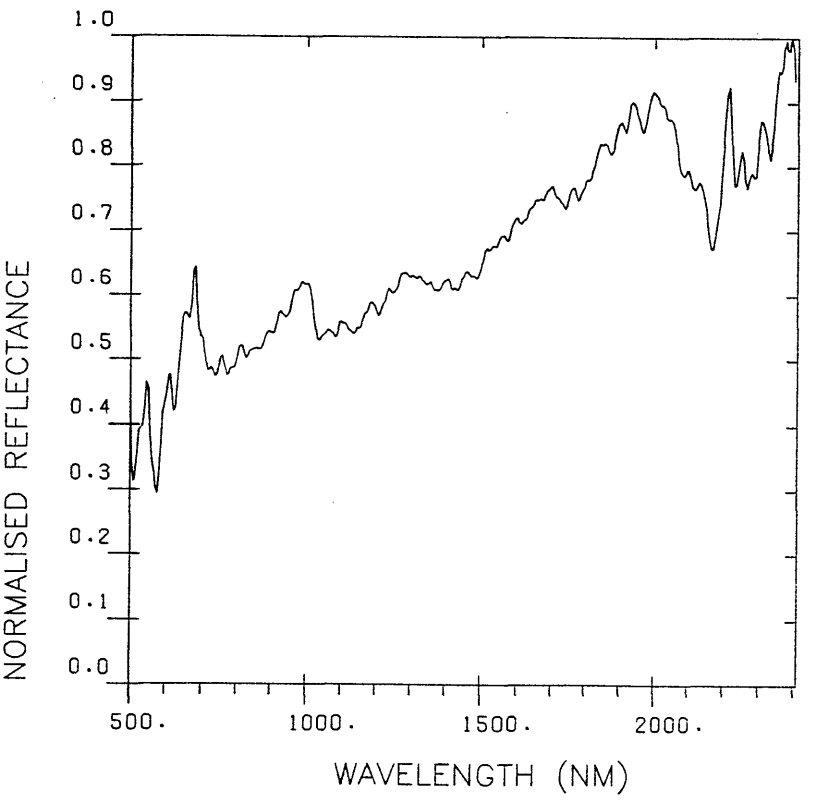

Figure 6.9 Comparative normalised spectral reflectance from the weathered and lichen covered (lower plot) and fresh surfaces (upper plot) of an alunitised tuff from Telephone Ridge.

processes. A stable substratum is an important requirement for desert varnish production. In the Summit Mountains the climate, rugged topography, steep slopes, thin soils and lack of vegetation all encourage mechanical weathering. The large number of scree slopes and rock strewn areas shows that mechanical weathering is a dominant erosional process. However on the lower, stable, colluvium covered areas, desert varnish may be present.

Generally my studies showed that locally *in-situ* weathering processes operating on the altered volcanics produce ferric and manganese oxide coatings which cause significant spectral masking of the underlying rock mineralogy. Lichens also cause significant flattening and damping of rock spectra, not only in the VNIR but also in the SWIR. The signatures of propylitic and non-altered rocks are much less affected by weathering surfaces and coatings.

The larger regional effects of these processes are difficult to assess, because it is difficult to measure the extent of weathering coatings and lichens without recourse to detailed field studies. However hydrothermal alteration was successfully mapped using the TM data and while the laboratory results show that locally lichens and weathering have a considerable masking effect, aerially these effects appear to be insignificant.

6.4 VEGETATION

While vegetation can be used to find geobotanical and bio-geochemical anomalies, its presence generally hinders mineralogical remote sensing by masking or contaminating the spectral signatures of the altered rocks.

The spectral reflectance properties of vegetation in the VNIR and SWIR are primarily due to plant pigments, morphology, physiology and water. Figure 6.10 shows laboratory reflectance curves for typical clay and iron oxide alteration minerals, green grass and dry grass. In the VNIR the steep rise in reflectance of both dry and green grass coincides with the 0.85 μm ferric iron absorption. In the SWIR both dry and green grass have strong absorption features which coincide with the diagnostic phyllosilicate feature. Siegal and Goetz (1977) have reported 60% green vegetation cover to completely mask the iron absorption feature but the 2.2 μm feature at this level is still recognisable.

Figure 6.11 shows the density of vegetation cover in the test area and table 6.1 expresses this information quantitatively. The vegetation density map was produced at 1:50,000 scale from natural colour aerial photographs of 1:30,000 scale. The photographs did not allow type identification except for scrub vegetation from trees. Vegetation details are given in Chapter 4.2. Canopy cover varies from zero to 100 per cent, but less than 10 per cent of the area has more than 60 per cent vegetation cover; the percentage at which, according to Siegal, iron oxide signatures in the SWIR are masked.

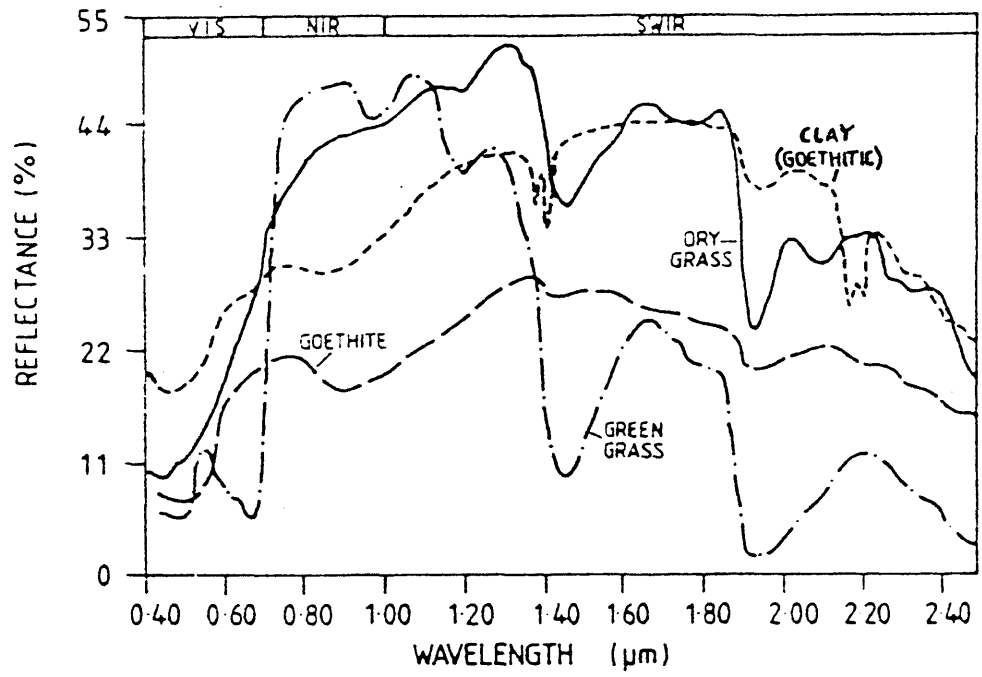

Figure 6.10 Reflectance of grasses and clay and iron rich altered rocks measured by a spectroradiometer (from Faser and Green 1986).

Key

A	100% Vegetated
B	>70
C	50 - 70
D	30 - 50
E	10 - 30
F	5 - 10
G	<5%
T	Unvegetated

Figure 6.11 Distribution and density of vegetation in the Summit Mountains test area interpreted from 1:30,000 scale colour aerial photographs and field survey.

Table 6.1 Vegetation cover in the Summit Mountains

Percentage vegetation Cover Ranges	Area Km2	Cummulative Area Km2
0	11	11
<10	153	164
10 - 30	28	192
30 - 50	14	206
50 - 70	14	220
70 - 90	12	232
90 - 100	3	235

Clay bearing alteration minerals were mapped without difficulty with the 5/7 ratio and there was no apparent difficulty in discriminating clays and vegetation. The HHRR measuremnts for vegetation show that the vegetation in the Summit Mountains has typical absorption features (Table 6.2).

On the north and eastern slopes of Telephone Ridge which are 70 - 90 % vegetated on a silicic-argillic substratum, vegetation is not sufficient to mask alteration spectra on TM imagery. This is probably because the vegetation here is surrounded by larger areas of altered rock with 30 % or less vegetation, which effectively dilutes the vegetation component. Generally the most heavily vegetated areas occur in patches too small to form pure vegetation pixels. From the aerial photographs it is estimated that this size is approximately 75 metres or less.

The iron oxide sensitive ratios were affected more by the vegetation than the clay ratio, in agreement with Siegal's experimental work. Yet all iron oxide bearing substrates were identified on the ratio imagery, with the exception of ratio 3/1 where ambiguous results occurred. On the 4/2 and 5/1 ratios images there is evidence suggesting that with increasing vegetation cover it would not be possible to separate vegetation from iron oxides on these images. In such a case the 3/2 or 5/4 ratios might prove superior because vegetation and iron oxides have opposite spectral responses with these ratios. However where considerable vegetation -iron oxide mixing occurs, separation using any of these simple ratios is unlikely to be successful.

Elvidge (1983) has proposed the use of ratio 3/1 in cases of spectral mixing, because this ratio is reportedly

Table 6.2 HHRR vegetation measurements and analysis

Vegetation Type	TM Ratio						
	5/7	3/4	5/1	5/4	4/2	3/2	3/1
Grass*1	1.88	0.26	4.30	0.63	3.44	0.88	1.75
Grass*1	1.60	0.50	3.30	1.00	2.44	1.20	1.70
Shrubs & Grasses	1.66	0.69	2.60	1.10	1.80	1.07	1.53
Cresote	1.86	0.69	1.10	0.64	3.50	1.07	1.50
Cactus	1.50	0.40	3.30	0.50	2.50	0.96	1.21
Green Creosote	1.83	0.21	2.70	0.48	3.60	0.74	0.69
Creosote/grass	1.11	3.30	2.80	0.40	3.00	0.92	1.30
Creosote/grass	1.20	0.37	0.44	0.66	2.30	0.90	1.28
Big Sage brush	1.80	0.48	2.50	1.00	1.90	1.00	1.25
Big Sage brush	1.87	0.35	3.00	0.65	2.80	1.00	1.25
Rabbit brush	2.00	0.35	3.20	0.76	2.60	0.87	1.60
Ant brush	1.83	0.27	4.30	0.85	3.20	0.58	1.40
Mean Value (scrub/grasses)	1.68	0.66	2.80	0.72	2.76	0.93	1.37
Juniper	1.30	0.23	2.30	0.40	3.80	0.73	0.88
Juniper	0.65	0.36	0.90	0.20	2.86	0.71	1.18
Juniper	2.25	0.09	4.50	0.27	6.60	0.60	1.50
Pinon	3.00	0.08	3.03	0.24	8.30	0.67	1.00
Pinon	2.30	0.12	2.32	0.22	5.20	0.66	1.33
Mean Value (Trees)	1.90	0.18	2.61	0.27	5.35	0.67	1.18
Mean Value (Vegetation)	1.79	0.42	2.70	0.49	4.05	0.80	1.27

Note 1 Grasses measured on lawn at Socorro, New Mexico

sensitive to iron oxides while being unaffected by vegetation (because leaf reflectance is broadly similar in TM bands 1 and 3). HHRR measurements of vegetation from the test area showed that reflectance values differ in bands 1 and 3, for both grasses and trees. On all but the 3/1 image it was possible to separate basaltic andesites with scattered scrub vegetation from altered iron oxide bearing areas (Chap. 5.4). Another weakness of the 3/1 ratio was the failure to identify known iron oxide alteration at Bitter Creek - recognised by the other ratios.

The evidence from the test area, from imagery and HHRR measurements clearly show that the 3/1 ratio confuses vegetation and iron oxides.

6.5 DISCUSSION

Neither the vegetation nor surface weathering and lichens affected alteration mapping with TM imagery because of their small extent relative to the surrounding unvegetated and unweathered area. Problems did not occur even in the most heavily vegetated areas where vegetation densities are 90 % or greater.

The alteration assemblages and rock types in the test area were discriminated with high resolution (10 - 30 nanometres) radiometry, with the following limitations. Siliceous rocks with spectral signatures in the thermal infrared (10 - 12 μm) cannot be identified with VNIR and SWIR data, but when phyllosilicates make up as little as

10 % of the rock surface, their spectra are similiar to those of clay rich alteration assemblages. Clay absorption bands occurring in devitrified acidic volcanics make it difficult to separate such rocks from argillic assemblages. It is difficult to identify propylitically altered rocks because the hydroxyl absorptions are small and tend to be drowned by the sensor noise.

The weather and related environmental conditions in which the data are collected crucially affect the usefulness of the data. In the test area the atmospheric corrections applied to the data (3.4 and 5.3) appreciably improved the interpretability of the ratio imagery for alteration mapping.

The accuracy of the atmospheric correction applied to the ratioed data is dependent on the scatter being equal all over the image. Where this is not so, as at Bitter Creek, the performance and reliability of the ratio are affected. For example, mist affecting band 1 affected the 3/1 ratio and prevented this ratio from mapping iron oxides which were detected by other iron oxide sensitive ratios which did not use band 1 (Chap. 5.5.). In such cases more complex atmospheric corrections are required.

Corrections were not needed for the PCA data or for the band colour composites because PCA separates uncorrelated information such as band variable scatter, into the lower components and contrast stretching of bands automatically corrects for scattering affects.

The spatial and spectral resolutions of TM were the most important factors affecting remote sensing of alteration in the test area, in the sense that the results were

affected most by the limitations of the TM performance as opposed to any external constraints from terrain, atmospheric and weather conditions.

Spectral resolution was insufficient to permit individual or assemblage identification. TM band 7 (band width = 270 nanometres) is too broad to allow separation of individual hydroxyl bearing minerals, but the combined absorptions of these minerals do significantly decrease reflectance in band 7. Thus the presence, but not the separation, of silicification, argillisation and sericitisation was possible. The visible TM bandwidths (70 nanometres for bands 1 2 and 3) and the NIR band (140 nanometres) are too broad to resolve individual iron minerals. But iron oxides are recognisable because of the decrease in reflectance which occurs in the visible bands.

Theoretically, Landsat TM with a nominal pixel size of 30 metres should detect an alteration zone with an area of 0.36 hectares (or 0.1 ha if the pixel is centred exactly on the alteration zone). However the alteration at East Camp, covering some 4 hectares was not identified. The narrowness of the zones (approximately 10 metres) and the lack of strong hydroxyl and iron bearing minerals were constraining factors.

Conversely it was possible to identify high contrast features less than 5 metres in width, e.g., rhyolite dykes. Additional factors to high contrast are probably subtle variations in topography, vegetation, and rock type (and alteration). Generally evidence suggests that an alteration zone size greater than 5 hectares is required for detection, although smaller zones of high spectral contrast are likely to be detected.

The high resolution laboratory results show that increased spatial, spectral and radiometric resolution beyond that of TM imagery would improve the capability of remotely sensed data to identify and discriminate alteration minerals, but because a larger percentage of pixels would be masked by lichens, weathering (including staining) and vegetation, there is the possibility that overall rock type classification accuracy would not improve significantly, unless new image processing techniques are used to cope with the increased image complexity.

Land cover and vegetation classification accuracy has been shown to decrease as image spatial resolution increases and the overall level of detail derived from the imagery increases (Heller and Ulliman, 1983; Shimoda et al, 1988), and similar results would be expected for geological classes. It is arguable that in the Summit Mountain, TM imagery is "cost effective" in the sense that potential improved mapping capabilities from improved sensor resolution are not worth the trade off of increased data handling (Chap. 3) and image processing difficulties caused by the introduction of image complexity.

This chapter has examined the main factors which affected remote sensing of alteration in the test area. It would be an over simplification to state that one particular factor is more important than another, given the complex interrelationships between the imagery the sensor performance, terrain and weather conditions. But there is some merit in listing the factors in order of relative importance. They are :

1. The spatial and spectral resolution of the sensor.
2. Weather and atmosphere at the time of data collection.
3. Spectra of the altered rocks.
4. Vegetation cover and distribution.
5. Iron and magnesium oxide mineral weathering veneers and lichens.

CHAPTER 7.

REGIONAL MAPPING

7.1 Introduction

This chapter describes and assesses the processing techniques used for regional mapping. The techniques were applied in various localities in southwest New Mexico with different relief (desert plain to high mountain), vegetation cover and vegetation type (shrub steppe to coniferous forest), (Fig. 7.1). The main characteristics of the regional test localities are listed in table 7.1.

The locations were chosen because of their physical variability and because they were known to have epithermal mineral deposits, or in the case of the Red Rock Basin locality, to have good potential to have epithermal deposits. Studies were concentrated in the Blue Creek Basin and its sub area the Red Rock Basin were the geology is poorly known (Chap. 3).

(a) Thematic Mapper Bands

Figure 7.2 is a processed 1 4 5 colour composite of the Blue Creek Basin. The image was selected as the best band combination for geological mapping by statistical analysis (MEV, Chap. 5.2) and visual assessment. A considerable amount of geological information can be extracted from this image. Colour and textural information allows

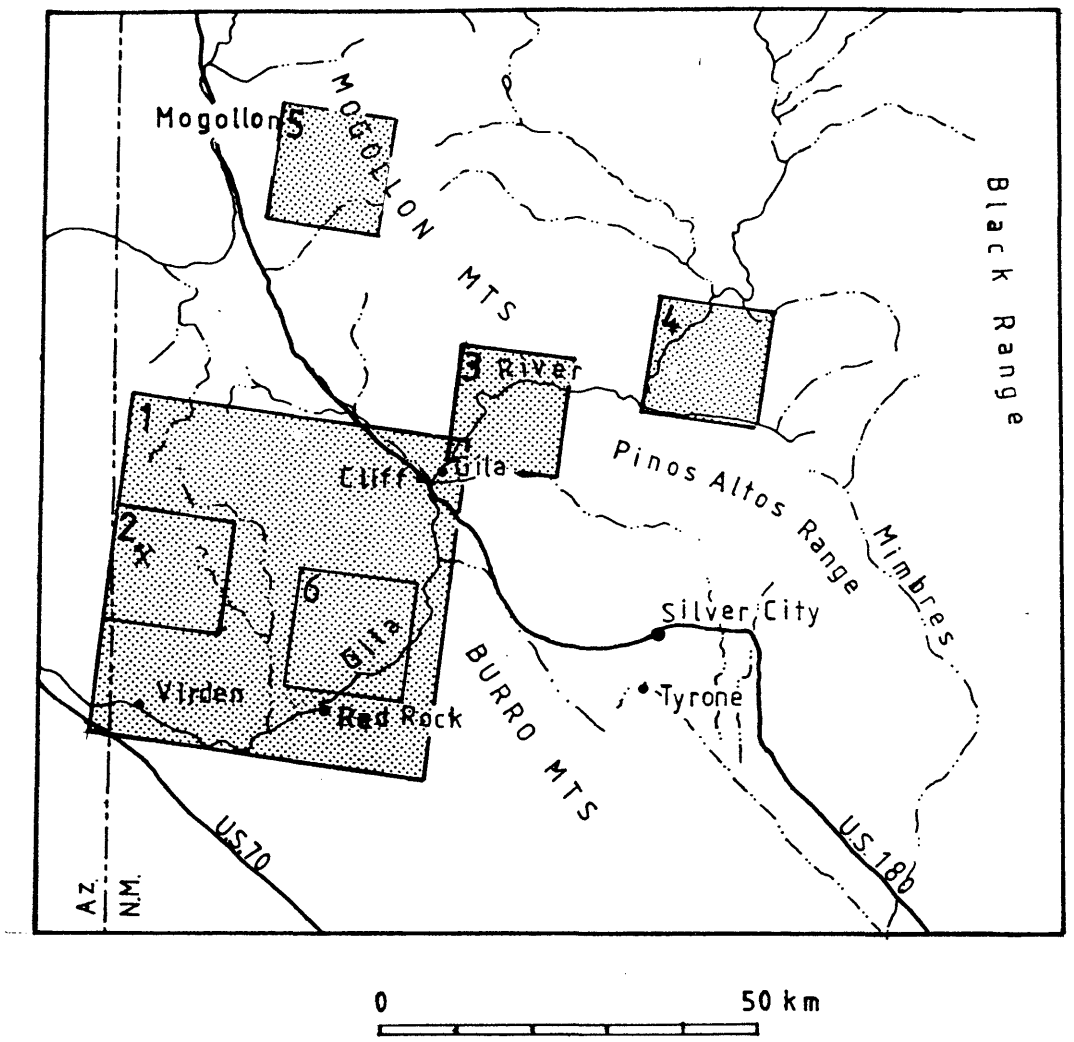

1. Blue Creek
2. Summit Mountain
3. Brock Canyon
4. Alum Mt. (Copperas Creek)
5. Mogollon
6. Red Rock

Figure 7.1 Location of the regional images.

Table 7.1 Physical characteristics of the regional test localities

Locality	Topography	Vegetation Area and Type	Geology	Hydrothermal Alteration and Mineralisation
ALUM MOUNTAIN Southern edge of Gila Wilderness	Lower foothills of Mogollon Mountains, all above 1667 m. Alum Mt - 2319 m	38 % Mixed coniferous forest of Pinon, Juniper, Pine and Douglas fir	Pre-caldera volcanic vent of calk-alkali type, overlain by Gila flat andesite and latites, with Gila conglomerate in the grabens	Oligocene siliceous pyritic pipes cutting argillised volcanics Widespread supergene alunite and halotrichite
BROCK CANYON 8 km northwest of Gila	Mountains above 2334 m Plains from 1667 - 2000 m	45 % On western plains are desert and shrub steppe with juniper woodland on Mt. slopes, and thick coniferous forests on the Mogollon Mt foothills	Calk-alkaline volcanic complex of altered and unlatered lava flows overlain by caldera ash flow tuffs on the north and Gila Conglomerate in the south	Oligocene. Argillised adnd sericitised volcanics cut by fault controlled silicified and pyritised areas
MOGOLLON SW Catron County	From 1833 m to 3000 m with deeply entrenched canyons up to 330 m deep	90 % Thick stands of coniferous forests on eastern slopes	Ash flow tuffs of the Bursum caldera	Gold and silver bearing quartz veins with silicic, argillic and propylitic alteration
BLUE CREEK BASIN	Elevation ranges from 1100 m on the plains to over 2000 m on the volcanic Peaks	9 % Mostly woodland but variable (see chapter 2)	Volcanic - tectonic basin with local intrusive extrusive centres, with underlying Mezozoic, and PreCambrian Basement (See Chapt. 3)	Known in Summit Mts (Chapt.4) and elsewhere (Chapt. 3.6)
RED ROCK BASIN (Sub region of Blue Creek Basin)	Rugged volcanic mountains from 1467 to 2285 m	18 % Woodland. Heavily wooded on east between Davis canyon and Gila river	Andesite - latite flows and tuffs overlying the Colorado Fm and Beartooth Quartzite	No known alteration.

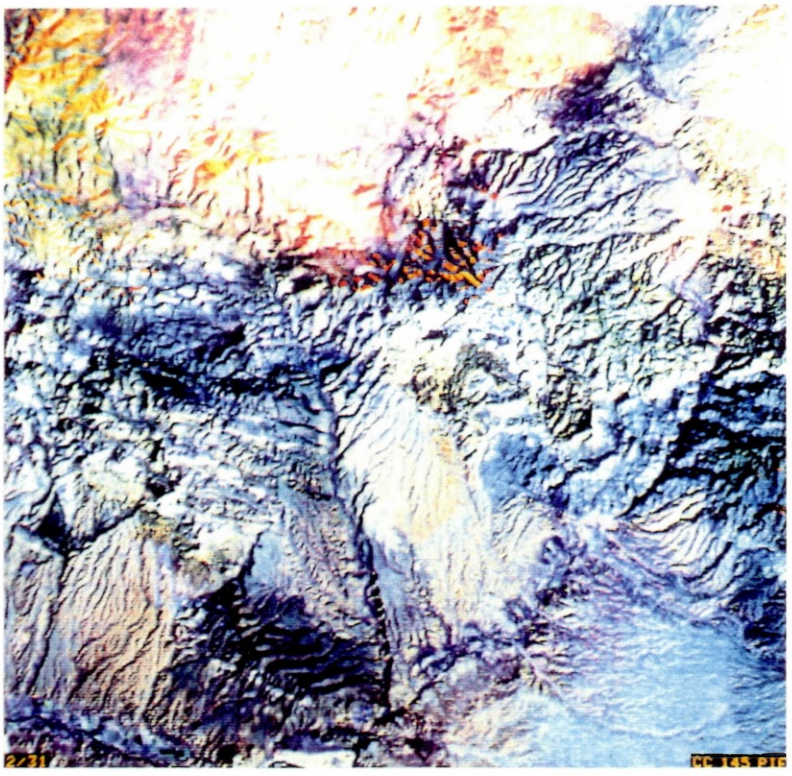

Figure 7.2 Colour Composite 1 4 5 of the Blue Creek basin.

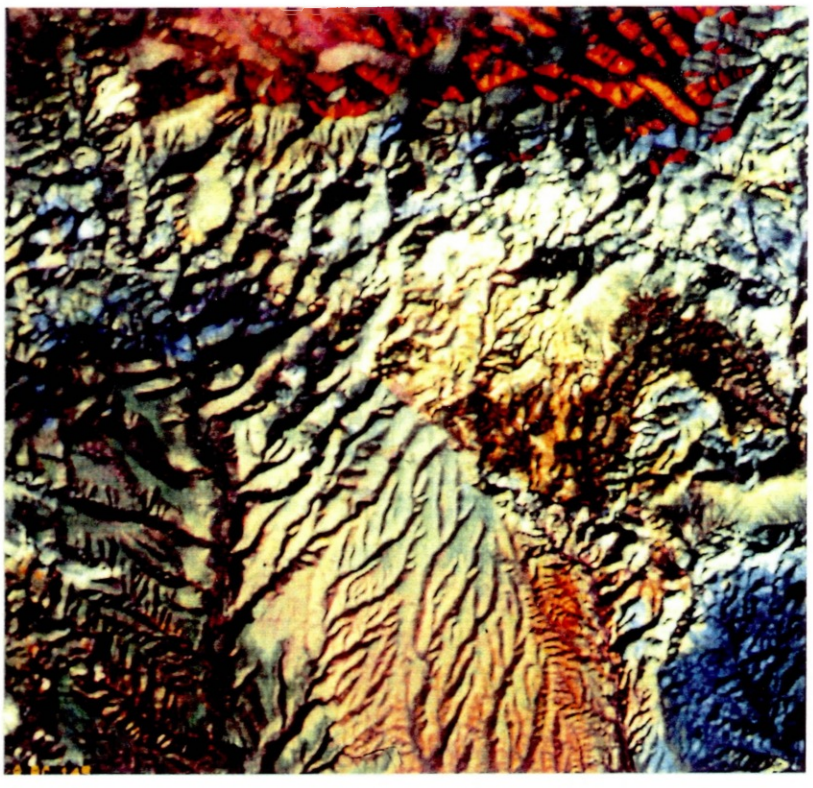

Figure 7.3 HSI transformed colour composite 1 4 5 of the Red Rock basin area (subscene of Fig. 7.2)

separation of the rocks into volcanics, sedimentary, granitoid and alluvial/fluvial areas. The volcanics in turn can be divided into classes approximating to their mineralogy (basic or acid) and origin of formation (intrusive or extrusive and as flows, tuffs or volcanoclastics). However, as in the test area it is not possible to spectrally discriminate altered rocks from acid volcanics, or indeed additionally in this image, from sedimentary formations (all appear white).

Colour transformations can improve spectral separation and show subtle spectral differences. Figure 7.3 of the Red Rock Basin is an excellent example of an HSI enhanced images were hue and saturation are "tweaked". However, even on this imagery it is not possible to identify mineral absorptions - only spectral differences.

Similar results occurred at the other localities, with the usefulness of the composite images becoming less as vegetation, snow and shadow increased. Altered rocks and acid volcanics were inseparable on all the images.

7.2 Ratio Imagery

As ratio imagery was the most effective imagery for mapping alteration in the test area the same image processing procedures were applied to the regional localities.

(a) Single Ratios

Figure 7.4 is the TM 5/7 ratio of the Blue Creek basin. Bright tones represent areas of strong 1.65/2.2 μm absorptions, which may be caused by strong hydroxyl absorptions. Comparison with the vegetation distribution map (Fig. 7.14) shows that many of these bright tones are vegetated areas. The strong vegetation absorptions are due to leaf water moisture (Chap. 6.4). Similar results occurred in the more vegetated terrain at Brock Canyon, Alum Mountain and Mogollon.

Table 7.2 shows the relative performance of the various iron oxide ratios for discriminating iron oxides from vegetation in the regional localities. As expected, given the results from the less vegetated test area, the iron oxide ratios were severely affected by vegetation. The 5/1 4/2 and 3/1 ratios are particularly poor in vegetated terrain.

The simple single band ratio images, effective in the Summit Mountains, are limited for mapping alteration in southwest New Mexico.

(b) Colour Composites

The incorporation of a vegetation index into the three band colour composite, as described in Chapter 5.6, is a common means of discriminating alteration from vegetation with multispectral imagery. As there are many possible ratio combinations (Chap. 3), there is a need for pre-selection. The statistical selection techniques were not used following the test area results (Chap. 5.6).

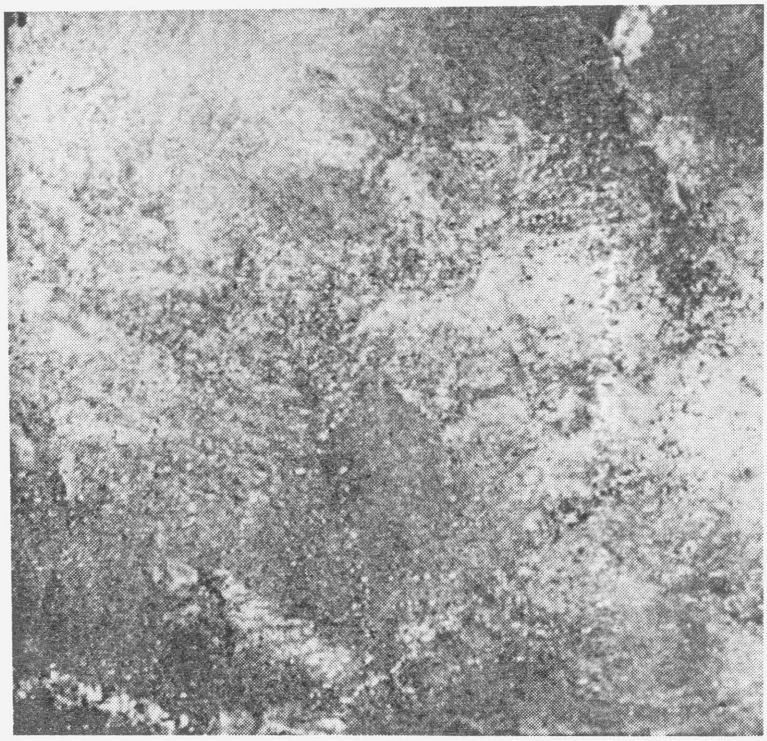

Figure 7.4 TM ratio 5/7 of the Blue Creek basin. Bright tones are due to either hydroxyl absorptions occurring in the rocks and soils or to water absorptions of vegetation. Compare with the vegetation map (Fig. 7.14).

Table 7.2 Performance of iron oxide ratios for separating alteration from iron oxides in south west New Mexico

SITE	VEGETATION COVER % AND TYPE		TM RATIOS 5/1	5/4	4/2	3/2	3/1
Summit Mountains	6	Woodland	Very good	Very good	Poor	Very good	Poor
Blue Creek Basin	9	Woodland desert grasses	Poor	Very Good	Poor	Very Good	Poor
Red Rock	10	Woodland	Poor	Satisfactory	Poor	Satisfactory	Poor
Alum Mountain	38	Mixed Coniferous forest	Poor	Good	Poor	Good	Poor
Brock Canyon	45	Woodland & desert grasses	Poor	Good	Poor	Good	Poor
Mogollon	70	Coniferous forest	Very Poor	Very Poor	Very Poor	Very Poor	Very Poor

A study was done of the main ratios at the various sites to identify the use of each ratio. TM ratio 5/7 was included in all combinations because it is the only TM ratio capable of identifying clay type minerals. Combinations without this ratio, e.g. two iron oxide ratios with a vegetation index, were not used because the test area studies showed iron oxide ratios are variable in their response to iron oxides, and alone need not be diagnostic of hydrothermal alteration.

From the earlier study (Table 7.2) the 5/4 and 3/2 iron oxide ratios were selected as the best iron oxide ratios for mapping iron oxides in the vegetated terrain of southwest New Mexico.

This analysis resulted in the identification of five potentially useful ratios for use in combination; ratios 5/7 (clay), 3/2, 5/4 (iron) and either the 3/4 or 4/3 or other similar vegetation indices. The five basic combinations are:

(1) 5/7 5/4 3/4
(2) 5/7 5/4 4/3
(3) 5/7 5/4 3/2
(4) 5/7 3/2 3/4
(5) 5/7 3/2 4/3

These ratio images were processed and assessed in each of the localities using the standard image processing techniques developed in the test area (Chap. 5.3d). Results are summarised in table 7.3.

Table 7.3 Performance of selected Colour Ratio Composites for mapping alteration at various localities in south west New Mexico

Locality	Ratio Combination 1 5/7 5/4 3/4	2 5/7 5/4 4/3	3 5/7 5/4 3/2	4 5/7 3/2 3/4	5 5/7 3/2 4/3
Blue Creek Basin	Poor	Very Good	Poor	Poor	Best
Red Rock Basin	Poor	Good	Poor	Poor	Good
Alum Mountain	Poor	Very Good	Best	Poor	Very Good
Brock Canyon	Poor	Best	Good	Poor	Very Good
Mogollon	Very Poor	Very Poor	Very Poor	Very Poor	Very Poor

The clay mineral and iron oxide ratios were not at all useful in the Mogollon Mountains. Here results were anomalous because the poor performance of the ratios was not, as was the case for the other localities, due to conflicting spectral signatures, but because of a lack of rock spectral information caused by high vegetation cover, snow cover and shadow from the very rugged topography combined with the low sun angle of the TM imagery. Therefore the following discussion excludes the Mogollon locality.

Combination 1 and combination 4 were poor for all sites. Combination 1 gave a image similar to the discarded 5/7 5/1 3/4 with vegetation and clay alteration appearing similar (as browns and reds). The high value of vegetation in ratio 5/7 dominates the low values of the 3/4 ratio causing confusion between clay and alteration.

Combination 2 worked well at all the sites, but was particularly good at Brock Canyon (Fig. 7.5). Alteration (clay and iron oxides) appears yellow, clays are red to pink, iron oxides are green (occurring in the Gila Conglomerate) and vegetation is magenta. The silicic ash flow tuffs overlying the Brock Canyon complex volcanics to the north also appear yellow (but less so than the hydrothermal alteration) probably due to the presence of clay bands and iron oxides from weathering, as was found in the test area (Chapters 6.2 and 6.5). Forests on the tuffs appear magenta.

Combination 3 (Fig. 7.6) was the best for mapping alteration in the Alum Mountain area. Vegetation is red, volcanics are cyan and snow is green. The alteration is a mottled pink-white colour indicating clay and iron oxide

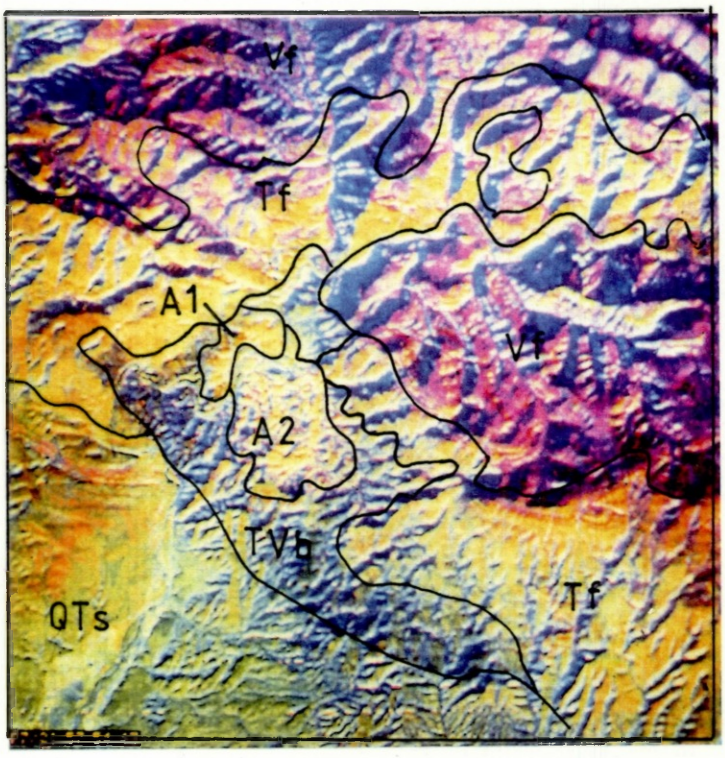

Figure 7.5 Colour Ratio Composite 5/7 5/4 4/3 of the Brock Canyon area. See text.

Key:

A1	Strong clay and Fe oxide alteration
A2	Hydrothermal alteration
Tvb	Volcanic complex of Brock Canyon (andesites and trachyandesites.
Tf	Ash flow tuffs
Vf	Ash flow tuffs with forest cover
QTs	Gila Conglomerate

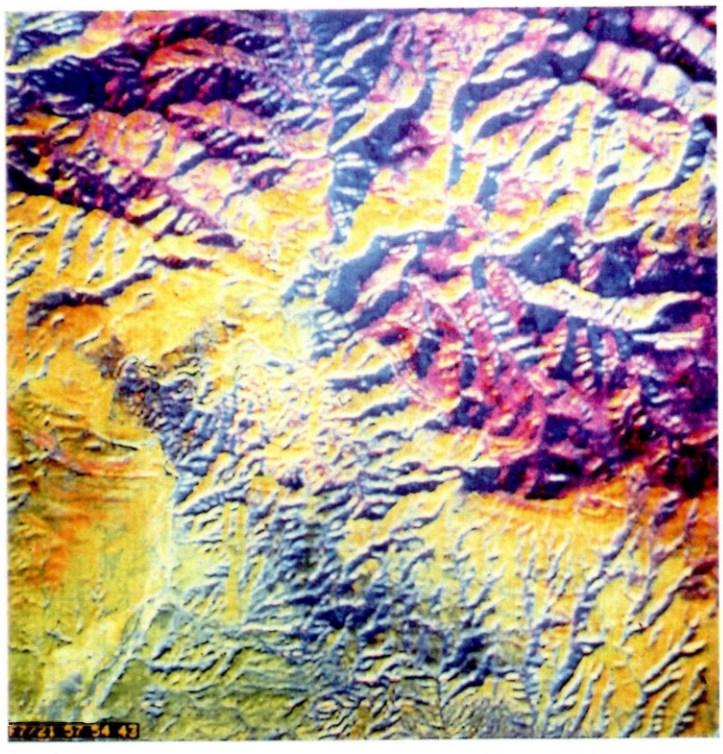

Figure 7.5 Colour Ratio Composite 5/7 5/4 4/3 of the Brock Canyon area. See text.

Key:

A1	Strong clay and Fe oxide alteration
A2	Hydrothermal alteration
Tvb	Volcanic complex of Brock Canyon (andesites and trachyandesites.
Tf	Ash flow tuffs
Vf	Ash flow tuffs with forest cover
QTs	Gila Conglomerate

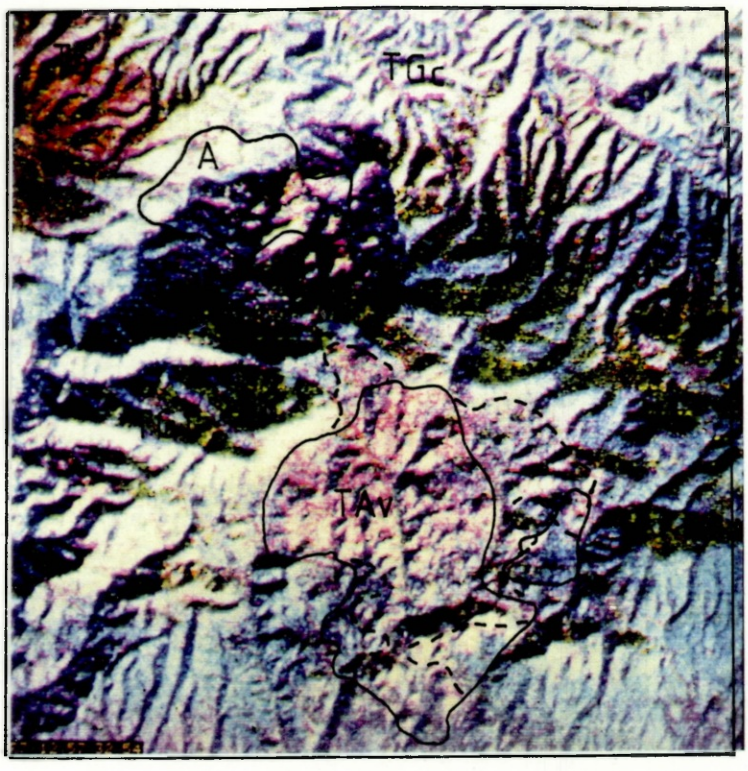

Figure 7.6 Colour Ratio Composite 5/7 3/2 5/4 of the Alum Mountain (Copperas Creek) area. See text for discussion.

Key:

	Extent of hydrothermal alteration mapped by Ratte and Gaskill 1975.
	Extent of hydrothermal alteration suggested by the TM imagery.
A	Area of strong clay and Fe oxide absorption on Alum Mt.
TGc	Gila Conglomerate
Ta	Andesites (Bearwallow Fm.)
TGf	Latite and Andesite of Gila Flat
TAv	Alum Mt. volcanic complex

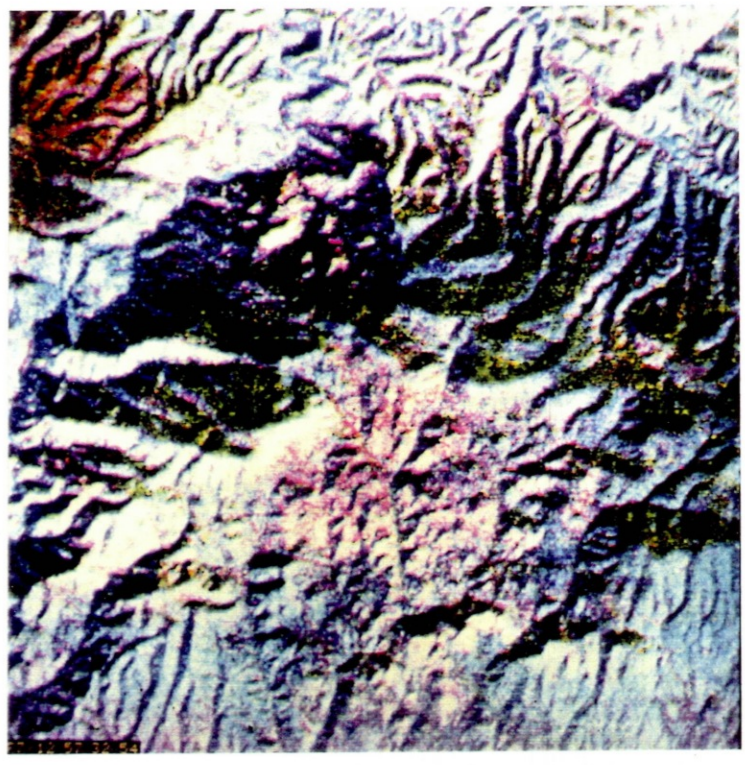

Figure 7.6 Colour Ratio Composite 5/7 3/2 5/4 of the Alum Mountain (Copperas Creek) area. See text for discussion.

Key:

	Extent of hydrothermal alteration mapped by Ratte and Gaskill 1975.
	Extent of hydrothermal alteration suggested by the TM imagery.
A	Area of strong clay and Fe oxide absorption on Alum Mt.
TGc	Gila Conglomerate
Ta	Andesites (Bearwallow Fm.)
TGf	Latite and Andesite of Gila Flat
TAv	Alum Mt. volcanic complex

alteration. At Alum Mt. itself and across the Gila River alteration is particularly strong. The imagery agreed with the previously known alteration distribution with minor differences, outlined on figure 7.6. Field mapping is recommended to check on the validity of the ratio results. Good results were also achieved at Brock Canyon where the vegetation cover is greater. The usefulness of combination 3 decreased as vegetation decreased.

Combination 5 was the best combination overall for all localities, although where vegetation is very heavy combination 2 is better (e.g. Brock).

On combination 5 clay, iron oxides, clay and iron oxides together and vegetation could all be mapped separately. Figure 7.7 shows the Blue Creek combination 5 image. Vegetation appears magenta and blue. The cultivation along the Gila River and the densely forested areas in the Burro Mountains and north east of Red Rock appear magenta indicating vegetation with strong leaf water absorptions (high 5/7) and strong chlorophyll absorptions (high 4/3). Vegetated areas which appear blue indicate vegetation with strong chlorophyll absorptions but no or small leaf water absorptions. These occur on densely forested areas northeast of the Summit Mountains and on scrub vegetated areas east of East Camp. These seem to occur exclusively on basaltic andesitic substrates, which seem to lower the 3/2 and 5/7 absorptions due to spectral mixing.

Clays (appearing red) occur at Deer Peak, the Gila fluorite area south of Cliff (Spring Canyon) and in the granite - gneiss terrain north east of Red Rock town. Iron oxides appear green. At Cliff small epithermal deposits of precious metals (Gillerman 1964, pages 151

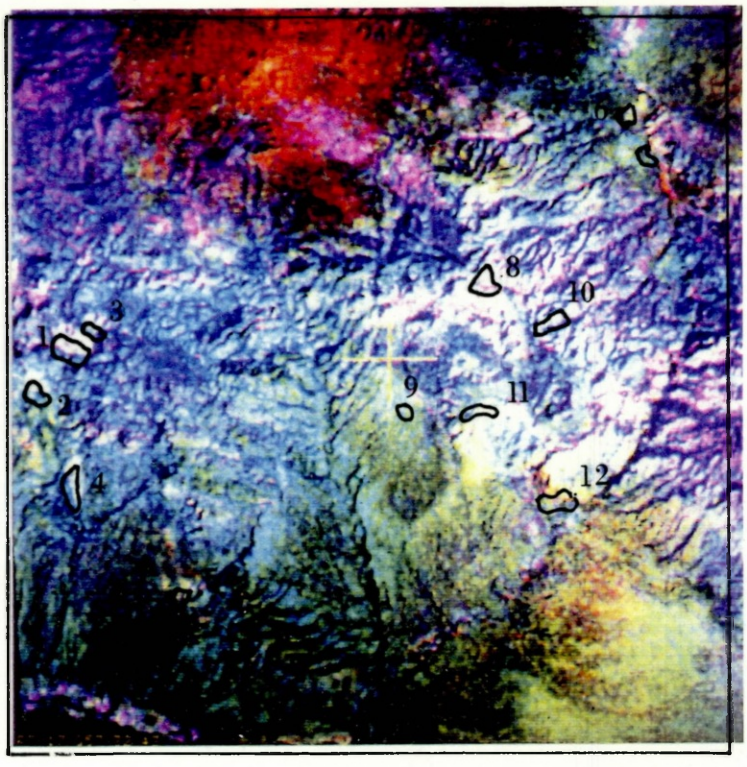

Figure 7.7 Colour Ratio Composite 5/7 3/2 4/3 of the Blue Creek basin. The best CRC for mapping hydrothermal alteration in the vegetated terrain of southwest New Mexico. The image has been low pass filtered and edge enhanced.

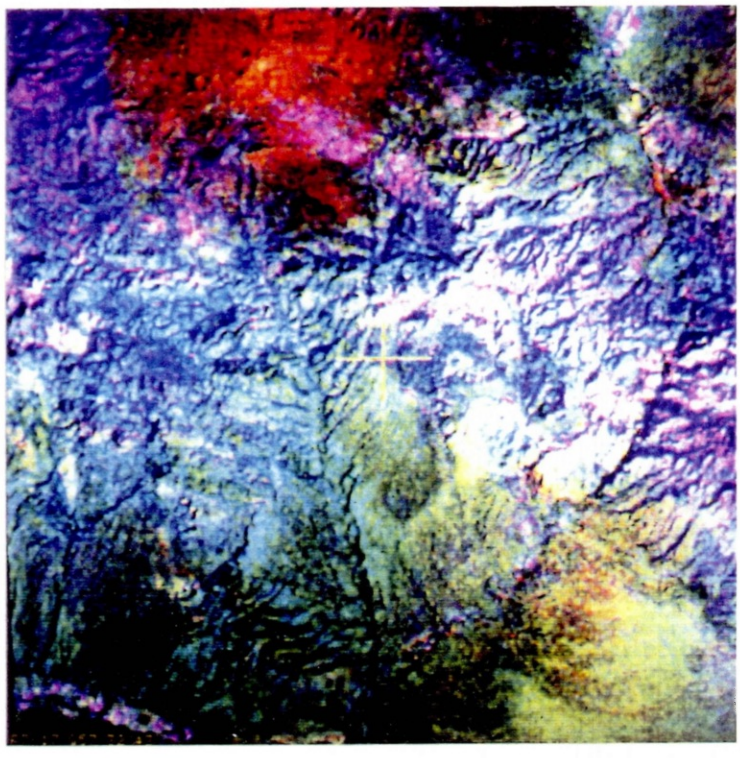

Figure 7.7 Colour Ratio Composite 5/7 3/2 4/3 of the Blue Creek basin. The best CRC for mapping hydrothermal alteration in the vegetated terrain of southwest New Mexico. The image has been low pass filtered and edge enhanced.

-153) and fluorite (pages 170 - 17) are known. Iron oxides (appearing green) occur mainly in the basinal areas probably originating from iron rich waters carried by the rains from the volcanic and granitic uplands.

Where clay and iron oxides occur together bright yellow hues result.[1] Such hues occurred at the following (the locations are shown on fig. 7.7) localities :

1	Telephone Ridge }	
2	Vanderbilt Peak }	Summit Mountains
3	Raeburn area }	Test Area
4	Mt. Royal }	
5	Riley Peak	
6	Sandy Canyon (Cliff)	
7	Red Rock Canyon }	
8	Fairground }	Red Rock
9	High Lonesome Peak }	Basin
10	Brushy Canyon }	
11	Ash Creek Camp	
12	Jack Canyon	
13	West of Burro Mountains Mts.	

The first four areas are in the Summit Mountains test area and have been described earlier (Chap. 5). At Riley Peak fluorite and manganese veins occur in quartz veins cutting Precambrian granites and the overlying volcanics. The alteration in the basinal areas west of the Burro Mountains is probably due to clays and iron oxide weathered rock surfaces, similar to the Lordsburg mining

1 *Unfortunately several of the yellow areas have appeared white on the image reproduced here, due to loss of colour resolution.*

district, some 40 kilometres to the south as noted by Kruse (1984).

No alteration or mineralisation is known at Sandy Canyon, at Cliff. Likewise no alteration or mineralisation is known in the Red Rock Basin area, although in 1960 Freeport Sulphur Company drilled 4 holes around High Lonesome Peak, searching for porphyry copper deposits. In the Red Rock area vegetation is a problem, particularly in the eastern part of the area, where spectral mixing of vegetation and acidic and/or altered rocks occurs (See fig. 7.14).

At Ash Creek Box and Jack Canyon the anomalies occur where Cretaceous Beartooth Quartzite and Colorado Shale are host to Tertiary rhyolite porphyry intrusives, on or near major northwest trending faults. Hydrothermal deposits are associated with faults near or in the granite and Tertiary volcanic contacts, including fluorspar, manganese, magnesite, lead silver and copper elswhere in the area (Gillerman, 1964, page 159). It is not clear however whether the ratios are responding to signatures from the sedimentary rocks, intrusive rhyolites, or associated hydrothermal alteration.

7.3 Principal Components Analysis

(a) Principal Components Analysis at Blue Creek

PCA was applied only to the Blue Creek Basin area. Figure 7.8 illustrates the six principal component images.

Eigenvectors of the Blue Creek Image

	TM Bands					
	1	2	3	4	5	7
PC1	0.31	0.19	0.30	0.30	0.70	0.42
PC2	0.74	0.27	0.27	0.21	-0.45	-0.25
PC3	-0.54	0.14	0.40	0.69	-0.22	-0.07
PC4	-0.14	0.22	0.51	-0.50	-0.34	0.56
PC5	0.16	-0.32	-0.41	0.37	-0.36	0.66
PC6	-0.12	0.85	-0.05	0.03	-0.03	0.10

(a) PC 1

(b) PC 2

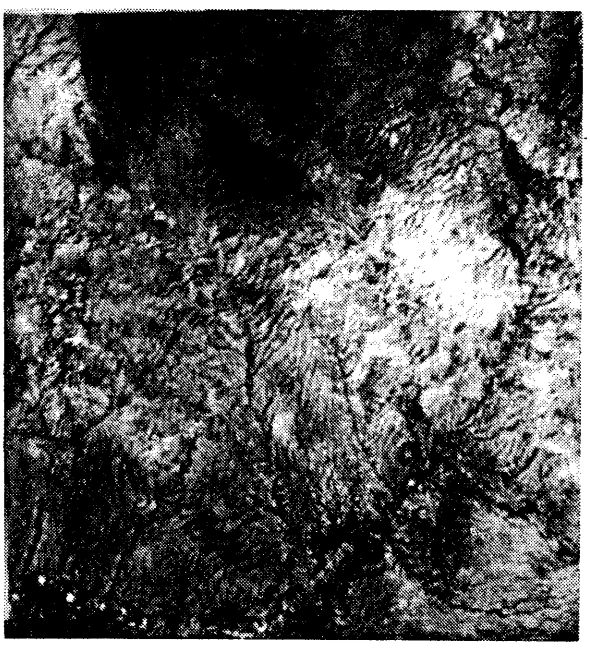

(c) PC 3

(d) PC 4

(e) PC 5

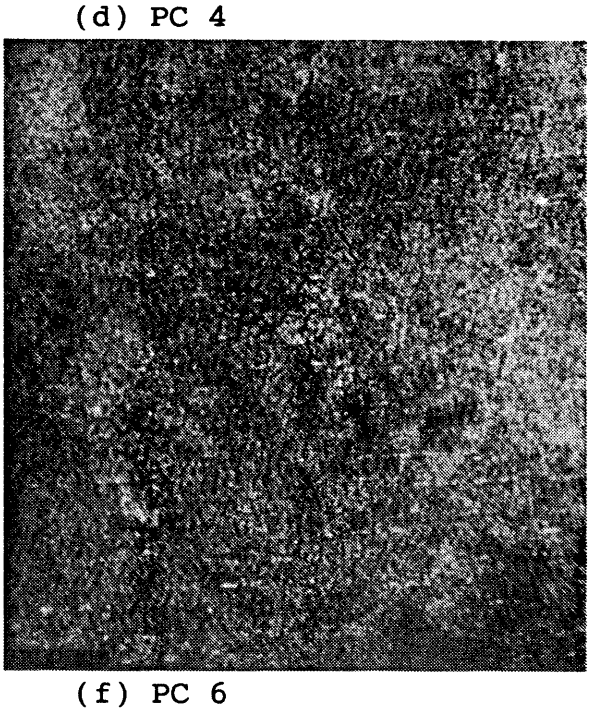

(f) PC 6

Figure 7.8 Principal Components images 1 - 6 of the Blue Creek basin. See text for details.

Processing included normalisation and contrast stretching using an ADJUST stretch.

PC1 shows topography and is a good image for structural interpretation, being free of noise, mist and other band dependent spectral features. The northern part of PC2 contains the mist and low cloud of the imagery and also shows the residual topography caused by uneven scattering typical of imagery illuminated by low sun angles. The fine textural detail of PC1 is absent. The Precambrian granite and metasediments show up clearly as a dark S shaped area on the east of the image.

PC4 and PC6 are the least useful for geological information. PC4 is a useful vegetation indicator which shows the "green" vegetation along the Gila river, the Summit Mountains, Blue Creek basin and elsewhere on the imagery. PC6 is predominantly noise.

Alteration appears on both PC3 and more prominently on PC5. On PC3 altered areas appear bright whereas on PC5 they appear dark. Rhyolitic rocks also appear dark on PC5, but less so than the known altered areas. Not all the dark areas on PC5 are altered, e.g., the basaltic plains of the Bearwallow Mt. Formation and Gila Conglomerate on the north of the image. As on the ratio imagery the Cretaceous age Beartooth Quartzite and Colorado Shale are particularly difficult to separate from altered and rhyolitic rocks.

PC composite 3 4 5 with a scale stretch was an excellent image for geological interpretation (Fig. 7.9). Red hues are altered areas. In the Red Rock area the Beartooth Quartzite and Colorado Shale appear orange, similar to

Figure 7.9 Principal Components 3 4 and 5 of the Blue Creek basin displayed as a colour compo site.

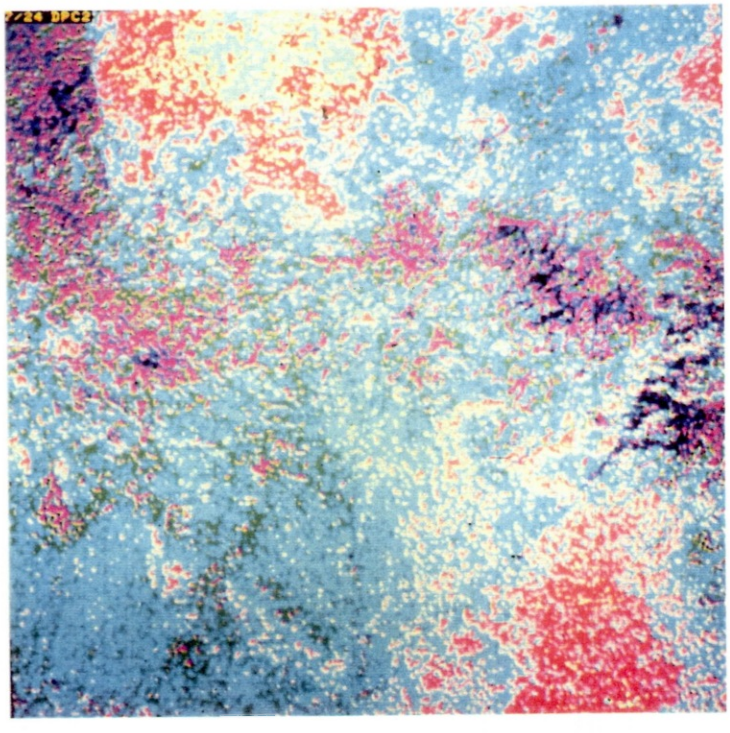

Figure 7.11 Directed Principal Components image 2 from TM ratios 5/7 and 3/4 of the Blue Creek Basin. Filtered, level sliced and psuedo-coloured.

deposits south of Cliff, Vanderbilt Peak and Anderson Ranch. Vegetation is magenta and is preponderant in the Red Rock area west of the Gila River and south of Davis Canyon. All these areas were identified on the ratio imagery except Anderson Ranch which was recognised on air photographs (Chap. 4.3g).

(b) Directed Principal Components

Directed Principal Components Analysis (DPCA) is a technique developed to separate conflicting vegetation and alteration spectra in multispectral imagery (Fraser and Green 1987). The technique uses two ratio images for input, a vegetation index neutral to alteration (clay and iron) and the clay (and vegetation contaminated) mineral ratio. The spectral information common to the two ratios should occur in DPC1. Theoretically this should be vegetation, leaving the clay mineral altered areas on DPC2 (Fig. 7.10).

The technique was expanded to use 3 input bands, 5/7, 5/1 and 3/4. Like the 2 band case, common information i.e. vegetation should occur in DPC1, with the remainder of the spectral information occurring in DPC2 and 3. This should improve spectral resolution and separate out noise in the imagery.

DPCA was done at Blue Creek, Alum Mountain, and the Red Rock Basin area. Figure 7.11 is the DPC2 from a DPCA consisting of band ratios 5/7 and 3/4 of Blue Creek. The image has been filtered and level sliced to 8 levels. Alteration appears light pink - but there are large unaltered areas appearing similar - a large area of

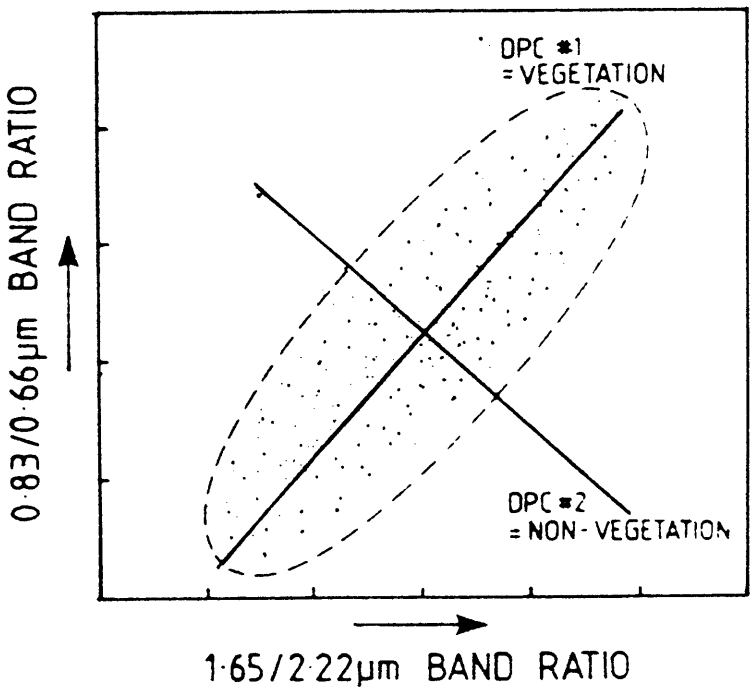

Figure 7.10 Schematic representation of a directed principal component analysis to separate the effect of clays from those of vegetation in the 1.65/2.22 µm band ratio.

alluvial material west of the Burro Mountains and on a concentric band around Mud Spring Mountain (but absent from vegetated areas on Applegate Mt. and Sycamore Creek).

The alluvial areas appeared spectrally similar to altered areas on ratio images (Chap. 7.2b) and is interpreted as ferric iron oxide stained. The area around Mud Springs is basalts and andesites, perhaps with surficial iron oxides staining. The image is good for delineating vegetation distribution and density (black to dark blue).

Figure 7.12 is a false colour composite of DPC 123 of Alum Mountain using DPCA of ratios 5/7 5/1 and 3/4. The image should be compared with figure 7.6. Alteration appears dark blue, vegetation is red, rocks are cyan and purple, shadow is yellow and snow is pink.

7.4 Vegetation Studies

(a) Introduction

The standard image processing techniques used to map alteration in the test area were not so successful for mapping alteration regionally, because of the difficulty of spectrally separating hydrothermally altered rocks from vegetation.

In order to determine with confidence that the areas identified by the ratio and PCA processes are hydrothermally altered rocks and not vegetation it is necessary to know the regional distribution of vegetation. More specifically it is necessary to identify those areas

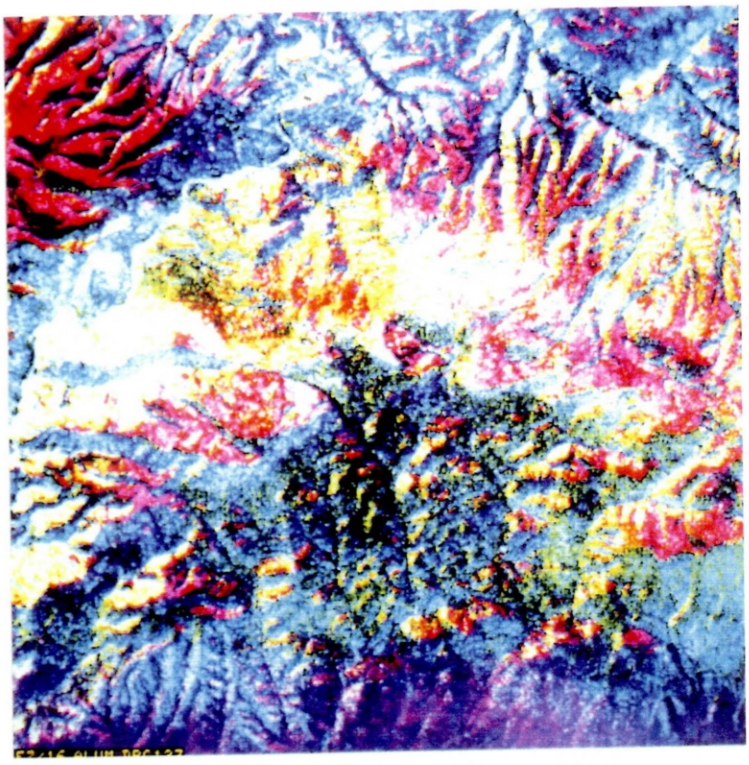

Figure 7.12 Directed Principal Components Composite of DPCs 1 2 and 3 from TM ratios 5/7 5/1 and 3/4 of the Alum Mt. area.

where vegetation density and distribution are sufficient to mask alteration spectra or to produce ambiguous results.

The test area studies suggest that alteration can be identified from mixtures of clay bearing altered rocks and vegetation where the vegetation is below 70 % (Chap. 6.4). Above 70 % we enter the mixed pixel area - here a pixel has neither the spectral signature of alteration (from 100 to 70 % of a pixel) or vegetation (100 % of a pixel). If all pixels with 70 % vegetation or more can be identified, alteration can be identified on the remaining imagery with a high degree of confidence.

The only information source available is the 1:250,000 scale regional vegetation map of New Mexico (Fig. 3.2) which has insufficient detail on vegetation type and distribution and no information on vegetation density. Consequently the easiest way of obtaining the required information is to extract it from Landsat satellite data. Several indices were assessed to find a useful regional vegetation index which could help indicate those areas where there would be difficulties in mapping alteration.

(b) Vegetation Indices

The most common way to extract information on vegetation using VNIR and SWIR data is to measure the difference of reflectance between the visible red and the infrared part of the spectrum. Broadly speaking two types of indices have been developed, both for the assessment of green biomass; N space based indices, such as the GVI of Kauth

and Thomas (1976) and the PVI of Richardson and Wiegand (1977) or ratio based indices. N space indices were not used in this study because they are computationally complex, unreliable and often require ground spectral measurements.

Several ratio based indices and a simple index based on the difference between the red and infrared bands were assessed. The indices were all tested in the Summit Mountains test area where vegetation types and distribution are well known. The results produced estimates of vegetation cover ranging from zero to 66 % (Table 7.4).

Table 7.4 Estimated percentage of vegetation cover of the Summit Mountains using TM indices.

Number	Name	Percent Vegetation
V1	4-3/4+3	3.2
V2	B7-V1/B7+V1	1.42
V3	4/3	3.2
V4	4-3 (cl=10)	0
	4-3 (cl=6	6
	4-3 (cl=5)	12
	4-3 (cl=1)	66

cl = clip level

These results were compared to the air photo study (Chap. 6.4) to determine the best estimate of vegetation density.

V1 and V2 are indices developed for differentiating between bed rock and superficial deposits in densely

vegetated areas (Peras et al. 1985). V2 uses the red/IR and the SWIR leaf water absorption feature. Subtraction of the VI from TM7 increases the difference between vegetated and non-vegetated substrates. Clay bearing rocks with a band 7 absorption are not confused with vegetation (with the leaf water absorption) because altered rocks do not have the red/IR feature. V3 is the standard TM equivalent of the widely used MSS 6/5 ratio.

Elvidge and Lyon (1985b) have shown that variation in rock and soil brightness strongly influences ratio based vegetation indices, resulting in over estimation of vegetation on dark backgrounds and under estimation on bright backgrounds, because of the radial way ratios divide up two dimensional space. In the Summit Mountains the ratio indices tended to under estimate the number of vegetated pixels, probably due to the bright volcanic substratum.

Several of the ratio indices based on the differences of red and infrared reflectance have been evaluated for measuring biomass and physiological status of vegetation (Tucker, 1977). Most were sensitive to green biomass but were dependent on the presence of sufficient green vegetation. As these techniques were developed for use on grasslands with high biomass and vegetation cover their usefulness in semi-vegetated terrain where soil and rock reflectance are high is questionable.

When tested under the more severe conditions existing at at Alum Mountain and Mogollon the ratio indices mixed shadow (in the case of V1) and snow (in the case of V2 and V3) with vegetation.

The 4-3 index with a clip level of 6 was the best index for the determination of vegetated pixels. On this index any pixel where the band 4 intensity is greater than the band 3 intensity is considered to be vegetated. Flexibility is added by the use of a variable clip level, where the value by which the band 4 level must be greater than the band three level is specified. This index correlated well with the determined 70 % vegetation level (Table 6.2).

Although this index does not suffer from the disadvantages of the ratio based indices discussed above, it does suffer from topographic effects and atmospheric variations (multiplicative errors) which are not present with ratioed data (Chapts. 3.6 and 5.3).

(c) The Hue HSI Index

Neither the N based, ratio based, or red - infrared difference indices are scene independent and therefore cannot be applied to TM imagery in other locations without detailed ground checking. For rapid processing of TM, repeatable and reliable processes are desirable. The HSI transform shows promise for such a process (Chap. 2.5c).

Visual inspection of TM images from New Mexico, Arizona and south eastern Spain show that the H value of vegetation always falls between certain well defined limits on a fully stretched hue image produced from an HSI transformed false colour image. As hue is independent of brightness changes caused by shadowing, solar elevation and azimuth variations it is a reliable and scene independent method of identifying vegetation.

Hue from an RGB image ranges from 0 - 360 degrees, but is scaled to 0 - 255 for display. Vegetation has an H value ranging between 130 and 160. As soil moisture increases there is a shift in hue towards the blue thus it is impossible to define absolute thresholds.

(d) Vegetation Masking

The HSI method of identifying vegetated pixels lends itself as an efficient means of identifying vegetated pixels from the imagery. A method using this technique involving masking out vegetated pixels prior to image processing was done based on a technique similar to that described by Knepper and Raines (1985) for masking vegetated pixels on Landsat MSS imagery.

The key to the success of this method when applied to alteration mapping is to identify only those pixels which are 70 - 100 % vegetated, while leaving altered pixels. The procedure is a follows:

(1) Select TM bands 4 3 2 (equivalent to the MSS false colour imagery).
(2) Apply an atmospheric correction (Chap. 5.3d).
(3) Transform the bands from RBG cartesian coordinates to HSI polar coordinates.
(4) Contrast stretch hue (H) to fill the display available (0 - 255).
(5) Check vegetation pixels fall between values of 130 and 160.

(6) Create a binary mask of the hue image to convert all vegetated pixels to 0 and all other pixels to 1.
(7) Multiply selected images by the binary mask to mask all vegetated pixels and leave all other pixels unaffected.

The atmospheric correction is crucial to produce reliable and repeatable results. If it is not possible to produce a reliable atmospheric correction then the imagery may be normalised using a gaussian or equalisation stretch. If this is necessary point 5 should be made carefully to ensure vegetated pixels are within the allowable limits.

Point 7 can be applied to any image, bands, ratios, PCs etc. However it is important that no processing techniques which utilise neighbourhood processes (i.e. spatial filtering) are applied to the image after vegetation masking.

Figure 7.13 is a split screen image of the western half of the Blue Creek image. The left side shows the original false colour composite and the right half shows the same image showing the areas identified as vegetated by the HSI binary mask. Figure 7.14 shows the areas in the Blue Creek Basin where pixels have vegetation levels greater than 70 %

Figure 7.15 is the TM 5/7 ratio of the Blue Creek image with the vegetation mask applied. The mask has identified and removed all those areas with 70 % vegetation cover or greater. Compare this image with figure 7.4. All absorptions resulting primarily from leaf water absorptions are removed i.e. from

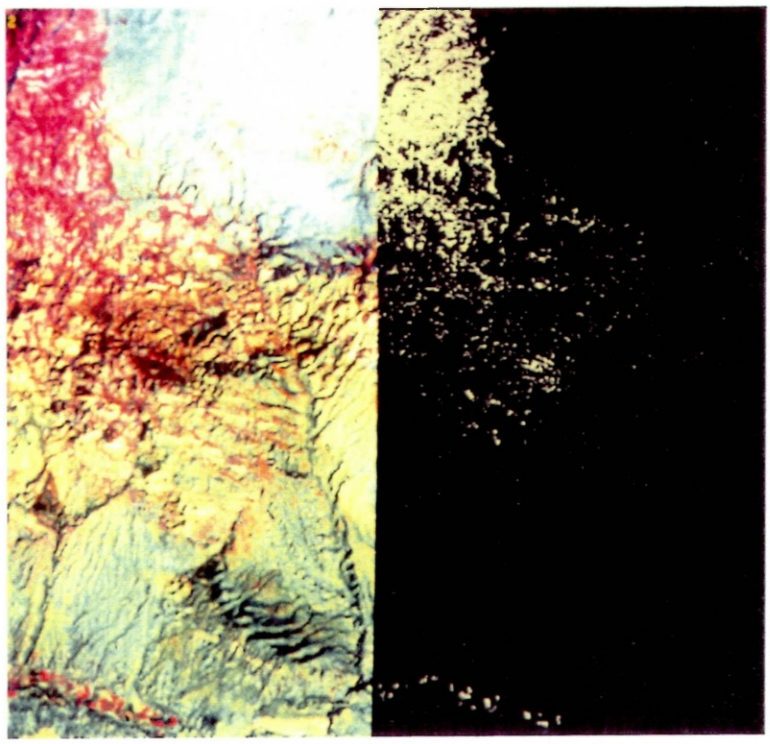

Figure 7.13 Split screen image of the western half of Blue Creek basin, showing a false colour composite with vegetation as red and the area identified as vegetated using the HSI mask.

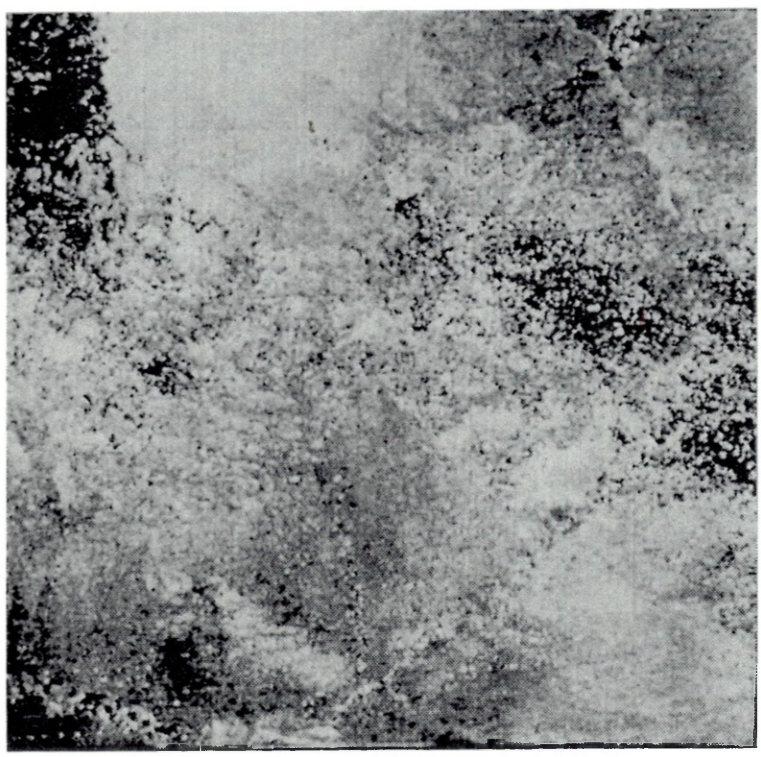

Figure 7.15 The TM 5/7 ratio of the Blue Creek Basin with vegetation removed. Compare with Fig. 7.4.

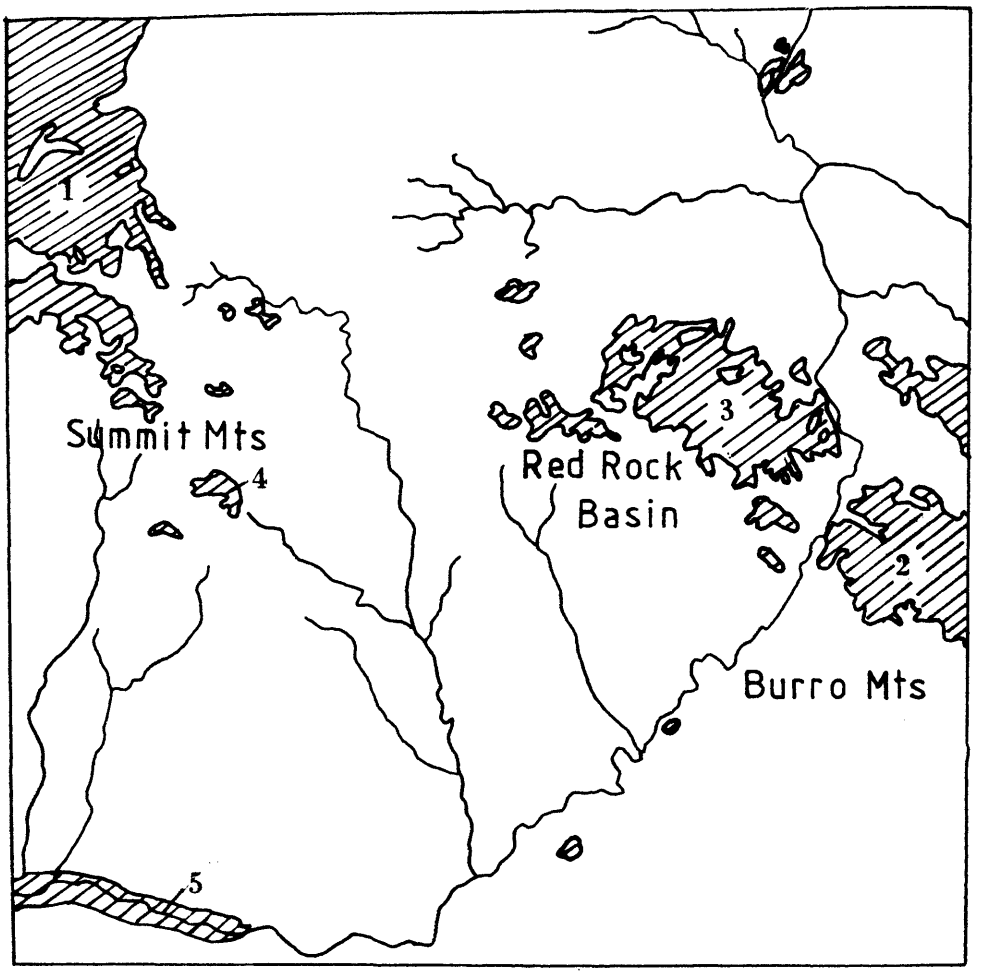

Figure 7.14 Areas of the Blue Creek basin where vegetation density exceeds 70% of a pixel area, and location of the vegetation training areas.

Key:

1. Gila Mountains
2. Burro Mountains
3. Red Rock basin
4. Summit Mountains
5. Gila River Valley

vegetation. Those remaining bright pixels are due to hydroxyl absorptions.

Of the potential altered areas identified earlier, two occur in areas of vegetation density above 70 %, Fairground, and Brushy Canyon, i.e. in areas of mixed pixels.

7.5 Mineral Indices

Two techniques have been developed to map alteration where mixed vegetation and substrate pixels are a problem, the Mineral Absorption Index, for mapping clays (MAI) (Elvidge and Lyon 1985) and the Iron Absorption Index (IAI) (Miller amd Elvidge 1985) for mapping iron oxides.[1]

(a) The Iron Absorption Index

The IAI establishes a baseline in DN space from where IAI values are measured. Deviations are based on iron oxides having a stronger absorption in TM band 1 relative to TM band 3. The IAI measures the deviation of limonite stained surfaces from a previously established rock-soil base line. This base line is transposed into digital space by extracting training sites on the imagery. Deviations from the transposed base line represent limonite stained areas on the imagery. The technique has

[1] Directed Principal Components Analysis and Least Square Residuals have also been used (Chapts. 7.3b and 8.6).

the advantage of being unaffected by the brightness variations which affect ratios.

The procedure requires reflectance measurements from limonite free rock - soil surfaces from the ground and on the satellite data. Such field reflectance data was not available (the technique was published after my field work had been completed). More importantly the entire procedure is dependent on vegetation having equal reflectance in TM bands 1 and 3, to avoid confusion between iron oxide and vegetated surfaces. This is not so in the Summit Mountains (Chap. 5.4d and 6.4).

(b) The Mineral Absorption Index

This technique estimates a background vegetation component, calculated from a regression technique between the 3/4 and 5/7 ratios, which is subtracted from the 5/7 ratio to leave residual absorptions either positive or negative which represent pixels with anomalous 5/7 absorptions.

The technique makes use of two important properties of TM ratio imagery. The first is the normally good correlation of vegetation in TM ratios 5/7 and 4/3. The second is the insensitivity of the 4/3 ratio to rock and soil variation. It is this characteristic which allows the prediction of the vegetation contribution to the 1.65/2.2 µm ratio.

The 1.65/2.22 µm ratio (TM 5/7) is an accurate indication of leaf water content (Rhode and Olsen 1971, Tucker 1980) because water moisture strongly absorbs at 2.2 µm and hence is a good indicator of the quantity of living

material. The 0.66/0.83 μm ratio (TM 3/4) is the TM equivalent of the widely used MSS 5/6 ratio vegetation index (Chapts. 6.5 and 7.4) which is inversely proportional to vegetation density. Band 5 (0.6 - 0.7 μm) is sensitive to chlorophyll absorptions, and band 6 (0.7 - 0.8 μm) is related to leaf chlorophyll concentrations. The two ratios commonly show a linear positive correlation for green vegetation.

c) Results in southwest New Mexico

Figure 7.16 plots 5/7 and 4/3 ratio values of altered rocks and vegetation measured from field data in the Summit Mountains. These results indicate that the two conditions necessary for successful implementation of the MAI hold for the Summit Mountains.

Band and ratio analysis were done on the TM imagery to determine if the required relationships also occur on the TM imagery. Vegetation was studied in five areas in the Blue Creek Basin (Fig. 7.14).

1. Gila Mountains (northwest of Summit Mountains)
Mixed coniferous and woodland consisting of Pine and Douglas fir, Juniper and Oak. Uniform tree canopy cover at 70 %. The terrain is fairly flat plateau between 2000 m and 2133 m. Rocks are andesite, basalt and basaltic andesites of the Bearwallow Mt. Formation.

2. Burro Mountains
Woodland association of Juniper Pinion and scrub Oak. Thickly developed and fairly continuous canopy

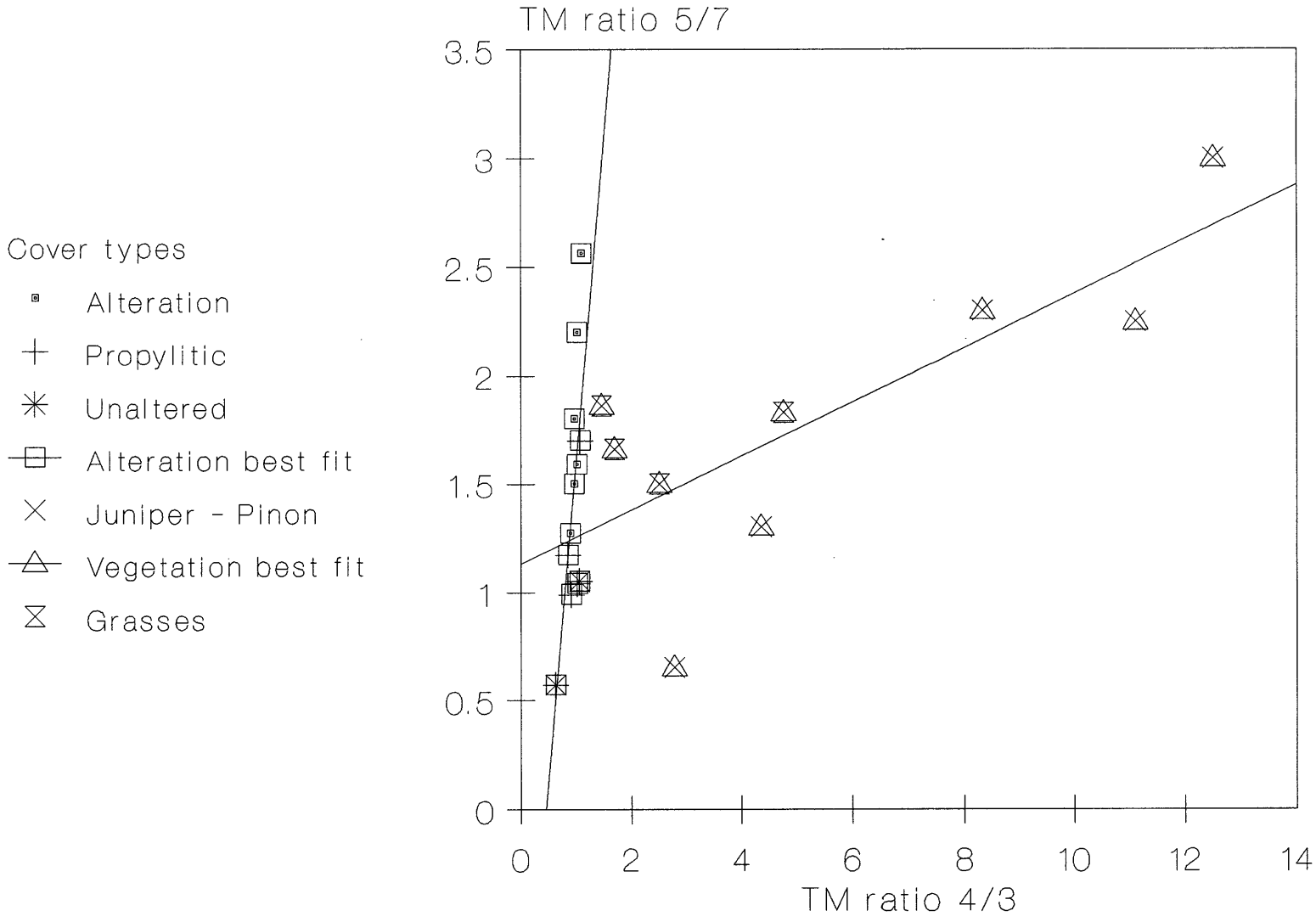

Figure 7.16 Plots of TM ratios 5/7 and 4/3 for vegetation and rocks of the Summit Mountains from HHRR measurements.

cover. About 70 % vegetated. The rocks are Precambrian granodiorite, granite and gneiss at elevation of 1666 - 1800 m.

3. Red Rock Basin
Vegetation is as in the Burro Mountains with very variable distribution. The substrate is predominately rhyolitic and trachyandesite ash flow tuffs and porphritic or andesite of the Cliff Eruptive Centre.

4. Summit Mts (East Camp)
Pine and Juniper on brown iron stained andesite soil (Fig. 5.2) with 60 - 70 % vegetation cover evenly distributed. Elevation is 1666 - 1800 m.

5. Gila River
Cultivated crop land with 100 % vegetation cover.

The correlation between ratios 5/7 and 3/4 for vegetation these vegetation types are shown in table 7.5.

The correlation calculated from the imagery varies between 0.1 and 0.6. As expected the highest correlations are from the uniformly vegetated cultivated areas. The correlations in the forested and scrub areas are all poor, probably due to spectral contamination from rock soil and shadows.

The linear relationship between the 4/3 and 5/7 is given by the formula $y = c + m x$, where y = the TM 5/7 value, X = the 4/3 value, m the slope of the line and c the intercept.

Table 7.5 Correlation of TM Ratios 5/7 and 4/3

Locality	Correlation	Slope	Intercept
Gila Mountains	0.10	-0.01	2.05
Burro Mountains	0.35	0.30	1.30
Red Rock Basin	0.50	0.79	1.03
Summit Mountains	0.28	0.45	1.36
Gila River	0.60	0.67	1.10

Using the most highly correlated 5/7 4/3 relationship (Gila River):

TM 5/7 Background = 1.1 + 0.67 (TM 4/3)

Anomalous areas with 5/7 absorptions i.e. those not due to vegetation are calculated from:

TM 5/7 original - TM 5/7 background

Figure 7.17 shows this difference image of the Blue Creek basin. All bright areas represent anomalous TM 5/7 ratio absorptions, i.e., areas where the absorptions in TM 5/7 are different from those expected from the TM 5/7 4/3 relationship.

Fairground clearly shows as a large area with anomalous TM 5/7 absorbtions. Other areas are Red Rock Canyon, High Lonesome Peak and a small area at Brushy Canyon. The Ash Creek Camp area does not have an anomaly, suggesting the alteration here is due to vegetation.

The main weaknesses in the technique is the dependence on the correlation of the 5/7 4/3 relationship for vegetation across the entire image. As can be seen from table 7.5 this relationship varies with vegetation type.

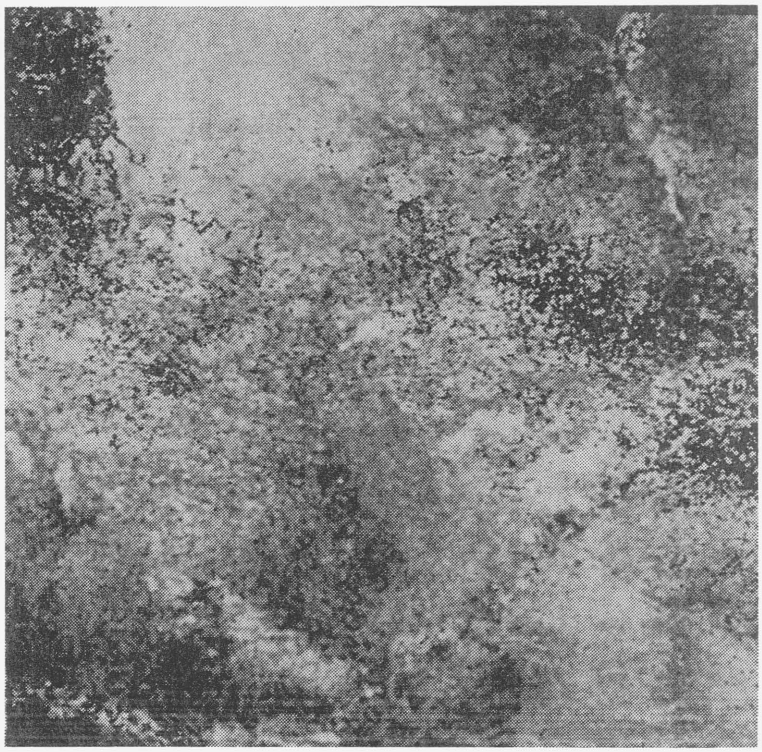

Figure 7.17 The Mineral Absorption Index (MAI) image for the Blue Creek basin. Bright tones represent areas of anomalous band 7 absorptions.

7.6 Epithermal Types in southwest New Mexico

The simple remote sensing model described in Chapter 5, developed from the Summit Mountain epithermal system (Chapter 4) was applied to the regional imagery to identify the epithermal types in southwest New Mexico. The model, developed for volcanic hosted epithermal deposits may not be suitable for sedimentary hosted deposits.

The results are presented on table 7.6 and the locations are shown on figure 7.18.

The area of the alteration zone in square kilometres was estimated from the imagery for each site. It may have hydroxyl absorptions from clay minerals, micas, alunite etc., iron oxide absorptions or both.

The main host rock to the alteration and the surrounding country rock were interpreted from the imagery or from the Silver City quadrangle geology map (see Drewes et al. 1985).

The presence and nature of the known faults or major lineaments of fracture traces recognised on the imagery and their relationship with any alteration are noted. Structural control is usual for epithermal deposits. Abundant fault and fracture systems particularly those kilometres in length are typical of adularia sericite systems.

Table 7.6 Details of the epithermal types mapped from TM imagery in south west New Mexico

	Locality Name	Location Reference	Mineral Absorptions	Estimated Alteration area (Km2)	Host Rocks	Faults	Intrusive Activity	Volcanic Vents/Domes	Known alteration or mineralisation	Epithermal Type
1	Fairground Red Rock Basin	Sec. 9, T.17S. R18W	Clay Fe	0.48	Tertiary silicic tuffs	On major NW trending zone	Numerous Tertiary rhyolite intrusives	Possible Vent	No	Adularia-sericite
2	Brushy Canyon Red Rock Basin	N. Sec. 23 T.17S R18W	Clay Fe	0.80	Sycamore Camp Eruptives	Pologonal fracture zone	Close to Tertiary intrusives of (1)	No	No	Unknown
3	Ash Creek Camp Red Rock Basin	Sec. 18 T.17S. R.18W	Clay Fe	2.00	Sycamore Camp Eruptives	?	Nearby Tertiary intrusives	No	No	Epithermal ?
4	Red Rock Canyon Red Rock Basin	Secs. 18 T.17S R18W	Clay Fe	10.00	Tertiary silicic tuffs and andesites	On prominent NE Trending lineament	No	No	No	Deuteric or Supergene
5	High Lonesome Peak Red Rock Basin	Sec. 26 T.17S R19.W	Clay Fe	0.40	Boundary of tertiary felsic, andesitic and Gila Congl.	On major NW trending fault	Minor rhyolite dykes	No	Minor Fe oxides No hypogene (Gillerman 1964)	Deuteric
6	Ash Creek Box Red Rock Basin	South of T.18S R.18W	Clay Fe ?	2.50	Colorado Shale, Beartooth Quartzite and granite	Near major N-NW fault	Tertiary rhyolite porphyry	No	Minor mineralisation (Gillerman, 1964)	Epithermal ? Sedimentary hosted
7	Jack Canyon	Secs. 11, 12 T.18S R.18W	Clay Fe ?	1.30	Colorado Shale, Beartooth Quartzite and granite	On major N-NW fault	Major Tertiary rhyolite porphyry	No	Minor hydrothermal deposits (Gillerman, 1964)	Epithermal Sedimentary hosted
8a	Spring Canyon Cliff	East Sec. 34 T.16S R.17W	Clay	0.90	Tertiary rhyolite tuffs	?	No	No	High grade silver (Cora Miller) reported (Gillerman, 1964)	Epithermal
8b	Dam Canyon Cliff	Sec. 22 T.16S R.17W	Clay Fe	0.26	Tertiary rhyolite tuffs	No	No		Small manganese deposit (Black Tower). (Gillerman, 1964)	Epithermal
9	Sandy Canyon Cliff	Sec. 9 T.16S R.17W	Clay Fe?	0.40	Gila Conglomerate	No	No	No	No	Unknown
10	Norris Ranch Sycamore Creek	NW Sec.14 T.16S R.18W	Clay Fe	1.20	Felsic volcanics	Major NNW	No	No	Perlite (Gillerman, 1964)	Epithermal
11	Deer Peak	Sec. 22 T.16S R.20W	Clay	0.60	Rhyolite flows and pyroclastics	East west	Intrusive Rhyolites	Yes	Clays (See Chapt. 5)	Deuteric
13	Sycamore Creek	Secs. 1-3 T.17S R.20W	Clay Minor Fe	2.70	Rhyolite flows and pyroclastics	Major east-west	Intrusive Rhyolites	Yes	Clays (See Chapt. 5)	Deuteric
12	Bitter Creek	Secs. 19-22, 26-30 T.16S R.21W	Clay Fe	18.00	Bloodgood Canyon tuff - Virden Dacite	Numerous major NW fault zone	Rhyolite dykes	Minor vents	Silicic & Advanced argillic (See Chapt. 4)	Acid-sulphate and Supergene
14	Raeburn	NW 1/4 Sec. 6 T.17S R.20W	Clay Fe	0.01	Bloodgood canyon tuff	Major NW fault	minor dykes	No	Silicic (See Chapt. 4)	Epithermal
15	Telephone Ridge	Sec. 1 T.17S R.21W	Clay Fe	1.00	Bloodgood Canyon tuff - Virden Dacite	Major locus of NW and EW faults	Rhyolite dykes	No	Extensive silicic, advanced argillic, lesser sericitic (See Chapt. 4 + 5)	Adularia-sericite super-imposed on Acid sulphate ?
-	Laura - Alabama	South 1/2 Sec. 3 T.17S R.21W	Fe, minor Clay	0.02	Amygdaloidal Andesite	Major N and NW faults	Rholite dykes and plugs	Minor vents	Chloritisation (See Chapt. 4)	Adularia-sericite
16	Park Spring	Sec. 36 T.17S R.21W	Clay Fe	0.50	Rhyolite flows and pyroclastics	No	Intrusive Rhyolite	Tuff ring vent	Clays (See Chapt. 5)	Deuteric
17	Riley Peak	Sec. 20 T.18S R.20W	Clay Fe	0.13	Granite, Older Volcanic Series	Minor	Rhyolite dykes	No	No	Epithermal
18	Anderson Ranch	Sec. 8 T.17S R.19W	Fe	0.10	Rhyodacite of Cherry Creek Rhyolite	Major NW	Rhyolite plug and dykes	No	No (See Chapt. 4 + 5)	Adularia-sericite ?
19	Brock Canyon	-	Clay Fe	5.00	Andesites and dacites	Major NW faults of Mogollon Front Range	No	Volcanic dome complex	Argillisation and Sereciti sation Ratte et al. 1979)	Acid-sulphate
20	Alum Mt.	-	Clay Fe	5.00	Andesite and latites	Near Mogollon Front range	Rhyolite plugs and dykes	Large Vent	Extensive advanced argillic (Ratte et al. 1979)	Acid-sulphate and Supergene
	Copperas Creek (Alum Mt.)		Clay Fe	19.00	Andesite and Latite	Near Mogollon Front range	Silicic pipes Numerous minor dykes	Eroded dome complex ?	Silicic, argillic (Ratte et al. 1979)	Acid-sulphate ?

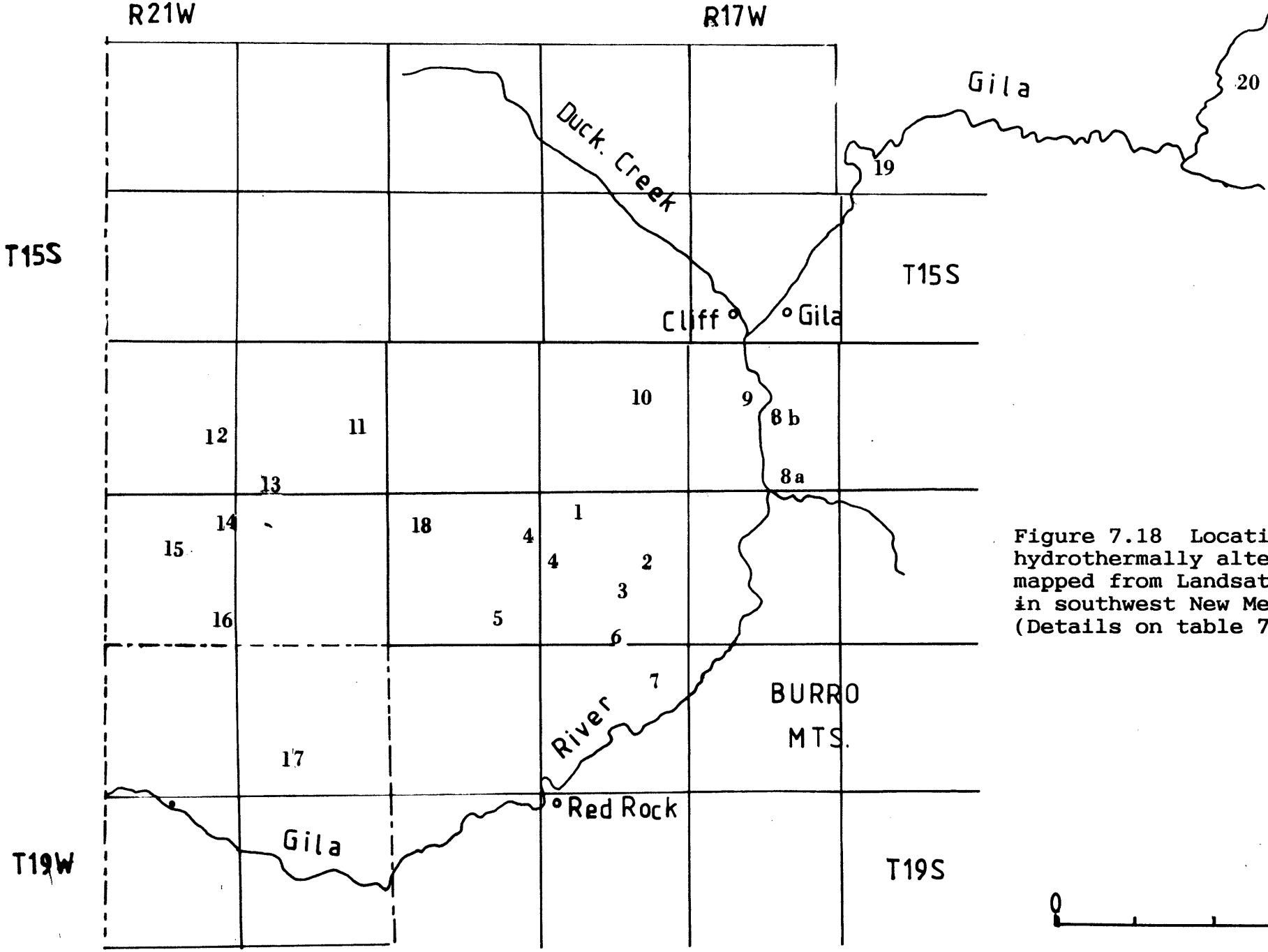

Figure 7.18 Location of hydrothermally altered rocks mapped from Landsat TM imagery in southwest New Mexico. (Details on table 7.6).

The presence of intrusives, either interpreted from the imagery or identified on the geological maps is indicated. The presence of intrusives while not directly related to an epithermal system is often positive evidence of the presence of an intrusion at depth, which can provide a heat source for an epithermal system.

Volcanic vents or domes are often visible on imagery as circular features. Vents often have associated deuteric alteration (Chap. 4.3j) and may rule out the presence of more extensive and mineral bearing epithermal systems. Domes or stratovolcanoes, particularly those associated with extensive argillic alteration are often acid-sulphate type epithermal deposits.

If alteration or mineralisation is documented in the literature this is indicated. Many of the areas have not previously been identified.

The alteration may be epithermal, deuteric or supergene in origin. Where possible the epithermal alteration is classified as acid-sulphate or adularia sericite type. A question mark denotes areas where the spectral signatures, although indicative of alteration, are thought unlikely to be so from geological evidence.

There are some areas where confusion occurs. At Rock Canyon the alteration is likely to be deuteric or supergene alteration of silicic tuffs, which exhibit a clay absorption band similar to epithermal minerals, and at Ash Creek Camp the MAI indicates the TM band 7 absorption is due to vegetation, not alteration. The majority of the altered areas identified have alteration zones greater than 0.1 km^2 (10 hectares). The acid

sulphate type deposits tend to form larger alteration zones, often many tens of kilometres in area. The adularia sericite type have smaller alteration zones, often around 0.5 km^2 and tend to be linear in shape.

The regional study has identified numerous areas of hydrothermal alteration in southwest New Mexico. Of these the Fairground area in the Red Rock Basin stands out as a locality where there may be an adularia sericite epithermal system.

7.7 DISCUSSION

The factors which influenced alteration mapping in the test area were also important for regional mapping, because of the geological and geographical similarities of the areas and because the same image data was used. However the relative importance of these factors is different and these influence the choice of image processing techniques applied to extract the information on alteration.

Local geographical variations were significant. As described in Chapter 2, there are significant variations in vegetation type and distribution and in topographic relief. In certain areas, such as the Mogollon Mountains the thick forests were sufficient to preclude spectral remote sensing and the rugged topography caused significant shadowing and specular reflectance. Elsewhere vegetation at or exceeding 70 % of a pixel may cause

confusion because of the spectral similarity between alteration minerals and vegetation (Chap. 6.5).

Variations in image quality e.g. mist or cloud or damaged pixels, affected results. Scattered cloud cover affected all the bands and occasional low mist affecting the visible bands. On the mountainous area snow cover was a problem e.g. Mogollon, Alum Mt.

The main problem was vegetation which appears spectrally similar to the key images used for alteration mapping. Two situations occur; the first is trivial, involving the separation of hydrothermally altered rocks from vegetation when individual pixels are easily identified as one or the other. The second situation is more complex, the extraction of rock soil information from pixels containing rock and vegetation information, so called mixed pixels, or mixels.

In the trivial case the main problem is the identification of the level of vegetation on an individual pixel which causes hydrothermally altered rocks to be misclassified. From studies in the Summit Mountains this was estimated to be approximately 70 % of a pixel (Chap. 7.4b). This figure was estimated by comparing those areas where alteration was successfully mapped with the imagery (Chap. 5) to a vegetation map produced from aerial photographs. The aerial survey was then matched with an HSI vegetation index to identify regional vegetation distribution.

There are limitations to this method. The photograph and satellite data were taken at different times (the photographs in November 1980 and the TM imagery in January 1983), but in southwest New Mexico, and generally in

[In practice it is very difficult to accurately measure vegetation cover, either in the field or by using remote sensing techniques such as aerial photographs or satellite imagery. Shadows can be a significant problem, particularly where sun illumination is low. As shadows within the vegetation canopy are included in the overall estimated vegetation cover figure, the actual vegetation cover is less than that indicated.]

semi-arid terrain, seasonal variations in vegetation distribution are usually small. In wetter periods (July to August) and in winter desert plants flower and grass grows, increasing biomass and hence vegetation indices. This was considered to have a minimal effect because the vegetation map constructed from the aerial photos was based on scrub and tree distribution which does not change significantly between seasons.

A number of image processing techniques were used to tackle the problems caused by the effects of mist, snow, low sun illumination and variable vegetation cover. These were:

(1) Colour ratio composites (CRC)
(2) Principal components analysis (PCA)
(3) Directed principal components analysis (DPCA)
(4) Single band ratios with Hue vegetation masking
(5) Mineral or iron absorption indices (MAI) and (IAI)

CRC, PCA and vegetation masked ratio imagery were very successful where vegetation was below the 70 % level. CRC provided useful spectral information and the substitution of various ratios allowed a large degree of flexibility. The vegetation masked ratio simplified image interpretation as all vegetated areas are removed leaving only altered pixels.

DPCA and MAI have been specifically tailored to solve the problem of mixed pixels; yet none worked particularly well in southwest New Mexico. The main problem is reliability. Both the IAI and the MAI cannot be used automatically as

they require ground spectral measurements. The MAI is dependent on the linkage between chlorophyll and leaf water moisture, and is susceptible to two types of error - those due to the relationships of the vegetation used to construct the regression curve and those if the relationships from the regression curve are not applicable to the vegetated areas outside that used in the regression.

It is important to ensure that the vegetation used for the regression calculation for detecting the background vegetation exhibits a relationship between the 3/4 and 5/7 ratios which holds for all the vegetated areas in the image, and that soil or rock spectra with low 5/7 absorptions are included. If the sample vegetation suffers from chlorosis or leaf water stress which does not occur in the remainder of the image (excepting altered areas) then the contribution of vegetation to the 5/7 image will be over estimated or under estimated respectively. If the reverse holds, i.e. parts of the vegetation except for the sample used for the regression suffer from chlorosis or leaf water stress the reverse occurs i.e. chlorosis causes under estimation and leaf water stress causes over estimation.

To use the Mineral Indices with any confidence detailed knowledge of the ground conditions are required. Even though a rigorous solution to the mixed pixel problem was not found adequate results were achieved.

Generally the more complex the processing used the greater is the likelihood that alteration targets are missed or imagery is misinterpreted because of a lack of a thorough understanding. Because of these problems it is not

possible to be absolutely certain that some of the target areas identified in figure 7.18 are hydrothermally altered.

The regional mapping in the Blue Creek basin used subsampled data (every 3rd pixel) to cover large areas and to minimise processing time. Epithermal deposits with alteration zones approximately 0.1 km^2 (10 hectares) were identified. Using full resolution data an increase in detection up to three times would be expected, suggesting TM would identify altered areas 3 - 5 hectares in size. A figure confirmed by the TM performance in the test area (Chap. 5).

It was difficult to separate hydrothermally altered rocks from the spectrally similar acid tuff rocks and quartzites and shales. The spectral similarity of the latter may be due to contact metamorphism and associated localised intrusives.

CHAPTER 8.

CONCLUSIONS AND RECOMMENDATIONS

8.1 Introduction

The objectives of this study were to assess TM data for mapping hydrothermally altered rocks and to identify areas of altered rocks in southwest New Mexico. The methodology is critically examined and the reliability and scope of the results are appraised. The results are presented separately as image processing and geological results and guidelines are presented for using TM in this type of application, together with recommendations for future work.

8.2 Critique of the Methodology

In short the methodology was to assess digital image processing techniques applied to TM data in the Summit Mountains test area, and to apply optimum arising processes to the Blue Creek Basin and surrounding areas of southwest New Mexico.

Of fundamental importance to the methodology is the applicability of the epithermal model (Chap. 4.8) and resultant remote sensing model (Chap. 5.8d) developed in the Summit Mountains, to the region. The characteristics

of the remote sensing epithermal model were categorised as direct and indirect.

(1) Direct features are those specific to the epithermal system directly observable by remote sensing i.e. faults, and surface hydrothermal alteration.

(2) Indirect characteristics are secondary geologic information interpreted from the imagery which are indicative of the epithermal type, i.e. regional structure, intrusions, vents, and country rocks (Chap. 4.7).

The Summit Mountain area is interpreted as an adularia sericite type epithermal deposit superimposed upon a probable acid sulphate system (Chap. 4.8). Because elements of both epithermal types are present it is likely that other epithermal deposits would have characteristics similar to those of the Summit Mountain based model.

One unusual aspect of the test area epithermal system is the dominance of natro-alunite in the advanced argillic assemblage of the acid sulphate system. However, this comparatively rare sodium rich alunite has the spectral signature of common alunite.

The characteristics of the epithermal model are sufficiently broad to permit identification of all significant volcanic hosted epithermal deposits occurring in New Mexico. The model is not applicable to sedimentary hosted epithermal deposits, such as those associated with the Mesozoic sedimentary formations.

Addendum to Critique

[The figure of 70 % pixel vegetation cover, as the cut off point, below which alteration can be mapped with 'standard' processes and above which special mixed pixel processes are required, is by no means absolute. This vegetation level is that estimated from the studies in the Summit Mountains test area. The extrapolation of this figure to other areas must be done with great care.

No attempt was made to rigorously define vegetation canopy cover on the ground on individual Landsat pixels, because of the difficulties involved. Rather, estimates were made from stereographic examination of small scale colour aerial photographs of the test area. The limitations of this method have already been discussed (Chap. 7.7, page 254-255). The author realises the difficulties of accurately measuring vegetation cover and accepts the actual cut-off point probably lies below 70 %.

The pixel vegetation cut-off figure would certainly be less in scenes with greater overall vegetation cover. The regional studies suggest the figure is approximately correct where overall scene vegetation cover is 40 - 50 %. (Chap. 8.4e).]

In addition to the alteration model, the successful extrapolation of the test area results to the region depends upon the similarities and differences between the geology, geography and imagery of the test area and the region. There are differences in all of these, particularly between the geography and the imagery. The increased vegetation cover, shadow (from rugged topography and low sun illumination) and snow affected the regional mapping (Chap. 7.7). These differences did influence the imaging processing techniques, but did not nullify the basic methodology.

8.3 TM Imagery Capability

The Landsat 4 TM imagery was affected by shadow, snow, cloud, and mist typical of winter images. The low sun illumination angle prevented the TM from mapping successfully in mountainous terrain. There was no choice of TM imagery available as this was the first available TM image acquired over southwest New Mexico.

Nevertheless, hydrothermally altered rocks were recognised by exploiting the spectral features typical of altered rocks; the absorptions in band 7 due to the presence of hydroxyl bearing minerals, and absorptions present in the visible bands due to the presence of iron oxides. Hydroxyl absorptions alone or with iron oxides indicated the presence of altered rocks, but the presence of iron oxides alone was not necessarily diagnostic of alteration.

It was not possible to separate individual alteration assemblages because of the poor spectral and spatial resolution of the imagery relative to the size of individual alteration assemblages, but the severity of the alteration was gauged qualitatively by measuring the relative strength of the band 7 absorption.

Hydrothermal alteration was mapped where:

(1) the altered rocks contain sufficient hydroxyl bearing minerals to produce strong band 7 absorptions. As little as 10 % is suggested (Chap. 6.5)

(2) the alteration zone was large enough to be resolved. No areas of hydrothermal alteration less than 5 hectares in size were mapped (Chap. 6.5), although evidence suggests the maximum capability is probably of the order of 1 hectare.

(3) the alteration is spectrally separable from the country rocks. There were some difficulties separating alteration from acid volcanics (Chap. 6.2b) and from quartzites and shales (Chap. 7.7).

(4) the alteration is not spectrally masked by weathering, lichens, or vegetation (Chap. 6.3 and 6.4).

The image processing techniques used to extract this information are presented below.

8.4 Image Processing results

A range of image processing techniques were used (Chap. 3) to exploit the spectral signatures of the altered rocks.

(a) Thematic Mapper Bands

Single TM bands and colour composites were of limited use for alteration mapping, because the high correlation of TM bands produced low contrast images which are difficult to interpret (Chap. 5.2 and 7.1). The removal of spectral vegetation information from the imagery gave poorer results (Chap. 5.2c) indicating that the vegetation component is an important factor of rock type discrimination in multispectral imagery.

Colour transformations of Intensity and Hue[1], and edge enhancements, produce images with excellent spectral, spatial and textural appearance for geological interpretation. Combinations 1 3 5 and 1 4 5 were the best. However on these images it is not possible to consistently identify and separate altered rocks from non altered rocks (Chap. 5.2d, 5.8a and 7.1). Such images are useful for providing "indirect" information for the epithermal model. "Direct" spectral information for the model was provided mainly by ratio and Principal Component imagery.

---

1 *Decorrelation stretching may be useful if results are not extrapolated to other images.*

(b) Principal Components

Single band Principal Components (PC) images were useful for alteration mapping and with careful interpretation were as useful as ratio images, but because they are image dependent it was difficult to identify alteration without good ground information. The first PC was good for providing structural information. As with ratio imagery, it was difficult to separate alteration from vegetation in areas of mixed pixels with a vegetation level of greater than 70 %. Directed Principal Components performed no better than conventional ratio or PC images (Chap. 7.3b).

(c) Band Ratios

Band ratios were the most effective imagery used for mapping alteration. They have the advantage of computational simplicity, and ease of interpretation. The only significant processes required are atmospheric corrections, and contrast stretching. However because of the severe way in which ratios effect data, it is important to examine the classes in feature space.

Vegetation density and distribution affected the ratios. Where vegetation cover is less than approximately 70 % over any pixel, simple processing techniques work well e.g. in the Summit Mountains. The single band TM 5/7 ratio (1.65/2.22 μm) effectively mapped clays, micas or alunitic rocks, and TM ratios 5/1 (1.65/0.48 μm), 5/4 (1.65/0.83 μm), 3/2 (0.66/0.56 μm) and 4/2 (0.83/0.56 μm) effectively mapped iron oxides. However the 3/1 ratio (0.66/0.48 μm) confused iron oxides and vegetation at low vegetation cover.

As vegetation cover increased above 70 %, the TM ratio 5/7 image confused clay bearing minerals and vegetation. Evidence from the Summit Mountains suggests that clays can be mapped at up to 90 % vegetation cover, so long as the vegetated area is not larger than approximately 0.4 hectares and is surrounded by a larger area with lower vegetation cover (Chap. 6.4). The TM iron oxide ratios 5/1 and 4/2 confused iron oxides with vegetation at vegetation cover at or above 60 % . TM ratios 3/2 and 5/4 were superior.

(d) Colour Ratio Composites

With increasing vegetation cover, colour ratio composites were more effective than individual ratio images. Certain combinations were more effective than others depending on the terrain conditions (vegetation, shadow, topography, snow and water). The standard ratio combinations, i.e. the clay ratios (5/7), a vegetation index to unscramble conflicting hydroxyl and leaf water absorptions e.g. 3/4 and either of the iron oxide ratios 5/1, or 4/2 is useful where less than 6 - 10 % of the scene was vegetated (defined as a pixel with greater than 70 % vegetation).

Combination 5/7 3/2 4/3 is recommended for mapping alteration in southwest New Mexico. It worked well over a wide range of conditions up to approximately 40 % scene vegetation cover. Under more severe conditions up to approximately 50 % scene vegetation cover, combination 5/7 5/4 4/3 is superior, although this may be unique to the situation at Brock Canyon.

(e) Vegetation Indices -

Subject to the overall scene vegetation constraints outlined above (i.e. up to approximately 50% scene vegetaion cover), where a pixel consists of mixtures of clay bearing altered rocks and vegetation, the alteration can be identified where the vegetation is below 70 % of the pixel area. Above 70 % we enter the mixed pixel area - here a pixel has neither the spectral signature of alteration (from 100 to 70 % of a pixel) or vegetation (100 % of a pixel), and was not identified by either ratio or PC imagery.

In areas of mixed pixels there is a need to separate vegetated pixels from mixed pixels. A number of vegetation indices were assessed. The red - infrared vegetation index was superior to ratio based indices for mapping vegetation but because neither the N based, ratio based, or red - infrared difference indices are scene independent, they cannot be applied to TM imagery in other locations without detailed ground checking.

The HSI transform provides a rapid, repeatable and reliable means for the identification of vegetation on TM Imagery (Chap. 2.5c and 7.4). With the HSI method only those pixels which are 70-100 % vegetated were identified. Interpretation of the ratio images was eased by removing vegetated pixels from the image prior to band ratio production.

(f) Mineral Indices

Mineral absorption indices (MAI) have been developed to identify altered areas in areas of mixed vegetation and alteration. The results were unreliable because the assumptions on which the technique relies did not always apply in southwest New Mexico. The technique also requires ground based reflectance measurements which are not always available (Chap. 7.5). However the MAI does show promise as a method for mapping alteration in areas of mixed pixels.

8.5 Geological Results

The interpretation of the processed imagery along with the epithermal model, produced new and improved geological knowledge of southwest New Mexico.

All known areas of hydrothermally altered rocks in southwest New Mexico, with the exception of the East Camp area in the Summit Mountains and the Mogollon mining areas, were mapped (Chap. 7). Alteration was not mapped at East Camp because of the small area (4 hectares) and width (approximately 10 metres) of the alteration zone and because there was little or no hydroxyl bearing minerals or iron oxides present to give absorptions sufficiently strong to be detected. In the Mogollon area the dense forests, shadow and snow coupled with the low sun angle of the imagery, made it impossible to detect spectral information from the rock surface.

Hydrothermal altered rocks were identified in both known

and previously unknown areas. The majority of the zones were greater than 0.1 km^2 in area. The alteration types were classified as deuteric, supergene or epithermal. It was impossible to separate acid sulphate from adularia sericite type epithermal deposits using spectral information alone, but in several cases information extracted from the imagery, supplemented by subsidiary geological information, enabled epithermal types to be identified.

Acid sulphate types tend to have larger alteration zones, often several tens of square kilometres, while adularia sericite types have smaller alteration zones (often less than 0.5 km^2) often aligned linearly and associated with regional fault zones.

The field and laboratory work in the Summit Mountains clarified the geology of the area (Chap. 4) and the details on the distribution and nature of the hydrothermal alteration were improved (Chap. 5.8).

8.6 Recommendations

The following guidelines are presented for alteration mapping using Landsat TM data:

It is important to formulate a model of the mineral type sought, and to relate the characteristics of this mineral type or types to the information extractable from the remotely sensed imagery used. Many of the characteristics

of such a model are unlikely to be extracted from remotely sensed data alone. The important characteristics of epithermal systems, (acid-sulphate or adularia - sericite in type), with TM were described earlier (Chap. 8.3). As this study has showns significant "indirect" supporting geological information is extractable from TM imagery (Table 4.5).

The image processing techniques to use to extract the "direct" and "indirect" data depend upon the characteristics of the imagery and the key remote sensing characteristics identified on the model.

Preliminary processing of the imagery should involve geometric correction if the data is to be transferred to other map data sources. TM is of sufficient geometric fidelity to permit 1:50,000 scale mapping with minimal distortion using 512 by 512 pixel full resolution imagery.

The "indirect" information is best provided by HSI enhanced colour composite bands with edge enhancements, or smoothing as required. Statistical measures of imagery content, such as described in Chapter 5 are useful for optimum band selection.

Band ratios, Principal Components Analysis or band subtraction should be used to extract direct "spectral" information. The success and necessity of image arithmetic and transformations are dependent on the terrain and image characteristics, particularly vegetation and sun illumination. The low sun illumination of the New Mexico imagery did not favour the use of subtraction techniques. Therefore the choice of imagery is very important. Choose imagery

with minimal cloud cover and other atmospheric disturbances, without snow and with an illumination angle preferably above 50 degrees. The MSS studies illustrate the importance of summer imagery for mapping in New Mexico (Appendix II).

It is important to determine the amount of vegetation in a pixel which can be tolerated by the mapping techniques employed, and to separate the image into areas were mapping can be done with confidence and those where mixed pixels may be a problem. The HSI technique potentially provides a means to identify vegetated pixels, independent of image location. More work is required to assess in detail how the Hue HSI technique performs in vegetated areas with varying vegetation types and density, and in different image types around the world.

Much important work is needed on mapping alteration in mixed pixels areas. Decorrelation stretching (Chap. 2.5c) and Directed Principal Components (Chap. 7.3) are not recommended. However, the MAI is a promising technique. The MAI could be used with more confidence in southwest New Mexico if a number of ground reflectance measurement are taken of the different vegetation types to estimate the local TM 5/7 4/3 ratio relationships.

A related technique not assessed in this thesis is Least-square Residuals (LSR). This technique has been developed for mapping hydrothermal alteration in vegetated and weathered terrain (Fraser et al. 1986) and good results are reported in conditions similar to those in New Mexico (Hook and Munday 1988). LSR

should be applied in the Summit Mountains area using the substantial geological data collected in this research. If successful, the study should be extended to the Red Rock basin area, supported by field studies including geological and vegetation mapping and *in-situ* reflectance measurements. Such studies should clear up the nature of the number of suspected areas of hydrothermal alteration identified in this work.

This research has shown that with appropriate and careful image processing, significant geological information on epithermal mineral deposits can be extracted from Landsat Thematic Mapper imagery, not only in arid and semi-arid terrain, but also in semi-vegetated, mountainous terrain. Useful results were achieved despite the affects of low illumination imagery affected by mist and snow. Similar techniques could be successfully applied to map hydrothermal alteration across much of the southwest USA and to approximately thirty per cent of the worlds land surface.

REFERENCES

Abrams, M.J., Ashley, R.P., Rowan, L.C., Goetz, A.F.H. Kahle, A.B., 1977 Mapping of hydrothermal alteration in the Cuprite mining district, Neveda, using aircraft scanner images for the spectral region 0.46 to 2.36 μm, Geology, vol. 5, pages 713 - 718.

Abrams, M.J., Brown, D., Lepley, L. and Sadowski, R., 1983 Remote sensing for Porphyry Copper deposits in Southern Arizona, Economic Geology, vol. 78, pages 591 - 604.

Adams, J.B. and McCord T.B., 1972 Electronic spectra of pyroxenes and interpretation of telescopic spectral curves of the moon, Geochemica et Cosmochimica Acta, Supplement 3, vol. 3, pages 3021- 3034.

Adams, J.B. and others, 1982 Interpretation of weathered surfaces in arid regions using Landsat multispectral images, Proceedings Thematic Conference on Remote Sensing of arid and semi-arid lands, Cairo, Egypt, January 1982, pages 685 - 694.

Adams, J.B.and Filice A.L., 1967 Spectral reflectance 0.4 to 2.0 microns of silicate rock powders, Journal of Geophysical Research, vol. 72, pages 5705 - 5715.

Albers, J.P. and Kleinhampl F.J., 1970 Spatial relationship of mineral deposits to Tertiary volcanic centres in Nevada, United States Geological Survey, Professional Paper 700 C, C1 - 10.

Baker, M.C.W. and Baldwin, J.A., 1981 Applications of Landsat Multispectral classifications for locating gossans in North Chile, Published in Remote Sensing in geological and terrain studies (Allan, J.A. and Bradshaw, M. eds.), Remote Sensing Society, London, pages 25-33.

Berger, B.R. and Eimon, P.I, 1983 Conceptual models of epithermal precious metal deposits, In Shanks, W.C. (ed), Cameroon vol. on unconventional mineral deposits; New York, American Institute of Mining, Metallurgical and Petroleum Engineers, pages 191 - 205.

Berstein, R., 1983 Image Geometry and rectification, in Chapter 21, Manual of Remote Sensing, Special Edition, publ. American Society of Photgrammetry, Colwell R.N. (ed), Sheridan Press.

Biggerstaff, B.P., 1974 Geology and ore deposits of the Steeple Rock - Twin Peaks area. Grant County, New Mexico, M.S. thesis, El Paso, University of Texas, 102 pages.

Blanchet, P.H., 1957 Development of fracture analysis as an exploration method, Bulletin of the Association of Petroleum Geologists, vol. 41, pages 1748-1759.

Buckingham, W.F. and Sommer, S.E., 1983 Mineralogical characterisation of rock surfaces formed by hydrothermal alteration and weathering - Application to remote sensing, Economic Geology, vol. 78, pages 664 - 674.

Burns, R.G., 1970 Mineralogical applications of crystal field theory, Cambridge, Md., Cambridge University Press, 224 pages.

Canas, A.A.D. and Barnett, M.E., 1985 The generation and interpretation of false-colour composite principal component images, International Journal of Remote Sensing, vol. 6, No. 6, pages 867 - 881.

Chavez, P. Jr., Berlin, G.L. and Sowers, L.B., 1982 Statistical method for selecting Landsat MSS ratios Journal of Applied Photographic Engineering, vol. 8, No.1, pages 23 - 30.

Coney, P.J., 1972 Cordilleran tectonics and North American plate motion, American Journal of Science, vol. 272, pages 603 - 628.

Conradsen, K. and Harpoth, O., 1984 Use of Landsat Multispectral Scanner data for detection and reconnaissance of iron oxide staining in mineral exploration, Central East Greenland, Economic Geology, vol. 79, No.6, pages 1229-1238.

Coren, S., Porac, C. and Ward, M.W., 1978 Sensation and Perception, Academic Press, 439 pages.

Corle, E., 1951 The Gila river of the Southwest, New York, Rinehart & Co.

Crippen, R.E., 1987a The regression intersection method of adjusting image data for band ratioing, International Journal of Remote Sensing, vol. 8, No. 2, pages 137 - 155.

Crippen, R.E., 1988a The dangers of underestimating the importance of data adjustments in band ratioing, International Journal of Remote Sensing, vol. 9, No. 4, pages 767 - 776.

Crippen, R.E., Blom, R.G. and Heyada, J.R., 1988b Directed band ratioing for the retention of perceptually-independent topographic expression in chromaticity-enhanced imagery, International Journal of Remote Sensing, vol. 9, No. 4, pages 749 - 765.

Crippen, R.E., Estes, J.E. and Hajic, E.J., 1987b Band and band ratio selection to maximise spectral information in colour composite displays, (in preparation - see Crippen 1987a).

Dee, W.F., Palmer, D.L., Williams, R.C. Jr. and Kisch, 1970 Bubonic plague in the southwest USA - a review of recent experience, Medicine (Baltimore), vol. 49, pages 465.

Drewes, H., Houser, B.B, Hedlund, D.C., Richter, D.H., Thorman, C.H. and Finnel T.L., 1985 Geologic map of the Silver City 1 X 2 Quadrangle, New Mexico and Arizona, United States Geological Survey Miscellaneous Investigations series, I - 1310 C.

Driscoll, T, and Walker,C., 1981 The evolution of image processing technology, Computer Graphics World, 6, pages 29 - 35.

Drury, S.A., 1987 Image interpretation in geology, Allen and Unwin.

Duggin, M.J., 1980 The field measurement of reflectance factors, Photogrammetric Engineering and Remote Sensing, vol. 46, pages 643-647.

Eaton, F.D. and Dirmhirn R.N., 1979 Reflected irradiance indicatrices of natural surfaces and their effect on albedo, Applied Optics, vol. 18, No. 7, pages 994-1008.

Elston, W.E. and Bornhorst, T.J., 1979 The Rio-Grande Rift in context of regional post 40 m.y. volcanic and tectonic events, in Rio-Grande Rift: Tectonics and Magmatism, Riecker, R.E. (ed), pages 416 - 438, AGU, Washington D.C.,

Elston, W.E., 1958 Burro uplift, northeastern limit of sedimentation of southwestern New Mexico and southeastern Arizona, American Association of Petroleum Geologists Bulletin, vol. 42, pages 2513 - 2417.

Elston, W.E., 1960 Reconnaissance geologic map of the Virden thirty minute quadrangle, New Mexico Bureau Mines and Mineral resources, Geologic map 15.

Elston, W.E., 1976a Tectonic significance of mid-Tertiary volcanism in the Basin and Range province; a critical review with special reference to New Mexico, New Mexico Geology Society, Special Publication No.5, pages 93 - 102, Elston W.E. and Northrop, S.A. (eds), 151 pages.

Elston, W.E., 1978 Mid-Tertiary Cauldrons and their relationship to mineral resources, Southwest New Mexico: A brief review, Field Guide to selected Cauldrons and mining districts of the Datil Mogollon volcanic field, New Mexico Geology Society Special Publication No.7, pages 107 - 1.

Elston, W.E., 1984a Mid-tertiary ash flow tuff cauldrons, Southwestern New Mexico, Journal of Geophysical Research, vol. 89, no. B10, pages 8733 - 8750.

Elston, W.E., 1984b Ore deposits hosted by Cenzoic volcanic rocks, Southwest New Mexico, Geological Society of America, Abstracts with Programs, 37th Annual Meeting Rocky Mt. Section, Fort Lewis, Durango, Colorado, vol. 16, No.4, May 11 - 12, 1984.

Elston, W.E., Rhodes, R.C. and Erb, E.E., 1976b Control of mineralisation by mid-Tertiary volcanic centres, southwestern New Mexico, New Mexico Geology Society. Special publication no. 5, pages 125 - 130.

Elvidge, C.D. and Lyon, R.J.P., 1985a Estimation of the vegetation contribution to the 1.65/2.22 μm ratio in airborne Thematic Mapper imagery of the Virginia Range, Nevada, International Journal of Remote Sensing, vol. 6, No.1, pages 75 - 88.

Elvidge, C.D., 1983 Affect of vegetation on Airborne Thematic Mapper imagery of the Kalamazoo porphyry copper deposit, Arizona, Proceedings of the Second Thematic Conference, International Symposium on Remote Sensing of Environment, pages 661 - 667.

Elvidge, D.E. and Lyon, R.J.P., 1985b Influence of rock - soil spectral variation on the assessment of green biomass, Remote Sensing of Environment, vol. 17, pages 265 - 279.

Estes, J.E., 1983 Fundamentals of image analysis: Analysis of visible and thermal infrared data Chapter 24, Manual of Remote Sensing, second edition, Vol. III, pages 987 - 1118, American Society of Photogrammetry, Sheridan Press.

Estes, J.E., Hajic, E.J. and Tinney, L.R., 1983 Fundamentals of image analysis: Analysis of visible and thermal infrared data, Chapter 24, Manual of Remote Sensing, Second Edition, Vol.I, American Society of Photogrammetry, Colwell, R.N. (ed), Sheridan Press, pages 987 - 1118.

Fahnestock, J.D. and Schowengerdt, R.A., 1983 Spatially variant contrast enhancement using local range modification, Optical Engineering, vol. 22, No.3, pages 378 - 381.

Farr, T.G., 1981 Surface weathering of rocks in semi-arid regions and its importance for geologic remote sensing, Unpublished PhD. thesis, University of Washington, 149 pages.

Ferguson, H.G., 1929 The mining districts of Nevada, Economic Geology, vol. 24, pages 115 - 148.

Fisher, W.A., 1975 History of remote sensing: in Reeves, R.G. (ed.) Manual of Remote Sensing, American Society of Photogrammetry, Falls Church, Virginia, pages 27 - 50.

Fraser, S.J. and Green, A.A., 1987 A software defoliant for geological analysis of band ratios, International Journal of Remote Sensing, vol. 8, pages 525 - 532.

Fraser, S.J., Gabell, A.R., Green, A.A. and Huntington, J.F., 1986 Targeting epithermal alteration and gossans in weathered vegetated terrain using aircraft scanners: Successful Australian case histories, Proceedings of the Fifth Thematic Conference, Remote Sensing for Exploration Geology, Reno, Neveda, September 29 - October 2.

Giles, D.,L., and Nelson, C.E., 1982 Principal features of epithermal lode gold deposits of the circum-Pacific rim, Circum-Pacific Energy Minerals Conference, 3rd, Honolulu, Hawaii, August 22 - 28, 1982, Transactions, pages 273 - 278.

Gillerman, E., 1964 Mineral deposits of western Grant County, New Mexico, Bulletin 83, New Mexico Bureau of Mines and Mineral Resources.

Gillespie, A.R., 1983 Digital techniques of Image Enhancement, Chapter 6, Remote Sensing in Geology, Siegal, B.S. and Gillespie, A.R. (eds), New York, John Wiley and Sons.

Gillespie, A.R., Kahle, A.B. and Walker, R.E., 1986 Colour enhancement of highly correlated images. I Decorrelation and HSI contrast stretchs, Remote Sensing of Environment, vol.20, p.209 - 235.

Gladwell, D.R., Lett, R.E., and Lawrence, P., 1983 Application of reflectance spectrometry to mineral exploration using portable radiometers, Economic Geology, vol.78, pages 699 - 710.

Gonzalez, R.C. and Wintz, P., 1977 Digital Image Processing, Addison - Wesley, 431 pages.

Graton, L.C., 1910 Steeple Rock District, The Ore deposits of New Mexico, United States Geologial Survey, Professional Paper 68, pages 327 - 328.

Green, A.A. and Craig, M.D., 1985 Analysis of aircraft spectrometer data with logarithmic residuals, Proceedings of the First Airborne Imaging Spectrometer Data Analysis Workshop, Jet Propulsion Laboratory Publication, 85-41, pages 111 - 119.

Griggs, R.L. and Wagner, H.C., 1966 Geology and ore deposits of the Steeple Rock mining district, Grant County, New Mexico, United States Geological Survey Bulletin 1222-E, 29 pages.

Hall, R.B, 1978 World Non Bauxite Aluminium resources - Alunite, United States Geological Survey, Professional Paper 1076 - A

Hayba, D.O., Bethke, P.M., Heald, P. and Foley, N.F., 1986 Geologic, mineralogic and geochemical characteristics of volcanic-hosted epithermal precious-metal deposits, Review Economic Geology, vol.2, pages 129 - 167.

Heald, P., Foley, N.K. and Hayba, D.O., 1987 Comparative Anatomy of Volcanic-hosted epithermal deposits: Acid-sulphate and Adularia-sericite types. Economic Geology, vol.82, No.1, pages 1 - 25.

Hedlund, D.C., United States Geological Survey, unpublished data in the Steeple Rock NW quadrangle, Grant County, New Mexico.

Hedlund, D.C., United State Geological Survey, unpublished data in the Steeple Rock SW quadrangle, Grant County, New Mexico.

Heiken, G. and Wohletz, K., 1985 Volcanic Ash, University of California Press, 1985.

Heller, R.C. and Ulliman, J.J., 1983 Forest Resource Assessments, Chapter 34, Manual or Remote Sensing, second edition, Colwell R. N. (ed.-in-chief), American Society of Photogrammetry, 2440 pages.

Holben, B.N. and Justice, C.O., 1980 The topographic effect on spectral response from nadir pointing sensors, Photogrammetric Enginering and Remote Sensing, vol. 46, pages 1101-1200.

Hook, S.J. and Munday T.J., 1988 Preprocessing and analysis of airborne visible near and shortwave infrared data for the detection of alteration in weathered vegetated terrain, Proceedings of IGARSS '88 Symposium, Edinburgh, Scotland, 13-16 Sept. 1988, pages 753-757, ESA Publications, Ref. ESA Sp284, (IEEE 88CH2497-6).

Horler, D.N., Barber, J. and Barringer, A.R., 1980 Effects of heavy metals on the absorbance and reflectance spectra of plants, International Journal of Remote Sensing, vol.1, pages 121 - 136.

Huckerby, J.A., Magee, R.W., Moore, McMahon Moore J. and Coates, D., Thematic Mapper applied to alteration zone mapping for gold exploration in South East Spain, presented at Remote Sensing for exploration Geology, Fifth Thematic Conference, Reno, Neveda, September 29 - October 2, 1986.

Hunt G.R., 1980 Electromagnetic radiation: the communication link in remote sensing, Remote Sensing in Geology (Siegal B.S. and Gillespie, A.R., eds.) New York, John Wiley, pages 5-45.

Hunt, J.R. and Ashley R.P., 1979 Spectra of altered rocks in the visible and infrared, Economic Geology vol.74, pages 1613 - 1629.

Hunt, J.R. and Salisbury J.W., 1970a Visible and near infrared spectra of minerals and rocks: I Silicate minerals, Modern Geology, vol.1, pages 283 - 300.

Hunt, J.R. and Salisbury J.W., 1970b Visible and near infrared spectra of minerals and rocks: II Carbonates, Modern Geology, vol.2, pages 23 - 30.

Hunt, J.R., Salisbury J.W. and Lenhoff C. J.,1971a Visible and near infrared spectra of minerals and rocks: III Oxides and hydroxides, Modern Geology, vol.2, pages 195 - 205.

Hunt, J.R., Salisbury J.W. and Lenhoff C. J., 1971b Visible and near infrared spectra of minerals and rocks: IV Sulphides and Sulphates, Modern Geology, vol 3, pages 1 - 14.

Hunt, J.R., Salisbury J.W. and Lenhoff C. J., 1973b Visible and near infrared spectra of minerals and rocks: VII Acid igneous rocks, Modern Geology, vol. 4, pages 217 -224.

Hunt, J.R., Salisbury J.W. and Lenhoff C. J., 1973c Visible and near infrared spectra of minerals and rocks: VIII Intermediate igneous rocks, Modern Geology, vol. 4, pages 237 -244.

Hunt, J.R., Salisbury J.W. and Lenhoff C. J., 1974 Visible and near infrared spectra of minerals and rocks: IX Basic and ultrabasic igneous rocks, Modern Geology, vol 5, pages 15 - 22.

Jenson, S.K. and Waltz, F.A., 1979 Principal Components Analysis and Canonical Analyis in remote sensing, Procceedings of the American Society of Photogrammetry Annual Meeting, March 1979.

Johnson, C.H., 1943 Steeple Rock district, Grant County, New Mexico, United States Bureau of Mines War Minerals Report 188, 11 pages.

Jones, W.R., Hernon, R.M. and Moore, S.L., 1967 General geology of the Santa Rita quadrangle, Grant County, New Mexico, United States Geological Survey, Professional Paper 555, 144 pages.

Kauth, R.J. and Thomas, G.S.,1976 The tasselled cap - a graphic description of the spectral - temporal development of agricultural crops as seen by Landsat, Proceedings Symposium on Machine Processing of Remotely Sensed Data, Purdue University, pages 41 - 51.

Kelly, V.C., 1982 New Mexico Geology Highway Map, New Mexico Geology Society and New Mexico Bureau of Mines and Mineral Resources.

Kelly, V.C., 1982 Tectonic map of New Mexico, New Mexico Geology Highway Map, New Mexico Geology Society and New Mexico Bureau of Mines and Mineral Resources.

Kent, B.H., 1957 Experiments in the use of colour aerial photographs for geologic study, Photogrammetric Engineering, vol. 23, pages 815 - 868.

Kepley, L.K., Abrams, M, and Readdy, L., 1982 Mineralogical remote sensing of surface expressions of deep seated porphyry copper deposits at Safford mining district, Arizona, International Symposium Remote Sensing of Environment, Second Thematic Conference, Remote Sensing for Exploration Geology, Fort Worth, Texas, December 6 - 10, 1982.

Knepper, D.H. and Raines, G.L., 1985 Determining stretch parameters for lithologic discrimination on Landsat MSS band-ratio images, Photogrammetric Engineering and Remote Sensing, vol. 51, No.1, pages 63-70.

Kolessar, J., 1983 The Tyrone copper deposit, Grant County, New Mexico, Chapter 15, Advances in geology of the Porphyry copper deposits, southwestern North America, Titley, S.R. (ed), University of Arizona Press, pages 327-334.

Kottlowski, F.E., 1965 Sedimentary basins of south-central and southwestern New Mexico, American Association Petroleum Geologists Bulletin, vol. 49, no.11, pages 2120 - 2139.

Kowalik, W.S., Lyon, R.J.P.and Switzer, P., 1983 The effects of additive radiance on ratios of Landsat data, Photogrammetric Engineering and Remote Sensing, vol. 49. pages 659 - 669.

Krauskopf, K.B., 1982 Introduction to Geochemistry, second edition, McGraw Hill.

Kriegler, F.J., Malia. W.A., Nalepka, R.F. and Richardson, W.,1969 Preprocessing transformations and their effects on multispectral recognition, Proceedings of the Sixth International Symposium Remote Sensing of Environment, vol.1, Ann Arbor, Michigan, pages 97 - 109.

Kruse, F.A., 1984a Evaluation of TM - simulator colour ratio composite images for hydrothermal alteration mapping, Lordsburg mining district, Hidalgo County, Geology Society of America, Abstracts and Programmes, vol. 16, No.4, pages 227.

Kruse, F.A., 1984b Munsell colour analysis of Landsat colour ratio composite images of limonitic areas in Southwest New Mexico, Presented at the International Symposium on Remote Sensing of Environment, Third Thematic Conference, Remote Sensing for Exploration Geology, Colorado Springs, USA.

Lake, M.C., 1950 Cerro Bolivar - US Steel's new bonanza, Engineering Mining Journal., vol. 151, pages 72-83.

Lattman, L.H., 1958 Technique of mapping geologic fracture traces and lineaments on aerial photographs, Photgrammetric Engineering, vol. 24, pages 166-181.

Lee, K. and Raines, G.L., 1984 Reflectance spectra of some alteration minerals a chart compiled from published data 0.4 - 2.5 μm, United States Geological Survey Open File report 84-96, 6 pages.

Lillesand T.M. and Kieffer, R.W., 1979 Remote Sensing and Image Interpretation John Wiley and Sons, 612 pages.

Lindgren, W., 1922 A suggestion for the terminology of certain mineral deposits, Economic Geology, vol. 17, pages 202-294.

Lindgren, W., 1933 Mineral deposits, 4th ed, New York, Mcgraw - Hill, 930 pages.

Lindgren, W., 1905 Description of the Clifton Quadrangle (Arizona), United States Geological Survey Folio 129, 149 pages.

Lindgren,W., Graton, L.C. and Gordon, C.H.,1910 The ore deposits of New Mexico, United States Geological Survey, Professional Paper 68, 361 pages.

Lipman, P.W and Sawyer, D.A., 1985 Mesozoic ash-flow caldera fragments in southeastern Arizona and their relation to porphyry copper deposits, Geology, vol. 13, pages 652-656.

Longshaw. T.G., 1974 Field Spectroscopy for multispectral remote sensing, an analytical approach, Applied Optics, vol.13, pages 1487-1493.

Loughlin, G.F. and Behre, C. H. Jr., 1933 Classification of ore deposits, Ore Deposits of the Western States (Lindgren vol.), New York, American Institute of Mining and Metallurgical Engineers, pages 17 - 55.

Loughlin, W.P and Tawfiq, M.A., 1985 Discrimination of rock types and alteration zones from airborne MSS data: the Samran - Shayban and Mahd Adh-Dhahab area of Saudi Arabia, Proceedings International Symposium Remote Sensing of Environment, 4th Thematic Conference, Remote Sensing for Exploration Geology, San Francisco, California, pages 207- 217.

Magee, R.W., M^{c}Mahon Moore, J.M., Brunner, J., 1986 Thematic Mapper data applied to mapping hydrothermal alteration in South West New Mexico, presented at Remote Sensing for Exploration Geology, Fifth Thematic Conference, Reno, Neveda, September 29 - October 2, 1986.

Marsh, S.E. and M^{c}Keon, J,B., 1983 Integrated analysis of high resolution field and airborne spectroradiometer data for alteration mapping, Economic Geology, vol.78, pages 618-632.

Martin, R.A., 1981 Geophysical surveys of the Hells Hole Further Planning Area (RAREII), Greenlee County, Arizona, and Grant County, New Mexico, United States Geological Survey, Miscellaneous Field Studies Map MF - 1344 - B.

M^{c}kee, E.H., 1979 Ash flow sheets and calderas: Their genetic relationship to ore deposits in Nevada, Geological Society of America Special Paper 180, pages 205 - 211.

Miller N.L. and Elvidge, C.D., 1985 The iron absorption index: a comparison of ratio - based and baseline - based techniques for the mapping of iron oxides, Proceedings Fourth Thematic Conference, Remote Sensing for Exploration Geology, San Francisco, California, April 1 - 4, 1985, pages 405 - 415.

Milton, E.J., 1986 Principles of field spectroscopy and its role in remote sensing, Proceedings of Remote Sensing Workshop, "Ground truth for remote sensing", University of Nottingham 17th April 1986, pages 14-39, Remote Sensing Society.

Morain, S.A., Budge, T.K. and White, M.E., 1977 Vegetation and landuse in New Mexico, Resource Map 8, New Mexico Bureau of Mines and Mineral Resources.

Norman, J.W. 1969 The role of photogeology in mineral exploration, Transactions of the Institution of Mining and Metallurgy, vol.78B, pages B101 - 107.

North, R.M. and McLemore, V.T., 1986 Silver and gold occurrences in New Mexico, Resource Map 15, New Mexico Bureau of Mines and Mineral Resources.

Oakes, G.D., 1987 Automatic lineament analysis techniques for remotely sensed imagery, Ph.D., thesis, Geology Department, Imperial College, University of London.

Perras S., Bonn F., Gwyn H. and Dubois, J.M., 1985 Classification multi-spectrale et apport de le bande TM7, dans la distinction des depots meubles de lile d'Anticosti, Quebec, Canadian Journal of Earth Sciences, vol. 22, No.8, pages 1139 - 1148.

Podwysocki M.H., Salisbury, J.W. and Jones, O.D., 1984 Evaluation of low sun illuminated Landsat 4 Thematic Mapper data for mapping hydrothermally altered rocks, presented at International Symposium on Remote Sensing of Environment, Remote Sensing for Exploration Geology, Colorado Springs, April 16 - 19, 1984.

Podwysocki, M.H., Siegal, D.B. and Abrams, M.J., 1983 Use of multispectral scanner images for assessment of hydrothermal alteration in the Marysvale mining area, Utah, Economic Geology vol. 78, pages 675 - 687.

Pontual, A., 1988 Applications of Landsat Thematic Mapper imagery to the study of subtle variations in lithology, Proceedings IGARSS'88, International Geoscience and Remote Sensing Symposium, Edinburgh,12 - 16 September, ESA SP -284, IEEE CH 2497 - 6.

Potter, R.M. and Rossman, G.R., 1977 Desert varnish: The importance of clay minerals, Science, vol. 196, pages 1446 - 1448.

Powers, R.S, 1976 Geology of the Summit Mountains and vicinity, Grant County, New Mexico and Greenlee County, Arizona, M.S. thesis, University of Houston, Texas, 107 pages.

Raines, G.L., Offield, T.W. and Santos E.S., 1978 Remotes sensing and subsurface definition of facies and structure related to uranium deposits; Powder River basin, Wyoming, Economic Geology, vol. 73, pages 1706-1723.

Ratte, J.C. and Hedlund D.C., 1981 Geologic map of the Hells Hole Further Planning Area (RARE II), Greenlee County, Arizona and Grant County, New Mexico, United States Geological Survey Map MF-1344A.

Ratte, J.C., Gaskill, D.L., Eaton, G.P., Peterson, D.L., Stotelmeyer, R.B. and Meeves, H.C., 1979 Mineral Resources of the Gila Primitive Area and Gila Wilderness Area, New Mexico, United States Geological Survey Bulletin, 1451, 229 pages.

Ratte, J.C., Hassemer, J. R.,Martin, R.A. and Briggs, J.P., 1982 Mineral resource potential of the Hells Hole Further Planning Area (RARE II), United States Geological Society Miscellaneous Field Studies, Map MF-1344E.

Ratte, J.C., Marvin, R.F., Naeser, C.W. and Bikerman, M., 1984a Calderas and ash flow tuffs of the Mogollon Mountains, Southwestern New Mexico, Journal of Geophysical Research, vol. 89, no. B10, pages 8713 - 8732.

Ratte, J.C., Marvin, R.F., Naeser, C.W., Brooks, W.E. and Finnel T.L., 1984b Volcanic history of the southwest Mogollon Datil volcanic field as recorded along the Morenci lineament, New Mexico and Arizona, Geological Society of America, Abstracts with Programs, vol. 16, no.4, 37th Annual Meeting, Rocky Mt. Section, May 11-12 1984, Fort Lewis, Durango, Colorado.

Rhodes, R.C. and Smith, E.I., 1972a Geology and tectonic setting of the Mule Creek caldera, New Mexico, U.S.A., Bulletin Volcanology, vol.36., pages 401 - 411.

Rhodes, R.C., 1976b Petrological framework of the Mogollon-Datil volcanic ring complex, New Mexico - Surface expression of a major batholith, New Mexico Geological Society Special Publication No.5, pages 103 - 112, Elston, W. E. and Northrop, S.A. (eds), 151 pages.

Rhode, W.G. and Olsen, C.E. Jr., 1971 Estimating foliage moisture content from infrared reflectance data, Third biennial workshop, colour aerial photography in the plant sciences: Falls Church, Virginia, American Society of Photogrammetry, pages 144 - 164.

Richardson, A.J. and Wiegand, C.L., 1977 Distinguishing vegetation from soil background information, Photogrammetric Engineering and Remote Sensing, vol.43, pages 1541 - 1522.

Richter, D.H. and Lawrence, V.A., 1983 Mineral deposit map of the Silver City 1 X 2 quadrangle, New Mexico - Arizona, United States Geological Survey Map I-1310-B.

Rickman, D.L., Sadowski, R.M., 1982 Application of Thematic Mapper type data over a Porphyry - Molybdenum deposit in Colorado, presented at International Symposium on Remote Sensing of Environment, Second Thematic Conference, Remote Sensing for Exploration Geology, Texas, December 6 - 10, 1982.

Ross, D.S., 1976 Atmospheric effects in multispectral photographs, Photogrammetric Engineering and Remote Sensing, vol. 39, pages 377 - 384.

Ross, H. P., Adler J.E.M. and Hunt, G.R., 1969 A statistical analysis of the reflectance of igneous rocks from 0.2 to 2.65 microns, Icarus, vol. 11, pages 46 - 54.

Rothery, D.A., 1982 The evolution of the Wuqbah Block and the applications of remote sensing in the Oman ophiolite, PhD. thesis, Open University, Milton Keynes, U.K.

Rothery, D.A., 1986 Improved discrimination of rock units using Landsat TM imagery of the Oman ophiolite, Journal of Geological Society, London, pages 587 - 598.

Rowan, L.C, Wetlauger, F.H., Goetz, A.F.H, Billingsley, F.C. and Stewart, J.H. 1976 Discrimination of rock types and detection of hydrothermally altered rocks in south central Nevada, United States Geological Survey, Professional Paper 883, 35 pages.

Rowan, L.C., and Lathram, E.H., 1980 Mineral Exploration, Chapter 17, Remote Sensing in Geology, Siegal, B.S and Gillespie, A. R. (eds), New York,J.Wiley & Sons.

Russel, P.L., 1943 Steeple Rock lead-zinc district, Grant County, New Mexico, United States Bureau of Mines Report Investigation 4073, 10 pages.

Sabins, F.F. Jr., 1978 Remote Sensing - Principles and Interpretation, San Francisco, W.H. Freeman and Co., 426 pages.

Sadowski, R.M. and Abrams, M.J., 1982 Mapping hydrothermal alteration using aircraft, VNIR scanners at the Rosemont Porphyry copper deposit, International Symposium Remote Sensing of Environment, 2nd Thematic Conference, Remote Sensing for Exploration Geology, Fort Worth, Texas, December 6 - 10, 1982.

Salisbury, J.W. and Hunt, G.R., 1968 Martian surface materials; effect of particle size on spectral behaviour, Science, vol. 161, pages 351 - 366.

Salomonson, V.V., Smith, P.L., Park, A.B., Webb, W. C. and Lynch, T.J., 1980 An overview of progress in the design and implementation of Landsat D systems, Transactions of the Institute of Electrical and Electronic Engineers, Geosciences and Remote Sensing, vol. 18, pages 137 - 146.

Satterwhite, M.B., Henley, J.P. and Carney, J.M., 1985 Effects of lichens on the reflectance spectra of granite rock surfaces, Remote Sensing of Environment, vol. 18, pages 105 - 112.

Schmidt, R.G. and Bernstein, R., 1977 Evaluation of improved digital processing techniques of Landsat data for sulphide mineral prospecting, United States Geological Survey, Professional Paper 1015, pages 201 - 212.

Schowengerdt, R.A., 1983 Techniques for image processing and classification in remote sensing, Academic Press Inc. (London) Ltd.

Segal, D.B., 1983 Use of Landat Multispectral scanner data for the definition of limonite exposures in heavily vegetated areas, Economic Geology, vol. 78, pages 711-722.

Sheffield, C., 1985 Selecting band combinations from multispectral data, Photogrammetric Engineeering and Remote Sensing, vol. 51, pages 681 - 687.

Shimoda, H., Fukue, K., Yamaguchi, R., Zhang, Zi-jue and Sakata, T., 1988 Accuracy of landcover classification of TM and SPOT data, Proceedings of the IGARSS '88 Symposium, Edinburgh, Scotland, 13 - 16 September, 1988, Ref. ESA SP-284 (IEEE 88CH2497-6), pages 529 - 535.

Siegal, B.S. and Goetz, A.F.H., 1977 Effect of vegetation on rock and soil type discrimination, Photogrammetric Engineering and Remote Sensing, vol. 43, no.2, pages 191 - 196.

Sillitoe, R.H. and Bonham, H.F. Jr., 1984 Volcanic landforms and ore deposits, Economic Geology, vol. 79, pages 1286 - 1298.

Sillitoe, R.H., 1983 Enargite bearing massive sulphide deposits high in porphyry copper systems, Economic Geology, vol. 78, pages 348 - 352.

Silva, L.R., 1978 Radiation and instrumentation in remote sensing, Remote Sensing: the quantitative approach, (Swain, P.H, and Davis, S.M, eds.), pages 21-135.

Skaley, J.E., 1983 Photo-optical techniques of image enhancement, Chapter 5, Remote Sensing in Geology, Siegal, B.S. and Gillespie, A.R. (eds), New York, John Wiley and Sons.

Slater, P.N., 1980 Remote sensing, optics and optical systems, Adison - Wesley ABP, Mass. USA.

Smith, D.M., 1983 Landsat 4, Measured performance versus design parameters, General Electric Co., Larcham Maryland.

Steven, T.A., Luedke, R.G. and Lipman, P.W., 1974 Relation of mineralisation to calderas in the San Juan volcanic field, southwestern Colorado, Journal of Research of the United States Geological Survey, vol. 2, No.4, pages 405-409.

Titley, S.R.and Hicks, C.L., 1966 Geology of the Porphyry copper deposits, Southwestern North America, University of Arizona Press.

Titley, S.R., 1983 Geologic Setting, Chapter 2, Advances in geology of the porphyry copper deposits, Southwestern North America, Titley, S.R., University of Arizona Press, 560 pages.

Trace, R.D., 1947 The Fourth of July and Luckie No.1 and No.2 fluorspar veins, Greenlee County, Arizona, United States Geological Survey, Strategic Minerals Investigation, Preliminary Report, 6 pages.

Tucker, C.J., 1977 Use of near infrared/red radiance ratios for estimating vegetation biomass and physiological status, X-Document, Goddard Space Flight Centre, Greenbelt, Maryland 20771, 70 pages.

Tucker, C.J., 1980 Remote sensing of leaf water content in the near infrared, Remote Sensing of Environment, vol. 10, pages 23 - 32.

Turner, G.L., 1962 The Demming Axis, southeastern Arizona, New Mexico and Trans-Pecos, Texas, New Mexico Geological Society, 13th Field Conference, Mogollon Rim Region, pages 58 - 85.

Vincent, R. K., 1972 An ERTS multispectral scanner experiment for mapping iron compounds, Proceedings of the Eighth International Symposium Remote Sensing of Environment, pages 1239 - 1247.

Wahl, D.E. Jr., 1980 Mid-Tertiary volcanic geology in parts of Greenlee County, Arizona, Grant and Hidalgo Counties, New Mexico, PhD. Thesis, Arizona State University, 144 pages.

Wertz, J.B., 1970 The Texas lineament and its economic significance in southeast Arizona, Economic Geological, vol. 65, pages 166 - 181.

Whitney, C.G., Abrams, M.J. amd Goetz, A.F.H., 1983 Mineral discriminatio using a portable ratio - determining radiometer, Economic Geology, vol. 78, pages 688 - 698.

Wilson, E.D., 1950 Fluorspar in Arizona, Arizona Bureau of Mines Circular 15, 13 pages.

Wise, D.U., 1982 Linesmanship and the practise of linear geo-art, Geological Society of America Bulletin, vol. 93, pages 886 - 888.

Wise, D.U., Funicello, R., Parotto, M. and Salvini, F., 1985 Topographic lineament swarms: clues to their origin from domain analysis of Italy, Geological Society of America Bulletin, vol. 96, pages 952 - 967.

Zara, S.J., 1986 A high spectral resolution study of vegetation reflectance in the red and near infrared PhD. thesis, Dept. of Pure and Applied Biology, Imperial College, University of London.

APPENDIX 1

FUNDAMENTALS OF ROCK SPECTRAL SIGNATURES IN THE VNIR AND SWIR.

The physical basis for spectral remote sensing is the interaction of electromagnetic radiation with the rock surface, which involves processes on the macroscopic and atomic-molecular scales. Only atomic-molecular processes are described here, the macroscopic processes are described in the context of the field radiometry measurements in Appendix III.

Atomic molecular processes

At an atomic level the interaction of electromagnetic radiation with materials can be described by quantum mechanics. All atoms exist in allowed energy levels which may change from interaction with electromagnetic radiation, manifested by absorptions or emissions of radiation. The energy levels are dependent upon the electronic, vibrational, rotational and translational energy of the molecular species. Measurement of the position and intensity of the absorption of emission bands in a spectrum may allow identification of that material. The complexity of the interactions are such that only energy levels of gases can be accurately described. The energy levels of solids, modified by crystal lattice effects, can only be approximated. The spectral features of rocks and minerals are caused by electronic and

vibrational processes.

Vibrational Processes

Vibrational processes in rocks and minerals are caused by the excitation of overtones and combination tones of the fundamental modes of anion groups, including the vibrations of such groups against the lattice structure, and from overtones and combinations of the fundamental modes of molecules trapped within the crystal structure (Hunt and Salisbury 1970a). The values and form of vibrational processes are determined by the number of constituent atoms, their spatial geometry and the magnitude of the binding forces. Transitions between vibrational energy levels cause absorption bands in a spectrum known as fundamentals, overtones or combination tones, depending on the energy levels and frequency. Overtones and combinations typically occur between wavelengths of 1.1 and 5 μm.

In the near infrared only a few materials with high fundamental frequencies show features from overtones and combinations. The most common and important of which are water and the OH stretching mode which occurs where the hydroxyl radical is present.

The water molecule has three fundamental vibrations at 3.106, 6.08 and 2.903 μm and prominent overtones and combinations in the near infrared at 1.875, 1.454, 1.38, 1.135 and 0.942 μm (Hunt 1980).

Water may occur in rocks and minerals as inclusions, hydrous minerals, zeolites and clays (adsorbed).

Laboratory spectra show two absorption bands when water is present at 1.4 and 1.9 μm (Appendix IV). The location and shape of these bands give precise information on the type and location of the water molecules in the rock or mineral. Generally sharp band indicate water in well ordered sites and broad bands indicates unordered or multiple occupied sites.

The fundamental OH stretching mode at 2.74 μm may form combinations with other fundamentals, including lattice and vibrational modes.

The Si-O fundamental vibration occurs beyond 10 μm and is not observable in the near infrared and visible. However when the silicate structure is joined to a hydroxyl the Si-O feature and the 2.74 feature combine to produce additional absorptions features between 2.04 and 2.37 μm.

The Al-OH and Mg-OH bending modes produce important features at 2.2 and 2.3 μm. The Al-OH absorption bands occur in minerals common in hydrothermal altered rocks, including lepidolite (2.2 μm), muscovite (2.208 μm) pyrophyllite (2.166 μm), montmorillonite (2.05 μm) kaolinite (2.162 - 2.009 μm doublet) (Fig. A1.1) and alunite (2.16 - 2.208 μm doublet) (Fig. A1.2). The Mg-OH feature occurs in chlorite (2.32 μm) (Fig. A1.1).

In addition to water and hydroxyl features, carbonate minerals display features between 1.6 and 2.5 μm, due to combination and overtones of the vibrations of the CO_3^{-2} radical ion. Features occur at 1.9, 2.0 2.16, 2.45 and 2.55 μm. e.g. calcite (Fig. A1.1).

Electronic Processes

Electronic spectral features are due to transition metal ions and crystal field effects. The transition metals iron, copper nickel, vanadium, manganese, chromium, titanium and scandium all show these features, but only iron occurs commonly geologically. Almost all electronic spectral features observed in earth resource mapping are due to the presence of iron.

The crystal field affects and conductive band charge transfer transitions for iron give spectral features below 1 μm. The charge transfer band between O^{2-} and Fe^{3+} causes an intense absorption centred in the ultraviolet, the longer wave wing extending into the visible spectrum, superimposed on which are crystal field features from Fe^{3+} in crystalline structures. Absorptions due to these affects are illustrated on figure A1.2.

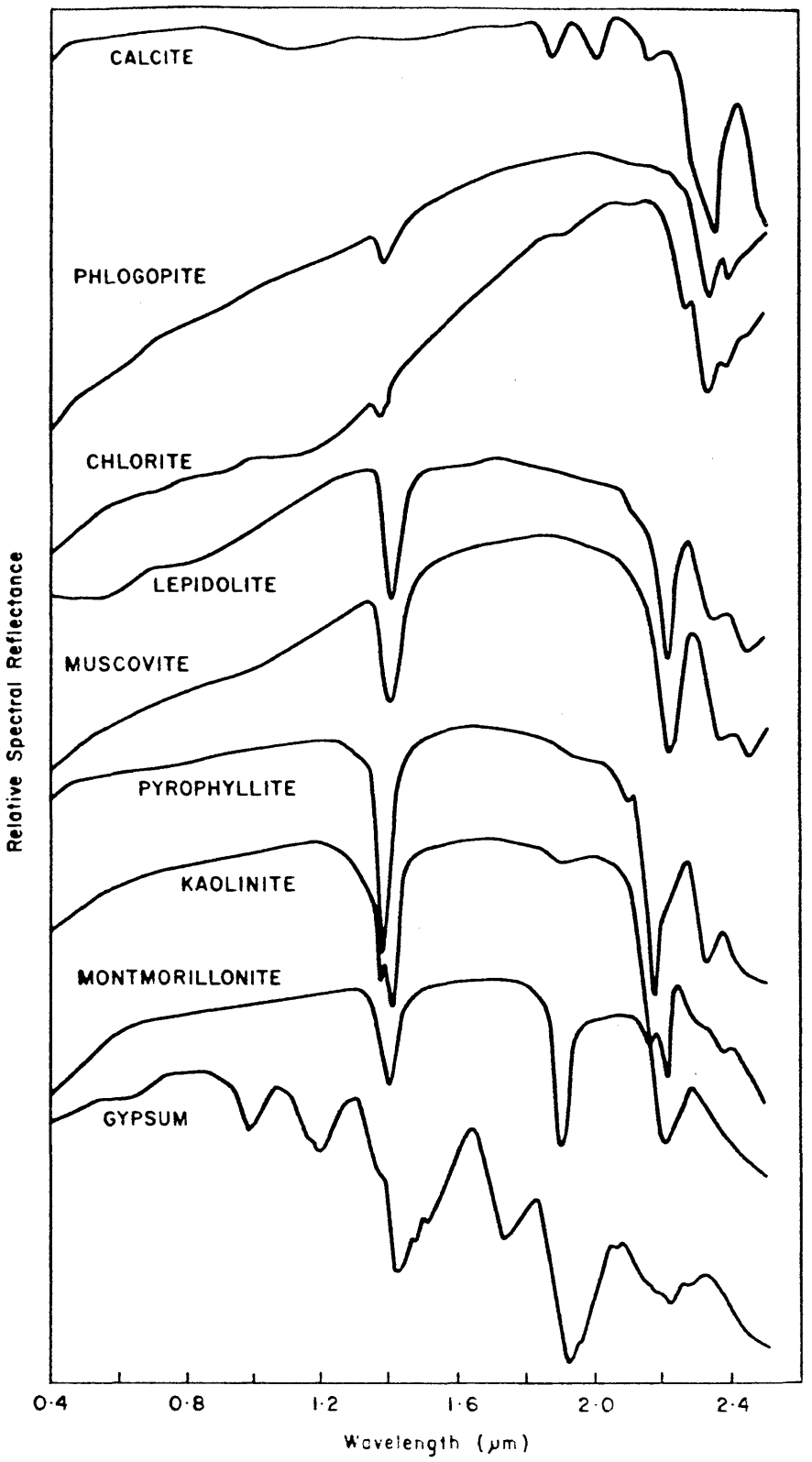

Figure A1.1 Reflectance spectra of alteration minerals I (adapted from Lee and Raines 1984).

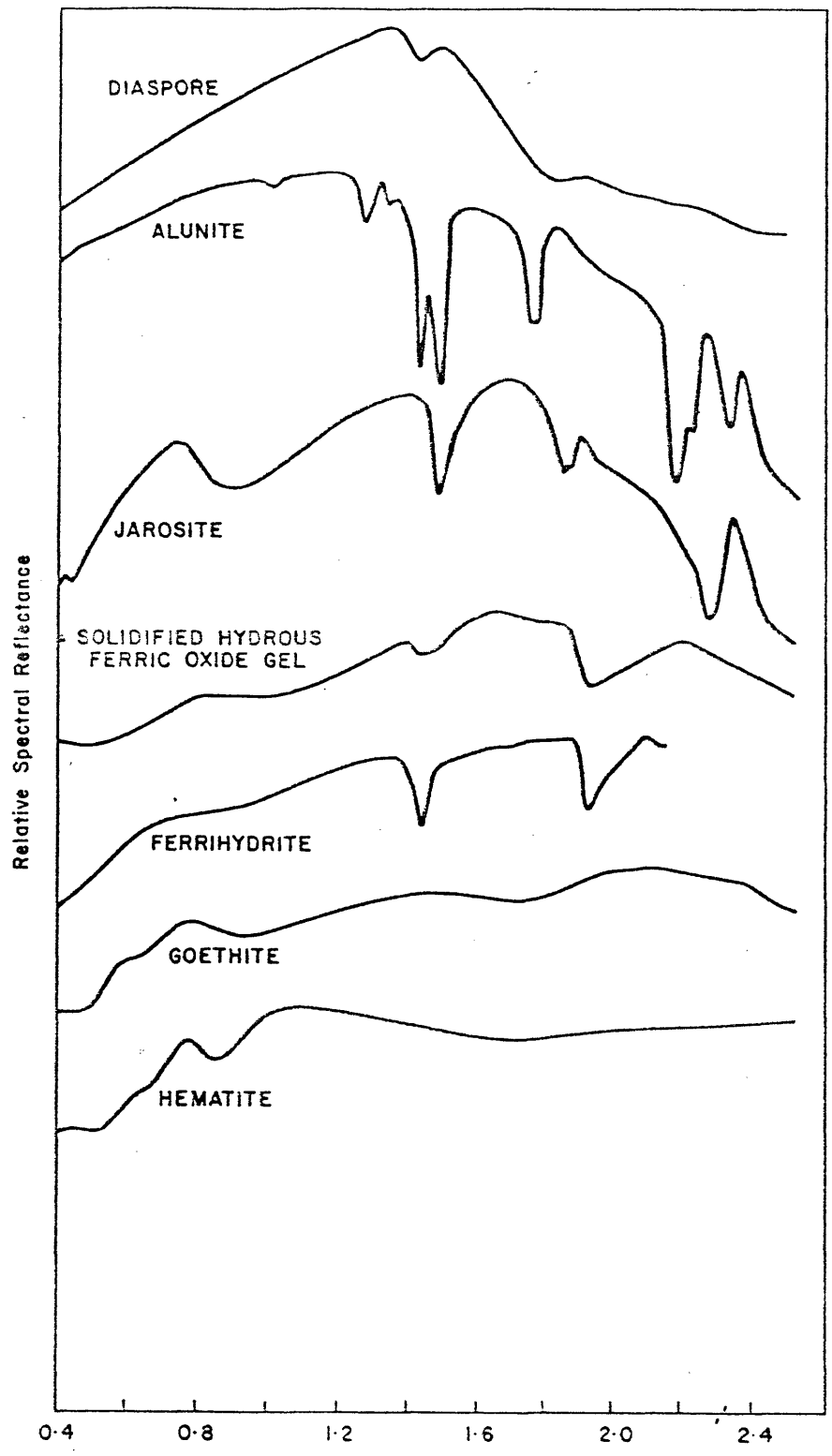

Figure A1.2 Reflectance spectra of alteration minerals II (adapted from Lee and Raines 1984).

APPENDIX II

LANDSAT MSS PROCESSING

1. Introduction

The objectives of the MSS study were to assess Landsat MSS data for mapping hydrothermal alteration in southwest New Mexico and to compare and contrast the imagery with the Landsat TM imagery.

MSS data was the primary source of satellite data for earth observation up until the widespread availability of Landsat TM data in the early and middle 1980s and SPOT data in the latter half of the decade. Therefore a comparative study of Landsat MSS with TM data was undertaken to fully assess the improvements of the TM sensor. (Chapter 1 and Table 1.1). In addition Landsat MSS data was used in preliminary stages of the research before TM data was available.

For mapping hydrothermal alteration the most important differences between MSS (and SPOT) is the absence of the SWIR band on the MSS data, capable of detecting clay bearing minerals (Appendix I), and the improved spatial resolution of TM.

The preliminary studies used MSS negatives of bands 4 5 and 7 which were used to produce black and white prints, and colour images by projection through an opto-electronic analyser. This imagery was poor for alteration mapping because of the inherent poor

resolution and the limitation of spectral band coverage to the near infrared (restricting the imagery to mapping iron oxides). This was exacerbated by both the poor image quality and restricted processing abilities of the analyser. However the imagery was useful for regional geological study and provided an introduction to the later detailed studies with digital MSS and TM.

2. Digital Processing

Digital image processing of the MSS data followed the steps outlined in Chapter 2 for the TM data. This involved geometric, radiometric and atmospheric corrections.

Preprocessing of the MSS data were eased because much of the IIS Software programmes were specifically written to process MSS data. The geometric corrections involved the application of two programmes to the entire MSS scene, DESKEW, to correct for pixel size variations in the line and sample directions and UTM, which transformed the imagery to Universal Transform Mercator. The primary radiometric correction was the DESTRIPE procedure (Chapter 3). Atmospheric correction for production of ratio images was as for the TM data.

Three MSS subscenes were used, named Grant (equivalent to the Blue Creek TM image), Mogollon (including the Brock Canyon TM image) and Alum Mt (equivalent to the Alum Mt. TM image) (See Fig. 2.1).

3. Previous Work

Colour composite ratio images of Landsat MSS imagery have been successfully used to map rocks with surface iron oxides (commonly referred to as limonite) in arid and semi-arid areas (Rowan et al., 1976,; Raines et al., 1978). MSS bands ratios identify iron oxides by recognising iron absorption bands occurring between 0.85 and 0.92 μm (MSS band 7) and by the sharp fall in iron reflectance in the visible bands (Appendix 1).

Previous work has shown that MSS band ratios composites 4/5 5/6 6/7, or 4/5 4/6 6/7 are the best for geological mapping in semi-arid terrain. For mapping limonite (iron oxides) workers have used 4/5 5/7 6/7 (red, green, yellow) (Conradsen 1984), 4/5 6/7 4/6 (red, green, blue) (Rowan et al., 1976, Raines et al., 1978).

However as vegetation density increases the standard techniques are ineffective, partly due to the spatial and spectral resolution limitations of MSS and to the relative positions of vegetation and limonite on the MSS ratios (Segal 1983). Segal (1983) developed a compound MSS ratio (4/5)/(6/7) specifically for mapping limonite in heavily vegetated terrain.

4. New Mexico Studies

In New Mexico I assessed both the standard colour ratio composites (CRC) and the improved CRC of Segal (1983) on the three subscenes.

Detailed analysis was undertaken on the Grant image,

because of the detailed data collected from the test area and regional studies. Four training classes were selected to evaluate the ability of MSS to discriminate limonitic materials from non-limonitic materials and vegetation. These were:

1. Limonite from Telephone Ridge and Bitter Creek
2. Granite from the Burro Mountains
3. Vegetation from the Gila River Valley at Virden and Cliff
4. Felsic volcanics from the Red Rock basin area.

Figure A2.1 shows class scatter plots for the main MSS ratios. Ratio 4/5 is the best for separating limonite from non-limonitic materials and vegetation. Ratio 4/6 confuses vegetation and limonite and ratio 5/6 and 6/7 confuse non-limonitic materials and limonite.

On MSS imagery where spectral mixing occurs results are affected most on ratios where the reflectance of the materials are different. Analysis of the spectral curves of limonite and vegetation (See Fig. 6.10, Chapter 6) show that ratios 5/6 and 6/7 are affected most by increasing vegetation content, while ratio 4/6 is least affected.

The usual contrast enhancements for the standard CRCs are linear stretches with saturation of 2 - 10 % at the black and white ends of the histogram. In sparsely vegetated terrain this stretch displays limonite as dark pixels. However in moderate to heavily vegetated areas vegetation is darker than limonite on ratios 4/6 and 5/6, while 4/5 and 6/7 are unchanged (Fig A2.1) thus the standard CRC with a linear contrast stretch will not enhance limonite.

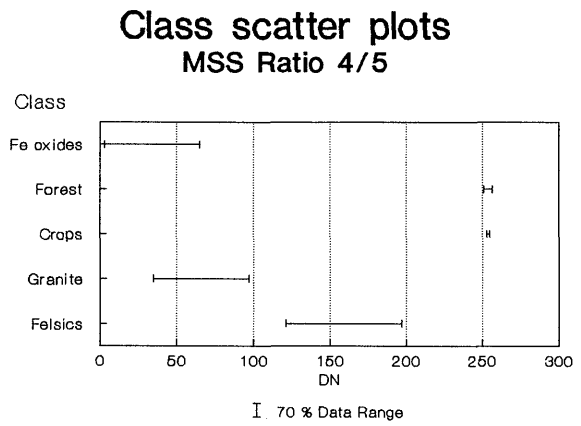

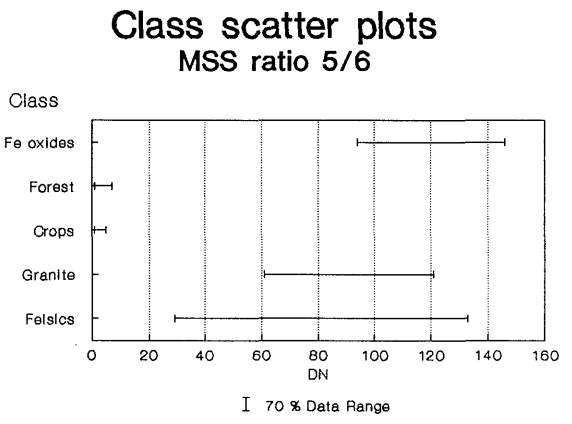

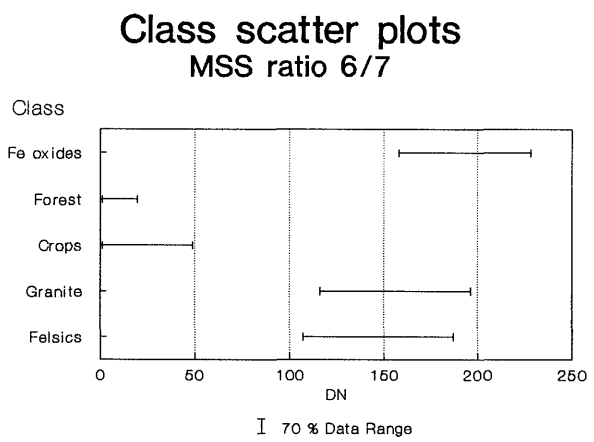

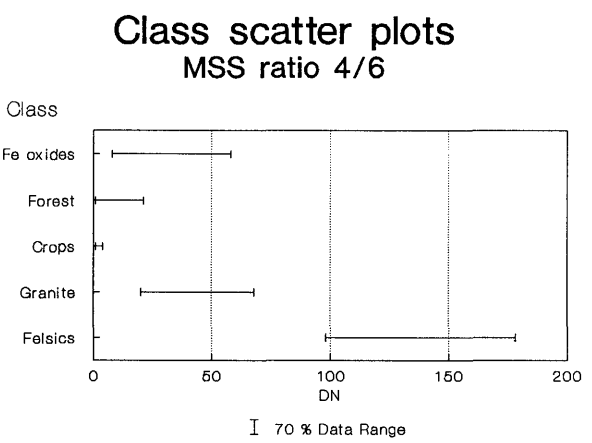

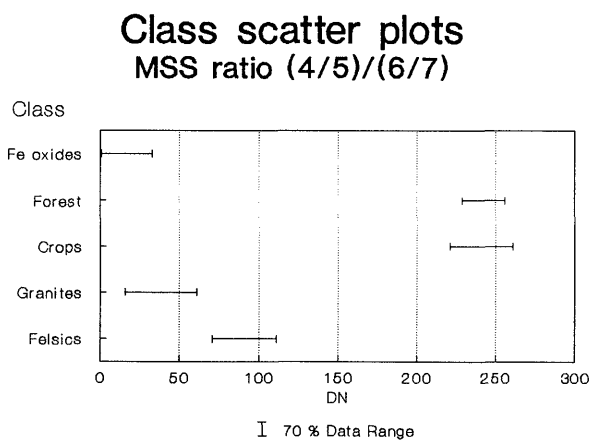

Figure A2.1 Co-incident spectral plots of MSS cover classes from southwest New Mexico.

These results were confirmed on the New Mexico imagery.

My studies confirmed the standard MSS ratios are poor for limonite mapping in vegetated terrain and that the compound ratio 4/5 (4/5)/(6/7) and 6/7 of Segal (1983) is superior for discriminating limonite from vegetated and non-limonitic rocks in moderately vegetated terrain. However the suggested display technique recommended by Segal did not produce optimum imagery in New Mexico.

5. An improved MSS Compound Ratio

An improved technique was developed for use in new Mexico. The method is to produce all the component ratios so that the cover classes occur with either high or low ratio values, and not as mixtures of the two.

This technique uses ratios 5/4, (4/5)/(6/7), 7/6 displayed through red, green and blue filters. Excellent images were produced for discriminating limonite from vegetation and non limonitic materials on the Grant, Mogollon and Alum MSS scenes. An exponential contrast stretch was the best for discriminating limonite. On the imagery limonite appeared white (or yellow), vegetation is black to dark green with increasing intensity, and non-limonitic rocks appear light blue.

On the Grant image limonite was identified at Steeple Rock (Telephone Ridge and Bitter Creek - Goat Camp Springs), Ash Creek in the Red Rock Basin, Brock Canyon, Mangas Creek, as well as on the Gila Conglomerates in the Mangas Valley and west of the Big Burro Mts. All these areas were identified on the TM imagery as altered areas

(Chap. 7). In addition limonitic areas were identified at Schoolhouse Canyon, and Lordsburg Mesa (10 km west of Lone Mt.). The TM data did not extend as far south as Lordsburg and the Schoolhouse area is difficult to interpret on the TM because of dense forest and rugged topography.

On the Mogollon image (where vegetation density is high) the standard CRC (4/5 5/6 6/7) is completely dominated by vegetation. Better imagery for geologic interpretation results from using the 4/5 4/6 6/7. However using the new ratio combination limonitic areas were identified at Mogollon, Alum Mountain and in the San Francisco Springs Area (Arizona).

6. Discussion

On the MSS imagery alteration was mapped in the mountainous forested areas where it was not possible to map with the TM data, despite the latters improved specifications. This is because the MSS imagery was acquired in summer where the high sun angle reduces shadowing and problems from non-Lambertian reflectance (Appendix III). In addition in summer in New Mexico high temperatures and low rainfall inhibit vegetation growth and reduce spectral mixing.

These results illustrate the importance of imagery selection. Despite the lack of the clay band and inferior spatial resolution the MSS was superior to the TM in the mountainous and forested areas.

However in the Blue Creek basin MSS did not provide the

level of detail available from the TM. Generally the MSS imagery gave geologic detail commensurate with mapping a 1:250,000 scale while with TM 1:50,000 mapping was achieved.

APPENDIX III

FIELD SPECTRAL STUDIES

1. Principles of Radiometry

Field radiometry is the set of techniques for measuring the interactions between electromagnetic energy and matter in the field environment (Milton 1986). The unit of measurement used is reflectivity of the target surface, defined as the dimensionless ratio of the reflected radiant flux to the incident radiant flux (Marsh and McKeon, 1983);

$$R = \frac{Er}{Ei} \times 100\ \%$$

where
Er is energy reflected
Ei is energy irradiated

Reflectance is a function of the properties of the surface under illumination and the intensity of the light source at a particular wavelength and is effected primarily by the surface roughness of the material relative to the wavelength of the impinging radiation. The scattering of the reflected radiation from interaction with the material is described as Lambertian (diffuse) or specular (mirror like) (Fig A3.1).

Reflectance for most natural objects is dependent upon the

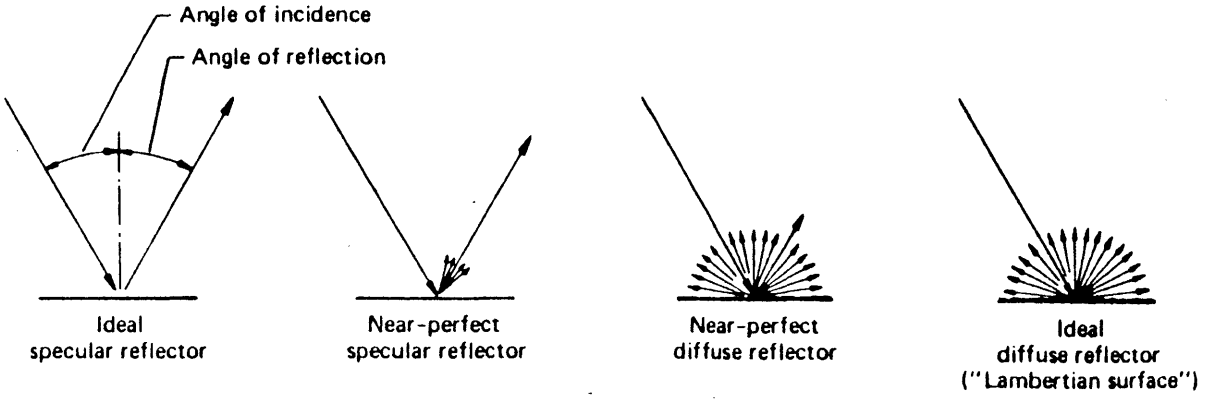

Figure A3.1 Lambertian and specular reflectance (after Lillesand and Kieffer, 1979)

direction of irradiance and the direction along which the reflected flux is detected, i.e. reflectance from a surface is strongly dependent upon the geometry of measurement.

The correlation of reflectance for different geometries is poor for non-Lambertian materials. As most natural objects are inherently non-Lambertian (Longshaw 1974), even from the restricted geometry of Landsat observations much valuable reflectance data are only valid for the unique conditions under which they were gathered. Rocks, soils and vegetation are often highly non-Lambertian and Eaton and Dirmhirn (1979) report bare soils may exhibit more specular behavior than vegetation.

Reflectance of Lambertian materials is independent of incidence and viewing angles, but for non-Lambertian surfaces the distribution is dependent on the view angle and the source incidence angle. The bi-directional dependence of reflectance of an object is measured by the Bi-directional Reflectance Distribution Factor (BRDF) and the spectral indicatrix defines the BDRF for all possible view angles for a specified solar position.

Measurement of BRDF is not practicable so a Bidirectional Reflectance Factor (BRF) is measured instead.
Bi-directional reflectance is defined as the ratio of the flux radiated by a target under specified conditions of irradiance and viewing angle to that reflected by a highly reflecting diffuse reference surface, identically irradiated and viewed (Silva 1978).

2. Field Measurement of Reflectance

In the field bi-directional reflectance can be measured if certain rules are followed.

Irradiance and target reflectance should be measured simultaneously to reduce error from atmospheric variations. Milton (1986) estimated that atmospheric variations could account for net changes in irradiance of 1 % over a period of microseconds to 5 % over several seconds, from random particulate movements in the atmosphere and high cirrus cloud respectively. Major changes occur when clouds pass in front of the sun.

With radiometers without the capability for simultaneous measurements of irradiance and target reflectance, measurements must be completed as quickly as possible. Alternatively two radiometers can be used, one to measure irradiance, the other to measure target reflectance. Duggin (1980) has described calibration methods for dual radiometer usage.

Ratioing radiometers have the advantage of simultaneous measurement and are thus freed from errors due to illumination changes. Ideally measurements should be taken under clear blue sky, but practical considerations may necessitate measurements under less than ideal conditions.

The angular relationships between the target, source and sensor should be the same, or within limits known not to affect reflectance, to ensure comparibality and repeatability of results. As noted above, if the surface is Lambertian the BRDF is independent of these angular

effects. Generally Lambertian behaviour can be assumed and is approximately true if :

(a) the azimuth of the target and sun are in the same plane and the azpect (the orientation of the slope measured clockwise from solar azimuth) is zero. This will keep shadows behind the target.

(b) Zenith is kept beteen 30 degress of maximum solar zenith. Ideally the affect of solar zenith angle on the BDR should be determined prior to operational use so that the limitations be known. Under low sun angles the assumptions of Lambertian properties may break down. As a rule of thumb incidence angles of 50 degrees or greater will give acceptable results.

(c) the target is flat.

However it was not always possible to measure under these conditions due to operational conditions. In New Mexico cloud build up in the early afternoon of summer months (when the measurements were taken) restricted ideal conditions from 9.30 am (Solar zenith = 50 degrees) to about 1.30 pm (Solar zenith = 80 degrees). (Table A3.1). Within these limits it was only possible to take 4 to 5 complete measurements per day because of the time required for filter changes and instrument calibration (A3.4), therefore to increase efficiency some measurements were taken earlier in the morning (from 8.45 am, zenith = 40 degrees) and under overcast conditions.

All measurements were taken from the vertical at an approximate height of 1 metre above the target to minimize errors from angle dependent variations. Dark clothing was

Table A3.1 Field Radiometry Measurement Conditions

Number	Zenith	Azimuth	Target	Azpect Incidence *		Time	Note
	Narrow band measurements						
3	64	70	Flat	0	64		Blue sky
4	64	70	Flat	0	64		Blue sky
5	40	81	Flat	0	40		Blue sky
7	54	108	Flat	0	54		Blue sky
8	54	108	Flat	0	54		Blue sky
9	60	100	Flat	0	60		Blue sky
10	60	100	Flat	0	60		Blue sky
11	79	93	Flat	0	79	1300	Blue sky
13	79	93	Flat	0	79	1330	Blue sky
14	39	92	074/060	4	19		Hazy and cloudy
15	39	92					Blue sky
16	64	120	080/044	(40)	38		Blue sky
17	90	134	080/044	(104)	35		Blue sky
23	40	90	080/044	0	23	0845-0902	Blue sky
24	48	94	Flat	0	48	0930	Blue sky
25	75	200	Flat	0	75	0114	Occasional cloud
26	44	83	Flat	0	44	0930	Blue sky
27	62	117			62	1039	Blue sky
	TM filter measurements						
19	78	196	Flat-210/20	4	58-78	1215	Blue sky
20	30-44	80-91	045/200	(35)-(46)	18-38	0815-0907	Blue sky
21	65	96			65	1030	Cloudy but bright
22	56	108	Flat	0	56		Blue sky

* Incidence = COS Z = COS E COS Z + SIN E SIN Z COS AZ

worn to avoid reflectance and the measurements were taken in bright sunshine without shadows. Where possible flat targets were chosen to minimise azpect problems but it was necessary to take several measurements on sloping targets. Table A3.1 shows the angular relationships for the ratio measurements. Effective incidence angles range from 10 to 79 degrees, with an average of approximately 60 degrees.

3. Hand Held Ratioing Radiometer (HHRR)

The radiometer used was the Barringer Hand Held Ratioing Radiometer (HHRR). Specifications of the HHRR are give on table A3.2.

The HHRR was used in narrow band and TM band modes of operation. The narrow band mode was used to identify particular alteration minerals in the field, and the TM mode was to provide TM ratio data of alteration types from the ground to compare to the TM satellite ratio imagery (Chapt. 5.3).

4. Operational Procedure

The operating technique was to divide one selected band by another by means of selecting filters mounted on filter wheels. The following considerations were important for filter selection:

(1) The minerals and rocks to be identified

(2) Simple and rapid operation in the field

SPECIFICATIONS:

RADIOMETER HEAD	
Spectral Range:	0.4 - 2.5 micrometres (Extended range 0.3 - 3.5 micrometres is optional).
Filters:	Not included. To be selected from available stock or custom ordered, Barringer will make a preliminary filter evaluation for any customer application.
Light Sources:	Scattered solar radiation, or artificial source.
Optics:	Standard unit has a 2° x 12° FOV
Noise Equivalent Reflectance:	1.5% @ 1 sec. response time and 60° solar zenith angle.
Dynamic Range:	Typically three orders of magnitude.
Response Time:	Typically selectable 1 second or 5 seconds; can be modified to suit customer requirements.
Display:	Reflectance ratio, or individual radiometer signal, or battery voltage or detector temperature on 4 digit LCD.
Analog Outputs:	Reflectance ratio signal and radiometer outputs: 0 to 10 VDC at 10 k output resistance.
Mechanical:	Size — 4" x 5.5" x 9" (10 cm x 14 cm x 24 cm) approximate Weight — 6 lbs (2.8 kg) approximate Pistol grip handle, shoulder strap.
Environmental:	Ambient temperature range: 0 to 40°C Dust sealed, splash & rain proof.
Power Requirements:	+ 6V DC: (8 hours operation from battery pack).
BATTERY PACK:	Belt mounted 6V rechargeable pack. 2" x 5" x 7" (5 x 13 x 18 cm) 4.5 lbs (2 kg).

Table A3.2 Specifications of the Barringer Hand Held Ratioing Radiometer.

The field area was known to be an epithermal mineral deposit in a Tertiary age volcanic setting. Minerals with unique visible and infrared spectral reflectance common in epithermal deposits were expected e.g. the Al rich clays (kaolinite, montmorillonite) and the Mg rich clays and chlorite with a 2.2 μm absoption; the sulphates, alunite and jarosite with absoptions at 2.17 and 0.43 μm respectively and carbonates with absorptions at 2.35 and 2.53 μm.

Having two wheels with five filter positions each, allowed 25 possible different ratios without having to change filters (a clumsy operation in the field). For simplicity only 7 filters were chosen (Table A3.3). The rationale used was the presence or absence of a particular mineral. The presence of a mineral was tested by ratioing its expected absorption filter against the 1.6 μm filter. A ratio value greater than one indicated that the mineral was present.

The field operational procedure involved:

(1) Selection of filters to be ratioed
(2) Balance channel gain to ensure ratio equals one.
(3) Calibrate against Fibrefax[1]
(4) Measure target reflectance

For the narrow band filter arrangement seven measurements were taken. TM measurements required 13 measurements.

---

1 *Fiberfrax is a non-water absorbant easily renewable fibrous material suited for field use. Fiberfax has an uneven spectral response between 0.4 - 2.5 um, with reflectance increasing in the infrared.*

Table A3.3 Filters used in the HHRR work.

Bottom	Centre	Top	1/2 Peak Band Width
390 +-6	430 +-5	470 +-6	40 +-6
580 +-4	600 +-5	620 +-4	20 +-4
910	920	930	10
1580 +-4	1600 +-5	1620+-4	20 +-4
2108	2150	2192	42
2170 +-4	2200 +-5	2230 +-6	30 +-6
2297	2350	2403	53

Note: All figures in nanometres and supplied by Barringer Research.

Even after experience of operation and under ideal weather conditions, it took 52 minutes to complete the 13 TM ratio measurements. Changes in solar irradiance required repeated calibration for ratios of visible and infrared bands. Time consuming calibration could be avoided if ground traverses were limited to the measurement of one ratio. However it was then difficult to ensure that the next ratio measurements are taken from the same target areas.

5. Narrow Band results

Results are tabulated on table A3.4. The table shows the HHRR interpretations and compares these with results from the laboratory spectroradiometer measurememts (Appendix V) and the geochemical mineralogical analyses.

The HHRR results were interpreted conservatively and qualitatively. Ratios values greater than 4 were categorised as very strong absorptions, from 1.8 to 4 as strong absorptions and from 1.2 to 1.8 as weak absorptions. Ratio values below 1.2 were interpreted as not being strong enough to indicate a mineral absorption.

6. Conclusions

The narrow band HHRR ratios chosen were designed to identify mineralogy typical of epithermal hydrothermal alteration assemblages in the Summit Mountains test area.

Ratio 4/2 successfully identified iron oxide bearing rocks; hematite, goethite and ferrihydrite. Ratio 4/3,

TABLE A3.4 HHRR Narrow Band Results.

No	Sample	HHRR Absorptions			Laboratory Radiometer Interpretation
		Strong	Medium	Weak	
3		Fe	Ja		
4	M4	C(Mo/Mu)	Al		Strong Py + K? + Mu?
5	430c	Fe Al Cl	Ja		Weak Al + Hm
6		Cl Ja Al	Fe		
7	432c	Fe	Ja	Al C	Subdued, flat, Weak OH
8	432b	Fe	C Ja	A	Subdued Mu + Go
9	432a	Fe	C(K) Ja	Al	Strong K + Dia
10		Fe	C(K) Ja	Al	
11A				Fe	Weak Mo? + Cl
11B	B1		Fe		
13A		Al	Fe	Ja	
13B	M132	Al	Fe	Ja	Strong Mo, Py + Mu
13C	m133	Fe Ja		Al	Strong Ja, Mu + Mo
14.1	41c		Ja	Fe	Weak OH + Fe
14.2	41b	Ca	Ja	C Fe	Weak Bip + Ho + Mu
14.3		Ca C(K)		Fe Ja A	
14.4	41g		C(K)	Fe	Moderate Mu + Hm
14.5	asc		C(K) Fe		Weak Ja + Mu
14.6	41e	C(Mu) Fe	Ja	Al	Strong Mo + Mu + Hm + Go
15A		C(K)	Al	Ja	
16.1					
16.2	16r	Fe Ja C Al			Strong K + Al? + Mu + Hm + Go
16.3					
16.4	16w		Fe C		Moderate KM + K?
16.5		Fe Ja			
16.6		Fe Ja			
17.1		Fe Ja C	Al C(K)		
17.2		C(K)	Al	Fe Ja	
17.3	M17g	Fe Ja C(K)	Al		Moderate Mu? - K? + Mi
17.4		Ja Al	Fe	C(K)	
17.5			C(K)		
17.6		Fe	C(K)		
18.1		Fe Ja	Ca		
18.2		Ja	Fe		
22.1	M22aw				Moderate Mu
22.2	M22bw	Fe Ja	C(K) Al		Moderate Mu
22.3	112A1	Fe Ja C(K)	Al		Strong OH + Fe
23.1	M23	Fe Ja		Al C	Moderate Al (masked)
23.2			Ja	Fe	
24.1	M24a		Al	C	Strong Al? + K + Mu
24.2		C Al			
24.3	M24b	C Al			Strong Py + K + Mu

Key

Al	Alunite
C	Clay
Fe	Iron Oxide
Go	Goethite
Hm	Hematite
Ja	Jarosite
K	Kaolinite
Mo	Montmorillonite
Mu	Muscovite
Py	Pyrophyllite

chosen to identify jarosite, worked well, but on hindsight it was a poor choice as jarosite is easily identified in the field. Although this ratio is theoretically capable of separating chlorite and muscovite it did not do so. Generally the ratio was high for altered rocks and low for weakly altered (Propylitic) and unaltered rocks.

Advanced argillic alteration assemblages were identified and separated from unaltered or weakly altered rocks with the 4/5 and 4/6 ratios. Ratio 4/5 was excellent for distinguishing pyrophyllite, alunite and clays.

The field measurements showed that siliceous cappings, and manganese stains severely mask hydroxyl absorptions of the hydrothermally altered rocks in the field situation, confirming the laboratory spectral measurements described in Chapter 6.

The HHRR is a useful field tool for determining alteration mineralogy and for distinguishing altered from non altered rocks in volcanic terrain were the fine grain size of the rocks makes it difficult to identify alteration minerals. The initial identification of the Bloodgood Canyon tuff as altered rock was due to the HHRR measurements.

However the HHRR has technial and operational problems. Under less than ideal weather conditions significant signal drifting occurred, particularly between ratios of infrared and visible bands. Scudding clouds in bright conditions caused irradiance fluctuations of around 14 % in the visible bands and 2 % in the infrared bands. This severe signal drifting required constant recalibration of the channels.

TM band 1 could could not be measured as tranmsission was too low for the sensor to give an accurate reading and TM band 7 could not be measured in bright sunlight because transmission was to high and the signal saturated the sensor range. Therefore ratio 4/1 could not be measured. The infrared ratios had to be measured under overcast conditions.

Clearly operation of the HHRR requires considerable skill and patience. Several of the problems could be solved by redesign e.g. easier access to the filter wheels to make filter changes, increased detector sensitivity for measurement of the smaller wavelengths and IR filters to enable IR measurements in full sunlight. An additional problem was the limited operational time. This could be increased by improved battery power or reduced operational electrical consumption.

APPENDIX IV

PROCEDURE TO MERGE AND DISPLAY SPECTRAL SCATTER PLOTS ON THE IIS SYSTEM 500

Scatterplots are a useful means of examining feature space between 2 bands. They show both the spread and the correlation of the data and is an essential analytical tool prior to band ratioing.

The clusters of separate classes in two dimensional feature space can be examined to determine separability, only if they can be displayed simultaneously. This appendix describes the procedure to achieve this, by overcoming the hardware (limited to 4 refresh and 4 graphics planes) and software (absence of graphic read or write capabilities) limitations imposed by the system 500. The procedure described allow 3 classes to be displayed in colour.

The procedure involves 8 stages:

1. Training Stage
2. Save Training Areas
3. Produce Scattergrams
4. Set Scattergrams
5. Feed and Save Scattergrams
6. Repeat from 3 for class 2
7. Repeat from 1 for class 3
8. Merge and Display Scattergrams

Stage 1. Training Stage

Select the image for the training procedure and use BLOTCH, an interactive programme which allows areas on the images to be selected. A good choice is a stretched colour composite. However if the training image is different from the scatterplot featured images it is posssible that classes separable on the colour composite may prove to overlap on the featured imagery.

During training using Blotch it is advisable to use 2 classes because of graphics limitations. Use planes 2 and 3 as 0 and 1 are overwritten by processes such as Histogram and Scattergram. It is important to be able to repeat the training procedure rapidly.

Stage 2. Save Training Areas

It is important to be able to extract data from the training area from other ratios or imagery. The original blotched area held in the bit plane is transient and is easily lost, so in the absence of a GRAPHICS SAVE command it is neccessary to save the blotch as an image. This can be done using the FEEDBACK command on a single band (usually TM band 5) with the bitplane holding the blotch. The image must then be LEVEL'SLICED to give the area outside the blotch DN values of 255 (while leaving the blotched area unchanged) for later Scattering.

The following command sequence loads and contrast stretches a false colour composite of band 1 4 and 5 (SR145) and designates a training area on bit plane 2. The training area ($B1) is then saved. The surrounding

grey levels outside the blotch area are set to 255 (white). This is required because the system will not save blank images.

```
1.  SR145 ADJUST > FAST DISPLAY > $A;
2.  $A > BLOTCH (PLANE=2);
3.  $A > DELETE;
4.  SR145 ADJUST(:3) > DISPLAY > $A1;
5.  > FEEDBACK(*BLOTCH BITPLANE=2) > $B1;
6.  $B1 > LEVEL'SLICE (GREYLEVEL=255 NOT BLOTCH);
7.  > FEEDBACK > $B1';
8.  $B1 > DELETE;
```

The procedure is then repeated for class 2.

```
 9. $A1 > SELECT;
10. > FEEDBACK (*BLOTCH PLANE=3) > $B2;
11. $B2 >LEVEL'SLICE (GREYLEVEL=255 NOT BLOTCH);
12. > FEEDBACK > $B2';
13. $B2 > DELETE;
```

The two classes are displayed and saved together.

```
14. $B1' $B2' > SELECT;
15. > FEEDBACK > $B12';
16. > SAVE > SR'BLO'CLASS12.
```

Stage 3. Produce Scattergrams

Read on the required bands for the scattergram and display them using SCATTERGRAM with the defined blotch plane for the desired training area.

If for example a TM band 5 ($B5) band 7 ($B7) scattergram is produced then:

```
17.  $B5 $B7 > SCATTERGRAM (PLANE=2) > $CLASS1;
```

Stages 4 and 5. Set Scattergrams Class Levels and

Feedback and Save the Scattergram

This is a crucial stage neccessary so that when several classes are displayed they are separable by density slicing and psuedocoloring. Feedback the set scattergram class set as above and save it as a one band monochrome image.

On FEEDBACK the grey level (GL) intensity of the data can be specified. Thus careful selection of individual class GLs will allow several classes to be displayed and discriminated in colour simultaneously.

Half byte intensity levels (IL) between 0 and 1023 are available.

Intensity Level	GL Output
4	0
8	1
260	64
516	128
772	192
1023	255

Overlaps between 3 classes can be calculated if the cumulative density levels are set to less than the display maxima (255). Thus:

Class	IN	GL
1	164	40
2	324	80
3	524	130
1 + 2		120
1 + 3		170
2 + 3		210
1 + 2 + 3		25

Thus:

```
18.  $CLASS1 > LEVEL'SLICE (IN = 164);
19.  > FEEDBACK > $CLASS1'N;
20.  $CLASS1'N > SAVE > SR'57'CL1;
```

The saved name designated the image (Steeple Rock), the bands (5/7) and the class (Class 1).

Stages 6 and 7. Repeat for next two classes

These classes are named SR'57'CL" and SR'57'CL3.

Stage 8. Merge and display

Once the 3 classes have been produced, intensity mapped and saved they are displayed, converted to a one band black and white image and psuedocoloured for analysis. The psuedocolour programme must be set to 8 levels, representing the possible number of levels in the image. For three classes this is 7, plus one for the screen background colour (black).

```
21.  SR'57'CL1 > FAST DISPLAY > $A;
22.  SR'57'CL2 > FAST DISPLAY > $B;
23.  SR'57'CL3 > FAST DISPLAY > $C;
24.  $A $B $C >SELECT;
25.  > FEEDBACK > $D;
26.  $D > PSUEDOCOLOUR (LEVELS=8);
```

If photographs are required the ANNOTATE and ZOOM facilities are useful. The DRAW command cannot be used as the graphics are lost on feedback.

Ratio scattergrams were done for six classes in the Summit Mountains area, alteration. rhyolite. latite, andesite, vegetation and colluvium (Chapter 5).

APPENDIX V

LABORATORY SPECTRAL MEASUREMENTS

The Barringer "Refspec" spectroradiometer was used to measure spectral reflectance of the rock samples. The Refspec measures hemispherical directional spectral reflectance with a spectral resolution of 1 - 3 nanometres in a range from 0.46 to 2.409 μm. A schematic of the machine is shown in figure A5.1. Light entering the sensor port is reflected through an integrating sphere and passes through unto a collimating lens focusing the light unto a diffraction grating and then through a filter wheel to either a silicon (for wavelengths to 1 μm) or cooled lead sulphide (for wavelengths above 1 μm) photocell.

Target radiance is collected over a 6 by 12 degree field of view and is directional. This is divided by hemispherical global irradiance (hemispherical) to give hemispherical directional reflectance.

The machine was designed for portable field use powered by a 12 volt portable shoulder battery pack. The measurements in this study were taken in the winter in the laboratory with artificial tungsten lighting.

The Refspec was interfaced with an Apple II microcomputer for automated data collection. The data was stored, digitally processed and graphically displayed. Hard copies were produced for interpretation.

The rock samples were held below the sensor head by clamps

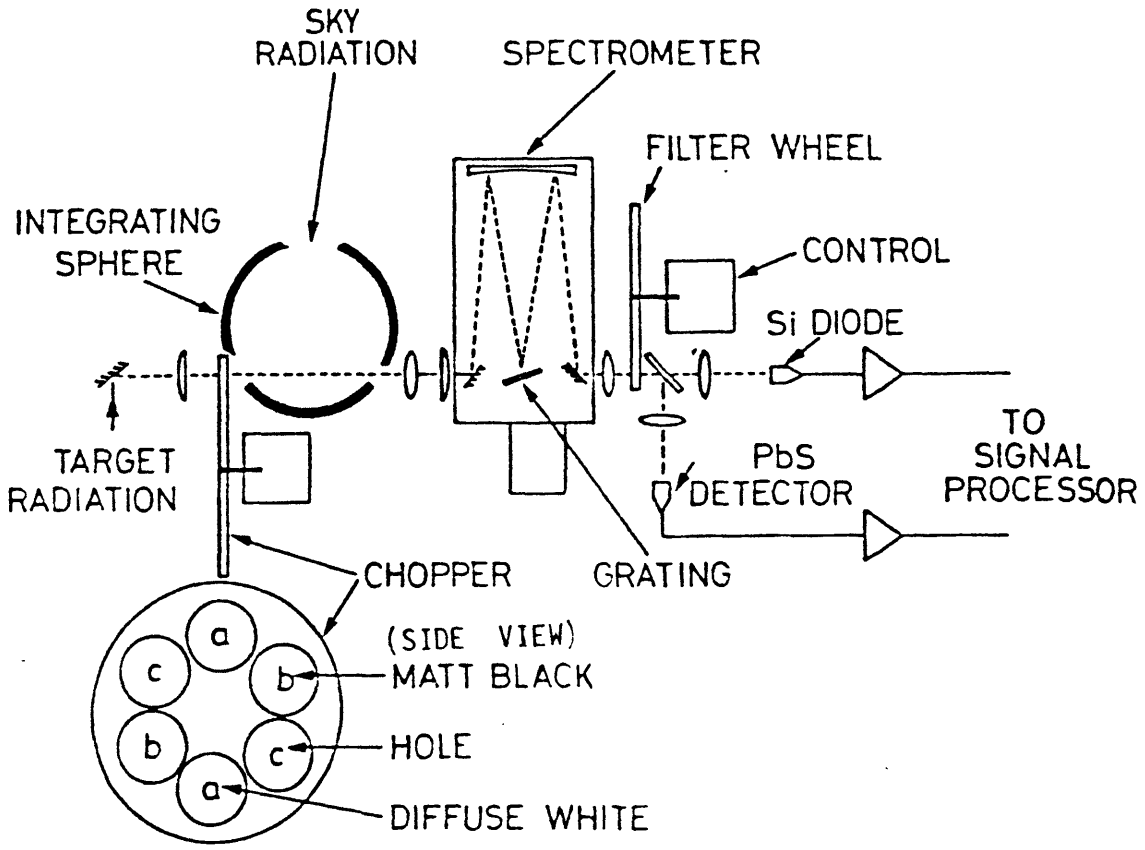

Figure A5.1 Schematic of the operation of the Barringer "Refspec" spectroradiometer.

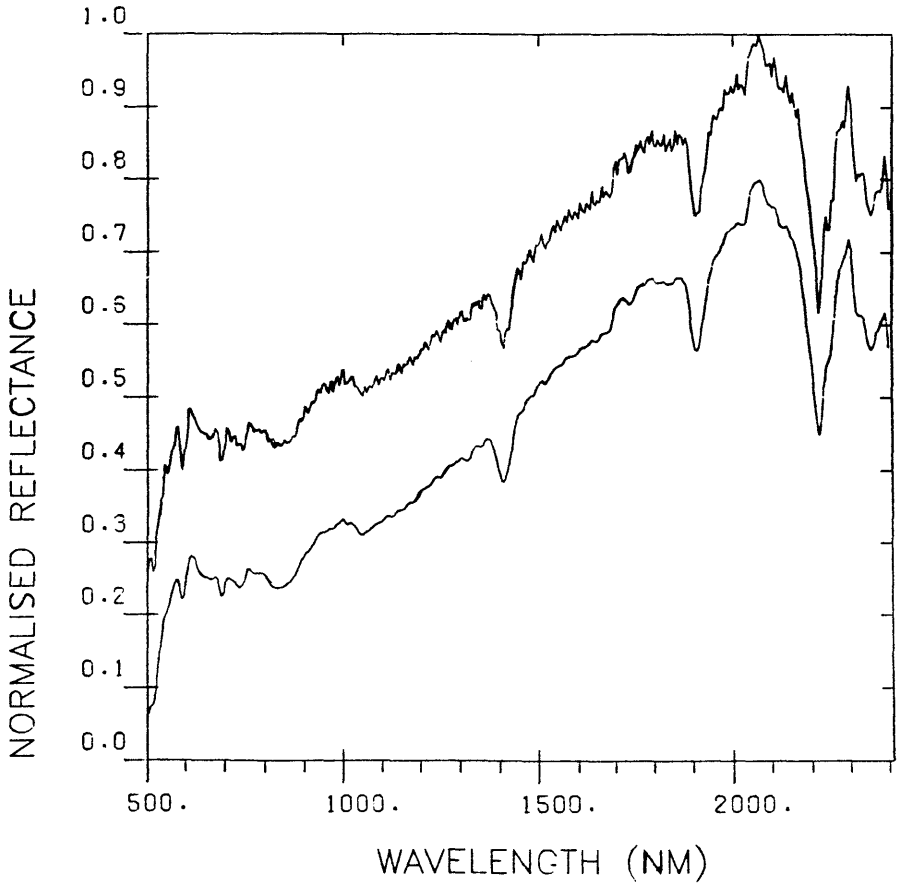

Figure A5.2 Smoothing of interpolated spectra data of an altered tuff.

at a distance of approximately 0.2 metres and illuminated by an incandescent tungsten light source. The sample was raised or lowered to find the optimum signal strength as indicated on the refspec reflectance meter. High signals can cause saturation and signal loss. As illumination intensity and direction affect results each sample was measured three times and an average taken and results were checked for anomalous reflectance.

Data processing software developed on the microcomputer by Zara (1986) was used to process the data. This involved averaging, interpolation, smoothing and normalisation. Interpolation at an interval of 5 nanometres was used to remove confusing peaks and noise. Goetz (1986) reports the optimum band width for remote sensing of geologic materials as 10 namometres. Noise was removed by an averaging filter. (Figure A5.2).

Initially it was hoped to calibrate the reflectance data so that results could be compared with other spectral data. However, since reflectance is dependent on the measurement method, the reference standard, surface roughness, particle size, and the properties of the mineral with respect to light (opaque, translucent, transparent) (See Annex III) the value of calibration is questionable.

To compensate for illumination variations the spectra were normalised. Normalised spectra convey no information on albedo, but the position of absorptions in the spectra are unchanged.

The spectra were interpreted on paper print-outs. Interpretations were based mainly on published spectral

data for rocks and minerals from Hunt and Ashley (1979), as shown on Appendix 1. Selected printouts are illustrated in Chapter 6.

Table A5.1 shows the results from laboratory reflectance measurements undertaken to compare reflectance of weathered and fresh rock surfaces.

The spectra differ in some respects to published work. A marked drop in reflectance at 1 micron is present in all the results. Although a ferrous iron absorption does occur here, it is due to a fault in the filter grating mechanism of the Refspec. Accentuated drops were interpreted as a ferrous iron absorption. A second anomaly occurred in some of the results between 1.85 and 2.0 μm, manifested as a steep rise in reflectance at 1.9 microns. Examination of the grating mechanism revealed the filter grating required lubrication.

It was considered unnecessary to repeat affected measurements since the faults occurred in regions which are not crucial for interpretation. Interpretations compared favourably with mineralogical analysis from X ray diffraction and thin sections. Details of the Refspec accuracy are given in Gladwell et al. (1983).

Table A5.1 Comparisons of reflectance between natural weathered and lichen covered rocks and and fresh rock surfaces

Sample No.	Rock Type	Location	XRD Mineralogy	Surface Details	Spectral Characteristics	Interpretation from Spectra	Comment
41E	Silicified dacite	Angelo Windmill Carlisle Canyon	Q: Ferri: K: Mus: MnO2 Sericitic-Argillic	Thin section silicified Fe stained	MW1.4: MB1.9: SB2.2 :WS2.35 MW1.4: MS1.9: SS2.2d: SB0.85	) Kaolinite -- Montmorillonite -- Muscovite) + Hematite	Little difference between fresh and weathered surfaces except for strong hematite at 0.85 um in the weathered
16r	Argillised dacite	Carlisle Fault	Q(low): Pyr-K: Go-Ja-He Argillic	Bleached Reddened	WS1.4: WS1.53: WB1.9: MB2.2 MB1.4: WW1.58d: MB1.9: SM2.2/2.17d	) Advanced argillic alteration) Alunite, Pyrophyllite, Muscovite -- Kaolinite	Little difference
M23	Silicified ashflow tuff	East Summit Ridge	Q: Nal-K; Pyr; Micas (Advanced Argillic)	Thin Section Natural Mn and Fe stained	WS1.42/1.47d: MS1.76: VSB2.17/SS2.2d: SB2.3 Sharp rise 1-1.2: Flattened beyond 1.3	Alunite -- Kaolinite Strong ferric iron	Fe and Mn totally mask OH absorptions
NB	Silicified ashflow tuff	Raeburn Pk SW	Q: K-Ferri: MnO2. Mu Silicic	Natural + lichens Underside	BS0.8: WB1.76: MB2.16: MS2.27: MS2.3 SB0.54: SB2.16/2.21d: MS2.3	Kaolinite, Hematite + Goethite Alunite ? + Kaolinite	Small difference. Fe on weathered surface is more pronounced
432A	Silicified ashflow tuff	Telephone Ridge	Q: N Dia Fe: An St Mn Le Silicic	Natural + lichens Underside	MS1.4: MB1.8: VSB2.16/2.21d: WB2.13 MB1.4: VBS1.8: MB2.17: VSS2.16/2.21d	) Kaolinite and) Diaspore	Small difference
M4	Bloodgood Canyon tuff	Estes Ranch	Q:K Py: Dia An Hm Advanced Argillic	Thin section Natural	MS1.4: MB1.74, SB1.9: VB2.22 WB0.7: MS1.4: SB2.2	) Pyrophyllite -- Kaolinite) -- Muscovite	No difference
17B	Rhyolitic tuff Silicic	Raeburn Pk. north slope	Q: K(Di) Dia Fe Silicic	Fresh Natural Fe stained	VSS1.42/1.48d: VSS1.76: MB1.9: VSB2.2: SS 2.32 MS1.4: SB1.9: SS2.18/2.22d	Alunite, Diaspore, Hematite, very flattened Diaspore + Kaolinite	Surface shows diaspore instead of alunite
46C	Silicic Capping Silicic	East Summit Ridge	Q: K: Fe An Silicic	Natural Thin section	SM1.4: VSB2.2/VSS2.21d: SS2.32 SB1.4: VSB2.162.2d: SB2.32	Kaolinite Kaolinite	Little difference Classic Kaolinite absorbtions
420	Silicic Capping Advanced Argillic	Telephone Ridge	Q Nal: Le: Mn Advanced Argillic	Fresh Natural + lichens	SB1.42/1.48d: SB1.76: VSB2.17: SS2.32 W1.4d: W1.76: SB2.2	Alunite Masked alunite	Strong difference, alunite subdued on surface
M25	Virden Dacite (Mild Propylitic)	Laura Canyon	Q Na-Ca feld Px: Mi(Chl Vm Bio): Ca Hm An?	Fresh Natural	) Very flat spectra, both show Fe) and NSS 2.26: 2.23: 2.24	) Micas, chlorite, calcite,) biotite and muscovite	Little difference
M24A	Silicified tuff Advanced Argillic	East Summit Ridge	Q Nal: D Hm Mi (Mu Verm) Advanced Argillic	Thin section Natural	VSB2.2: WB1.76: SS2.32 Flat spectra SS0.55: SB2.14/2.17d: Flat	Alunite + Kaolinite Kaolinite + Fe	Strong difference, surface Fe masks alunite -
M26C	Bloodgood Canyon tuff Advanced Argillic	Whiskey Creek	Q D K: Py: Fe	Natural + lichens Fresh - vesicular	SB 0.89-9: W1.4d: W1.76: MB2.1 WB0.85: MB2.2: SS2.3 very flat	Alunite + Kaolinite + Hematite or Goethite Kaolinite + hematite or Goethite	Little difference except Fe more pronounced on altered surface
ASC	Ashflow tuff	Angelo Windmill	Clays and Jarosite	Natural Thin section	BO.89-9: VW1.4: WB1.85: SB2.2: W2.23 BWO.85: W1.4: W2.0: MW2.21: WS2.25	Jarosite + Kaolinite + Muscovite Muscovite	Weathered spectra flatter
28A	Rhyolite	Estes Valley East Camp fault	Not Available	Natural Fresh	) Regular increase in reflectance from) 0.4 to 2.1 with WB2.2	Not possible	No difference
14B	Bloodgood Canyon tuff	Pennsylvania Canyon	Q Nal Py: Dia K Le	Mn Fe stained Fresh (red)	) SO.85-9: VWB1.76: VW1.4: MB2.17 2.13d) large rise from 1 - 1.3	) Alunite + hematite +) Goethite	No difference
44A	Ash flow tuff	Angelo Windmill	Not Available	Fresh Natural	) WBO.85: WB1.4: SB2.2)	) Muscovite)	No difference
32	Virden Dacite	Bank Mine	Not Available	Fresh Natural	) WBO.85-9.0: WB2.2) very flat	) Hornblende)	OH more pronounced on weathered surface
432B	Rhyolite	Telephone Ridge	Not Available Silicic ?	Fresh Natural (red/brown stain)	) VWB1.4: VWB 1.9: W2.2	) Water in fluid inclusions) or opalisation	No difference

Key to Table A5.1

XRD Mineralogy

: Key from Table 4.3

Spectral Characteristics

Number refer to position of absorptions in micrometres. The first letter refers to the absorption depth (S-Strong, M-Moderate, W-Weak) the second letter to the width of the absorption (S-Sharp, M-Moderate, B-Broad)

A "V" prefix may be added to designate "Very".

A "d" refers to an absorption doublet.

GEOLOGY OF THE SUMMIT MOUNTAINS AREA, GREENLEE COUNTY, ARIZONA, AND GRANT AND HIDALGO COUNTIES, NEW MEXICO.

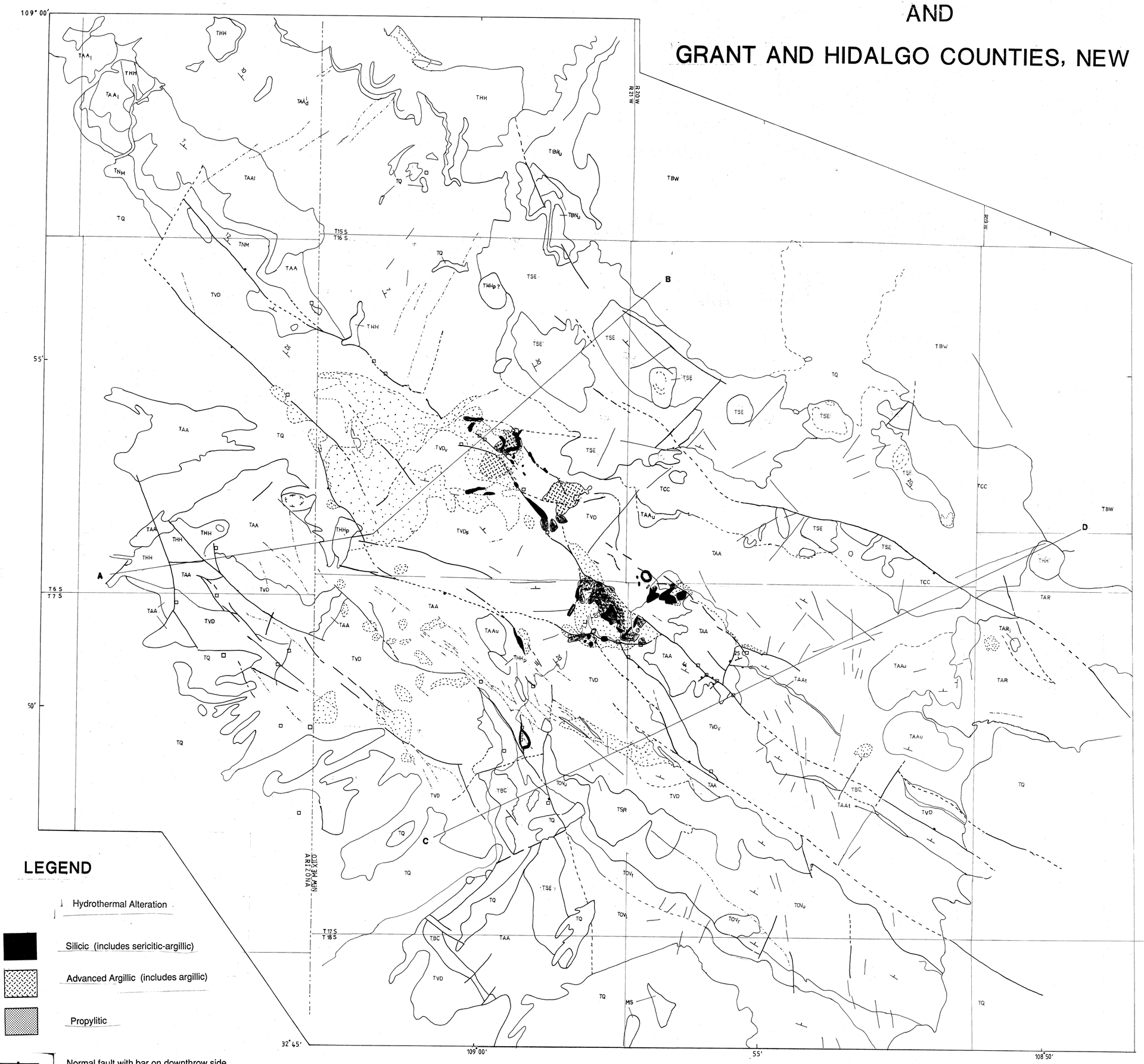

LEGEND

- Hydrothermal Alteration
- Silicic (includes sericitic-argillic)
- Advanced Argillic (includes argillic)
- Propylitic
- Normal fault with bar on downthrow side
- Wrench fault
- Tectonic linear feature
- Strike and dip of bedding
- Dyke
- Lithological boundary
- Selected mine location

DESCRIPTION OF MAP UNITS

TQ Gila Conglomerate
Gila Conglomerate and younger colluvial and alluvial material

TSE Sycamore Eruptives
Rhyolitic to dacitic tuffs and flows of the Sycamore Eruptive Centre

TBW Bearwallow Mountain Formation
Andesite and basaltic andesite flows from shield volcanoes

TCC Cherry Creek Rhyolite
Intermediate to acid flows and tuffs (photogeologic unit)

THH Hells Hole Unit
Rhyolite intrusive - extrusive flow complex
- THHp (Satellite plugs and intrusives)

TAA Amygdaloidal Andesite Unit
Rhyodacite to basaltic andesite lava flows and flow breccias with discontinous felsic tuff and volcanoclastic lenses:
- TAAu (Porphyritic andesite flows of Vanderbilt Peak)
- TAAd (Andesite flows of Dark Thunder Canyon)
- TAAl (Latite of Apache Creek)

TAR Anderson Ranch Unit
Acid to intermediate flows and tuffs (photogeologic unit)
- TARi (Rhyolite intrusives)

TBC Bloodgood Canyon Tuff
Welded rhyolite ash flow tuff

TVD Virden Dacite Unit
Andesitic to dacitic flows, tuffs and flow breccias with intercalated felsic tuff horizons
- TVDs (Andesitic to dacitic flows of Summit Mountains)
- TVDv (Felsic tuffs and volcanoclastic lenses)

TSR Steeple Rock Rhyolite
Flow banded rhyolite

TOV Older Volcanic Series
Moderately welded tuffs with andesitic flow breccias and volcanoclastics
- TOVu (Upper andesite flows)
- TOVt (Tuffs)
- TOVr (Rhyolite flows and tuffs of Horse Camp Springs)
- TOVl (Lower Andesite)

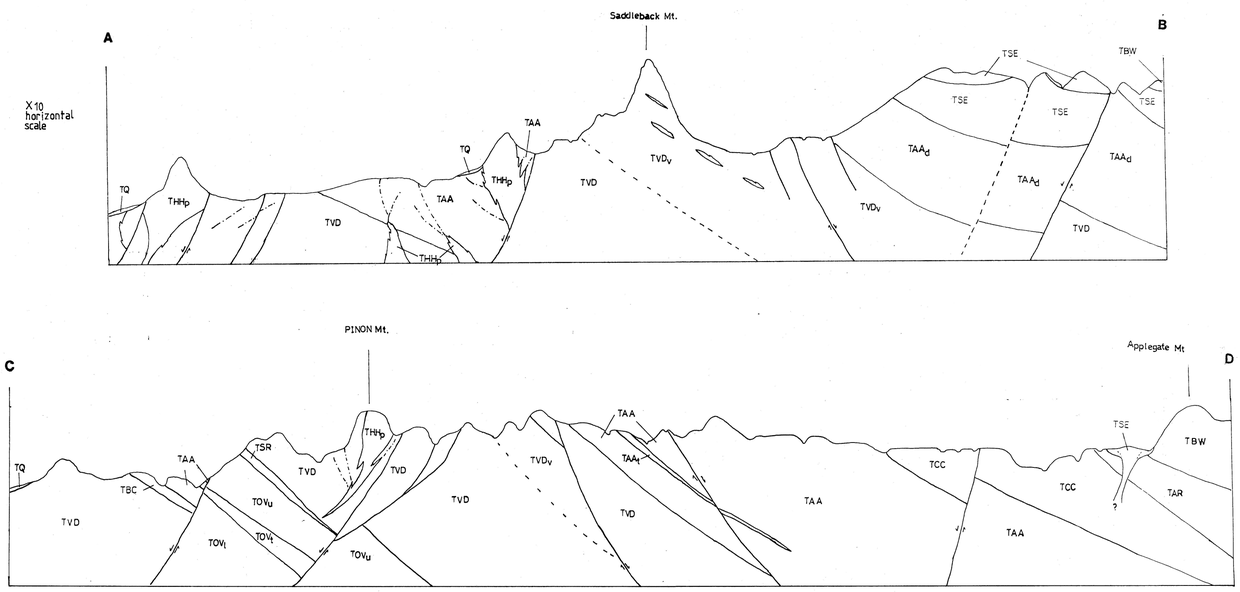

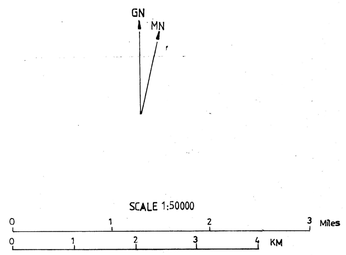

CORRELATION OF MAP UNITS

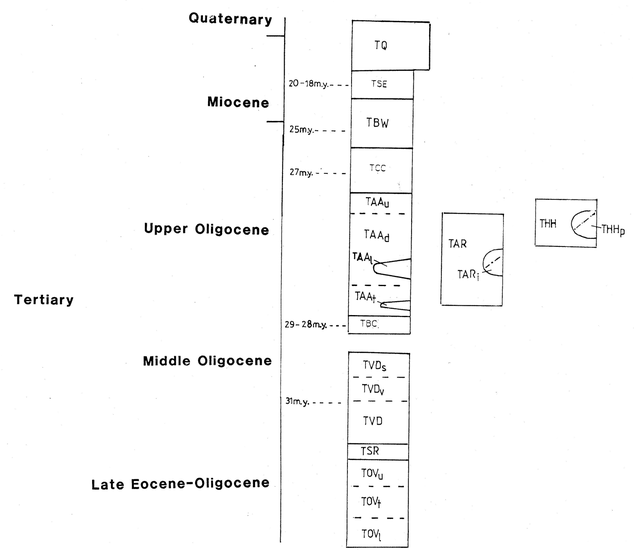

map compiled from field data and aerial photographs.

R.W.Magee 1986